Laboratoire Charles Fabry
Institut d'Optique Graduate School

THESE DE DOCTORAT DE L'ECOLE POLYTECHNIQUE

présentée par

Pierre Lugan

pour obtenir le grade de Docteur de l'Ecole Polytechnique

Sujet de la thèse:

GAZ DE BOSONS ULTRA-FROIDS DANS DES POTENTIELS DESORDONNES : EXCITATIONS COLLECTIVES ET EFFETS DE LOCALISATION

ULTRACOLD BOSE GASES IN RANDOM POTENTIALS: COLLECTIVE EXCITATIONS AND LOCALIZATION EFFECTS

Soutenue le 25 janvier 2010 devant le jury composé de :

M.	A. ASPECT	Membre invité
M.	P. BOUYER	Directeur de thèse
M.	T. GIAMARCHI	Président
M.	R. KAISER	Examinateur
M.	L. SANCHEZ-PALENCIA	Codirecteur de thèse
M.	L. SANTOS	Rapporteur
M.	B. VAN TIGGELEN	Rapporteur

Aknowledgements

The work reported in this thesis was carried out at the Charles Fabry laboratory of the ***Institut d'Optique***, in Palaiseau, France. Funding for this thesis was provided by both the doctoral school of ***Ecole Polytechnique*** via a scholarship of the French Ministry for Higher Education and Research, and the ***Université Paris-Sud*** in Orsay via a teaching assistantship. The *Institut d'Optique* is a joint research institute of the *Université Paris-Sud* and the French ***Centre National de la Recherche Scientifique (CNRS)***. I am grateful to all of the above institutions for providing the framework of my PhD thesis, and I would like to thank their staff for their essential administrative support.

I would like to thank **Pierre Chavel**, the director of the Charles Fabry laboratory. I have been struck by how attentive Pierre Chavel is to the well-being of his collaborators, and how naturally, in spite of his busy schedule, he would take time to enquire about how things are going.

I would like to thank **Alain Aspect** for welcoming me in the Atom Optics Group at *Institut d'Optique*. I very much appreciated the frequent discussions where he would share his inspiring knowledge on experimental as well as theoretical matters. I will recollect his acute sense for pedagogy, and his effort to promote doctoral students within the academic world and outside. Last but not least, I would like to thank him for his warm support during these years, especially in these critical months of writing up.

I am grateful to my advisor **Philippe Bouyer**, who guided my steps with an open mind and good humor, and left me a lot of freedom in the initial direction of this thesis. I will remember as a fruitful recipe this combination of trust, openness, and aptitude to sustain multiple projects.

I would like to express my deep gratitude to my co-advisor **Laurent Sanchez-Palencia**, who directed our theoretical research. I have strongly appreciated Laurent's patient, kind and insightful guidance throughout these years. Laurent's door was open any time for questions, and on so many occasions, our understanding improved by Laurent's reflecting a few minutes to extract precise and relevant physics from fuzzy ideas. Finally, I simply feel indebted to Laurent for the outcome of this PhD. I also feel lucky to have been given the exciting opportunity to work on theoretical aspects of disordered systems just as experiments on disorder were gaining momentum in the group.

Luis Santos and **Bart van Tiggelen** kindly accepted to be thesis referees. I would like to thank them for the interest they showed for our work, the numerous comments they made on this document, and the reflection these comments triggered. I would like to thank **Thierry Giamarchi** and **Robin Kaiser** for having accepted to be members of the jury, and for the questions and comments put forward during the oral defense.

Even before my arrival in the Atom Optics Group, **David Clément** greeted me with an enthusiastic e-mail, which, I think, reflects his personality very well. David was at that time working on the "BEC1" experiment, which had produced the first disordered condensate in our group. David introduced me to the experiment, and I had the opportunity to discuss with

him many theoretical aspects of disordered bosons. I also thank David for the good tips about cultural life in Paris. I thank **Jocelyn Retter** too, for time spent both in the lab and on climbing walls.

I would like to aknowledge fruitful collaboration and helpful discussions with **Maciej Lewenstein**. In particular, I remember profitable discussions in the privileged setting of a summer school in Trieste. On the same occasion, but also on others back in Orsay, I benefited from the advice of **Gora Shlyapnikov**. I do now consider with a different eye the sapience contained in Landau and Lifshitz.

We had a collaboration with **Dominique Delande, Benoit Grémaud, Cord Müller**, and **Christian Miniatura**. I would like to thank them, for this collaboration was an exhilarating experience. I have had extended discussion time with Cord and Dominique, and I must say that their enthusiasm is contagious. Cord has many things to share beyond the beauty of wild diagrams. Dominique is equally generous in sharing his deep understanding. Come up with a few trivial questions, and you will be baffled to learn about universal scaling laws, instantons and tunneling in momentum space.

I would like to thank **Christopher Gaul** for sharing his ideas, notes and results. Our subjects have had overlaps, and I am glad these overlaps stirred not only emulation, but also profitable exchange.

For the analysis of the data of their experiment, I had the opportunity to join **Vincent Josse, Juliette Billy, Zhanchun Zuo** and **Alain Bernard** in the basement of the deserted building of the old institute in Orsay. We spent some extensive time together fighting stacks of prints and electronic data. Vincent played a major role leading the experiment. I am grateful to him for drafting me for the task. Special thanks also go to Juliette. I will remember the lifts to the train station as some of the happy occasions where we would let loose about the joys and hardships of a PhD.

I enjoyed working with **Ben Hambrecht** and **Luca Pezzé** in the theory group. It has always been amazing to be around Ben for his culture in physics and beyond. I would like to wish him good luck on his future endeavors. **Marie Piraud** and **Lam Dao** recently joined the theory group. I would like to seize the present opportunity to thank Ben, Luca, Marie and Lam for the uplifting atmosphere in the group.

Repeated discussions with **Isabelle Bouchoule** and an encounter with **Victor Gurarie** have contributed to my understanding of excitations in bosonic systems. I would also like to aknowledge interesting discussions with **Luca Fontanesi, Michiel Wouters** and **Vincenzo Savona** about the transition from superfluid to Bose glass.

Quite often, I would have been helpless with my computer hardware without the good-humored help of **Frédéric Moron**. I am also grateful to **André Villing** for having lent me a laptop computer. I am secretly hoping he will never ask for this ageing but valiant machine back.

I enjoyed teaching with **Denis Boiron, Sylvie Lebrun, François Goudail, Carlos Garrido-Alzar** and **Felix Kröger** at the *Institut d'Optique*. I am also sincerely grateful to **Jocelyne Armand** from the administration of the institute, who kindly adapted to my last-minute requests on several occasions.

A number of people at the *Institut d'Optique* and in our group contributed to making this PhD a good time. I am thinking of **Francesca** as a precious friend, of **Gaël, Patrick** and **Karen** as office neighbors, of **Andrés, Ronald, Jean-Baptiste, Robert, Aurélien,**

Martijn, Valentina, Jean-François, David, Jean-Philippe, Jean-Christophe, Karim, Sébastien, Martin, Simon, Julien, Rémi, Marie... as former or present members of the Atom Optics Group.

I wish to thank some friends and relatives in particular, for both their support and the recreation they offered in Paris and elsewhere, without (maybe) hoping for much in return: **Laëtitia, Adrien, Virginie, Mircea, Simona, Julien, Frédérique, Denis, Mathilde, Antoine, Camille, Giuliana, Stefan, Diana, Tim, Pam, Kate, Tony, Becky, Tasha, Christian, Alastair and Lindy**...

These years, of course, would have been a different experience without the steady support of my brother **Hermann** and my **parents**. I am grateful to my father for having made me develop a serious taste for physics, to my brother for tempering it through occasional sarcasm, and to my mother for nurturing likings of an alternative, linguistic nature.

Last but not least, I would like to thank **Andrea** with all my heart, for her patience in face of the long itinary of my thesis, for her interest in my coupled equations, her moral support, her skilled and precious advice, her logistic help during my writing up, and the milestones we took on to pass not only on endless train journeys, but also in our common life during this thesis.

November 2009
March 2010

Contents

Introduction **9**

1 Disorder and interactions: condensed-matter physics and ultracold atoms **13**
1.1 Localization of non-interacting waves . . . 13
1.1.1 Coherent transport . . . 14
1.1.2 Anderson localization . . . 17
1.1.3 Localization in one dimension . . . 20
1.1.4 Experimental observations . . . 22
1.2 Disorder in interacting systems . . . 24
1.2.1 Insulators, conductors, and superfluids . . . 25
1.2.2 Disordered bosons: weak and strong interactions . . . 27
1.2.3 Ultracold atomic Bose gases . . . 29
1.3 Random potentials . . . 32
1.3.1 Correlation functions . . . 32
1.3.2 Gaussian disorder . . . 34
1.3.3 Speckle potentials . . . 35
1.4 Conclusion . . . 41

2 Anderson localization of single particles in correlated 1D disorder **43**
2.1 Framework . . . 44
2.1.1 Single particles in correlated one-dimensional disorder . . . 44
2.1.2 One-dimensional Anderson localization . . . 45
2.2 Weak-disorder expansion for the Lyapunov exponent . . . 47
2.2.1 Phase formalism for the Schrödinger operator . . . 47
2.2.2 Born approximation . . . 49
2.2.3 Phase formalism beyond the Born approximation . . . 54
2.2.4 Summary of the leading orders . . . 61
2.3 Localization in weak speckle potentials . . . 64
2.3.1 Speckle potentials . . . 65
2.3.2 The simplest speckle model . . . 68
2.3.3 Transfer matrix calculations . . . 70
2.3.4 Anderson localization of matter waves in speckle potentials . . . 74
2.4 Conclusion . . . 78

3 Weakly-interacting Bose gas in a correlated 1D random potential **81**
3.1 Introduction . . . 82
3.2 Framework of the analysis . . . 84
3.2.1 Weakly-interacting Bose gases . . . 84

3.2.2 Trap geometry and disorder . . . 86
3.3 Delocalized BEC regime . . . 87
3.3.1 Quantum field for condensates and quasi-condensates . . . 87
3.3.2 Mean-field description of the ground state . . . 89
3.3.3 Perturbation of the density profile by a weak potential . . . 91
3.3.4 Trapped Bose gas in one-dimensional disorder . . . 101
3.4 Lifshits glass regime . . . 105
3.4.1 Non-interacting case: the Lifshits tail . . . 105
3.4.2 Lifshits regime . . . 111
3.4.3 Domain of validity . . . 115
3.4.4 Mean-field equation of state . . . 117
3.5 Quantum state diagram . . . 121
3.5.1 Quantum states . . . 121
3.5.2 Crossover boundaries . . . 123
3.5.3 Scaling . . . 126
3.6 Conclusion . . . 127

4 Elementary excitations of disordered weakly-interacting Bose gases 129
4.1 Bogolyubov quasi-particles . . . 130
4.1.1 Symmetry-breaking approach . . . 131
4.1.2 Density-phase picture . . . 136
4.1.3 Summary . . . 138
4.1.4 Homogeneous case . . . 139
4.2 Perturbation expansion for Bogolyubov quasi-particles in weak potentials . . . 140
4.2.1 Ground-state density background . . . 141
4.2.2 Decoupling basis for the Bogolyubov-de Gennes equations . . . 142
4.2.3 Effective Schrödinger equation (first order) . . . 144
4.2.4 Scattering by weak potentials . . . 145
4.3 Anderson localization of Bogolyubov quasi-particles in one-dimension . . . 148
4.3.1 Phase formalism in the Born approximation . . . 148
4.3.2 Localization regimes . . . 149
4.3.3 Validity of the leading-order result . . . 152
4.3.4 Numerical calculations . . . 153
4.4 Beyond the Born approximation . . . 155
4.4.1 Discussion . . . 155
4.4.2 Decoupling beyond the first-order approximation . . . 156
4.4.3 Lyapunov exponent in one dimension . . . 159
4.5 Conclusion . . . 163

Conclusion and outlook 165

A Correlation functions of speckle potentials 169

B Fourth-order Lyapunov exponent in a speckle potential 173

C The dilogarithm function 183

D Gross-Pitaevskii equation in standard geometries **185**

E Perturbative solution of the Gross-Pitaevskii equation **191**

F Lifshits tail in a speckle potential **199**

G Decoupling basis for the Bogolyubov-de Gennes equations **203**

Bibliography **211**

Introduction

Disorder is present in all natural media to a certain degree, but its effects are often neglected in first approaches to the description of physical systems. However, even a small amount of disorder may produce large and counter-intuitive effects.

One such emblematic effect in quantum systems is Anderson localization [1], which demonstrates that even weak disorder may alter the transport properties of quantum particles, up to the point of inhibiting any transport, and turning a conductor into an insulator. Although the concept of Anderson localization was formulated more than fifty years ago to explain certain metal-insulator transitions in solids, evidence for localization remained elusive for decades [2]. The mechanism underlying Anderson localization is a subtle interference process which localizes single-particle wave functions in space. It has since been realized that Anderson localization may affect all kinds of waves and quantum particles, as its elementary ingredients are just coherence and disorder. Anderson localization has therefore been embraced by a variety of fields outside of solid-state physics, including optics [3], acoustics [4] and atomic physics [5].

In its original form, the concept of Anderson localization applies to non-interacting particles. The question as to how disorder combines with interactions in many-body systems is a fundamental issue in the understanding of the effects of disorder. One of the most notorious results of the interplay of disorder and interactions in condensed-matter systems is the destruction of superfluidity in "dirty" superconductors and liquid helium in porous media. Above a certain amount of disorder, superfluidity is lost in these systems because of particle localization [6–8]. The influence of disorder in superconductors and liquid helium has been studied intensively since the beginning of the eighties [9–11]. Strong correlations and a limited control over both the randomness and the strength and range of interactions often complicate the interpretation of experiments with condensed-matter systems [10]. Thus, many questions on the influence of disorder in interacting systems are still open.

The achievement of Bose-Einstein condensation (BEC) in ultracold atomic gases [12–14] has opened a new avenue in the study of disordered quantum systems [15, 16]. Ultracold atomic gases offer a high degree of control and versatility [17–19]. Both bosons and fermions can be cooled down to degeneracy, and their interactions can be tuned from non-interacting to strongly correlated regimes by means of Feshbach resonances. Also, trapping potentials can be designed so as to choose the effective dimensionality of the system, and laser light fields can be used to tailor potentials for the atoms. The realization of a strongly correlated Mott-insulator phase in optical lattices [20] and the observation of Berezinskii-Kosterlitz-Thouless physics in a two-dimensional trap [21] have illustrated the degree of flexibility and control available with ultracold atoms. Remarkably, while laser light may be used to create phonon- and defect-free lattice potentials for the atoms, optical potentials can also be employed to generate disorder in a controlled way [22–24]. Hence, since 2005, experiments have been investigating the influence of disorder on ultracold Bose gases [25–28]. The observation of Anderson localization in a regime of vanishing interactions has been one of the results of this activity [29, 30].

The study of disorder with ultracold atoms has many appealing features. Interactions and disorder in these systems are not only controllable, but also well characterized. The statistical properties of the optical random potentials currently used in experiments are very well known. They may be calibrated *in-situ* by using the atoms themselves as probes [31], in order to avoid systematic errors. Additionally, and in contrast for instance to liquid helium, ultracold atomic gases are dilute. Their low-temperature collision properties are thus accurately described by a single parameter, the scattering length [32]. This allows *ab initio* calculations and analytical approaches to give a clear picture of the processes at work.

This thesis

In this thesis, we examine the localization properties of weakly-interacting Bose gases in one-dimensional random potentials, a subject which is currently attracting both theoretical and experimental attention [33]. Here the emphasis is set on a microscopic description of the disordered Bose gas and on the role of the statistical correlations of the random potential. In the absence of interactions and in the presence disorder the bosons are expected to be localized. In the absence of disorder and in the presence of weak repulsive interactions the bosons form a delocalized superfluid (quasi-) BEC phase at sufficiently low temperature. The core questions are therefore: How do statistical correlations affect the Anderson localization of non-interacting bosons? How do interactions alter the Anderson localization of bosons? How does disorder affect the (quasi-) condensate phase? What is the localization-delocalization scenario between the regime of Anderson localization and the superfluid (quasi-) BEC regime? What are the forms of collective localization in the interacting case?

Outline

This thesis is organized as follows.

In chapter 1 we present a few general notions about disordered systems. We introduce key concepts of the theory of Anderson localization of non-interacting particles, such as multiple scattering, the exponential localization of eigenstates, the Lyapunov exponent or inverse localization length, and the dependence on dimensionality. Experimental results are briefly reviewed. We then turn to many-body systems, and point out the challenges associated with the understanding of disorder in interacting systems. Available results for the case of disordered 1D bosons are presented. A few general ideas related to weakly-interacting Bose gases are discussed. In the last part of the chapter, we focus on the statistical properties of disorder, and discuss a few elementary properties of correlation functions. As a model of disorder, we present speckle potentials and their fundamental properties.

Chapter 2 is devoted to the one-dimensional Anderson localization of non-interacting particles in correlated random potentials. In 1D all single-particle states are known to be localized under fairly general assumptions, and exact solutions are available for uncorrelated random potentials. We show that statistical correlations may introduce new features, such as a strong dependence of the localization process on the single-particle energy. A strong dependence arises for instance in random potentials with a high-momentum cutoff in their spatial Fourier spectrum. Speckle potentials are a particularly important example of such random potentials, as

they are used in current experiments with ultracold atoms, and have been shown to give rise to interesting localization properties [29, 34]. For those potentials the standard perturbative estimate of the Lyapunov exponent, called the Born approximation, vanishes on extended regions of the single-particle energy spectrum. We carry out a weak-disorder expansion of the Lyapunov exponent two orders beyond the Born approximation, and discuss the regimes of localization on such spectral regions. While our approach is general, speckle potentials appear as an original class of disorder, which allows the exploration of correlated, non-Gaussian statistics.

In chapter 3, we investigate the ground-state properties of a weakly-interacting Bose gas in a correlated 1D random potential, and establish a zero-temperature quantum state diagram of the Bose gas as a function of the chemical potential and the disorder strength. Three regimes are identified: the (quasi-) BEC regime, the regime of fragmented BEC, and a regime which we call the Lishits glass regime. In the delocalized BEC regime, which correponds to the limit of intermediate interactions and weak disorder, we analyze precisely the density modulations imposed on the Bose gas by the random potential. With increasing disorder, the BEC ultimately fragments. We analyze the dependence of the fragmentation threshold on the strength of interactions (or the chemical potential), and both the amplitude and the correlation length of the disorder. The crossover from BEC to fragmented BEC is expected to correspond to the transition from the superfluid to the Bose glass expected at weak interactions. The Lifshits glass denotes the insulating regime found for very weak interactions and strong disorder. In that regime, the bosons populate strongly localized single-particle states which belong to the low-energy tail of the single-particle spectrum. We derive a mean-field equation of state of the Bose gas, and use scaling arguments to locate the crossover to the regime of fragmented BEC.

Finally, in chapter 4 we study the elementary excitations of a disordered, weakly-interacting Bose gas deep in the BEC regime (or quasi-BEC regime in 1D), where the mean-field interactions are larger than the amplitude of the disorder. The Bogolyubov theory for condensates and quasi-condensates is briefly reviewed. In the framework of this theory, the elementary excitations of the Bose gas are quasi-particles (Bogolyubov quasi-particles, BQPs) which experience both the presence of the external potential and the interactions with the density background of the Bose gas. We develop a perturbation expansion around the exact Bogolyubov-de Gennes equations which govern the quasi-particle excitations, and find a mapping on an effective Schrödinger equation which describes the scattering of BQPs in weak inhomogeneous potentials. We then specialize to the 1D case, and examine the Anderson localization of BQPs in a correlated random potential. We discuss in detail the role of disorder correlations, and the screening of the random potential by the interactions.

CHAPTER 1

Disorder and interactions: condensed-matter physics and ultracold atoms

Disorder plays an important role in condensed-matter systems. Usually, our understanding of solid-state physics starts from the concepts of crystalline order, Bloch bands, and metallic conduction. However, Anderson, Mott and others have shown that disorder might be a fundamental aspect to consider, as it may cause a phase transition from metal to insulator in solids because of a localization of the electronic wave functions in space. This effect, known as Anderson localization, was originally put forward for non-interacting electrons. Anderson localization is nowadays a field of intense research as it is has be recognized to be transversal to various areas of physics beyond electrons in solids [2], and because localization has many facets which are not yet fully understood. In particular, the interplay of disorder and interactions is a long-standing question of condensed-matter physics, which has become acute with the discovery that disorder may destroy superconductivity or superfluidity due to localization effects. Ultracold atomic gases offer appealing possibilities to study the physics of disordered quantum systems, as many parameters, including disorder and interactions, may be controlled in these ultracold gases.

This chapter is devoted to the presentation of concepts which form the background of chapters 2 to 4. In section 1.1 we review a few key elements of the theory of Anderson localization of non-interacting waves and quantum particles. In section 1.2 we turn to localization effects in interacting many-body systems, and review available results in the case of disordered one-dimensional bosons. Finally, in section 1.3 we discuss models of disorder and introduce fundamental properties of the speckle random potentials which are used in current experiments with ultracold atoms.

1.1 Localization of non-interacting waves

In this section, we focus on the localization of non-interacting waves and quantum particles. Illuminating introductions to the subject can be found e.g. in Refs. [2,35–37]. In section 1.1.1, we emphasize the origin of Anderson localization in coherence effects which entail the breakdown of diffusive transport. Key concepts of the theory of localization, such as the exponential localization of single-particle states, mobility edges, and a strong dependence on dimensionality are presented in section 1.1.2. In section 1.1.3, we specialize to the case of the one-dimensional geometry, where localization effets are known to be the strongest, and exact results are available. Finally, an overview of available experimental results is provided in section 1.1.4.

1.1.1 Coherent transport

In his 1958 publication [1], Anderson showed how an electron (a "spin"), initially placed at some site of a disordered lattice, might remain localized in the vicinity of its initial position under the effect of the random potential, instead of diffusing and spreading to infinity. In the language developed throughout the years, the electron is prevented from diffusing because of (coherent) scattering from the random variations of the potential landscape, and destructive interference effects which localize the electron. The precursor of Anderson localization is a phenomenon called weak localization, whereby the diffusive motion of classical waves and quantum particles is *reduced* by such coherent scattering and interference effects. This reduction of diffusion signals the breakdown of the semi-classical theory of electron transport.

Limitations of the semi-classical theory of transport

In the semiclassical (Drude-Bloch-Boltzmann) theory of electronic transport, electrons are Bloch waves which are free to move across a perfectly ordered lattice. These electrons are scattered on impurities, dislocations, and phonons representing the thermal vibrations of the lattice. The static conductivity of a sample is given by [38]

$$\sigma_B = \frac{ne^2\tau}{m}, \tag{1.1}$$

where m is the (effective) electron mass, n is the density of electrons participating to transport (i.e. those which lie at the Fermi energy E_F), and τ is the elastic transport mean free time i.e. the average time an electron travels before its direction is randomized through collisions with scatterers [35]. All types of collisions are treated on the same footing, and it is assumed that each collision redistributes the quasi-momentum of a Bloch wave *and causes it to lose phase coherence*. The result is a diffusive motion, which allows the wave to extend to infinity [37]. According to the so-called Mathiessen rule, the collision rates $1/\tau_i$ of independent sources of scattering (static disorder, phonons, ...) add up: $1/\tau = \sum_i 1/\tau_i$ [35, 36]. If the temperature of the sample is lowered, the scattering with phonons steadily decreases until the scattering from the static disorder dominates. The semi-classical theory of electron transport hence predicts a monotonous increase of conductivity (i.e. a monotonous decrease of resistivity) towards the lower temperatures. However, a series of experiments has shown that in samples with strong disorder or confinement in lower-dimensional geometries (1D, 2D), the resistivity eventually regrows at low temperatures [36]. Fig. 1.1 shows the temperature dependence of the resistance in a 2D copper sample and the regrowth observed at low temperature [39].

Multiple scattering

The reason for the failure of the semi-classical theory to explain the increase of resistivity at low temperature is the fact that, while scattering with a bath of phonons indeed destroys the phase coherence of the Bloch waves, elastic scattering from the static impurities does *not*. We can associate a phase-coherence length L_ϕ to the scattering with phonons (and other sources of decoherence), and define a scattering mean free path ℓ_s as the average distance travelled by the waves between two collisions with a static impurity. If L_ϕ is smaller than ℓ_s, the phase accumulated by the wave between two scattering events on the impurities is random,

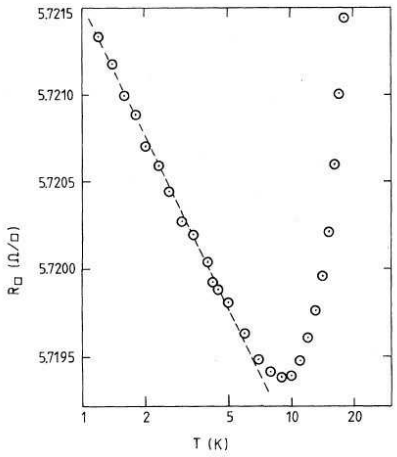


Figure 1.1: Dependence on the temperature of the resistance of a thin copper film [39].

the scattering amplitudes of the waves on different impurities have no phase correlation, and transport is well described by the semi-classical law (1.1) with diffusion constant D_B. At low temperature, however, the phase-coherence length L_ϕ may exceed the scattering mean-free-path ℓ_s, and (coherent) multiple scattering from the impurities has to be taken into account.

Weak localization

Multiple scattering can be described within the framework of an elaborate theory of transport [35, 40–42]. This theory has proven able to describe the aforementioned deviations from semi-classical predictions [35, 43]. For the purpose of this chapter, we simply borrow a few qualitative arguments from the presentation given in Ref. [35].

To understand the effect of multiple scattering on transport properties, let us consider the situation depicted in Fig. 1.2. The disordered medium is represented by a random arrangement of static, point-like impurities. Schematically, the propagation of the wave (field) associated with the particle from point $\mathbf{r}$ to $\mathbf{r}'$ is described by the sum $\sum_i a_i(\mathbf{r}, \mathbf{r}')$ of the complex amplitudes a_i correponding to all possible scattering paths i between $\mathbf{r}$ and $\mathbf{r}'$. One such path is represented in solid line in Fig. 1.2(a). As the particle density is given by the squared modulus of the field, a trajectory of the complex conjugate field is represented as well. The particle density at $\mathbf{r}'$ is determined by a product of the form $\sum_{i,j} a_i^*(\mathbf{r}, \mathbf{r}')\, a_j(\mathbf{r}, \mathbf{r}')$, and depends on the interference of all the scattering paths. The average conduction properties of the medium are obtained by considering a product of the form [35, 44]

$$P(\mathbf{r}, \mathbf{r}') = \left\langle \sum_{i,j} a_i^*(\mathbf{r}, \mathbf{r}') a_j(\mathbf{r}, \mathbf{r}') \right\rangle = \sum_i \left\langle |a_i(\mathbf{r}, \mathbf{r}')|^2 \right\rangle + \sum_{i \neq j} \left\langle a_i^*(\mathbf{r}, \mathbf{r}') a_j(\mathbf{r}, \mathbf{r}') \right\rangle , \tag{1.2}$$

where $\langle \cdots \rangle$ denotes statistical averaging over the distribution of scatterers. The quantity $P(\mathbf{r}, \mathbf{r}')$ represents the probability of a quantum particle initially located at position $\mathbf{r}$ to reach $\mathbf{r}'$ at a later time.[1] The phase of a $a_i^*(\mathbf{r}, \mathbf{r}')\, a_j(\mathbf{r}, \mathbf{r}')$ term is directly related to the different lengths

[1] The time dependence in not included in expression (1.2) for the simplicity of the discussion.

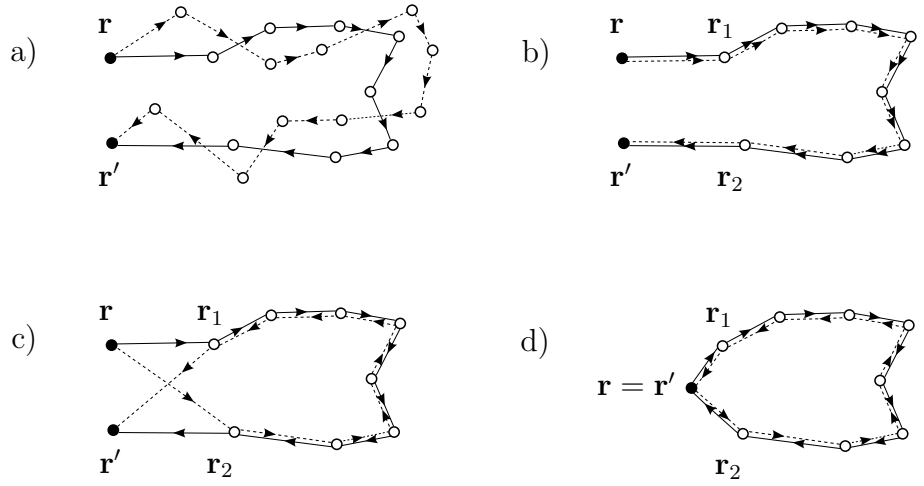


Figure 1.2: Interference contributions to the transport of intensity between two points $\mathbf{r}$ and $\mathbf{r}'$. Scattering paths followed by the field (solid line) and its complex conjugate (dashed line). The contributions such as (a), where the field and its conjugate do not visit the same scatterers, vanish on average. Diagram (b) is the classical diffusion contribution to transport, and (c) is an interference contribution. Diagram (d) is the same as (c) with $\mathbf{r} = \mathbf{r}'$ as represents an increased probability of return of the wave to its starting point.

of the paths taken by the field and its complex conjugate. Therefore, contributions such as the one shown in Fig. 1.2(a) cancel out of the sum once the average is taken.

The contributions which survive the disorder average are those where the field and its complex conjugate visit the same scatterers. Such is the case of the term

$$P_{\mathrm{cl}} = \sum_i \left\langle |a_i(\mathbf{r}, \mathbf{r}')|^2 \right\rangle , \tag{1.3}$$

which corresponds to contributions such as the one depicted in Fig. 1.2(b), where the field and its complex conjugate follow exactly the same path, and no relative phase is accumulated. These contributions, where coherence plays no role, correspond to the diffusive transport of the classical Drude-Boltzmann theory. It turns out, however, that other terms survive the disorder average, such as the one shown in Fig. 1.2(c), where the field and its conjugate follow reversed paths. Such interference terms are not present in the Drude-Boltzmann theory. Diagram 1.2(d), where $\mathbf{r}'$ is set equal to $\mathbf{r}$, shows that such interference terms enhance the probability of return of the wave to its starting point. From the point of view of transport, this means that both the diffusion and the conductivity σ in the sample are reduced with respect to the classical Drude theory [45]:

$$\sigma = \sigma_B - \delta\sigma. \tag{1.4}$$

As the reduction of conductivity originates from an increased dwell time of the electrons in certain regions of the sample, one speaks of a weak-localization correction to the diffusive motion.

In the regime of weak localization, transport is hampered by multiple scattering and interference in the disordered medium, but a residual diffusive motion nevertheless allows quantum

particles and waves to spread to infinity. Eventually, however, the destructive interference effects may be so strong as to forbid any diffusive transport at all. This situation corresponds to the regime of Anderson (or strong) localization, which we discuss below.

1.1.2 Anderson localization

Exponential localization of single-particle states

The idea that the presence of disorder might lead to a complete absence of transport in a system of non-interacting quantum particles was first formulated by Anderson in 1958. In his seminal paper [1], Anderson considered non-interacting particles ("spins") on a lattice, described by a tight-binding Hamiltonian [36, 46]

$$H = \sum_i \epsilon_i \hat{c}_i^\dagger \hat{c}_i - \frac{1}{2} \sum_{\langle i,j \rangle} (J_{ij} \hat{c}_i^\dagger \hat{c}_j + h.c.), \tag{1.5}$$

where i and j denote lattice sites, $\hat{c}_i$ and $\hat{c}_i^\dagger$ are particle destruction and creation operators, J_{ij} are hopping amplitudes, $\langle i,j \rangle$ indicates a summation over nearest neighbors, and the ϵ_i are uncorrelated, random on-site energies uniformly distributed in an interval $[-W/2, W/2]$. Anderson analyzed the time evolution of the probability amplitude of a particle initially located on some site j to occupy it at a latter time, and found that for a given particle energy E and for a sufficient strength of disorder (measured in the model by the breadth W), the particle remains localized around its orginal location, with a probability amplitude decreasing exponentially with the distance from the center. A connection is thereby established between the absence of transport and the exponential localization of the single-particle states of the electrons. The typical length scale on which localized states decay is called localization length L_{loc}. Strong (Anderson) localization affects the transport properties of the system when the localization length is much smaller than the system size.

Mobility edges

In the Anderson model, the single-particle states at a given energy are localized if the disorder is strong enough. Conversely, for a given strength of disorder, some single-particle states are localized, while some others may be delocalized (extended). A qualitative picture of localization in the Anderson model is shown in Fig. 1.3. According to an argument attributed to Mott, no localized state can exist in energy regions with extended states, as an infinitesimal change in the random potential would couple this localized state with extended states and hybridize it into new extended states [41, 43].[2] Localized and extended states are therefore separated by critical energies called mobility edges [48–51]. For weak disorder, the electron states close to the band edge are localized, but the states close to band center remain extended. With increasing disorder, the mobility edges move towards the band center with increasing disorder, and eventually merge at a critical disorder strength W_c, above which all states are localized [36, 52]. As the transport properties are determined by the electrons at the Fermi surface, the system is expected to be conducting if the states at the Fermi energy are delocalized, and insulating if they are localized. When the Fermi energy crosses a mobility edge under a change

[2] The argument does not apply to inhomogeneous random potentials. See e.g. Ref. [47].

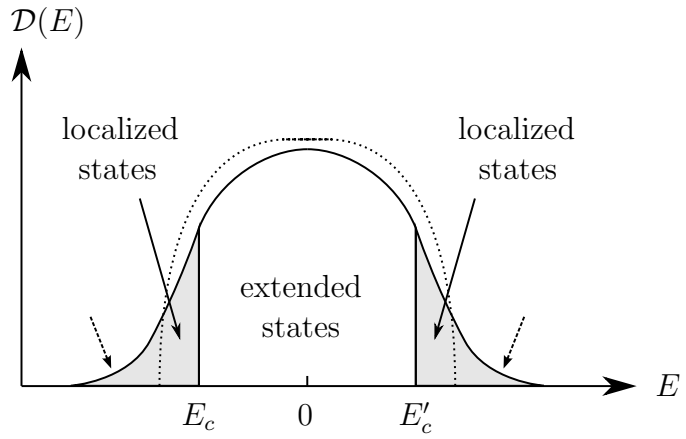


Figure 1.3: Qualitative picture of localization in the 3D Anderson model (following Refs. [36, 43, 45]). The density of states $\mathcal{D}(E)$ (solid line) has no singularities as in the disorder-free case (dashed line), and develops smooth tails at the band edges (dashed arrows) under the influence of disorder (see section 3.4.1 and Ref. [43]). The states close to the band edges are localized, and separated from the extended states at the band center by mobility edges E_c and E_c'.

of the disorder strength or of the electron density, the system undergoes a (metal-insulator) phase transition between the metallic and the insulating regime.

Scaling theory

Anderson localization strongly depends on the dimension of the system, and one of the central results of the theory of localization is that, while both extended and localized states may exist in 3D, all states are generally localized in 1D and 2D, provided the waves are non-interacting.

One important step towards such a qualitative description of the effect of dimensionality was provided by the scaling theory developed by Abrahams *et al.* [53]. These authors considered the "dimensionless conductance" $g(L)$ (a conductance measured in nuits of $e^2/\hbar$) of a hypercube of volume L^d, where d is the dimension of space. The transport properties of the system are examined as some Fermi energy E_F. A scaling function

$$\beta = \frac{\mathrm{d}\ln g}{\mathrm{d}\ln L} \tag{1.6}$$

is introduced to analyze how the conductance evolves with the system size. The result of the analysis of Abrahams *et al.* is reproduced in Fig. 1.4. The curved lines with arrows represent the trajectories of $(\ln g, \beta)$ as L grows. In 3D, two situations arise. If the disorder is weak enough so that, for some finite value of L, the conductance $g(L)$ exceeds the critical value g_c, then β is positive, and the conductance g grows with L. On the other hand, if the disorder is so strong that we have $g(L) < g_c$ for some L, then the system follows the path at negative β. In the limit of very large L, the three-dimensional system is hence either a conductor or an insulator, depending on the strength of disorder. This result agrees with the analysis of the Anderson model. In 1D and 2D, however, the trajectories all lead into the insulating state $g \to 0$, whatever the initial situation and the amount of disorder are. This indicates a localization of

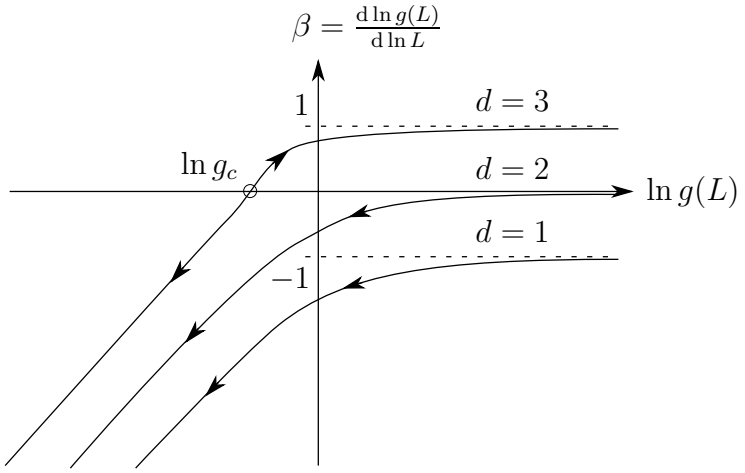


Figure 1.4: Scaling flow of the one-parameter scaling theory of localization [53]. The behavior of the conductance $g(L)$ for $L \to \infty$ depends crucially on the dimension d of the system.

all states for an arbitrarily small amount of disorder. As this is a fundamental result, let us outline the reasoning behind it.

The scaling arguments developed to establish diagram 1.4 are summarized in a number of review papers (see e.g. Refs. [37, 43, 54]). In brief, the key assumption in the scaling theory of Abrahams *et al.* is that, for large enough samples, the scaling function β does not depend on the microscopic details of the sample (e.g. the amplitude of disorder), nor on the absolute value of the length L, but only on the dimensionless conductance $g(L)$ itself.[3] The assumption that β depends only on g is known as the one-parameter scaling hypothesis. With this assumption at hand, the diagram is obtained by interpolating between two limiting regimes. In the limit of weak disorder ($g \gg 1$, metallic regime), g is related to the usual Ohmic conductance $G(L) = L^{2-d}\sigma_B$, where σ_B is the classical Drude conductivity [see Eq. (1.1)]. In this limit, the scaling function β takes the value

$$\beta \simeq 2 - d \qquad (g \gg 1), \tag{1.7}$$

which defines the horizontal asymptotes towards large g in the figure. In the limit of strong disorder ($g \ll 1$), exponential localization is assumed in all dimensions, and g is argued to fall off exponentially with L: $g = g_0\,\mathrm{e}^{-\alpha L}$, so that

$$\beta \simeq \ln g + c_d \qquad (g \ll 1), \tag{1.8}$$

where c_d is some constant. Between the limits at large and small g, the quantity β is assumed to be a monotonous continuous function of g, which yields the curves in Fig. 1.4.

The scaling theory predicts that no true metallic (conducting) state exists in 1D and 2D, as an insulator is obtained for large systems. The two-dimensional geometry is identified as the marginal case where this occurs [58, 59], and localization is found to be the strongest in 1D. Let us now introduce a few tools and concepts of localization theory in 1D.

[3] In the regime where L exceeds the mean free path, the dimensionless conductance g is actually not related directly to the macroscopic conductivity. Following earlier studies by Edwards, Thouless and Licciardello [55–57], the conductance g is then rather defined as a number which uniquely describes how the transport properties of a hypercube are modified when it is matched with another hypercube to build a larger system. The quantity g is therefore put forward as the only relevant variable is the scaling of the system properties with L [37, 43].

1.1.3 Localization in one dimension

As all states are generally strongly localized in 1D, the length scale on which the states localize, called localization length, is usually one of the observables sought in the first place. Other physical quantities, such as the density of states [60, 61], or the conductance of an equivalent, open system [62], may be derived from it. Generally, however, instead of the localization length $L_{\rm loc}$, one rather calculates its inverse

$$\gamma = 1/L_{\rm loc}, \tag{1.9}$$

which is called the Lyapunov exponent. Below, we briefly discuss how the Lyapunov characterizes the eigenstates and conduction properties of disordered 1D systems.

Lyapunov exponent

A vast body of literature on disordered one-dimensional systems relies on their description by products of random matrices [59, 63–76]. The concept of Lyapunov exponent, or inverse localization length, naturally emerges from such approaches.

Transfer matrices - Consider the discretized Schrödinger equation

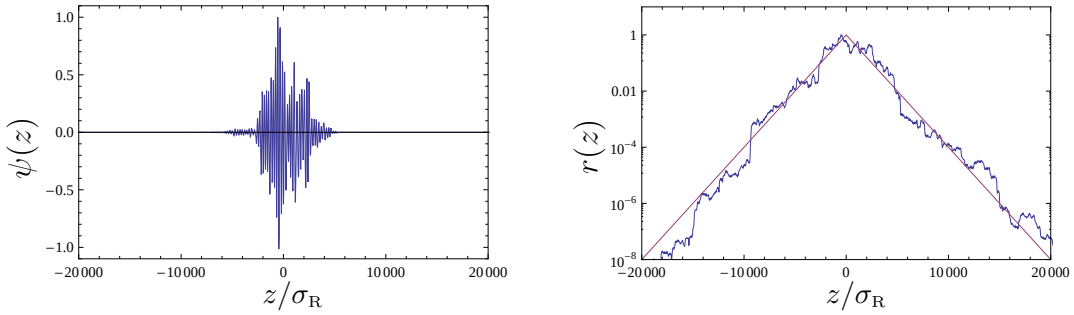
$$-J\left[\psi_{n+1}+\psi_{n-1}-2\psi_n\right]+V_n\psi_n = E\psi_n, \tag{1.10}$$

where $J=\hbar^2/2m(\Delta z)^2$ is the kinetic term, $\Delta z = z_{n+1}-z_n$ is the discretization step, $\psi_n \equiv \psi(z_n)$ and V_n is the value of a random potential V at point z_n.This equation rewrites as a recursion formula for ψ_{n+1} as a function of ψ_n and ψ_{n-1}. For any initial condition $\{\psi_0,\psi_1\}$, the value of the wave function ψ at point z_{n+1} is determined by a product of transfer matrices T_j:

$$\begin{pmatrix}\psi_{n+1}\\ \psi_n\end{pmatrix} = T_n\cdots T_1\begin{pmatrix}\psi_1\\ \psi_0\end{pmatrix} \qquad \text{with} \qquad T_j=\begin{pmatrix}\frac{V_j-E}{J}+2 & -1\\ 1 & 0\end{pmatrix}. \tag{1.11}$$

The matrix $T_{1\cdots n}=T_1\cdots T_n$ is the product of a large number of random matrices, parametrized by the energy E and a realization of the random potential V. Theorems by Oseledec [77] and Furstenberg [78] are invoked to describe the behavior of such products [43, 59, 79–81]. One finds that, for almost all sets $\{V_n\}_n$ (i.e. for almost all "realizations" of the random potential), an initial vector $(\psi_0,\psi_1)^{\rm T}$ grows or decays asymptotically as $\mathrm{e}^{\pm\gamma'(E)n}$ for $n\to\infty$, where $\gamma'(E)$ is a positive, non-random quantity. This defines a Lyapunov exponent, which in absolute units reads $\gamma(E)=\gamma'(E)/\Delta z$. The Lyapunov exponent $\gamma(E)$ describes the exponential growth or decay of ψ.

Localized eigenstates - For every set $\{V_n\}_n$, there is only one vector which decays exponentially as $n\to\infty$ [81]. Therefore, if one imposes the energy E and the initial condition $(\psi_0,\psi_1)^{\rm T}$, numerical and analytical calculations almost surely yield a function ψ_n which grows exponentially at rate $\gamma'(E)$ as $n\to\infty$ (see chapter 2). Such functions are not normalizable, and the energy E is therefore not part of the spectrum. For E to be part of the spectrum, two branches need to be connected which ensure the decay of ψ_n for both $n\to-\infty$ and $n\to+\infty$. *The corresponding eigenstates of the system are localized, and decay exponentially on either sides of a localization center on the length scale* $L_{loc}(E)=1/\gamma(E)$ [81, 82]. The aforementioned calculations at fixed E and $(\psi_0,\psi_1)^{\rm T}$ can be used to determine the Lyapunov exponent $\gamma(E)$. An example of localized eigenstate is shown in Fig. 1.5.



(a) Wave function (b) Envelope on semi-log scale

Figure 1.5: Wave function amplitude (a) and envelope (b) of a localized state, obtained by numerical solution of the Schrödinger equation (1.10). The length scale σ_R is the correlation length of the (speckle) random potential used for the calculation (see section 1.3). Fig. (b) shows that the eigenstate tends to decay exponentially.

Exponential decay of the transmission - While the above considerations apply to eigenstates in a closed system, the Lyapunov exponent also describes the asymptotic behavior of waves sent across an open, disordered 1D system. The transmission of such waves can also be described by a product of transfer matrices. These matrices take a slightly different form than the T_j matrices above [75, 83], but they share the same asymptotic behavior. It can be shown that the intensity transmission coefficient T of a wave which is sent across a sample of size $L = n\Delta z$ writes [70, 75, 83]

$$T = \frac{1}{\cosh^2(x)}, \tag{1.12}$$

where, almost surely, x scales asymptotically as $x \sim \gamma(E)L$ with the system size. As $T \propto \mathrm{e}^{-2x}$ for $x \gg 1$, this relation indicates an exponential decay of the transmission. The intensity transmission coefficient T itself is related to transport properties of the medium. In the context of electronic systems, for instance, the conductance G of the sample is $G = Te^2/\pi\hbar$ according to Landauer's formula [63, 75].

Fluctuations

The asymptotic decay of eigenfunctions and transmission coefficients is determined by the Lyapunov exponent, which does not depend on the realization of the random potential. At finite distances, however, fluctuations are observed from one realization to the next. In Fig. 1.5(b), the logarithmic profile is also seen to fluctuate around the straight red lines which indicate the rate of asymptotic decay. These fluctuations at finite distance are characterized by a probability distribution. For the transmission coefficient T and in the case of uncorrelated random potentials, a probability distribution is obtained in the form[4] [81, 84, 85]

$$P[\ln T] = \frac{1}{\sqrt{2\pi}\sigma_L}\,\mathrm{e}^{-\frac{1}{2}(-\ln T-\mu_L)^2/\sigma_L^2} \qquad \text{with} \qquad \mu_L = -\frac{2L}{L_{\mathrm{loc}}} \qquad \text{and} \qquad \sigma_L = \sqrt{\frac{4L}{L_{\mathrm{loc}}}}. \tag{1.13}$$

[4] We identify here identify here L_{loc} with the mean free path l of Ref [84] and the localization length ξ of Ref. [75]. Note that this distribution makes sense in the regime $T \ll 1$, as the Gaussian cannot extend to values $T > 1$. As an additional caveat, let us note that the Gaussian distribution (1.13) is the result of a perturbative calculation [84].

The fluctuations of the observable $\ln T$ hence obey a Gaussian distribution with mean μ_L and standard deviation σ_L. As $\sigma_L \propto \sqrt{|\mu_L|}$, the probability distribution of $\ln T$ narrows down to a well-defined value, which coincide with $-2L/L_{\rm loc} = -2\gamma L$, in the limit $\gamma L = L/L_{\rm loc} \gg 1$. Because of this property, the observable $\ln T$ is said to be self-averaging [86,87]. Equation (1.13) shows that the Lyapunov exponent γ can be obtained as[5] $\gamma = \lim_{L\to\infty}\langle -\frac{1}{2}\ln T\rangle$. The self-averaging property of $\ln T$ means that a good estimate of γ can be obtained by averaging over a small number of realizations at large distances. Conversely, the Lyapunov is a quantity which is well representative of the distribution of $\ln T$.

Uncorrelated potentials

A Lyapunov exponent $\gamma(E) > 0$ indicates that the states at energy E are localized, and its magnitude measures the rate of exponential decay of the eigenstates around their localization center. In the case where the values of the random potential at different points are uncorrelated, the Lyapunov exponent can be calculated exactly. In the case of the continuous Schrödinger equation, the Lyapunov exponent reads[6] [86]

$$\gamma(E) = \sqrt{\frac{2mE_\delta}{\hbar^2}}\frac{\int_0^\infty {\rm d}y \frac{\sqrt{y}}{2}\,{\rm e}^{-\frac{y^3}{12}-\frac{E}{E_\delta}y}}{\int_0^\infty {\rm d}y \frac{1}{\sqrt{y}}\,{\rm e}^{-\frac{y^3}{12}-\frac{E}{E_\delta}y}}, \tag{1.14}$$

where $E_\delta = (mD^2/2\hbar^2)^{1/3}$, and the quantity D, which parametrizes the auto-correlation function $C_2(z) = D\delta(z)$ of the potential [see Eq. (1.36) below], measures the strength of disorder.

The Lyapunov exponent (1.14) is plotted in Fig. 1.6 as a function of the single-particle energy E. The origin $E = 0$ corresponds to the average value of the potential. This figure shows that, in an uncorrelated potential, the Lyapunov exponent is strictly positive for all E, and decreases monotonously with increasing energy. The state with large negative energy have a Lyapunov exponent roughly proportional to $\sqrt{|E|}$, and resemble in this respect the bound states of a quantum well (although interference phenomena are still important to localize the particles). For $E \gg E_\delta$, although the energy of the particle lies well above the typical amplitude of the potential, the states are also localized. Their Lyapunov exponent scales as

$$\gamma(E) \propto \frac{\langle V^2\rangle}{E} \qquad [E \gg E_\delta], \tag{1.15}$$

as indicated by the dashed line in Fig. 1.6. High-energy states are thus localized on longer length scales.

1.1.4 Experimental observations

Anderson localization is remarkable in the sense that i) as a process which originates from coherent scattering, it contrasts with the classical physics of trapping, percolation and random walk in complex media [41], ii) the insulating behavior is due neither to trivial band-gap effects, nor to interactions between the particles [36], and iii) above all, it is rather ubiquitous in the

[5] See Eq. (2.7) for a similar definition of the Lyapunov exponent for eigenstates.

[6] In the formula on page 142 of Ref. [86], y^2 should be replaced by y^3.

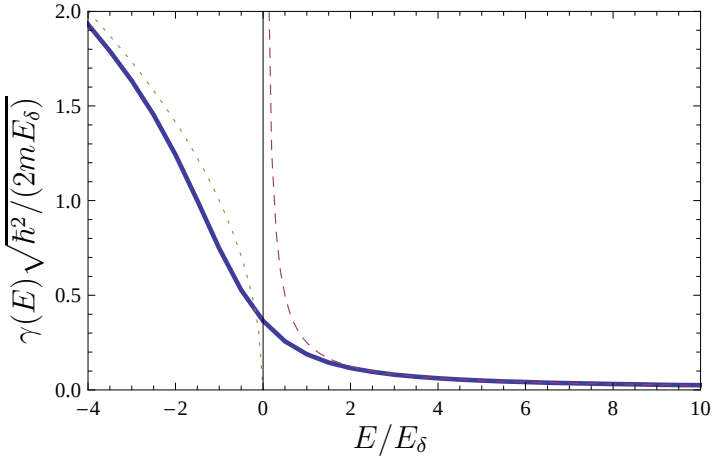


Figure 1.6: Lyapunov exponent of a Schrödinger particle in an uncorrelated 1D random potential, as a function of the particle energy E. The Lyapunov exponent $\gamma(E)$ [solid blue line] is determined by Eq. (1.14). Energy and Lyapunov exponent are normalized with $E_\delta = (mD^2/2\hbar^2)^{1/3}$, where D is defined as the parameter of the two-point correlator $C_2(z) = D\delta(z)$ and measures the strength of disorder. The dashed and dotted lines correspond to the asymptotes at large positive energy $[\gamma(E)\sqrt{\hbar^2/2mE_\delta} \sim E_\delta/(4E)]$ and at large negative energy $[\gamma(E)\sqrt{\hbar^2/2mE_\delta} \sim \sqrt{|E|/E_\delta}]$, respectively [86].

sense that it may affect the behavior of a great variety of waves in disordered media [2, 5]. As a consequence, it has been studied in a number of contexts beyond the physics of electrons in solids. One of the motivation for studies with other systems was the absence of Coulomb interaction, the effect of which is difficult to measure and control in electronic systems.

Localization has been reported so far with ultrasound [4,88,89], microwaves [90,91], light at optical wave lengths in "free" space [92,93] and disordered photonic band-gap material [94,95], as well as cold [96–98] and ultracold atoms [5, 29, 30].

The first experiments performed in the nineties with microwaves and visible light involved measurements of the sole transmission coefficient T as a function of the sample size, and raised questions about the role of absorption. Later experiments with microwaves [91] took account of the statistics of T, in particular its variance [see Eq. (1.13)], to provide evidence of localization even in the presence of absorption. In time-resolved transmission experiments with light [93], the long-time decay of short pulses sent through the samples was measured, and evidence of path lengths that are incompatible with diffusion were found. More recently, 1D and 2D disordered photonic crystals were used to observe directly the localization of light by imaging the light intensity profiles in transmission experiments [94, 95]. In those experiments, the light was sent into the sample on one facet, and its transverse spreading was measured on the opposite facet. Evidence of strong localization was provided by the transverse intensity profiles, localized within a few lattice sites of the photonic crystal.

Localization of ultrasound in a three-dimensional sample of aluminium beads was reported in Ref. [88]. As in the case of photonic crystals, a source and a detector were placed on opposite facets of the sample, and the transverse intensity profile was measured. Transmission measurements resolved both in space and time were performed in the localized regime. Taking

the localization length and a few other parameters as inputs, the data was well fitted by a novel version [42] of the self-consistent theory used to describe localization in higher dimensions [41].

Disorder with cold atoms - Cold atomic clouds may be used as disordered medium for light. This approach has been successfully used to study signatures of weak localization in so-called coherent backscattering effects [99]. Conversely, light fields may be used to introduce disorder into cold atomic gases. Following this path, cold atoms have been employed to realize a quantum version of so-called kicked rotors [100, 101] and observe Anderson localization in momentum space [96–98]. In such experiments, the atoms experience the presence of a periodically pulsed 1D optical lattice potential, and the spreading of their momentum distribution with time is measured. In the pioneering experiments of Refs. [96,97], the momentum distribution was measured after some drift time to convert velocities into positions, and the equivalent of exponential 1D localization was found in momentum space. In Ref. [98], an analog of the 3D Anderson model was realized, the momentum distribution of the atoms was directly measured by Raman spectroscopy, and the Anderson transition was studied precisely, leading to the determination of a critical exponent.

Ultracold atoms - Ultracold atoms have allowed a direct observation of the 1D Anderson localization of matter waves in coordinate space [5, 29, 30]. In those experiments, Bose-Einstein condensates (BECs) were left to expand in random [29] and quasi-periodic [30] 1D potentials created with laser light. A regime of negligible interactions was reached either by sufficient dilution of the BEC [29], or with the help of a so-called Feshbach resonance [30]. Absorption images were taken to measure directly the density profiles of the localized matter waves. In Ref. [29], localization lengths were extracted directly from the absorption images, and were found to be in good agreement with theoretical *ab initio* calculations. The observation of higher-dimensional versions of Anderson localization can also be envisioned with BECs released from a harmonic trap. Such a scheme to observe 3D Anderson localization has been studied theoretically in Ref. [102].

As we shall see below, two interesting features of ultracold atoms are the ability i) to control interactions, so as to study the interplay of localization and interactions (see section 1.2 below), and ii) to implement a variety of random potentials in order to examine the role of statistical correlations (see section 1.3). Let us first turn to the former aspect. Indeed, Anderson localization in its original form is a single-particle phenomenon, and one of the related challenges is to describe how it is affected by interactions. In a broader scope, this question is about understanding how interactions and disorder determine the properties of quantum systems.

1.2 Disorder in interacting systems

Disorder lies at the heart of some of the most complex phenomena in many-body systems, such as localization-induced metal-insulator transitions, the physics of spin glasses, high-T_c superconductivity, or quantum chaos (see Ref. [19] and references therein). In particular, the interplay of disorder and interactions is one of the important puzzles of condensed-matter physics. In this context, questions arise on two prominent fronts. The first one concerns the effect of interactions on Anderson localization, and the second one, the possible destruction

of superfluidity (or superconductivity) by disorder. These two aspects may be interrelated, as shown below.

1.2.1 Insulators, conductors, and superfluids

The combined action of disorder and interactions give rise to a rich variety of phenomena in many-body systems. We shall outline here a few results and open questions which form the background of the following chapters.

Anderson localization

The effect of Coulomb interactions on the localization and transport of electrons in disordered solids has been considered for a number of years (for reviews on the subject, see e.g. Refs. [103, 104]). For weak interactions, Altshuler and coworkers [44, 105, 106] have shown that the effect of disorder and interactions amplify each other, so that interactions help localizing the particles. In particular, this result suggests that in the 2D geometry, which is the marginal dimension according to the scaling theory of Abrahams *et al.* [53] (see section 1.1.2), all states should remain localized at $T = 0$ [104]. Support for such a scenario is given in a more recent publication [107], where it is shown that in regimes where all the single-particle states are localized by the disorder, no delocalization transition takes place under the effect of weak interactions at zero temperature. On the other hand, renormalization group calculations by Finkel'stein [108] have shown that, for weak disorder and sufficiently strong interactions, the resistivity of a 2D system might scale towards a finite value at low temperature. These calculations are considered not to be conclusive on the existence of a metallic phase because of the limited regime of validity of the approach [104]. On the experimental side, observations of conductor-insulator transitions driven by the electron density have been reported [104, 109]. However, the interpretation of the experimental results lead to a considerable debate, and the nature of the phases on either side of the observed transitions seems to be an open question [103].

The above considerations apply to fermions with repulsive interactions, and to the transition from a normal (metallic) conductor to an Anderson insulator. In certain systems, however, the disorder-free system is superfluid at low temperatures. In that case, the focus lies on the effects of disorder on the superfluid phase and on the transition from the normal to the superfluid phase, or the possibility of a direct transition from the superfluid to an insulating state at low temperatures.

Superfluidity

Macroscopically, superfluidity characterizes an absence of viscosity, dissipationless flow, and the possibility of persistent currents [32, 110]. Superfluidity is common to condensed bosons found in liquid ^{4}He, atomic Bose gases (^{23}Na, ^{87}Rb, ...), and bosonic excitations (polaritons, ...), and to paired fermions in superconductors, atomic Fermi gases (^{6}Li, ^{40}K), and liquid ^{3}He [18, 32, 110, 111]. In all cases, the superfluid behavior originates from the presence of interactions. Interestingly, experiments with "dirty" electronic systems [112, 113] and ^{4}He in porous media [114, 115] have shown that superfluidity may be destroyed by disorder [7].

Disordered superconductors - In the Bardeen-Cooper-Schrieffer (BCS) theory of conventional superconductivity, electrons pair due to a weak effective attraction mediated by phonons and form a superfluid many-body state at sufficiently low temperatures [116]. Investigations into the effect of disorder on the properties of superconductors started in the fifties [117], mostly focusing on the modification of the critical temperature T_c of the normal-to-superconductor transition. These investigations culminated with the question of whether a localization of the electrons may affect pairing and superconductivity altogether [9, 37]. It has been recognized that, while the presence of weak (non-magnetic) impurities does not affect significantly T_c [118–120], stronger disorder may completely suppress superconductivity [9].[7] In the latter regime, the theoretical analysis is complicated by the fact that disorder modifies simultaneously several ingredients in the system, such as the coupling between electrons and phonons, the Coulomb repulsion of electrons, and the density of states of the normal state [37, 122]. It is also believed that the dominant processes in the destruction of superfluidity (phase fluctuations or a suppression of the amplitude of the "order parameter") may depend on the type of disorder [9], and whether it is homogeneous, or rather coarse grained, as in granular superconductors [11, 112, 123].

Superfluid helium - The effect of disorder on superfluid bosons, on the other hand, has been studied with ^{4}He in porous media (see e.g. Ref. [124] for an early publication, and Ref. [10] for a review). Interesting phenomena have been observed in these disordered systems, such as a modification of the critical behavior at the normal-superfluid transition [125]. The most remarkable result of this activity, however, has been the observation of a complete suppression of superfluidity in films of ^{4}He adsorbed on a porous substrate [114,126,127]. In these experiments, the superfluid behavior is lost when the density of ^{4}He covering the substrate is lowered below a critical value. Superfluidity is recovered above that threshold. In 1979, Hertz *et al.* [6] proposed that the insulating behavior may be due to a localization of the bosons below the critical density (for small chemical potentials), and probably coined the term of "Bose glass" (see below). The picture which emerged from the experiments was that of a superfluid-to-insulator transition connected with a localization or delocalization of the bosons, and determined by the interplay of the disorder and interactions. This discovery triggered an intense activity around the "boson localization problem" [7, 8, 121, 128–133], many aspects of which are not yet fully understood.

The role of quantum statistics

Non-interacting particles are generally localized by disorder at all energies in 1D and 2D, and below the mobility edge in 3D.[8] The addition of interactions gives rise to a complex interplay, even in the ground state of many-body systems. Quantum statistics play an essential role in this respect, as an infinite number of non-interacting bosons can populate the same single-particle ground state, whereas fermions cannot occupy the same state due to the Pauli exclusion principle, and fill all the single-particle states up to the Fermi energy instead [134]. The effect of finite but very weak interactions on many-body system is therefore expected to be qualitatively

[7] See e.g. Refs. [8, 121] for a description of the superconductor-insulator transition in 1D.

[8] However, we will see in chapter 2 that the localization length in 1D might experience sharp crossovers, where it changes by orders of magnitude as a function of the single-particle energy, in certain types of correlated disorder, like speckle potentials.

quite different in the case of bosons and fermions. Bosons are interesting in their own right since i) even for weak interactions, their behavior is expected to be a collective one, and ii) disorder-free bosonic systems often exhibit superfluidity for weak interactions. Moreover, the problem of boson localization may help understanding some features of disordered superconductors, in regimes where the picture of Cooper pairs is adequate [135].

1.2.2 Disordered bosons: weak and strong interactions

In this section, we focus on the ground-state ($T = 0$) properties of interacting bosons in a disordered potential. Such disordered bosons have a different behavior depending on the regime of interactions, and on whether additionally they experience a periodic lattice potential or not. Below, we summarize a few general ideas and results which are known for the 1D geometry.

General phenomenology

Non-interacting bosons - At $T = 0$, non-interacting bosons all populate the single-particle ground state, which is extended (delocalized) in the absence of disorder, and form a Bose-Einstein condensate (BEC).[9] In the presence of disorder, the single-particle ground state is localized, and so are all the bosons.

Weak interactions - In the absence of disorder and in the presence of weak interactions, the bosons form a condensate[10] and, additionally, display superfluidity. In the presence of disorder, however, the bosons may be localized in accordance with the non-interacting limit, and in that case superfluidity is unlikely. However, weak repulsive interactions are expected to have a delocalizing effect on an assembly of bosons localized by disorder in some region of space, as those particles otherwise pay the price of mutual interaction for occupying the same location. Weak interactions might therefore restore superfluidity.

Strong interactions (lattice bosons) - It is known that strong repulsive interactions may localize particles, even in the absence of disorder, and destroy superfluidity. A prime example of such a localization induced by interactions is provided by the Mott-insulator phase [136] which is formed for strong interactions or small tunneling *in the presence of a lattice*. For an integer average number of particles per lattice site ("integer" or "commensurate" filling), the system forms a Fock state in which the particles are localized on single sites. Phase coherence is lost because of the vanishing number fluctuations. The strong on-site interaction creates an energy gap in the excitation spectrum, turning the system into an insulator. The transition to this state has been studied extensively for fermions [137, 138] and since the eighties for bosons [128, 139–141]. It has recently been observed with ultracold atoms [20, 142–145]. In the context of the Mott transition, localization occurs because of the interplay of the lattice potential, the kinetic energy which tends to delocalize the particles, and the strong inter-particle interactions which impose a toll on such a delocalization [146,147]. In the Mott insulating phase,

[9] In 1D, the density of state prevents the formation of a BEC in the homogeneous case. If interactions are turned on, however, 1D bosons form a quasi-condensate with superfluid properties, as in higher dimensions.

[10] Or a quasi-condensate in 1D. See section 3.3.1.

the boson density remains homogeneous on long length scales, and the term of "localization" is used to characterize the many-body state.

The above considerations show that interactions may either hamper or favor localization in inhomogeneous systems. Let us now review how this shapes the behavior of bosons in 1D. The one-dimensional geometry is interesting, as the effects of both the disorder and the interactions are generally expected to be at their strongest [147]. Another advantage of one-dimensional systems is that they can be, to some extent, treated analytically, and that they may give some insight into the physics governing their higher-dimensional analogues.

Disordered bosons in 1D

Quantum phase diagrams - We reproduce in Fig. 1.7 the quantum phase diagrams worked out in Refs. [8, 148] for disordered bosons with and without lattice.

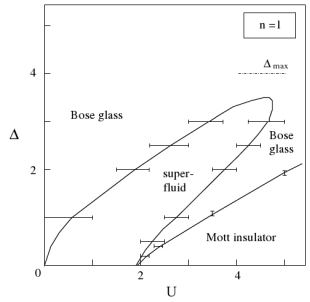
For strong interactions, disordered bosons enter an insulating phase.[11] In the presence of a lattice and for integer filling, this insulating phase is either a Mott insulator, characterized by a gapped excitation spectrum and vanishing compressibility, or a gapless compressible phase called Bose glass [128] [see Fig. 1.7(a)]. In the absence of a lattice, however, there is no insulating Mott phase, and the only phase present for strong interactions is the Bose glass [see Fig. 1.7(c)]. The gapless Bose glass is an insulator because of the localization effects of the disorder [128].

For moderate repulsive interactions and weak disorder, on the other hand, an extended (delocalized) superfluid phase is predicted. Starting from this superfluid phase, as put forward in Refs. [8,148,149], stronger disorder drives the system back into an insulating phase, identified with the same Bose glass. In diagrams such as those reproduced in Fig. 1.7, the superfluid phase is enclosed in a lobe attached to the line of vanishing disorder, and separated from the line of vanishing interaction by an insulating phase. The prevailing argument explaining the latter feature is that for an infinitesimal amount of disorder non-interacting bosons in 1D all populate the Anderson-localized single-particle ground state, with no superfluid properties.

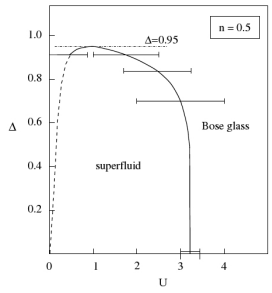
Open questions - It seems well established numerically that there is no phase transition between the strongly- and weakly-interacting regimes of the insulator found in the continous case, and that the phase enclosing the superfluid lobe is a unique Bose-glass phase [148]. However, this phase is expected to exhibit qualitative differences between the two regimes. In particular, the processes leading to localization and an insulating behavior in the two regimes are recognized to be different.[12] Much attention has been devoted to the strongly-interacting part of the quantum phase diagram of disordered 1D bosons, especially to the lattice case.

[11] This has been shown analytically for the continuum case using Luttinger liquid theory and renormalization group (RG) techniques [8], and for the lattice case using scaling arguments [128], Monte-Carlo [130, 149], real-space renormalization [150, 151] or density matrix renormalization group (DMRG) [148] calculations.

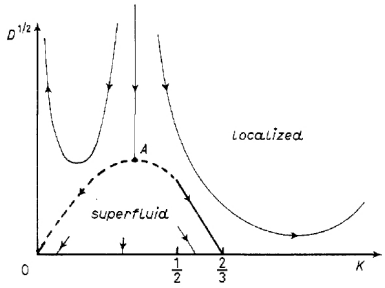
[12] The precise shape of the lobe displayed in Fig. 1.7(b) confirms that disorder and interactions cooperate in the transition to the Bose glass in the regime of strong interactions, while they compete for weak interactions. Strictly speaking, the data displayed in Fig. 1.7(b) does not correspond to the continuous case. Because of the absence of Mott phase, however, it probably lies closer to the continuous case than the commensurate case shown in Fig. 1.7(a). Note that in the latter case, there are points in the Bose glass phase from which a stronger disorder and constant interactions drive the system back into the superfluid phase. This introduces a nuance in the rule of thumb indicating that strong interactions cooperate with disorder. An explanation is given in Ref. [148].



(a) DMRG study of the commensurate lattice case (Fig. 1 of Ref. [148]).



(b) DMRG study of the lattice case at half filling (Fig. 2 of Ref. [148]).



(c) Luttinger liquid and renormalization group study of the continuous case (Fig. 3 of Ref. [8]).

Figure 1.7: Quantum phase diagrams of strongly interacting 1D bosons in disorder. (a),(b) Results of DMRG calculations performed for the lattice case from the Bose-Hubbard Hamiltonian with on-site interaction energy U and random on-site energies ϵ_i uniformly distributed in an interval $[-\Delta, \Delta]$. The energies in the figures are normalized by $t = 1$ where $t/2$ is the (kinetic) hopping term of the Hubbard model. (c) Analysis of the continuous case. The arrows show the RG flow of the disorder strength D and the Luttinger liquid parameter K, which are renormalized when a short-wavelength cutoff in the low-energy Luttinger liquid theory is sent to infinity. In this figure, K is zero for non-interacting bosons, and increases with the strength of repulsive intreactions. The quantity D parametrizes an uncorrelated disorder with autocorrelation function $C_2(z) = D\delta(z)$ [see Eq. (2.45)].

Interestingly, the weakly-interacting regime itself is not well characterized. The dashed lines left in Figs. 1.7(b) and 1.7(c), for instance, raise questions about the location of the phase-transition boundary. Further important issues are connected with the dominant mechanisms triggering the transition, a characterization of the weakly-interacting Bose glass beyond that boundary, and a description of the Bose glass found close to the line of vanishing interactions, where pure Anderson localization occurs.

1.2.3 Ultracold atomic Bose gases

At sufficiently low temperatures, atomic Bose gases form a Bose-Einstein condensate (BEC), or a quasi-BEC in low-dimensional geometries [32, 111, 152]. Condensates and quasi-condensates exhibit (quasi-) long-range order, which makes them ideal tools to study the effects of coherence and disorder. The theory of Bose-Einstein condensation can be found in standard textbooks [153] and review articles [111]. We touch upon a few points below. We also highlight a few well-known but significant aspects of theory and experiment with ultracold atomic Bose gases. Ultracold Bose gases are naturally weakly-interacting, and can therefore be described accurately with simple theoretical tools. From the experimental point of view, ultracold gases offer a high degree of control.

Bose-Einstein condensation

Non-interacting case - Bose-Einstein condensation is often introduced by considering non-interacting bosons at thermal equilibrium in the grand-canonical ensemble. Then, the system

is described on a basis of single-particle states with energies E_i. The occupation of these states at temperature T is given by

$$N_i = \frac{1}{\mathrm{e}^{\beta(E_i-\mu)} - 1}, \tag{1.16}$$

where $\beta = 1/k_{\mathrm{B}}T$, and the chemical potential μ is determined by the average number N of bosons: $\sum_i N_i(\mu, \beta) = N$. In this framework, Bose-Einstein condensation is a phase transition which occurs if, for some temperature T_c, the population of excited states saturates below T_c, and the occupation N_0 of the single-particle ground state becomes of the order of N. Such is the case in free space in 3D, and in harmonic traps in 3D and 2D [32]. Key ingredients for condensation to occur in the single-particle ground state are the indistinguishability of the bosons, their ability to occupy the same single-particle state, and the saturation of the population of excited states. The occurence of such a saturation depends on the single-particle density of states, hence also on the dimensionality. In a homogeneous 1D geometry, bosons do not form a true BEC, even at $T = 0$. In the presence of weak interactions, however, they form a quasi-condensate (see section 3.3.1), which displays some form of coherence (quasi-long-range order), and shares with higher-dimensional analogues the property of superfluidity [18].

Interacting case - Bose-Einstein condensation is not restricted to non-interacting systems. In general, the description of Bose-Einstein condensation in an interacting system requires the explicit consideration of its many-body states. All the statistical and quantum-mechanical information about the state $|\Psi\rangle$ of a many-body system is contained in its density matrix $\hat{\rho}$. Few-body correlation functions describing $|\Psi\rangle$ are obtained from the p-body density matrices $\hat{\rho}_p$, whose elements in the position basis are $\rho_p(\mathbf{r_1}, \cdots, \mathbf{r_p}, \mathbf{r'_1}, \cdots, \mathbf{r'_p}) = \langle\Psi|\hat{\Psi}(\mathbf{r_1})^\dagger \cdots \hat{\Psi}(\mathbf{r_p})^\dagger \hat{\Psi}(\mathbf{r'_1}) \cdots \hat{\Psi}(\mathbf{r'_p})|\Psi\rangle$. In this expression, $\hat{\Psi}(\mathbf{r})$ is the bosonic field operator which creates a particle at position $\mathbf{r}$. The one-body density matrix

$$\rho_1(\mathbf{r}, \mathbf{r}') = \langle\Psi|\hat{\Psi}(\mathbf{r})^\dagger \hat{\Psi}(\mathbf{r}')|\Psi\rangle, \tag{1.17}$$

in particular, reflects the one-particle properties of the many-body state. The density matrix is a key concept for the definition of Bose-Einstein condensation in interacting systems. The one-body density matrix is Hermitian and positive semi-definite, and can be diagonalized in an orthonormal basis of eigenfunctions χ_i:

$$\rho_1(\mathbf{r}, \mathbf{r}') = \sum_i N_i \chi_i^*(\mathbf{r}) \chi_i(\mathbf{r}'), \tag{1.18}$$

with $N_i \geq 0$. A Bose-Einstein condensate is said to be present when at least one of the eigenvalues N_i is of the order of the average number N of particles in the system (and remains so if N is sent to infinity at constant particle density) [111, 154–157]. Now the system might have different properties depending on whether only one or several eigenvalues have a magnitude comparable to N. If a single eigenvalue N_0 is comparable to N, the system displays a *simple BEC*, and χ_0 is called the wave function of the condensate. On the other hand, if several eigenvalues N_i are comparable to N, the system is said to be in a state of *fragmented BEC* [111, 157]. The latter situation will be encountered and discussed in sections 3.3.3 and 3.4.2.

Weakly-interacting Bose gases

Modeling interactions - Ultracold atomic gases are naturally dilute and weakly-interacting. This has several advantages. First, interactions between the atoms can be described by two-body scattering processes [110]. In the case of bosons at temperatures below the millikelvin (i.e. even far above the typical condensation temperatures), these processes are dominated by s-wave scattering, and determined by a single parameter, the s-wave scattering length a_s [18]. Hence, interactions can be modeled with a simple contact interaction potential

$$V_{\text{int}}(\mathbf{r}-\mathbf{r}') = \frac{4\pi\hbar^2 a_s}{m}\,\delta(\mathbf{r}-\mathbf{r}'), \tag{1.19}$$

where m is the mass of the atoms [32]. In contrast, a complicated interaction potential is required to describe interactions in liquid ^{4}He [158]. Second, the atom density n and the scattering length a_s in ultracold Bose gases are usually such that $na_s^3 \ll 1$, which defines a regime of weak interactions.[13] As a consequence i) almost pure BECs can be obtained in systems of ultracold atoms (in 3D), with condensate fractions N_0/N close to one, ii) mean-field approaches provide a reasonable starting point to explain a wealth of phenomena [32].

Description of the many-body system - In the standard mean-field picture, the many-body state $|\Psi\rangle$ is simply represented by a macroscopic coherent matter wave of the form $\Psi_0(\mathbf{r}) = \sqrt{N_0}\chi_0(\mathbf{r})$ [18]. In the Bogolyubov approach [159], correlations beyond the mean field are included by considering *small* quantum fluctuations $\delta\hat{\Psi}(\mathbf{r})$ around the mean field, and writing the field operator as

$$\hat{\Psi}(\mathbf{r}) \simeq \Psi_0(\mathbf{r}) + \delta\hat{\Psi}(\mathbf{r}). \tag{1.20}$$

The concept of a macroscopic wave function is also known from the field of superconductors and superfluid ^{4}He. In those cases, however, it only provides a phenomenological description of the superfluids [18]. In the case of ^{4}He, for instance, interactions are generally strong, and the condensate fraction is believed to be typically 10% only, even at zero temperature [155]. On the contrary, the mean-field and the mean-field-plus-Bogolyubov pictures provide accurate microscopic descriptions of BECs in atomic gases.

Experiments with ultracold gases

Since the achievement of Bose-Einstein condensation in 1995, ultracold atomic gases have demonstrated their versatility by allowing the exploration of topics from fields as diverse as condensed-matter physics [20] and quantum optics [160]. Assets of ultracold gases are the high degree of control and the number of available diagnostic tools.

Control and versatility - With ultracold atoms, the experimentalist can choose the quantum statistics, and has control over the temperature and the number of atoms. Laser light, magnetic fields or radio-frequency fields can be used to design potentials for the atoms. Those potentials may serve as waveguides, traps, coupled wells or lattice potentials. Tightly-confining

[13] Strong interactions can nevertheless be achieved by tuning a_s with Feshbach resonances. Alternatively, strongly correlated regimes can be reached at small na_s^3 by loading the atoms into an optical lattice, which quenches their kinetic energy [18, 146].

traps can be used to reduce the effective dimension of the system. Periodic lattice potential, on the other hand, are used mimic solid state physics. The strength of interactions may be tuned by means of Feshbach resonances. Finally, special atomic species and internal structures give access to new types of interactions in spinor gases and dipolar gases.

Diagnostic tools - Many types of measurements can be performed on systems of ultracold atoms. Absorption, fluorescence or phase-contrast imaging can be used to measure density profiles *in-situ*, or velocity distributions after time-of-flight. The position and the energy of the atoms may be very finely measured by using light-shift tomography. Internal states can be resolved by adapting the probe laser light. Collective excitations can be measured by modulating trapping potentials. One- and two-body correlation functions can be measured with interference experiments, Raman or Bragg spectroscopy, and noise correlation spectroscopy.

For the above reasons, ultracold atoms also constitute an excellent arena to study the physics of disordered quantum systems. One of the appealing features of ultracold atoms in this respect is the controlled generation of random potentials. In the following section, we address the statistical properties of random potentials, and possible implementations of disorder in systems of ultracold atoms.

1.3 Random potentials

Disorder may take different shapes. In the Anderson Hamiltonian (1.5), for instance, either the on-site energy ϵ_i or the hopping term J_{ij}, or even both, may be random functions of the position. What is more, these quantities could be random function of time as well, and this would just be one of the many conceivable ways to model disorder. In this thesis we only consider quenched disorder (i.e. time-independent disorder) which takes the form of a random potential V. Below, we present those properties and ways of characterizing random potentials which are relevant to our study (sections 1.3.1 and 1.3.2). In section 1.3.3, we provide a brief description of speckle potentials. Those speckle potentials are relevant to current experiments with ultracold atomic gases, and have original statistical properties.

1.3.1 Correlation functions

A random potential is a random function $V(\mathbf{r})$ of the position $\mathbf{r}$, associated to a probability measure $P[V]\mathcal{D}V$. A *realization* of the random potential is a particular outcome of the process of drawing the potential values $V(\mathbf{r})$ for all $\mathbf{r}$. For simplicity, we sometimes also refer to such an outcome as "the random potential" itself. We denote by

$$\langle \cdots \rangle = \int \cdots P[V]\mathcal{D}V \tag{1.21}$$

the statistical average with respect to the probability P. In the framework of the following chapters, we need not know the complete probability density P, and the set of n-point autocorrelation functions $\langle V(\mathbf{r}_1)V(\mathbf{r}_2)\cdots V(\mathbf{r}_n)\rangle$ is sufficient. Without loss of generality, we assume that V has a vanishing spatial average: $\langle V(\mathbf{r})\rangle = 0$. We detail below two additional (key)

assumptions, namely that the statistical properties of the potential are "homogeneous", and that statistical correlations disappear at infinity.

Spatial homogeneity

The random potential is assumed to be homogeneous in the sense that its statistical properties do not depend on the absolute position in the sample. As a consequence, the n-point correlation functions C_n depend on $n-1$ relative coordinates only:

$$C_n(\mathbf{r}_1,\ldots,\mathbf{r}_{n-1}) = \langle V(\mathbf{r}_0)V(\mathbf{r}_0+\mathbf{r}_1)\cdots V(\mathbf{r}_0+\mathbf{r}_{n-1})\rangle. \tag{1.22}$$

Disappearance of statistical correlations at infinity

Another standard assumption on the random potential is the disappearance of statistical correlations between values of the potential at points with infinitely large separation. This is expressed by the factorization of averages [86]

$$\langle V(\mathbf{r}_0)\cdots V(\mathbf{r}_{m-1})V(\mathbf{r}_m+\mathbf{d})\cdots V(\mathbf{r}_{n-1}+\mathbf{d})\rangle \xrightarrow[|\mathbf{d}|\to\infty]{} \langle V(\mathbf{r}_0)\cdots V(\mathbf{r}_{m-1})\rangle\times\langle V(\mathbf{r}_m)\cdots V(\mathbf{r}_{n-1})\rangle. \tag{1.23}$$

In particular, the two-point correlator, or auto-correlation function C_2, drops to zero at infinity by virtue of the assumption $\langle V\rangle = 0$. We call correlation length $\sigma_{\rm R}$ a typical width of the correlation function C_2.

The function C_3 also vanishes in a factorization such as the one encountered on the right-hand side of formula (1.23). For higher-order correlation functions, however, this is in general not the case. For instance, the four-point correlation function may not vanish in the limit

$$\langle V(\mathbf{r}_0)V(\mathbf{r}_1)V(\mathbf{r}_2+\mathbf{d})V(\mathbf{r}_3+\mathbf{d})\rangle \xrightarrow[|\mathbf{d}|\to\infty]{} \langle V(\mathbf{r}_0)V(\mathbf{r}_1)\rangle\times\langle V(\mathbf{r}_2)V(\mathbf{r}_3)\rangle. \tag{1.24}$$

This means that the absence of correlation between two points does not imply the disappearance of *all* correlations.

Cumulants

The correlation functions C_n correspond to various moments of the continuous random variable $V(\mathbf{r})$. For the analysis of higher-order correlations, it proves useful to define also the cumulants K_n of the random potential [35, 161]. In brief, the cumulants K_n are obtained from the moments C_n by substracting all possible factorized contributions:

$$K_2(\mathbf{r}_1) = \langle V(\mathbf{r}_0)V(\mathbf{r}_0+\mathbf{r}_1)\rangle - \langle V(\mathbf{r}_0)\rangle\times\langle V(\mathbf{r}_0+\mathbf{r}_1)\rangle \tag{1.25}$$

$$\begin{aligned} K_3(\mathbf{r}_1,\mathbf{r}_2) &= \langle V(\mathbf{r}_0)V(\mathbf{r}_0+\mathbf{r}_1)V(\mathbf{r}_0+\mathbf{r}_2)\rangle - \langle V(\mathbf{r}_0)V(\mathbf{r}_0+\mathbf{r}_1)\rangle\times\langle V(\mathbf{r}_0+\mathbf{r}_2)\rangle \\ &\quad -\langle V(\mathbf{r}_0+\mathbf{r}_1)V(\mathbf{r}_0+\mathbf{r}_2)\rangle\times\langle V(\mathbf{r}_0)\rangle - \langle V(\mathbf{r}_0+\mathbf{r}_2)V(\mathbf{r}_0)\rangle\times\langle V(\mathbf{r}_0+\mathbf{r}_1)\rangle \end{aligned} \tag{1.26}$$

$$\cdots = \cdots$$

Since $\langle V\rangle = 0$, the lower-order cumulants K_2 and K_3 coincide with the moments C_2 and C_3, respectively. The fourth-order cumulant reads

$$\begin{aligned} K_4(\mathbf{r}_1,\mathbf{r}_2,\mathbf{r}_3) &= C_4(\mathbf{r}_1,\mathbf{r}_2,\mathbf{r}_3) - C_2(\mathbf{r}_1)\,C_2(\mathbf{r}_2-\mathbf{r}_3) \\ &\quad -C_2(\mathbf{r}_2)\,C_2(\mathbf{r}_3-\mathbf{r}_1) - C_2(\mathbf{r}_3)\,C_2(\mathbf{r}_1-\mathbf{r}_2). \end{aligned} \tag{1.27}$$

Owing to the factorization of averages [see Eq. (1.23)], the cumulant $K_4(\mathbf{r}_1, \mathbf{r}_2, \mathbf{r}_3)$ vanishes as soon as any of its arguments $\mathbf{r}_i$ becomes infinitely large.

Symmetries

The assumption of homogeneity implies the symmetries

$$C_2(\mathbf{r}_1) = C_2(-\mathbf{r}_1) \tag{1.28}$$

$$\hat{C}_2(\mathbf{q}_1) = \hat{C}_2(-\mathbf{q}_1) \tag{1.29}$$

$$C_3(\mathbf{r}_1, \mathbf{r}_2) = C_3(-\mathbf{r}_1, \mathbf{r}_2 - \mathbf{r}_1) = C_3(-\mathbf{r}_2, \mathbf{r}_1 - \mathbf{r}_2) = C_3(\mathbf{r}_2, \mathbf{r}_1) \tag{1.30}$$

$$\hat{C}_3(\mathbf{q}_1, \mathbf{q}_2) = \hat{C}_3(\mathbf{q}_1, -\mathbf{q}_1 - \mathbf{q}_2) = \hat{C}_3(\mathbf{q}_2, -\mathbf{q}_2 - \mathbf{q}_1) = \hat{C}_3(\mathbf{q}_2, \mathbf{q}_1), \tag{1.31}$$

where $\hat{C}_n(\mathbf{q}_1, \ldots, \mathbf{q}_{n-1})$ is the Fourier transform

$$\hat{C}_n(\mathbf{q}_1, \ldots, \mathbf{q}_{n-1}) = (2\pi)^{-(n-1)d/2} \int \mathrm{d}\mathbf{r}_1 \cdots \int \mathrm{d}\mathbf{r}_{n-1} C_{n-1}(\mathbf{r}_1, \ldots, \mathbf{r}_{n-1}) \mathrm{e}^{i(\mathbf{q}_1.\mathbf{r}_1 + \cdots + \mathbf{q}_{n-1}.\mathbf{r}_{n-1})}. \tag{1.32}$$

However, homogeneity alone does not guarantee the symmetries[14] $C_3(\mathbf{r}_1, \mathbf{r}_2) = C_3(-\mathbf{r}_1, -\mathbf{r}_2)$ and $\hat{C}_3(\mathbf{q}_1, \mathbf{q}_2) = \hat{C}_3(-\mathbf{q}_1, -\mathbf{q}_2)$.

1.3.2 Gaussian disorder

Gaussian random potentials form a particular class of disorder, described by a probability measure[15] [35]

$$P[V]\mathcal{D}V = \frac{1}{\mathcal{Z}} \mathrm{e}^{-\frac{1}{2}\iint \mathrm{d}\mathbf{r}\, \mathrm{d}\mathbf{r}'\, V(\mathbf{r}) B(\mathbf{r}-\mathbf{r}') V(\mathbf{r}')} \mathcal{D}V, \tag{1.33}$$

where $\mathcal{Z}$ is a normalization factor, the function B satisfies

$$\int \mathrm{d}\mathbf{r}''\, B(\mathbf{r} - \mathbf{r}'')\, C_2(\mathbf{r}' - \mathbf{r}'') = \delta(\mathbf{r} - \mathbf{r}'), \tag{1.34}$$

and C_2 is the two-point correlation function $C_2(\mathbf{r}' - \mathbf{r}) = \langle V(\mathbf{r}) V(\mathbf{r}') \rangle$.

Essential property - Gaussian random potentials have the fundamental property that all *cumulants* K_n of order $n > 2$ vanish identically.[16] Since $\langle V \rangle = 0$, this implies that all correlation functions (i.e. moments) C_n of odd order n vanish identically, and that correlation functions C_n of even order expand into products of two-point correlation functions C_2. In particular the four-point correlator of a Gaussian potential reads

$$C_4^G(\mathbf{r}_1, \mathbf{r}_2, \mathbf{r}_3) = C_2(\mathbf{r}_1)\, C_2(\mathbf{r}_2 - \mathbf{r}_3) + C_2(\mathbf{r}_2)\, C_2(\mathbf{r}_3 - \mathbf{r}_1) + C_2(\mathbf{r}_3)\, C_2(\mathbf{r}_1 - \mathbf{r}_2). \tag{1.35}$$

The statistical properties of a Gaussian random potential are hence entirely determined by the two-point correlator C_2.

[14] A simple counter-example is found with a 1D potential made of scarcely, randomly placed impurities with asymmetric shape [see model (1.37)]. It can be checked that such a potential is not isotropic and that $C_3(\mathbf{r}_1, \mathbf{r}_2) \neq C_3(-\mathbf{r}_1, -\mathbf{r}_2)$.

[15] In certain specific contexts, one may find that a random potential is said to be Gaussian when its single-point probability distribution $P[V(\mathbf{r})]$ is a Gaussian, or when its two-point correlation function $C_2(\mathbf{r}_1)$ Gaussian. In both cases, the random potential may not be Gaussian in the sense of the definition given here.

[16] This property is known as a consequence of the so-called Gaussian moment theorem. It also directly follows from the very definition of the cumulants with the help of a generating functional [35, 161].

Gaussian white noise - The model of uncorrelated Gaussian disorder, or Gaussian white noise [162], corresponds to

$$C_2(\mathbf{r}_1) = D\,\delta(\mathbf{r}_1), \tag{1.36}$$

where δ is the d-dimensional Dirac function, and $D = \int \mathrm{d}\mathbf{r}_1 C_2(\mathbf{r}_1)$ parametrizes the strength of the potential. Note that D has dimension $(energy)^2 \times (length)^d$, where d is the spatial dimension.

Example - A standard model of disorder is the random impurity potential, or Edwards model, in which the random potential arises from the contribution of identical and randomly placed impurities [35]:

$$V(\mathbf{r}) = \sum_i f(\mathbf{r} - \mathbf{r}_i). \tag{1.37}$$

In this expression, the $\mathbf{r}_i$ denote the random positions of the impurities, and f is the single-impurity potential. The potential V is characterized by the impurity density n, i.e. the average number of impurities per unit volume, and the typical amplitude f_0 of the single-impurity potential f [e.g. $f_0 = f(0)$]. In the limit of dense impurities, which corresponds to taking $n \to \infty$ while keeping nf_0^2 constant, the impurity potential is Gaussian, and its correlation function is

$$C_2(\mathbf{r}) = n \int \mathrm{d}\mathbf{r}' f(\mathbf{r}') f(\mathbf{r}' + \mathbf{r}). \tag{1.38}$$

Quite often, the single-impurity potential is assumed to be proportional to a Dirac distribution, in which case the disorder is uncorrelated [162, 163].

Gaussian random potentials are widely used in the literature [162–167] because i) they often allow explicit calculations and ii) they offer a good description of processes which result from the sum of a large number of random variables (for uncorrelated variables, the central limit theorem ensures the convergence to a Gaussian distribution). It is common to approximate true disorder by an uncorrelated Gaussian random potential if the correlation length of the true potential is much smaller than all other relevant length scales in the physical problem [167]. We examine in the following chapters situations where such is not the case.

1.3.3 Speckle potentials

Optical potentials have proved to be an efficient tool to trap and manipulate ultracold atoms. In the field of a laser light which is close to resonance with a transition from the ground state to an excited state, atoms experience the potential [18]

$$V_{\mathrm{dip}}(\mathbf{r}) = \frac{3\pi c^2 \Gamma}{2\omega_0^3} \frac{I(\mathbf{r})}{\delta}, \tag{1.39}$$

due to the electric dipole coupling of atom and field. In this expression, Γ is the decay rate (width) of the excited state, ω_0 is the transition frequency, $\delta = \omega_{\mathrm{L}} - \omega_0$ is the detuning of the laser frequency from the transition, and $I(\mathbf{r})$ is the intensity of the field at position $\mathbf{r}$:

$$I(\mathbf{r}) = \frac{1}{2} c\epsilon_0 |\boldsymbol{\mathcal{E}}(\mathbf{r})|^2, \tag{1.40}$$

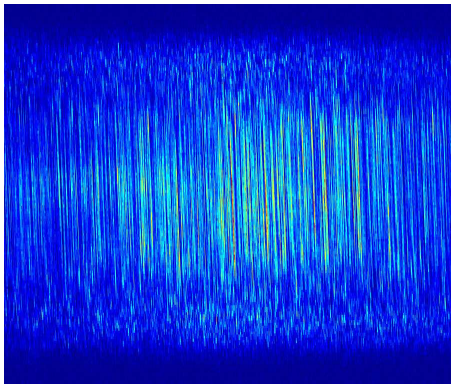


Figure 1.8: Experimental speckle pattern (courtesy of J. Billy). False colors indicate the intensity of the light field (blue: minimim; red: maximum). Here the optical set-up is built so as to produce elongated speckle grains, with a correlation length exceeding the system size in the vertical direction. The speckle potential is then effectively 1D.

where $\mathcal{E}$ is the amplitude of the electric field.[17] Expression (1.39) holds for $\Gamma \ll |\delta| \ll \omega_0$. If the laser is blue-detuned with respect to the transition ($\omega_L > \omega_0$), the potential is repulsive, and the atoms seek low field intensities. If the laser is red-detuned ($\omega_L < \omega_0$), the potential is attractive, and the atoms seek strong intensities.

The high degree of control offered by optical dipole potentials has been used to confine ultracold atoms into low-dimensional geometries and to create lattice potentials for the atoms, allowing an exploration of condensed-matter problems [20, 21, 168, 169]. Optical potentials can also be used to create disorder in a controlled way [25–27, 30, 170–173], e.g. in the form of speckle patterns [22–24]. Such a speckle pattern is displayed in Fig. 1.8. Other schemes exist or have been proposed to impose random or pseudo-random potentials on ultracold atoms. They include the use of disordered magnetic traps on atom chips with rough wires [174, 175], static impurity atoms [176–178] or radio-frequency fields [179]. Speckle potentials have advantages from both a practical and a fundamental point of view. First, speckle potentials are easily implemented with simple optical components, and their statistical properties are well known (see Refs. [180, 181] and below). Second, speckle potentials are correlated random potentials, and their correlation functions can be designed by adapting the geometry of the optical setup used to produce them. Speckle potentials thereby allow to investigate the effect of statistical correlations. Finally, both the amplitude and the correlation length of speckle potentials can be precisely controlled and calibrated [31], so that quantitative comparisons with the theory are possible [29].

What is speckle ?

Speckle fields typically arise as a result of the reflection or transmission of a coherent wave on a rough surface. Such a situation is depicted schematically in Fig. 1.9(a). A laser beam is passed through a diffusive plate, giving rise to partial waves with different phases (and possibly

[17] With this standard notation the intensity I is homogeneous to the energy flux of the laser light, rather than the squared modulus of the electric field. For simplicity, we also refer to the latter quantity as the intensity.

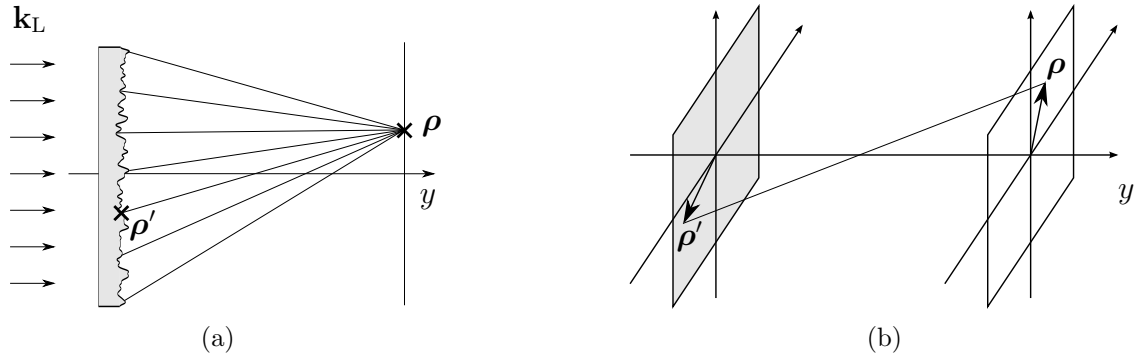


Figure 1.9: Transmission through a ground-glass diffuser. The partial waves created on the diffuser interfere at the observation spot $(\boldsymbol{\rho}, y)$. In coherent light (wave vector $\mathbf{k}_\mathrm{L}$), this interference produces a speckle pattern.

different amplitudes) due to the tickness variations of the diffusive plate. The complex field amplitude $\mathcal{E}(\mathbf{r})$ at some observation point $\mathbf{r} = (\boldsymbol{\rho}, y)$ results from the interference of these partial waves, and forms a random pattern.

Elementary properties

The statistics of speckle are reviewed in detail in Refs. [180, 181]. Let us summarize here some elementary properties. For simplicity, we assume that the field is scalar, and the diffuser is regarded as being composed of N independent elementary scatterers. Then, at every position $\mathbf{r}$, the complex electric field amplitude can be written as a sum of elementary contributions (see Fig. 1.9(a))

$$\mathcal{E} = \frac{1}{\sqrt{N}} \sum_{n=1}^{N} |e_n| \mathrm{e}^{\mathrm{i}\phi_n}. \tag{1.41}$$

The roughness of the diffuser is assumed to be such that the phases ϕ_n are uniformly distributed in the interval $[0, 2\pi]$, and that, for all n, the amplitude $|a_n|$ and the phase ϕ_n are uncorrelated. Then, the sum (1.41) appears as the result of a random walk in the complex plane. The real and imaginary parts $\mathcal{R} = \mathrm{Re}[\mathcal{E}]$ and $\mathcal{I} = \mathrm{Im}[\mathcal{E}]$ are uncorrelated variables with zero mean and equal variance. The central limit theorem ensures that, as sums of N independent and identically-distributed random variables, $\mathcal{R}$ and $\mathcal{I}$ have Gaussian probability distributions for large N. The field $\mathcal{E}$ itself is a complex Gaussian random field.

Light intensity - As a first consequence of their Gaussian distribution, $\mathcal{R}$ and $\mathcal{I}$ have the joint probability density

$$P_{\mathcal{R},\mathcal{I}}(\mathcal{R}, \mathcal{I}) = \frac{1}{2\pi\sigma^2} \mathrm{e}^{-\frac{\mathcal{R}^2+\mathcal{I}^2}{2\sigma^2}}, \tag{1.42}$$

where σ^2 is the variance of both $\mathcal{R}$ and $\mathcal{I}$. Switching to a polar representation with $|\mathcal{E}|^2 = \mathcal{R}^2 + \mathcal{I}^2$ and $\Phi = \arctan(\mathcal{I}/\mathcal{R})$, the probability distribution for the field intensity $I = c\epsilon_0|\mathcal{E}|^2/2$ is readily derived as

$$P_I(I) = \begin{cases} \frac{\mathrm{e}^{-I/\langle I\rangle}}{\langle I\rangle} & \text{if } I > 0 \\ 0 & \text{otherwise} \end{cases}, \tag{1.43}$$

where $\langle I \rangle$ is the average value of the intensity. Note that this distribution is highly asymmetric around the mean, and that it has a lower bound, but no upper bound.

The speckle random potential is defined as $V = V_{\rm dip} - \langle V_{\rm dip} \rangle = V_{\rm R}(I/\langle I \rangle - 1)$, where

$$V_{\rm R} = \frac{3\pi c^2 \Gamma}{2\omega_0^2} \times \frac{\langle I \rangle}{\delta}. \tag{1.44}$$

Then, V has a vanishing average, a root-mean-square amplitude $|V_{\rm R}|$, and a single-point probability distribution

$$P[V(\mathbf{r})] = \begin{cases} V_{\rm R}^{-1} \mathrm{e}^{-\frac{V(\mathbf{r})}{V_{\rm R}}+1} & \text{if } \frac{V(\mathbf{r})}{V_{\rm R}} > -1 \\ 0 & \text{otherwise} \end{cases}. \tag{1.45}$$

Equation (1.44) shows that the disorder amplitude $|V_{\rm R}|$ is directly controlled by the laser power via $\langle I \rangle$. The sign of $V_{\rm R}$, on the other hand, is controlled by the sign of the detuning δ. For blue-detuned laser light, $V_{\rm R}$ is positive, and the potential is bounded below. For red-detuned light, $V_{\rm R}$ is negative and the potential is bounded above.

Speckle grain size - The typical grain size of the speckle pattern is determined by the width of its (two-point) autocorrelation function. We denote by $\mathcal{E}_i$ the value of the complex field at some point $\mathbf{r}_i$. For all i, j, the correlation functions $\langle \mathcal{E}_i \mathcal{E}_j \rangle$ and $\langle \mathcal{E}_i^* \mathcal{E}_j^* \rangle$ vanish [181], so that the two-point correlation properties of the field $\mathcal{E}$ are entirely determined by correlators of the form $\langle \mathcal{E}_i^* \mathcal{E}_j \rangle$. Moreover, the Gaussian moment theorem applies to $\mathcal{E}$ (see section 1.3.2), so that all higher-order correlation functions factorize into products of two-point correlators. In particular, the two-point intensity correlation function $\langle I_0 I_1 \rangle \propto \langle \mathcal{E}_0^* \mathcal{E}_1^* \mathcal{E}_0 \mathcal{E}_1 \rangle$ is obtained from the expansion

$$\langle \mathcal{E}_0^* \mathcal{E}_1^* \mathcal{E}_0 \mathcal{E}_1 \rangle = \langle \mathcal{E}_0^* \mathcal{E}_0 \rangle \langle \mathcal{E}_1^* \mathcal{E}_1 \rangle + \langle \mathcal{E}_0^* \mathcal{E}_1 \rangle \langle \mathcal{E}_1^* \mathcal{E}_0 \rangle. \tag{1.46}$$

This result can be cast in the form[18]

$$\frac{\langle I_0 I_1 \rangle}{\langle I \rangle^2} = 1 + \frac{\langle \mathcal{E}_0^* \mathcal{E}_1 \rangle \langle \mathcal{E}_1^* \mathcal{E}_0 \rangle}{\langle \mathcal{E}^* \mathcal{E} \rangle^2} \tag{1.47}$$

or, equivalently,

$$\frac{\langle V_0 V_1 \rangle}{V_{\rm R}^2} = \frac{\langle \mathcal{E}_0^* \mathcal{E}_1 \rangle \langle \mathcal{E}_1^* \mathcal{E}_0 \rangle}{\langle \mathcal{E}^* \mathcal{E} \rangle^2}. \tag{1.48}$$

For points $\mathbf{r}_i = (\boldsymbol{\rho}_i, y)$ located in a plane at distance y from the diffusive plate [see Fig. 1.9(b)], the field correlation function $\langle \mathcal{E}_0^* \mathcal{E}_1 \rangle = \langle \mathcal{E}^*(\boldsymbol{\rho}_0, y) \mathcal{E}(\boldsymbol{\rho}_1, y) \rangle \equiv C_{\mathcal{E}}^{\perp}(\boldsymbol{\rho}_1 - \boldsymbol{\rho}_0)$ obeys [181]

$$\frac{C_{\mathcal{E}}^{\perp}(\boldsymbol{\rho}_1 - \boldsymbol{\rho}_0)}{C_{\mathcal{E}}^{\perp}(\mathbf{0})} = \frac{\int \mathrm{d}\boldsymbol{\rho}' F(\boldsymbol{\rho}') \, \mathrm{e}^{-\mathrm{i}\frac{k_{\rm L}}{y}(\boldsymbol{\rho}_1 - \boldsymbol{\rho}_0).\boldsymbol{\rho}'}}{\int \mathrm{d}\boldsymbol{\rho}' F(\boldsymbol{\rho}')}, \tag{1.49}$$

where $F(\boldsymbol{\rho}') = \langle |\mathcal{E}'(\boldsymbol{\rho}')|^2 \rangle$, and $\mathcal{E}'(\boldsymbol{\rho}')$ is the complex amplitude at the level of the diffusing plate. The parameter $k_{\rm L} = 2\pi/\lambda_{\rm L}$ is the wave number of the laser light. Hence, Eq. (1.48) and the non-constant term of Eq. (1.47) write

$$\frac{C_2^{\perp}(\boldsymbol{\rho}_1 - \boldsymbol{\rho}_0)}{V_{\rm R}^2} = \frac{\langle \mathcal{E}_0^* \mathcal{E}_1 \rangle \langle \mathcal{E}_1^* \mathcal{E}_0 \rangle}{\langle \mathcal{E}^* \mathcal{E} \rangle^2} = \left| \frac{\int \mathrm{d}\boldsymbol{\rho}' F(\boldsymbol{\rho}') \mathrm{e}^{-\mathrm{i}\frac{k_{\rm L}}{y}(\boldsymbol{\rho}_1 - \boldsymbol{\rho}_0).\boldsymbol{\rho}'}}{\int \mathrm{d}\boldsymbol{\rho}' F(\boldsymbol{\rho}')} \right|^2, \tag{1.50}$$

[18] We assume that $\langle I \rangle$ and $V_{\rm R}$ are constant in the spatial region of interest.

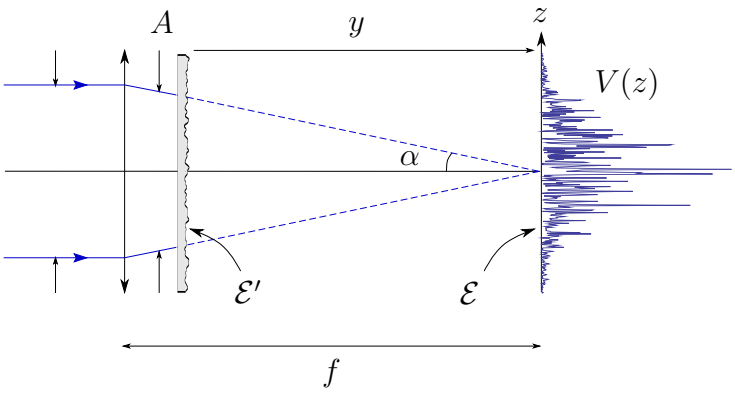


Figure 1.10: Typical set-up for an experiment with speckle potentials. The speckle pattern is observed behind a diffusing plate, in the back focal plane of a lens, where the atoms are placed. The correlation functions of the speckle field $\mathcal{E}$ can be designed by choosing the shape and size of the aperture A and the intensity profile of the free laser beam. A speckle potential V can be created which, on the scale of the cloud of atoms, varies only along the z-direction.

where $C_2^{\perp}(\boldsymbol{\rho}_1 - \boldsymbol{\rho}_0)$ is the two-point autocorrelation function of the speckle potential. Equation (1.48) shows that the two-point correlation function of the intensity pattern (and of the speckle potential V) in the transverse plane directly depends on the Fourier transform of the intensity distribution $F(\boldsymbol{\rho}')$ on the diffuser. Therefore, the typical speckle grain correponds to the diffraction spot associated with the illuminated portion of the diffuser. A broad intensity distribution $F(\boldsymbol{\rho}')$ implies small speckle grains (i.e. a small correlation length σ_{R}), while a narrow distribution creates large grains.

Experiments - The correlation functions can be directly controlled in the experiments by changing the aperture of the optical system, thereby modifying the intensity pattern $\langle|\mathcal{E}'(\boldsymbol{\rho}')|^2\rangle$ on the diffuser. A typical experimental setup is sketched in Fig. 1.10. A lens is added in front of the diffusive plate to concentrate the laser power on the atoms, but the wave-front curvature imposed by the lens does not modify the correlation properties of the speckle pattern in the back focal plane. The aperture A, on the other hand, limits the portion of the diffuser which is illuminated, and its geometry is used to control the correlation functions. High numerical apertures allow to produce correlation lengths σ_{R} of the order of the laser wave length λ_{L}.[19] Small correlation lengths are important, for instance, for the observation of Anderson localization on small, measurable length scales. Conversely, the aperture can be made narrow in a given direction to create random potentials which are effectively translation invariant in that direction. Figure 1.8 shows the speckle pattern obtained with a rectangular aperture which is wide in one direction, and narrow in the other. The result is a highly anisotropic speckle pattern, which can be used as a truly 1D random potential.

[19] A correlation length σ_{R} of $0.26\,\mu$m was achieved in Ref. [29]. A precise definition of the correlation length in the context of speckle potentials is given below.

Original features

Speckle potentials are easily tuned in amplitude, geometry and correlation length. They are also interesting from a fundamental point of view for a number of reasons. First, speckle potentials have special long-range correlations that correspond to a sharp cutoff in their spatial Fourier spectrum. Second, they form a class of non-Gaussian potentials, which nevertheless inherit some of the properties of a Gaussian field. Both of these features can be exploited to study the role of correlations in an original (but realistic) model of disorder.

Cutoff in the Fourier spectrum - Information about the spatial Fourier components of the speckle potential in a transverse plane (at constant distance y in Fig. 1.9(b)) are obtained from the Fourier transforms of Eqs. (1.46) and (1.48). For the field correlation function, the Fourier transform reads

$$\hat{C}_{\mathcal{E}}^{\perp}(\mathbf{q}) \propto F\left(-\frac{y}{k_{\mathrm{L}}}\mathbf{q}\right), \tag{1.51}$$

where $F(\boldsymbol{\rho}') = \langle|\mathcal{E}'(\boldsymbol{\rho}')|^2\rangle$ is the intensity profile on the diffuser. Due to the finite aperture of the optical system, F has a compact support, and $\hat{C}_{\mathcal{E}}^{\perp}(\mathbf{q})$ vanishes identically for $|\mathbf{q}|$ exceeding some critical value k_c. For speckle potentials, we now *define* the correlation length σ_{R} as the inverse of this cutoff:[20]

$$\sigma_{\mathrm{R}} \equiv \frac{1}{k_c}. \tag{1.52}$$

For the two-point correlation function of the potential, one obtains

$$\frac{\hat{C}_2^{\perp}(\mathbf{q})}{\hat{C}_2^{\perp}(\mathbf{0})} = \frac{\int \mathrm{d}\boldsymbol{\rho}' F(\boldsymbol{\rho}')F(\boldsymbol{\rho}' + \frac{y}{k_{\mathrm{L}}}\mathbf{q})}{\int \mathrm{d}\boldsymbol{\rho}' F(\boldsymbol{\rho}')^2}. \tag{1.53}$$

For $|\mathbf{q}| > 2k_c$, the supports of $F(\boldsymbol{\rho}')$ and $F(\boldsymbol{\rho}' + \frac{y}{k_{\mathrm{L}}}\mathbf{q})$ have no overlap, and the Fourier transform of the autocorrelation function of the potential vanishes. In other words, the random potential V has no spatial Fourier component such that $|\mathbf{q}| > 2k_c$. The presence of a cutoff k_c is a generic property of speckle potentials, which is related to the way they are produced. This cutoff distinguishes speckle potentials from white-noise potentials, which have a flat Fourier spectrum, but also from other standard models of disorder with a Fourier spectrum which decays smoothly at infinity (e.g. impurity potentials with exponential, Gaussian, or Lorentzian two-point correlator). The sharp cutoff in Fourier space also implies that speckle potentials have long-range correlations. We shall see in chapter 2 that it has a strong effect on localization in 1D.

Higher-order statistics - Speckle potentials derive from the intensity of a speckle pattern, that is, from the squared modulus of the field amplitude $\mathcal{E}$. Since $\mathcal{E}$ is a Gaussian random field, all the correlation functions of a speckle potential can be expressed in terms of an elementary brick, the two-point field-field correlation function $\langle\mathcal{E}_j^*\mathcal{E}_i\rangle$ [181]. The first example is provided by Eqs. (1.46) to (1.48). More generally, the n-point correlation function of the speckle potential

[20] As such, σ_{R} corresponds typically to a minimal length scale on which the speckle potential varies, i.e. to the speckle grain size.

is found to expand as

$$\langle V_0 V_1 \cdots V_{n-1} \rangle \propto \sum_{\Pi \in S'_n} \langle \mathcal{E}^*_{\Pi(0)} \mathcal{E}_0 \rangle \langle \mathcal{E}^*_{\Pi(1)} \mathcal{E}_1 \rangle \cdots \langle \mathcal{E}^*_{\Pi(n-1)} \mathcal{E}_{n-1} \rangle, \tag{1.54}$$

where S'_n denotes an ensemble of permutations of the indices $0, \ldots, n-1$. Precisely, the elements of S'_n are those permutations which leave no index unchanged.[21] The latter criterion stems from the requirement $\langle V \rangle = 0$. Expression (1.54) reveals that i) since the third-order correlation function ($n = 3$) does not vanish, speckle potentials are non-Gaussian, ii) they nevertheless factor almost as Gaussian potentials do, iii) each of the factors in Eq. (1.54) has the same cutoff at a critical value k_c for Fourier components in the transverse plane. In the following, we shall examine systems confined to the transverse plane, so that each of the field-field correlators has a cutoff in Fourier space.

1.4 Conclusion

Disorder is present everywhere, and understanding its repercussions on the properties of physical systems is of prime importance, as even as small amount of disorder may have large effects.

From condensed-matter physics emerged the concept of Anderson localization, or the discovery that the presence of disorder at the microscopic scale may completely suppress the transport of quantum particles and waves, due to coherent scattering and inteference. As the basic ingredients of Anderson localization are just disorder and coherence, this phenomenon is transversal to various domains of physics, ranging from solid-state to atomic physics, and from optics to acoustics. Anderson localization is a pure single-particle effect, which is particularly strong in lower dimensions.

The physics of disordered quantum systems is even richer when interactions are present, as the interplay of disorder and interactions may trigger transitions to quantum phases which are absent from clean systems. Among those, the superfluid-insulator transition of disordered bosons is an interesting case, as the system becomes insulating both at strong and at very weak interactions, for quite distinct reasons. A precise picture of the insulating regime at weak interactions is lacking. In particular, the transition from the superfluid to the insulating regime, the limiting case of very weak interactions, and the regime in between are of particular interest.

Ultracold quantum gases offer appealing possibilities to study disordered quantum systems, as many parameters, such as the quantum statistics, the dimensionality and the strength of interactions, may be chosen in the experiments [16]. Furthermore, disorder may be created in a controlled fashion with optical potentials. These potentials are easily implemented, and allow to study the effect of disorder correlations.

In the following chapters, we examine the role of both statistical correlations of the random potential and interactions on the localization of bosons in one dimension.

[21] Formula (1.54) is discussed in further detail in appendix A.

CHAPTER 2

Anderson localization of single particles in correlated one-dimensional disorder: beyond the Born approximation

A small amount of disorder can strongly affect the properties of non-interacting waves and quantum particles. While incoherent scattering from the random defects of a disordered medium results in diffusive transport, coherent interference effects may lead to a complete suppression of diffusion and prevent the waves from extending to infinity [37]. This was first put forward by Anderson in 1958 to explain certain metal-insulator transitions in electronic systems [1]. In his analysis, Anderson showed that single electrons introduced into a disordered lattice may not diffuse away from their original location, and that the presence of a random potential may instead *localize* them by leading to an exponential decay of their wave functions in space. Subsequent theoretical and experimental work revealed that Anderson localization arises with a great variety of waves [2, 35].

The onset of Anderson localization depends crucially on the dimension of the system [53]. The effect of disorder is at its strongest in 1D, where the particles are scattered either in the forward or the backward direction, and single particles are exponentially localized on a length scale (the *localization length*) which is simply proportional to the transport mean free path [75].

Rigorous proofs have been given for the 1D localization problem (see section 2.1.2), and all particles are known to be localized under fairly general assumptions, irrespective of their energy [2]. This strong property should not eclipse subtles dependencies of the localization process on the statistical properties of the disorder, e.g. long-range correlations. Interesting effects have been shown to arise with models of disorder whose power spectrum has a finite support [29,34,182,183], and for which leading-order perturbation theory predicts an absence of backscattering and, hence, of localization on an extended region of the single-particle spectrum.

In this chapter, we study the localization of non-interacting particles in weak, correlated random potentials. A perturbative calculation of the Lyapunov exponent, or inverse localization length, is carried out beyond the usual leading-order approximation to account for higher-order scattering processes. The results are applied to speckle potentials [181] such as those currently used in experiments with ultracold atoms [15, 26, 29]. In addition to a high-momentum cutoff in their power spectrum, speckle potentials have special non-Gaussian statistics deriving from a Gaussian field (see chapter 1). For this class of disorder, we show the existence of a series of sharp crossovers (*effective mobility edges*) between regions of the single-particle energy spectrum where the localization lengths differ by orders of magnitude.

The chapter is organized as follows. In section 2.1, we define the framework of our study, and we briefly present the body of studies and proofs of localization in 1D. In section 2.2 we carry out a perturbation calculation of the Lyapunov exponent two orders beyond the usual Born

approximation, and obtain formulas which are valid for any model of correlated disorder. In section 2.3 we apply our expressions to speckle potentials. The existence of a series of effective mobility edges is discussed for generic speckle potentials. The first few orders of the Lyapunov exponent are calculated explicitly for a simple speckle model and compared to the results of numerical transfer matrix calculations. Finally, we use our results to examine localization beyond the effective mobility edge found in recent theoretical and experimental studies with ultracold atoms in speckle potentials.

2.1 Framework

2.1.1 Single particles in correlated one-dimensional disorder

In this chapter, we consider non-interacting particles in an infinite 1D system. These particles are described by the time-independent Schrödinger equation

$$-\frac{\hbar^2}{2m}\partial_z^2\psi(z) + V(z)\psi(z) = E\psi(z), \tag{2.1}$$

where E is the energy of the particle, and V is a random potential drawn from some statistical ensemble. Without loss of generality, we assume that V has zero average, i.e. $\langle V\rangle = 0$, where $\langle .\rangle$ denotes statistical averaging. The statistical properties of the potential are assumed to be homogeneous, which means that they do not depend on the (absolute) position in the system.

Correlation functions

In the framework of this chapter, a sufficient characterization of the random potential is given by the set of n-point autocorrelation functions

$$\begin{aligned} C_2(z_1) &= \langle V(z_0)V(z_0+z_1)\rangle & (2.2)\\ C_3(z_1,z_2) &= \langle V(z_0)V(z_0+z_1)V(z_0+z_2)\rangle & (2.3)\\ \cdots &= \cdots & \\ C_n(z_1,\cdots,z_{n-1}) &= \langle V(z_0)V(z_0+z_1)\cdots V(z_0+z_{n-1})\rangle & (2.4)\\ \cdots &= \cdots & \end{aligned}$$

A key assumption is the disappearance of statistical correlations between the values taken by the potential at points with infinitely large separation.[1] Since $\langle V\rangle = 0$, this implies that the correlation function C_n vanishes as soon as any point in $\{z_0, z_0+z_1, \cdots, z_0+z_{n-1}\}$ is sent to infinite distances from *all* the other points. In particular, the two-point correlator $C_2(z_1)$ drops to zero for $z_1 \to \infty$.

We call correlation length σ_{R} a typical width[2] of C_2, and define reduced correlation functions c_n by

$$C_n(z_1, z_2, \cdots, z_{n-1}) = V_{\text{R}}^n c_n(u_1, u_2, \cdots, u_{n-1}), \tag{2.5}$$

[1] This requirement naturally excludes periodic potentials, or the quasi-periodic potentials used in certain studies of Anderson localization [184].

[2] A precise definition might depend on the model of disorder or some choice of normalization (see chapter 1).

where $u_i = z_i/\sigma_{\mathrm{R}}$. The factor V_{R} may take positive as well as negative values. Allowing negative values of V_{R} is useful for the description of potentials with asymmetric probability distribution, such as speckle potentials (see section 2.3). The magnitude of V_{R} is defined as the root-mean-square amplitude of the disorder

$$|V_{\mathrm{R}}| = \sqrt{\langle V^2 \rangle} = \sqrt{C_2(0)}. \tag{2.6}$$

The limit of *white noise*, or uncorrelated disorder, corresponds to taking $\sigma_{\mathrm{R}} \to 0$ while keeping $V_{\mathrm{R}}^2 \sigma_{\mathrm{R}}$ constant [see Eq. (2.46)].

Lyapunov exponent

Single-particle states in 1D, which are defined as solutions of the Schrödinger equation (2.1) with the requirement that their wave function ψ_E be normalizable, are almost surely localized in the presence of disorder. The rate of exponential decay of the wave functions is given by the Lyapunov exponent

$$\gamma_E = - \lim_{|z-z_0|\to\infty} \left\langle \frac{\ln\left[\|\psi_E(z)\| \,/\, \|\psi_E(z_0)\|\right]}{|z - z_0|} \right\rangle. \tag{2.7}$$

In definition (2.7), $\|.\|$ is a norm, chosen as the modulus $|\,.\,|$ if the wave functions ψ_E are complex, and defined by $\|\psi_E(z)\| = \sqrt{\psi_E(z)^2 + \alpha[\partial_z \psi_E(z)]^2}$ if they are required to be real. In the latter case, α is a positive constant, which is introduced to avoid the cancelling of $\|\psi_E(z)\|$ at the nodes of $\psi_E(z)$, and can be chosen arbitrarily without altering γ_E. A common choice is $\alpha = \hbar^2/2mE = 1/k^2$ (see section 2.2.1). The angular brackets in expression (2.7) indicate averaging with respect to the probability law of V.

A convenient way to calculate the Lyapunov exponent, both numerically and analytically, consists in solving the Schrödinger equation for fixed E and initial conditions at some point z_0 in space, e.g. $\psi_E(z_0) = a$ and $\partial_z \psi_E(z_0) = b$. With probability one, such a function grows exponentially instead of decaying (see section 1.1.3), and the rate of asymptotic growth is obtained by using expression (2.7) with a plus sign. In that case, ψ_E does not correspond to an eigenstate of the system, but the Lyapunov exponent extracted from its asymptotic behavior nevertheless yields the rate of exponential decay of the eigenstates which lie (almost) at the same energy.

2.1.2 One-dimensional Anderson localization

Proofs of localization in 1D

The localization problem in one dimension has been studied for decades, with various techniques, and a wealth of results is available [37, 65, 75, 185–187].

The most important result might be that in 1D, quite loosely stated, almost all single-particle states are localized. Mott and Twose [188] are credited for having first pointed out with qualitative arguments that it might be so, and a first proof in the physical literature is attributed to Borland [189], who showed the exponential localization of all states in a chain of identical, non-overlapping potential barriers with random separation. In an earlier work of 1959, Gertsenshtein and Vasil'ev had actually already derived and solved Fokker-Planck equations describing the complete transmission statistics of waves sent through a 1D waveguide

with weak uncorrelated disorder [75, 190]. The conclusion that all states are localized in 1D is now well established, as it was also reached from scaling arguments [53, 66], diagrammatic calculations [185, 191], as a by-product of exact scaling equations for the (multi-channel) quasi-1D geometry [75, 76] or field-theoretical methods [192].

First mathematical proofs of Anderson localization in 1D for the continuous Schrödinger operator appeared in the late seventies [193–195]. These early proofs assumed some kind of absence of correlation. Interestingly, localization in models with correlations is an active field of research in the mathematical literature (see e.g. [196–198]).

Why study correlations ?

The absence of spatial correlations in the random potential is a very common assumption in the physical literature[3] because (i) calculations and proofs can be carried out much more easily with delta correlation functions, (ii) the replacement of the true disorderd potential by a delta-correlated one might not be the strongest approximation made in certain fields (e.g. in condensed matter), (iii) under certain physical circumstances only long-wavelength excitations might be relevant to determine the properties of a system, and on the scale of those excitations the random potential appears as uncorrelated disorder [147], (iv) some qualitative conclusions may indeed remain unchanged in the presence of correlations.

Nevertheless, considering correlations may be relevant, for instance, in the context of ultracold atoms, as these systems both offer a high degree of control, and a relatively easy *ab initio* description. What is more, the observation that certain correlated potentials might give rise to interesting physics or require special care is supported by two well-known models.

The first of these models is the bichromatic lattice potential of the Aubry-André model [184], which is immediately relevant to experiments with ultracold lattice gases [30], and which yields an interesting localization-delocalization transition even in 1D. Such a potential has only a discrete set of incommensurate Fourier components and is therefore called quasi-periodic. While this potential may locally resemble true short-range disorder, one quite naturally expects almost identical copies of a given potential pattern, analogous to a revival of Rabi oscillations in the time domain, to occur in systems that are large enough. Such revivals traduce long-range correlations even for highly incommensurate frequencies.[4] Some recent experiments have provided evidence of the striking features of this 1D model [30, 199].

The second example is the random dimer model, a lattice Schrödinger model akin to the Anderson model [1], with the difference that the random on-site energies are distributed among pairs of neighboring sites instead of individual ones [200]. This model was first said to exhibit a considerable set of extended states and a so-called superdiffusive behavior, that is, a departure from the diffusionless localized regime. This claim led to some controversy, and it is now established mathematically that the eigenstates in this model are exponentially localized for all but two critical energies [201], and yet there is mathematical support for superdiffusive behavior [202]. This particular behavior can be attributed to the strong pair correlation enforced by the model.

Neither of the above examples contradicts the approximate statement that in 1D, and for

[3] See e.g. the scaling theory exposed in Ref. [66], to cite only one of the most prominent examples.

[4] Correlation functions in quasi-periodic systems do not fall off at infinity. For this reason at least, quasi-periodic potentials cannot be handled with the techniques of the present chapter.

true disorder, all states are localized in the spectral sense except, possibly, for a set of measure zero. They do however show that there is room for rich physics and interesting considerations beyond such a general statement, due to correlations. The speckle potentials which have been used in recent experiments with ultracold atoms [25–27, 203] have a twofold appeal in this respect. First of all, from the experimental point of view, they are easily set up and calibrated [31]. Their properties are robust against experimental imperfections and determined by a small number of parameters (amplitude and correlation length) which can be tuned in the experiments. Then, from the theoretical point of view, speckle potentials form a class of disorder with interesting statistical properties, namely (i) a skewed single-point probability distribution (the potential is not invariant under the change $V_{\mathrm{R}} \to -V_{\mathrm{R}}$), (ii) particular non-Gaussian statistics deriving from a Gaussian process, and (iii) particular long-range correlation functions, which are associated with a sharp cutoff in their Fourier spectrum. The impact of this cutoff on localization properties is discussed in section 2.3.

2.2 Weak-disorder expansion for the Lyapunov exponent

Exact results are difficult to derive for disorder of arbitrary strength, except in a few limiting cases, and one has to resort to numerical calculations or perturbation expansions around an exactly solvable situation to gain insight. Notable exceptions are non-perturbative results obtained for white-noise potentials, for potentials of non-overlapping impurities, or in the vicinity of some special points of the spectrum [162,163,204–208]. No such exact results are available for correlated potentials.[5] The Lyapunov exponent can nevertheless be calculated perturbatively. A robust formalism to do so in 1D, while covering most of the single-particle energy spectrum and all types of correlated continuous potentials, is the phase formalism presented below.

Subsections 2.2.2 and 2.2.3 contain the technical details of the perturbation expansion. The results are summarized in subsection 2.2.4.

2.2.1 Phase formalism for the Schrödinger operator

Phase variable

Consider a real-valued solution ψ of the Schrödinger equation (2.1) at energy E. A representation which proves efficient for the localization problem in 1D is obtained by introducing amplitude and phase coordinates (r, θ) such that

$$\psi(z) = r(z)\sin[\theta(z)] \tag{2.8}$$

$$\partial_z\psi(z) = k\, r(z)\cos[\theta(z)], \tag{2.9}$$

where k is defined from the energy E by

$$E = \frac{\hbar^2 k^2}{2m}. \tag{2.10}$$

This transformation simply amounts to a polar representation of the vector $[\psi(z), \partial_z\psi(z)/k]^{\mathrm{T}}$, and is always possible once ψ is chosen real (see Fig. 2.1). Note that the phase θ and the

[5] The scattering from non-overlapping impurities, for instance, can still be treated as a random sequence of uncorrelated events.

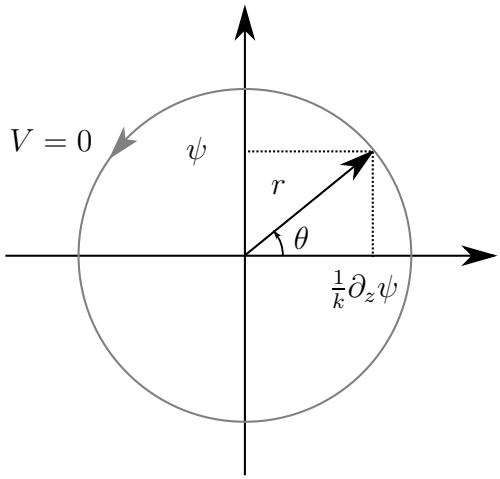


Figure 2.1: Phase formalism for the Schrödinger particle of energy $E = \hbar^2 k^2/2m$. In the absence of an external potential ($V = 0$), the evolution of the eigenstate ψ with respect to coordinate z is described by a circular orbit $r(z) = r_0$, and the Prüfer phase $\theta(z)$ grows linearly at rate k.

amplitude r introduced in this picture differ from those which would be obtained in the polar representation of a complex wave function $\tilde{\psi} = \tilde{r}\exp(\mathrm{i}\tilde{\theta})$.

With these coordinates, the logarithmic derivative of the wave function reads

$$\frac{\partial_z\psi(z)}{\psi(z)} = k\,\mathrm{cotan}[\theta(z)]. \tag{2.11}$$

Taking the derivative of both sides of this expression with respect to z and using the Schrödinger equation (2.1) we obtain

$$-\frac{k\,\partial_z\theta}{\sin^2(\theta)} = \frac{\partial_z^2\psi}{\psi} - \left(\frac{\partial_z\psi}{\psi}\right)^2 = \frac{2m}{\hbar^2}V - k^2(1+\mathrm{cotan}^2\theta), \tag{2.12}$$

and a closed equation for θ follows:

$$\partial_z\theta(z) = k - \frac{2mV(z)}{\hbar^2 k}\sin^2[\theta(z)]. \tag{2.13}$$

In the process, we have traded the linear, second-order Schrödinger equation, for a first-order, non-linear differential equation for the phase θ alone. The absence of the amplitude r from the equation for the phase θ has to be traced back to the representation of the real-valued function ψ [see Eqs. (2.8) and (2.9)]. No such closed equation is found for the phase $\tilde{\theta}$ of a complex function $\tilde{\psi} = \tilde{r}\exp(\mathrm{i}\tilde{\theta})$. The formal solution of Eq. (2.13) is

$$\theta(z) = \theta_0 + kz - \frac{2m}{\hbar^2 k}\int_0^z \mathrm{d}z' V(z')\sin^2[\theta(z')], \tag{2.14}$$

where $\theta_0 = \theta(0)$ is taken as initial condition.

Remark - The phase variable θ sometimes appears in the mathematical literature under the name of Prüfer phase.[6]

Lyapunov exponent

The spatial dependence of the amplitude

$$r = \sqrt{\psi^2 + \frac{(\partial_z \psi)^2}{k^2}} \tag{2.15}$$

is determined by

$$\partial_z \ln(r) = \frac{\partial_z r^2}{2r^2} = \frac{1}{2r^2}\partial_z \left[\psi^2 + \frac{(\partial_z\psi)^2}{k^2}\right] = \frac{\partial_z \psi}{r^2}\left[\psi + \frac{\partial_z^2 \psi}{k^2}\right] = \frac{2mV\psi\,\partial_z\psi}{\hbar^2 k^2 r^2}, \tag{2.16}$$

where the last equality follows from (2.1). The amplitude r is a norm of the wave function ψ, such as the one defined below Eq. (2.7), with $\alpha = \hbar^2/2mE = 1/k^2$. Finally, using Eqs. (2.8) and (2.9) we obtain

$$\partial_z \ln[r(z)] = \frac{mV(z)}{\hbar^2 k}\sin[2\theta(z)], \tag{2.17}$$

or, equivalently,

$$\ln[r(z)/r_0] = \frac{m}{\hbar^2 k}\int_0^z \mathrm{d}z' V(z')\sin[2\theta(z')]. \tag{2.18}$$

The latter expression is especially relevant in the context of localization, since the amplitude $r(z)$ of localized eigenstates is expected to scale exponentially with the distance z from the origin. In the framework of the phase formalism, the Lyapunov exponent is defined as

$$\gamma(k) = +\lim_{|z|\to\infty} \frac{\langle \ln[r(z)/r_0]\rangle}{|z|}, \tag{2.19}$$

which is left to compute from Eq. (2.18). The plus sign in Eq. (2.19) is set assuming that the function ψ is determined by initial conditions.[7]

2.2.2 Born approximation

Equation (2.14) is a closed equation for the phase which, for a weak potential V, can be solved in a perturbation expansion

$$\theta(z) = \sum_{n=0}^{\infty} \theta^{(n)}(z), \tag{2.20}$$

[6] The phase angle θ was originally introduced by Prüfer [209]. It is a standard tool for the study of the 1D Schrödinger equation, as well as a broader class of differential equations called Sturm-Liouville problems [210]. Sturm theory is associated to the well-known result that, for the Schrödinger operator, the number of states up to energy E is related to the number of nodes found in an eigenfunction at energy E. The phase formalism has been used extensively since the early studies on the localization problem in the physics litterature, with a special emphasis on the density of states [186], and in some mathematical proofs of localization (see e.g. Refs. [193, 211]). The connection with more general Sturm-Liouville problems, as e.g. obtained from coupled 1D Schrödinger equations, is interesting to keep in mind, as it might be possible to calculate the Lyapunov exponent for quasi-1D geometries as well, using a matrix version of the Prüfer phase [210, 212–216].

[7] See section 1.1.3 and the discussion below Eq. (2.7).

where the superscripts indicate increasing powers of the potential amplitude $V_{\rm R}$ [see Eq. (2.6)]. As we are interested in asymptotic properties of the wave function and will ultimately take the limit $|z| \to \infty$, we choose the origin $z_0 = 0$ such that $\theta_0 = 0$ to simplify the notations.[8] Hence, we have

$$\theta^{(0)}(z) = kz \tag{2.21}$$

$$\theta^{(1)}(z) = -\frac{2m}{\hbar^2 k}\int_0^z \mathrm{d}z' V(z')\sin^2(kz'). \tag{2.22}$$

For notational convenience, we define $x(z) = \ln[r(z)/r_0]$. Then, we write the expansions of Eqs. (2.18) and (2.19) in the form

$$\ln[r(z)/r_0] = \sum_{n=1}^{\infty} x^{(n)}(z) \tag{2.23}$$

$$\gamma = \sum_{n=1}^{\infty} \gamma^{(n)}. \tag{2.24}$$

Equation (2.24) can be called the Born series for the Lyapunov exponent, in analogy with the infinite perturbation series solving implicit problems like Eq. (2.14) by iterated insertions. Expanding the sine function in the integrand of Eq. (2.18) to first order as

$$\sin[2\theta(z')] = \sin[2\theta^{(0)}(z')] + 2\cos[2\theta^{(0)}(z')]\theta^{(1)}(z') + \cdots, \tag{2.25}$$

we obtain

$$x^{(1)}(z) = \frac{m}{\hbar^2 k}\int_0^z \mathrm{d}z' V(z')\sin(2kz') \tag{2.26}$$

$$x^{(2)}(z) = \left(\frac{m}{\hbar^2 k}\right)^2 \int_0^z \mathrm{d}z' \int_0^{z'} \mathrm{d}z'' V(z')V(z'')\left[-4\cos(2kz')\sin^2(kz'')\right]. \tag{2.27}$$

Taking the average of Eq. (2.26), and owing to the prescription $\langle V\rangle = 0$, we have

$$\langle x^{(1)}(z)\rangle = \frac{m}{\hbar^2 k}\int_0^z \mathrm{d}z' \langle V(z')\rangle \sin(2kz') = 0 \tag{2.28}$$

$$\gamma^{(1)} = \lim_{|z|\to\infty} \frac{\langle x^{(1)}(z)\rangle}{|z|} = 0. \tag{2.29}$$

The average of Eq. (2.27) reduces to

$$\langle x^{(2)}(z)\rangle = \left(\frac{m}{\hbar^2 k}\right)^2 \int_0^z \mathrm{d}z' \int_0^{z'} \mathrm{d}z'' C_2(z''-z')\left[-4\cos(2kz')\sin^2(kz'')\right] \tag{2.30}$$

$$= \left(\frac{m}{\hbar^2 k}\right)^2 \int_0^z \mathrm{d}z' \int_{-z'}^{0} \mathrm{d}z_1 C_2(z_1)\left[-4\cos(2kz')\sin^2(kz'+kz_1)\right]. \tag{2.31}$$

From this expression we need to extract

$$\gamma^{(2)} = \lim_{|z|\to\infty} \frac{\langle x^{(2)}(z)\rangle}{|z|}. \tag{2.32}$$

[8] This is always possible with a suitable translation to a node of the wave function, provided the energy of the particle is high enough for the wave function to have a node. In practice, this will always be the case in the regime of validity of the perturbative results derived in this chapter (see below).

The quickest route

Integral (2.31) is represented schematically in Fig. 2.2. An inspection of the integrand and the domain of integration allows a quick calculation which circumvents an explicit evaluation of $\langle x^{(2)}(z)\rangle$ for all z.

The limit (2.32) can be argued to follow from (2.31) as [9]

$$\gamma^{(2)} = \Big(\frac{m}{\hbar^2 k}\Big)^2 \int_{-\infty}^{0} \mathrm{d}z_1 C_2(z_1) \lim_{z\to\infty} \frac{1}{z} \int_0^z \mathrm{d}z' \left[-4\cos(2kz')\sin^2(kz'+kz_1)\right]. \tag{2.33}$$

Between Eq. (2.31) and Eq. (2.33), the order of integration on z' and z_1 has been interchanged, and the integration boundary for z_1 sent to $-\infty$. The latter step is reasonable if C_2 falls off "quickly enough" when z_1 becomes larger than a few σ_{R}. The limit in the integral (2.33) is then easily obtained as an average of the trigonometric integrand with respect to z'. A straightforward calculation leads to

$$\gamma^{(2)} = \Big(\frac{m}{\hbar^2 k}\Big)^2 \int_{-\infty}^{0} \mathrm{d}z_1 C_2(z_1)\cos(2kz_1). \tag{2.34}$$

The assumption that V has homogeneous statistical properties implies that $C_2(z)$ is an even (and real-valued) function of z. The above result therefore also writes

$$\gamma^{(2)} = \frac{\sqrt{2\pi}}{2}\Big(\frac{m}{\hbar^2 k}\Big)^2 \hat{C}_2(2k), \tag{2.35}$$

where $\hat{C}_2$ is the Fourier transform of the two-point correlation function C_2. This Fourier transform can also be referred to as the power spectrum[10] of V.

Formulation in Fourier space

Result (2.34) can be given a rigorous footing by considering

$$\langle x^{(2)}_{\eta_1}(z)\rangle = \Big(\frac{m}{\hbar^2 k}\Big)^2 \int_0^z \mathrm{d}z' \int_{-z'}^{0} \mathrm{d}z_1\, C_2(z_1)\, \mathrm{e}^{+\eta_1 z_1} \left[-4\cos(2kz')\sin^2(kz'+kz_1)\right], \tag{2.36}$$

where $\eta_1 > 0$. Then, the exponent $\gamma^{(2)}$ is given by

$$\gamma^{(2)} = \lim_{z\to+\infty} \lim_{\eta_1\to 0^+} \frac{\langle x^{(2)}_{\eta_1}(z)\rangle}{z}. \tag{2.37}$$

[9] The argument reads as follows. Without loss of generality, we can restrict z to the positive axis as $\langle x^{(2)}(z)\rangle$ is an even function of z. A schematic picture of the integrals in Eqs. (2.30) and (2.31) is given in Fig. 2.2. Partial integration on the domain $z' \in [0, z_{\mathrm{part}}]$ in Eq. (2.31), where z_{part} is some constant, yields a finite result whose contribution to $\langle x^{(2)}(z)\rangle/z$ vanishes once z is send to infinity. For every z_{part}, the distance z can be chosen large enough to make this contribution negligible in the evaluation of the Lyapunov exponent. Thus, we can consider that only large z' contribute to the asymptotic form of the double integral. By large we mean that a minimum value of z' can be chosen which exceeds an arbitrary number of correlation lengths. The lower bound of the integral on z_1 can then be approximated by $-\infty$ due to the decay of the correlator C_2 beyond a few correlation lengths. Once the lower bound for z_1 has been sent to $-\infty$, the order of integration can be swapped, which yields Eq. (2.33).

[10] The Wiener-Khintchin theorem establishes the equality $\hat{C}_2(q) = (2\pi)^{d/2}\langle|\hat{V}(q)|^2\rangle$, where $\langle|\hat{V}(q)|^2\rangle$ is the power spectrum of V, and the factor $(2\pi)^{d/2}$ comes from the normalization of the Fourier transform.

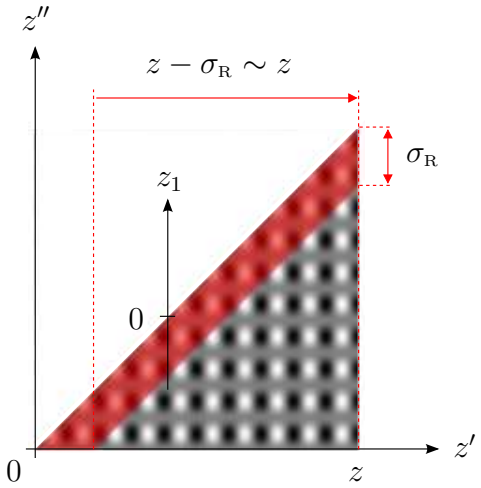


Figure 2.2: Domain of integration for the evaluation of the Lyapunov exponent $\gamma^{(2)}$. The periodic structure represents the trigonometric part of the integrand in Eqs. (2.30) and (2.31). The two-point correlator is constant on lines parallel to the diagonal, and is assumed to drop off "quickly" outside a stripe of typical width σ_{R}, shown in red. For large z', the lower boundary on z_1 can then be effectively taken to $-\infty$. The length of the stripe along z' grows asymptotically as z.

Expressing $C_2(z_1)$ in terms of Fourier components, we have

$$\langle x^{(2)}_{\eta_1}(z)\rangle = \left(\frac{m}{\hbar^2 k}\right)^2 (2\pi)^{-1/2} \int \mathrm{d}q_1 \hat{C}_2(q_1) h_2(q_1, k, \eta_1, z), \tag{2.38}$$

where

$$h_2(q_1, k, \eta_1, z) = \int_0^z \mathrm{d}z' \int_{-z'}^0 \mathrm{d}z_1 \, \mathrm{e}^{\mathrm{i}(q_1 - \mathrm{i}\eta_1)z_1} \left[-4\cos(2kz')\sin^2(kz' + kz_1)\right]. \tag{2.39}$$

An explicit calculation of this integral shows

$$h_2(q_1, k, \eta_1, z) = \frac{z}{2\mathrm{i}} \left[\frac{1}{q_1 - 2k - \mathrm{i}\eta_1} + \frac{1}{q_1 + 2k - \mathrm{i}\eta_1}\right] + \underset{z\to\infty}{\mathcal{O}}(1). \tag{2.40}$$

Hence, for Eq. (2.37) we obtain[11]

$$\gamma^{(2)} = \lim_{\eta_1 \to 0^+} \left(\frac{m}{\hbar^2 k}\right)^2 \frac{(2\pi)^{-1/2}}{2\mathrm{i}} \int \mathrm{d}q_1 \hat{C}_2(q_1) \left[\frac{1}{q_1 - 2k - \mathrm{i}\eta_1} + \frac{1}{q_1 + 2k - \mathrm{i}\eta_1}\right], \tag{2.41}$$

Using the symmetry[12] $\hat{C}_2(q) = \hat{C}_2(-q)$, and the identity

$$\lim_{\eta \to 0^+} \frac{1}{q - \mathrm{i}\eta} = \mathcal{P}\left(\frac{1}{q}\right) + \mathrm{i}\pi\delta(q), \tag{2.42}$$

[11] One has to check that the limits $\eta_1 \to 0^+$ and $z \to +\infty$ commute by looking precisely at the $\mathcal{O}(1)$ term in Eq. (2.40). We leave this calculation aside here.

[12] As $C_2(z)$ is an even and real-valued function of z, its Fourier transform $\hat{C}_2$ is also real and even.

where $\mathcal{P}$ denotes the Cauchy principal value, we find

$$\gamma^{(2)} = \frac{\sqrt{2\pi}}{2} \left(\frac{m}{\hbar^2 k}\right)^2 \hat{C}_2(2k), \tag{2.43}$$

in agreement with result (2.34).

Born approximation

Equation (2.43) is a standard result. Since the first order $\gamma^{(1)}$ vanishes, $\gamma^{(2)}$ provides the leading-order approximation of the exact Laypunov exponent in the weak-disorder expansion. As such, $\gamma^{(2)}$ is called the Born approximation to the Lyapunov exponent.

Result (2.43) calls for a few comments. First, as $\gamma^{(2)}$ is proportional to V_{R}^2, changing the sign of the potential does not change the Lyapunov exponent at this level of approximation. Then, the term $\hat{C}_2(2k)$ suggests that the particle essentially samples the disordered potential at spatial frequency $2k$, and that localization occurs because of elastic backscattering.[13] Finally, the $m/\hbar^2 k$ factor is directly related to the unperturbed kinetic energy of the Schrödinger particle. All other factors left aside, a larger kinetic energy reduces the strength of localization, as expected from the scattering by a weak potential [217].

Altogether, the Lyapunov exponent is determined by the kinetic energy of the particle, and by the availability and amplitude of a Fourier component in the disorder which is able to backscatter the particle elastically.

White-noise limit

A given model of disorder is defined by the set of reduced correlation functions c_n defined in Eq. (2.5). The corresponding white-noise potential is obtained by taking the limit $\sigma_{\mathrm{R}} \to 0$ while keeping $V_{\mathrm{R}}^2 \sigma_{\mathrm{R}}$ constant. The quantity

$$D = \int_{\mathbb{R}} \mathrm{d}z\, C_2(z) = V_{\mathrm{R}}^2 \sigma_{\mathrm{R}} \int_{\mathbb{R}} \mathrm{d}u\, c_2(u) \tag{2.44}$$

is left invariant in the process, and the two-point correlation function tends to[14]

$$C_2^{\mathrm{w.n.}}(z) = D\delta(z). \tag{2.45}$$

For this white-noise potential, the Born approximation for the Lyapunov exponent reads

$$\gamma_{\mathrm{w.n.}}^{(2)} = \frac{m^2 D}{2\hbar^4 k^2}. \tag{2.46}$$

[13] Here the wave function ψ is real-valued, and corresponds in principle to two counter-propagating waves, but the $2k$-component in Eq. (2.43) and the higher-order results (2.81) and (2.41) indicates that the process at work is a process of elastic backscattering in which the potential imparts a momentum $-2\hbar k$ to the particle (wave) and transfers it from $\hbar k$ to $-\hbar k$. The important feature of Eq. (2.43) is the absence of *forward* scattering which, at the level of the Born approximation, involves the component $\hat{C}_2(0)$. Such a contribution is known from the one-particle Green function calculation of the scattering mean-free path [35], and causes dephasing, but no localization.

[14] The constant D appears with different normalizations in the literature [86, 147, 162]. It is sometimes normalized to represent a diffusion term [86]. Here, we simply define D as the integral of the two-point correlator, thereby following Ref. [147].

This expression is also obtained with other techniques, which are suitable for white-noise potentials only[15] [86, 162, 206, 218]. Result (2.43) offers a generalization of (2.46) to correlated potentials.

2.2.3 Phase formalism beyond the Born approximation

The Born term (2.43) provides the leading term of the expansion of the Lyapunov exponent in powers of the disorder amplitude $V_{\rm R}$. Not so much to deal with stronger disorder amplitudes, but rather to study the properties of potentials with special correlations, it proves useful to carry out the weak-disorder expansion a few orders beyond the Born term. In particular, this is the case when the power spectrum $\hat{C}_2(q)$ vanishes identically on some range of Fourier components, and the Born approximation predicts an absence of localization at the corresponding single-particle energies (see section 2.3).

Setup of the expansion

Our starting point is the set of equations (2.14), (2.18) and (2.19) with $\theta_0 = 0$:

$$\theta(z) = \sum_{n=0}^{\infty} \theta^{(n)}(z) = kz - \frac{2m}{\hbar^2 k} \int_0^z \mathrm{d}z' V(z') \sin^2[\theta(z')] \tag{2.47}$$

$$\ln[r(z)/r_0] = \sum_{n=1}^{\infty} x^{(n)}(z) = \frac{m}{\hbar^2 k} \int_0^z \mathrm{d}z' V(z') \sin[2\theta(z')] \tag{2.48}$$

$$\gamma(k) = \sum_{n=1}^{\infty} \gamma^{(n)}(k) = \lim_{|z|\to\infty} \frac{\langle \ln[r(z)/r_0] \rangle}{|z|}. \tag{2.49}$$

The superscripts (n) indicate increasing powers of $V_{\rm R}$ in the series. The various orders are obtained by expanding the functions $\sin^2(\theta)$ and $\sin(2\theta)$ in the above equations into Taylor series around the homogeneous solution $\theta(z') \simeq kz' = \theta^{(0)}(z')$.

Expansion of the phase - The Taylor expansion of Eq. (2.47) takes the form

$$\sum_{n=0}^{\infty} \theta^{(n)}(z) = kz - \frac{m}{\hbar^2 k} \int_0^z \mathrm{d}z' V(z') \left\{ 1 - \sum_{m=0}^{\infty} \frac{2^m}{m!} \cos^{(m)}(2kz') \left[\sum_{p=1}^{\infty} \theta^{(p)}(z') \right]^m \right\}. \tag{2.50}$$

The superscript on the cosine indicates differentiation [$\cos^{(m)}(u) = \mathrm{d}^m \cos(u)/\mathrm{d}u^m(u)$], and should not be confused with the order in $V_{\rm R}$. As each term on the right hand side picks up of factor $V(z')$, the $\theta^{(n)}$ can be calculated recursively. For an expansion of γ up to $\gamma^{(4)}$, we only need to expand the term in the curly brackets above as far as

$$\begin{aligned} 2\sin^2[\theta(z')] \;\simeq\; & 1 - \cos(2kz') \\ & + 2\sin(2kz') \left[\theta^{(1)}(z') + \theta^{(2)}(z') \right] \\ & + 2\cos(2kz') \left[{\theta^{(1)}}^2(z') \right]. \end{aligned} \tag{2.51}$$

[15] In particular, result (2.46) corresponds to the high-energy or weak-disorder expansion $\gamma(E) \sim \sqrt{2m/\hbar^2} \times E_\delta^{3/2}/(4E)$ found for $E_\delta \ll E$ from Eq. (1.14) [86].

Identifying the contributions of same order in $V_{\rm R}$ on the left- and right-hand sides of Eq. (2.50) yields

$$\theta^{(0)}(z) = kz \tag{2.52}$$
$$\theta^{(1)}(z) = -\frac{m}{\hbar^2 k}\int_0^z \mathrm{d}z' V(z')\left[2\sin^2(kz')\right] \tag{2.53}$$
$$\theta^{(2)}(z) = -\frac{m}{\hbar^2 k}\int_0^z \mathrm{d}z' V(z')\left[2\sin(2kz')\,\theta^{(1)}(z')\right] \tag{2.54}$$
$$\theta^{(3)}(z) = -\frac{m}{\hbar^2 k}\int_0^z \mathrm{d}z' V(z')\left[2\sin(2kz')\,\theta^{(2)}(z') + 2\cos(2kz')\,{\theta^{(1)}}^2(z')\right]. \tag{2.55}$$

For notational convenience, we define the functions

$$c_k(z) = \cos(2kz) \tag{2.56}$$
$$s_k(z) = \sin(2kz) \tag{2.57}$$
$$S_k(z) = 2\sin^2(kz). \tag{2.58}$$

The first few terms obtained in the recursive procedure for θ read

$$\theta^{(0)}(z) = kz \tag{2.59}$$
$$\theta^{(1)}(z) = \frac{m}{\hbar^2 k}\int_0^z \mathrm{d}z' V(z')\left[-S_k(z')\right] \tag{2.60}$$
$$\theta^{(2)}(z) = \left(\frac{m}{\hbar^2 k}\right)^2 \int_0^z \mathrm{d}z' \int_0^{z'} \mathrm{d}z'' V(z')V(z'')\left[2s_k(z')S_k(z'')\right] \tag{2.61}$$
$$\theta^{(3)}(z) = \left(\frac{m}{\hbar^2 k}\right)^3 \int_0^z \mathrm{d}z' \int_0^{z'} \mathrm{d}z'' \int_0^{z''} \mathrm{d}z''' V(z')V(z'')V(z''') \left[-4s_k(z')s_k(z'')S_k(z''') - 4c_k(z')S_k(z'')S_k(z''')\right]. \tag{2.62}$$

In the last term of Eq. (2.62) we have used

$${\theta^{(1)}}^2(z') = \left(\frac{m}{\hbar^2 k}\right)^2 \int_0^{z'} \mathrm{d}z'' \int_0^{z''} \mathrm{d}z''' V(z'')V(z''')\left[2S_k(z'')S_k(z''')\right], \tag{2.63}$$

where the original integration domain $[0, z']^2$ has been halved by using the symmetry of the integrand.

Expansion of the amplitude - A similar procedure applied to Eq. (2.48) with the expansion

$$\sum_{n=1}^{\infty} x^{(n)}(z) = \frac{m}{\hbar^2 k}\int_0^z \mathrm{d}z' V(z') \sum_{m=0}^{\infty} \frac{2^m}{m!}\sin^{(m)}(2kz') \left[\sum_{p=1}^{\infty} \theta^{(p)}(z')\right]^m \tag{2.64}$$

yields

$$x^{(1)}(z) = \frac{m}{\hbar^2 k}\int_0^z \mathrm{d}z' V(z')\,[s_k(z')] \tag{2.65}$$

$$x^{(2)}(z) = \frac{m}{\hbar^2 k}\int_0^z \mathrm{d}z' V(z')\,\left[2c_k(z')\theta^{(1)}(z')\right] \tag{2.66}$$

$$x^{(3)}(z) = \frac{m}{\hbar^2 k}\int_0^z \mathrm{d}z' V(z')\,\left[2c_k(z')\theta^{(2)}(z') - 2s_k(z'){\theta^{(1)}}^2(z')\right] \tag{2.67}$$

$$x^{(4)}(z) = \frac{m}{\hbar^2 k}\int_0^z \mathrm{d}z' V(z')\,\left[2c_k(z')\theta^{(3)}(z') - 4s_k(z')\theta^{(1)}(z')\theta^{(2)}(z') - \frac{4}{3}c_k(z'){\theta^{(1)}}^3(z')\right]. \tag{2.68}$$

The first two orders have been discussed in section 2.2.2 [see Eqs. (2.26) and (2.27)]. We recall, in particular, that $\langle x^{(1)}(z)\rangle$ vanishes for all z since $\langle V\rangle = 0$. The analysis of higher orders seems complicated by the growing number of terms involved and the fact that these various contributions are multi-dimensional integrals with different domains. Fortunately, symmetries can be used to reduce the integrals, as in Eq. (2.63). Those integrals which do not have the proper symmetries can be split up into pieces which all have the same domain upon a change of variables. In particular, we can write

$$\begin{aligned}\theta^{(1)}(z')\theta^{(2)}(z') = {} & \left(\frac{m}{\hbar^2 k}\right)^3 \int_0^{z'}\mathrm{d}z''\int_0^{z''}\mathrm{d}z'''\int_0^{z'''}\mathrm{d}z''''\, V(z'')V(z''')V(z'''') \\ & [-2S_k(z'')s_k(z''')S_k(z'''') - 4s_k(z'')S_k(z''')S_k(z'''')]\end{aligned} \tag{2.69}$$

$$\begin{aligned}{\theta^{(1)}}^3(z') = {} & \left(\frac{m}{\hbar^2 k}\right)^3 \int_0^{z'}\mathrm{d}z''\int_0^{z''}\mathrm{d}z'''\int_0^{z'''}\mathrm{d}z''''\, V(z'')V(z''')V(z'''') \\ & [-6S_k(z'')S_k(z''')S_k(z'''')]\,.\end{aligned} \tag{2.70}$$

Collecting all terms in Eqs. (2.67) and (2.68), we obtain

$$x^{(3)}(z) = \left(\frac{m}{\hbar^2 k}\right)^3 \int_0^{z}\mathrm{d}z'\int_0^{z'}\mathrm{d}z''\int_0^{z''}\mathrm{d}z'''\, V(z')V(z'')V(z''')g_3(z',z'',z''') \tag{2.71}$$

$$x^{(4)}(z) = \left(\frac{m}{\hbar^2 k}\right)^4 \int_0^{z}\mathrm{d}z'\int_0^{z'}\mathrm{d}z''\int_0^{z''}\mathrm{d}z'''\int_0^{z'''}\mathrm{d}z''''\, V(z')V(z'')V(z''')V(z'''')g_4(z',z'',z''',z''''). \tag{2.72}$$

where

$$g_3(z',z'',z''') = [\,4\,c_k(z')s_k(z'')S_k(z''') - 4\,s_k(z')S_k(z'')S_k(z''')] \tag{2.73}$$

$$\begin{aligned}g_4(z',z'',z''',z'''') = {} & [-8\,c_k(z')s_k(z'')s_k(z''')S_k(z'''') - 8\,c_k(z')c_k(z'')S_k(z''')S_k(z'''') \\ & + 8\,s_k(z')S_k(z'')s_k(z''')S_k(z'''') + 16\,s_k(z')s_k(z'')S_k(z''')S_k(z'''') \\ & + 8\,c_k(z')S_k(z'')S_k(z''')S_k(z'''')\,]\,.\end{aligned} \tag{2.74}$$

In these expressions, the variables are fully ordered according to $0 \leq z'''' \leq z''' \leq z'' \leq z' \leq z$. The averages of Eqs. (2.71) and (2.72) evaluate to

$$\langle x^{(3)}(z)\rangle = \left(\frac{m}{\hbar^2 k}\right)^3 \int_0^z \mathrm{d}z' \int_{-z'}^0 \mathrm{d}z_1 \int_{-z'}^{z_1} \mathrm{d}z_2\, C_3(z_1,z_2) g_3(z', z'+z_1, z'+z_2) \tag{2.75}$$

$$\langle x^{(4)}(z)\rangle = \left(\frac{m}{\hbar^2 k}\right)^4 \int_0^z \mathrm{d}z' \int_{-z'}^0 \mathrm{d}z_1 \int_{-z'}^{z_1} \mathrm{d}z_2 \int_{-z'}^{z_2} \mathrm{d}z_3\, C_4(z_1,z_2,z_3) g_4(z', z'+z_1, z'+z_2, z'+z_3). \tag{2.76}$$

The asymptotic behavior of $\langle x^{(3)}(z)\rangle$ and $\langle x^{(4)}(z)\rangle$ determines the next orders in the expansion of the Lyapunov exponent.

Exponent $\gamma^{(3)}$

The term $C_3(z_1,z_2) = \langle V(z_0)V(z_0+z_1)V(z_0+z_2)\rangle$ in Eq. (2.75) decays whenever either z_1 or z_2 exceeds a few correlation lengths, due to the factorization property

$$\langle V(z_i)V(z_j)V(z_k)\rangle \to \langle V(z_i)V(z_j)\rangle\langle V(z_k)\rangle \quad \text{for } \min(|z_k - z_i|, |z_k - z_j|) \to \infty. \tag{2.77}$$

As in the derivation of Eq. (2.33), the lower integration boundaries on z_1 and z_2 in Eq. (2.75) can be sent to $-\infty$ and we obtain

$$\gamma^{(3)} = \left(\frac{m}{\hbar^2 k}\right)^3 \int_{-\infty}^0 \mathrm{d}z_1 \int_{-\infty}^{z_1} \mathrm{d}z_2\, C_3(z_1,z_2) \lim_{z\to\infty} \frac{1}{z} \int_0^z \mathrm{d}z' g_3(z', z'+z_1, z'+z_2). \tag{2.78}$$

As g_3 consists only of trigonometric functions, the limit is easily computed as a spatial average, and gives

$$\gamma^{(3)} = -2\left(\frac{m}{\hbar^2 k}\right)^3 \int_{-\infty}^0 \mathrm{d}z_1 \int_{-\infty}^{z_1} \mathrm{d}z_2\, C_3(z_1,z_2) \sin(2kz_2). \tag{2.79}$$

This result can be expressed in terms of

$$\hat{C}_3(q_1,q_2) = \frac{1}{2\pi} \int_{-\infty}^{+\infty} \mathrm{d}z_1 \int_{-\infty}^{+\infty} \mathrm{d}z_2\, C_3(z_1,z_2)\, \mathrm{e}^{-\mathrm{i}(q_1 z_1 + q_2 z_2)}, \tag{2.80}$$

which is called bispectral density (or simply bispectrum) of the random potential V. We obtain

$$\gamma^{(3)} = -2\left(\frac{m}{\hbar^2 k}\right)^3 \mathcal{P} \int \mathrm{d}q \frac{\hat{C}_3(q,2k) + \hat{C}_3(-q,-2k)}{2q}, \tag{2.81}$$

where $\mathcal{P}$ denotes a Cauchy principal value.

Remark - Result (2.81) is also obtained from a careful derivation along the lines of Eqs. (2.36) to (2.43). The calculations involved in such a derivation are cumbersome. Using a software for symbolic calculus, we find

$$\begin{aligned}\gamma^{(3)} = \lim_{\eta_1,\eta_2\to 0^+} \left(\frac{m}{\hbar^2 k}\right)^3 \frac{\mathrm{i}}{2\pi} \int \mathrm{d}q_1 \int \mathrm{d}q_2\, \frac{\hat{C}_3(q_1,q_2)}{(q_1 - \mathrm{i}\eta_1)} \times \\ \left[\frac{1}{(q_2 - 2k - \mathrm{i}\eta_2)} - \frac{1}{(q_2 + 2k - \mathrm{i}\eta_2)} \right. \\ \left. - \frac{1}{(q_1+q_2-2k-\mathrm{i}\eta_1-\mathrm{i}\eta_2)} + \frac{1}{(q_1+q_2+2k-\mathrm{i}\eta_1-\mathrm{i}\eta_2)}\right],\end{aligned} \tag{2.82}$$

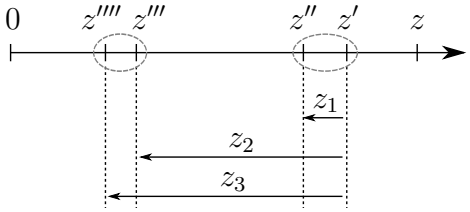


Figure 2.3: Ordering of coordinates in the expression for the fourth-order Lyapunov exponent. As explained in the text, a large separation of z'' and z''' does not imply a vanishing $C_4(z_1, z_2, z_3)$ correlator.

Using the identity (2.42) and the symmetries of the bispectrum[16] $\hat{C}_3$, we recover expression (2.81). This agreement validates the arguments used in Eq. (2.78) for a quick calculation in coordinate space.

Exponent $\gamma^{(4)}$

Factorization of averages - Unlike C_2 and C_3, the four-point correlator C_4 does not necessarily decay as soon as one of its arguments grows beyond a few correlation lengths. Consider, for instance, the case depicted in Fig. 2.3, where the points $z', ..., z''''$ are ordered as in the integrals (2.72) and (2.76). If z'' is sent away from z''' (and from z'''' because of the ordering), we have the factorization

$$\langle V(z')V(z'')V(z''')V(z'''')\rangle \xrightarrow[z''-z'''\to+\infty]{} \langle V(z')V(z'')\rangle\langle V(z''')V(z'''')\rangle. \tag{2.83}$$

If z' and z'' on the one hand, and z''' and z'''' on the other hand are kept at finite distances, the four-point correlator does not necessarily vanish. Therefore, the argument developed for Eqs. (2.31) and (2.75) does not directly apply to the correlator C_4 in Eq. (2.76). This correlator can always be written in the form

$$C_4(z_1, z_2, z_3) = K_4(z_1, z_2, z_3) + C_2(z_1)C_2(z_2 - z_3) + C_2(z_2)C_2(z_3 - z_1) + C_2(z_3)C_2(z_1 - z_2), \tag{2.84}$$

where $K_4(z_1, z_2, z_3)$ is the fourth-order cumulant of the potential (see section 1.3.1). As discussed below Eq. (1.27), $K_4(z_1, z_2, z_3)$ vanishes when one or several of its arguments are sent to infinity. Therefore the technique used for Eqs. (2.31) and (2.75) can be applied to the K_4 part of C_4 at least. The remaining contribution to $\gamma^{(4)}$, which contains the products of two-point correlators, needs to be calculated carefully.

Non-Gaussian part - The fourth-order cumulant K_4 vanishes for Gaussian disorder (see section 1.3.2). Therefore, we may call non-Gaussian part $\gamma^{(4)}_{\rm NG}$ the contribution to $\gamma^{(4)}$ which arises from K_4 alone [219, 220]. Applying the argument developed in Eqs. (2.33) and (2.78), we

[16] Here we use $\hat{C}_3(q_1, q_2) = \hat{C}_3(q_1, -q_1 - q_2)$. This symmetry is derived from $C_3(z_1, z_2) = \langle V(0)V(z_1)V(z_2)\rangle = \langle V(-z_2)V(z_1 - z_2)V(0)\rangle = C_3(z_1 - z_2, -z_2)$, which follows from the assumption of homogeneous statistics.

have

$$\gamma_{\rm NG}^{(4)} = \left(\frac{m}{\hbar^2 k}\right)^4 \int_{-\infty}^{0} \mathrm{d}z_1 \int_{-\infty}^{z_1} \mathrm{d}z_2 \int_{-\infty}^{z_2} \mathrm{d}z_3 K_4(z_1, z_2, z_3) \lim_{z\to\infty} \frac{1}{z} \int_0^z \mathrm{d}z' g_4(z', z'+z_1, z'+z_2, z'+z_3). \tag{2.85}$$

Evaluating the limit in the integral, we find

$$\gamma_{\rm NG}^{(4)} = -2\left(\frac{m}{\hbar^2 k}\right)^4 \int_{-\infty}^{0} \mathrm{d}z_1 \int_{-\infty}^{z_1} \mathrm{d}z_2 \int_{-\infty}^{z_2} \mathrm{d}z_3 K_4(z_1, z_2, z_3) \left\{\cos[2k(-z_1+z_2+z_3)] + 2\cos[2kz_3]\right\}. \tag{2.86}$$

It turns out that this compact formula in coordinate space can be extended to the "Gaussian" part of C_4, which contains products of two-point correlators (see below).

Formulation in Fourier space - Following the approach of Eqs. (2.36) to (2.43), the long-range behavior of the complete four-point correlator is controlled by considering

$$\begin{aligned}\langle x_{\{\eta_i\}}^{(4)}(z)\rangle \;=\; & \left(\frac{m}{\hbar^2 k}\right)^4 \int_0^z \mathrm{d}z' \int_{-z'}^{0} \mathrm{d}z_1 \int_{-z'}^{z_1} \mathrm{d}z_2 \int_{-z'}^{z_2} \mathrm{d}z_3\, C_4(z_1, z_2, z_3) \times \\ & \mathrm{e}^{\eta_1 z_1 + \eta_2 z_2 + \eta_3 z_3} g_4(z', z'+z_1, z'+z_2, z'+z_3).\end{aligned} \tag{2.87}$$

Then, the Lyapunov exponent is given as

$$\gamma^{(4)} = \lim_{z\to+\infty} \lim_{\eta_i\to 0^+} \frac{\langle x_{\{\eta_i\}}^{(4)}(z)\rangle}{z}. \tag{2.88}$$

After a lengthy (computer-assisted) calculation along the lines of Eqs. (2.38) to (2.41), we obtain

$$\begin{aligned}\gamma^{(4)} \;=\; & \lim_{\eta_1,\eta_1,\eta_3\to 0^+} \left(\frac{m}{\hbar^2 k}\right)^4 \frac{-\mathrm{i}}{(2\pi)^{3/2}} \int \mathrm{d}q_1 \int \mathrm{d}q_2 \int \mathrm{d}q_3\, \hat{C}_4(q_1, q_2, q_3) \times \\ & \Bigg[\frac{1}{(q_1+q_2+q_3-2k-\mathrm{i}\eta_1-\mathrm{i}\eta_2-\mathrm{i}\eta_3)(q_2+q_3-4k-\mathrm{i}\eta_2-\mathrm{i}\eta_3)(q_3-2k-\mathrm{i}\eta_3)} \\ & + \frac{1}{(q_1+q_2+q_3+2k-\mathrm{i}\eta_1-\mathrm{i}\eta_2-\mathrm{i}\eta_3)(q_2+q_3+4k-\mathrm{i}\eta_2-\mathrm{i}\eta_3)(q_3+2k-\mathrm{i}\eta_3)} \\ & + \frac{2}{(q_1+q_2+q_3-2k-\mathrm{i}\eta_1-\mathrm{i}\eta_2-\mathrm{i}\eta_3)(q_2+q_3-2k-\mathrm{i}\eta_2-\mathrm{i}\eta_3)(q_3-2k-\mathrm{i}\eta_3)} \\ & + \frac{2}{(q_1+q_2+q_3+2k-\mathrm{i}\eta_1-\mathrm{i}\eta_2-\mathrm{i}\eta_3)(q_2+q_3+2k-\mathrm{i}\eta_2-\mathrm{i}\eta_3)(q_3+2k-\mathrm{i}\eta_3)}\Bigg].\end{aligned} \tag{2.89}$$

The limits $\eta_i \to 0$ $(i = 1, 2, 3)$ are calculated with the help of identity (2.42). This gives rise to large number of terms, even more so since C_4 may expand into several constituants (K_4 and two-point correlators).[17] For the factorizable ("Gaussian") part of C_4, this expression can be simplified.

[17] As in the case of $\gamma^{(2)}$ and $\gamma^{(3)}$, though, it might be possible to simplify this expression by using the symmetries of C_4.

Example - Consider the term $C_2(z_1)C_2(z_3-z_2)$ in Eq. (2.84).[18] For easy reference, we denote this term by C_4^A. In Fourier space, we have $\hat{C}_4^A(q_1,q_2,q_3) = \sqrt{2\pi}\hat{C}_2(q_1)\hat{C}_2(q_3)\delta(q_2+q_3)$, so that the corresponding contribution to $\gamma^{(4)}$ is

$$\begin{aligned}\gamma_A^{(4)} &= \lim_{\eta_1,\eta_1,\eta_3\to 0^+}\left(\frac{m}{\hbar^2 k}\right)^4 \frac{-\mathrm{i}}{2\pi}\int \mathrm{d}q_1 \int \mathrm{d}q_3\, \hat{C}_2(q_1)\hat{C}_2(q_3)\times \\ &\quad\Bigg[\frac{1}{(q_1-2k-\mathrm{i}\eta_1-\mathrm{i}\eta_2-\mathrm{i}\eta_3)(-4k-\mathrm{i}\eta_2-\mathrm{i}\eta_3)(q_3-2k-\mathrm{i}\eta_3)} \\ &\quad+\frac{1}{(q_1+2k-\mathrm{i}\eta_1-\mathrm{i}\eta_2-\mathrm{i}\eta_3)(+4k-\mathrm{i}\eta_2-\mathrm{i}\eta_3)(q_3+2k-\mathrm{i}\eta_3)} \\ &\quad+\frac{2}{(q_1-2k-\mathrm{i}\eta_1-\mathrm{i}\eta_2-\mathrm{i}\eta_3)(-2k-\mathrm{i}\eta_2-\mathrm{i}\eta_3)(q_3-2k-\mathrm{i}\eta_3)} \\ &\quad+\frac{2}{(q_1+2k-\mathrm{i}\eta_1-\mathrm{i}\eta_2-\mathrm{i}\eta_3)(+2k-\mathrm{i}\eta_2-\mathrm{i}\eta_3)(q_3+2k-\mathrm{i}\eta_3)}\Bigg]. \end{aligned} \tag{2.90}$$

Taking the limits $\eta_i \to 0$ and using the symmetry $\hat{C}_2(q) = \hat{C}_2(-q)$, which is always valid, we find

$$\gamma_A^{(4)} = -\frac{5}{2k}\left(\frac{m}{\hbar^2 k}\right)^4 \hat{C}_2(2k)\ \mathcal{P}\int \mathrm{d}q \frac{\hat{C}_2(q+2k)}{q}. \tag{2.91}$$

The other contributions to $\gamma^{(4)}$ have more complicated expressions (see appendix B).

Extension of the formula in coordinate space - The infinitesimals $\eta_i > 0$ in Eq. (2.87) can also be used to extend directly formula (2.86) to the complete correlator C_4. For each positive set of parameters $\eta_i > 0$, the function $C_4(z_1,z_2,z_3)\,\mathrm{e}^{\eta_1 z_1+\eta_2 z_2+\eta_3 z_3}$ decays for $z_i \to -\infty$, so that the arguments leading to Eq. (2.86) apply. Taking $\eta_i \to 0^+$ at the end of the calculation, we obtain the Lyapunov exponent for the correlation function C_4:

$$\begin{aligned}\gamma^{(4)} &= -2\left(\frac{m}{\hbar^2 k}\right)^4 \lim_{\eta_i\to 0^+}\int_{-\infty}^{0}\mathrm{d}z_1\int_{-\infty}^{z_1}\mathrm{d}z_2\int_{-\infty}^{z_2}\mathrm{d}z_3\, C_4(z_1,z_2,z_3)\,\mathrm{e}^{\eta_1 z_1+\eta_2 z_2+\eta_3 z_3}\times \\ &\qquad \{\cos[2k(-z_1+z_2+z_3)]+2\cos[2kz_3]\}. \end{aligned} \tag{2.92}$$

A straightforward calculation shows that this expression is identical to formula (2.89).

[18] This term is represented by the circles in Fig. 2.3.

2.2.4 Summary of the leading orders

We summarize here the results found in the previous sections [see Eqs. (2.34), (2.35), (2.79), (2.81), (2.89), and (2.92)].

The three leading orders of the Lyapunov exponent for a particle of energy $E = \hbar^2 k^2/2m$ in a correlated disorder can be written in the form:

$$\gamma^{(n)}(k) = \sigma_{\rm R}^{-1} \left(\frac{\epsilon_{\rm R}}{k\sigma_{\rm R}} \right)^n f_n(k\sigma_{\rm R}), \tag{2.93}$$

where

$$\epsilon_{\rm R} = \frac{V_{\rm R}}{E_\sigma} = \frac{2m\sigma_{\rm R}^2 V_{\rm R}}{\hbar^2}. \tag{2.94}$$

The parameter $E_\sigma = \hbar^2/2m\sigma_{\rm R}^2$ is sometimes called the correlation energy of the random potential [221]. The function $f_n(\kappa)$ depends only on the reduced n-point correlation function c_n of the random potential, defined in Eq. (2.5). The first few terms read

$$f_2(\kappa) = +\frac{1}{4}\int_{-\infty}^{0} {\rm d}u\, c_2(u)\cos(2\kappa u) \tag{2.95}$$

$$f_3(\kappa) = -\frac{1}{4}\int_{-\infty}^{0} {\rm d}u \int_{-\infty}^{u} {\rm d}v\, c_3(u,v)\sin(2\kappa v) \tag{2.96}$$

$$\tilde{f}_4(\kappa) = -\frac{1}{8}\int_{-\infty}^{0} {\rm d}u \int_{-\infty}^{u} {\rm d}v \int_{-\infty}^{v} {\rm d}w\; c_4(u,v,w)\left\{\cos[2\kappa(-u+v+w)] + 2\cos[2\kappa w]\right\}. \tag{2.97}$$

The tilde on $\tilde{f}_4$ indicates that the c_4 correlator should be replaced by $c_4(u,v,w)\,{\rm e}^{\eta_1 u+\eta_2 v+\eta_3 w}$, with $\eta_i \to 0^+$, to ensure a convergence of the integral. The equivalent representations in momentum space are:

$$f_2(\kappa) = +\frac{\sqrt{2\pi}}{8}\,\hat{c}_2(2\kappa) \tag{2.98}$$

$$f_3(\kappa) = -\frac{1}{4}\,\mathcal{P}\int {\rm d}q \frac{\hat{c}_3(q,2\kappa)+\hat{c}_3(-q,-2\kappa)}{2\,q}. \tag{2.99}$$

The fourth-order term has a cumbersome expression. We leave it here in the form

$$\begin{aligned} f_4(\kappa) = \lim_{\eta_1,\eta_1,\eta_3\to 0^+} \frac{-{\rm i}}{16(2\pi)^{3/2}} \int {\rm d}q_1 \int {\rm d}q_2 \int {\rm d}q_3\, \hat{c}_4(q_1,q_2,q_3) \times \\ \left[\frac{1}{(q_1+q_2+q_3-2\kappa-{\rm i}\eta_1-{\rm i}\eta_2-{\rm i}\eta_3)(q_2+q_3-4\kappa-{\rm i}\eta_2-{\rm i}\eta_3)(q_3-2\kappa-{\rm i}\eta_3)} \right. \\ + \frac{1}{(q_1+q_2+q_3+2\kappa-{\rm i}\eta_1-{\rm i}\eta_2-{\rm i}\eta_3)(q_2+q_3+4\kappa-{\rm i}\eta_2-{\rm i}\eta_3)(q_3+2\kappa-{\rm i}\eta_3)} \\ + \frac{2}{(q_1+q_2+q_3-2\kappa-{\rm i}\eta_1-{\rm i}\eta_2-{\rm i}\eta_3)(q_2+q_3-2\kappa-{\rm i}\eta_2-{\rm i}\eta_3)(q_3-2\kappa-{\rm i}\eta_3)} \\ \left. + \frac{2}{(q_1+q_2+q_3+2\kappa-{\rm i}\eta_1-{\rm i}\eta_2-{\rm i}\eta_3)(q_2+q_3+2\kappa-{\rm i}\eta_2-{\rm i}\eta_3)(q_3+2\kappa-{\rm i}\eta_3)} \right]. \end{aligned} \tag{2.100}$$

Comments

Isotropy - It is clear from Eqs. (2.93) to (2.97) that $\gamma^{(n)}$ is left unchanged under the replacement of k by $-k$. However, as ψ is real-valued, this replacement does not imply a propagation in opposite direction, but the choice of a different phase [see Eqs. (2.8), (2.9) and (2.14)]. The isotropy of the Lyapunov exponent is analyzed by replacing z by $-z$ in the previous derivations or, equivalently, $c_n(u_1, .., u_{n-1})$ by $c_n(-u_1, .., -u_{n-1})$ and $\hat{c}_n(q_1, .., q_{n-1})$ by $\hat{c}_n(-q_1, .., -q_{n-1})$ in the above results. Expressions (2.98) and (2.99) clearly yield an isotropic Lyapunov exponent even if the random potential itself is not isotropic. Note also that Eq. (2.99) simplifies if V itself is isotropic [$\hat{c}_3(q_1, q_2) = \hat{c}_3(-q_1, -q_2)$].

The third-order term - To our knowledge, the third-order term had not been derived and documented in the literature prior to our work [222],[19] even in studies of non-Gaussian potentials [219]. In such potentials, however, C_3 does not vanish in general. Interestingly, for the same model of disorder (i.e. for the same reduced correlators c_n), the sign of $\gamma^{(3)}$ changes with the sign of V_{R}. This contrasts with the Born approximation, where the strength of localization appears independent of the overall sign of the potential. The third-order term in non-Gaussian potentials may thus enhance or reduce localization.[20]

Validity - The results summarized above are general, as we have made no other assumptions on the potential than homogeneous statistics and statistical independence of the values taken by the potential at points with infinite separation.[21] A truncated perturbation expansion $\gamma^{(2)} + \cdots + \gamma^{(n)}$ provides an accurate approximation of the exact Lyapunov exponent γ if the leading-order terms dominate the (sum of the) following orders in the perturbation series. Quite generally, owing to the factor $(\epsilon_{\mathrm{R}}/k\sigma_{\mathrm{R}})^n$ in Eq. (2.93), this requires the potential amplitude V_{R} to be small or the energy of the particle to be large. This leads to the definition of a small parameter for the perturbation expansion, which is discussed below. However, the amplitude of the n-th order term in the Lyapunov exponent may also crucially depend on the details of the correlation functions. In particular, if a function f_n is small or even vanishes for some values of $k\sigma_{\mathrm{R}}$, then the other perturbation orders need to be examined.

Small parameter

In Eq. (2.93), the total Lyapunov exponent appears as an expansion in powers of the parameter

$$\frac{\epsilon_{\mathrm{R}}}{k\sigma_{\mathrm{R}}} = \frac{V_{\mathrm{R}}}{\sqrt{E_\sigma E}}. \tag{2.101}$$

Because of this factor, all the individual perturbation orders $\gamma^{(n)}$ blow up in the limit $k \to 0$ ($E \to 0$). This signals a breakdown of the perturbation expansion, as it is known that the Lyapunov exponent tends to a finite value at vanishing energy [162, 207]. It is tempting to

[19] See, however, the study which was published simultaneously in Ref. [220].

[20] See the inset of Fig. 2.6. The exponents γ^+ and γ^- displayed in the inset refer to the exact Lyapunov exponent in a speckle potential with $V_{\mathrm{R}} > 0$ and $V_{\mathrm{R}} < 0$, respectively. In this example, the reduction or enhancement of localization by odd terms in the expansion amounts to half the magnitude of the Born term.

[21] Going back to the analysis of Eqs. (2.36) and (2.43), for instance, it should be possible to determine how fast correlations have to decay at the level of the Born approximation.

identify $\epsilon_{\rm R}/k\sigma_{\rm R}$ as the small parameter of the perturbation expansion. Requiring it to be much smaller than one would guarantee a good approximation of γ by the the first few perturbation terms. However, this criterion appears not to be sufficient in general. The low-energy limit has been analyzed in detail by Derrida and Gardner [207] (see also Refs. [162,206,223]), and it turns out that the smallness of higher-order terms rather requires

$$\epsilon_{\rm R}^{2/3} \ll k\sigma_{\rm R}. \tag{2.102}$$

This conclusion follows from the comparison of $\gamma^{(2)}$, $\gamma^{(3)}$ and $\gamma^{(4)}$ in a model of uncorrelated disorder, and the observation that, while $\gamma^{(n)}$ scales as $(V_{\rm R}/k)^n$ for $n = 2, 3$, the fourth-order term $\gamma^{(4)}$ scales as $V_{\rm R}^4/k^5$ because of the contribution of factorizable ("Gaussian") terms.[22] Then, the comparison of the Born and fourth-order terms leads to criterion (2.102). As the Born term itself obeys $\gamma^{(2)}\sigma \propto (\epsilon_{\rm R}/k\sigma_{\rm R})^2$ at low energy (assuming that $\hat{c}_2(q)$ tends to a finite value for $q \to 0$), criterion (2.102) rewrites $\gamma^{(2)} \ll k$, or simply [86]

$$\gamma \ll k. \tag{2.103}$$

This criterion is understandable in physical terms, as the potential can be said to be weak if the decay of the wave function on the length scale of a wavelength is small.

Effective mobility edges

Equation (2.98) shows that $\gamma^{(2)}$ may vanish identically on some extended region of the single-particle energy spectrum. This happens, for instance, when the Fourier transform $\hat{c}_2(q)$ of the two-point correlation function has a finite support, bounded above by a cutoff $2\kappa_c$. If so, the Lyapunov exponent calculated in the Born approximation vanishes for $\kappa > \kappa_c$ (i.e. $k > k_c = \kappa_c/\sigma_{\rm R}$) and, if the potential is weak, the strength of localization for $k > k_c$ is expected to be significantly reduced. Then, k_c defines an *effective mobility edge* [34,183], which separates the region $k < k_c$ where the localization is significant from the region $k > k_c$ where localization occurs with a much smaller Lyapunov exponent. In 3D, the so-called *mobility edge* separates localized states from extended ones (see section 1.1.2). In 1D, on the other hand, as general results exclude delocalization on some extended region of the spectrum (see section 2.1.2), the states at $k > k_c$ are expected to be localized. In system of finite size, however, an effective mobility edge may separate states which are well localized inside the system, and states with localization lengths exceeding by far the system size [225].

The fact that the leading-order approximation of the Lyapunov exponent may have a cutoff was naturally pointed out a while ago (see e.g. Ref. [182]). Interestingly, such a cutoff at the level of the Born approximation has been shown to have significant consequences on the transport and localization of waves packets in 1D [34] and quasi-1D [225] geometries. Both numerical

[22] See Eq. (13) in Ref. [207], which we translate here in our notations. The results of Ref. [207] have been derived for uncorrelated potentials on a lattice, but the conclusions are expected to be more general, as the lattice and the detailed correlations should play a marginal role in the limit $k \to 0$. Numerical calculations performed with correlated speckle potentials by D. Delande [224] have shown to be in agreement with the non-trivial scaling of the exact Lyapunov exponent at low energy which was worked out by Derrida and Gardner. Note also that, starting from criterion $\gamma \ll k$, and the high-energy or weak-disorder expansion $\gamma(E) \propto V_{\rm R}^2/E$ of the exact Lyapunov exponent in a continuous white-noise potential [see Eq. (1.15)], one finds a criterion similar to Eq. (2.102).

[34, 182, 183, 225, 226] and experimental studies [29] have confirmed these predictions, and the question naturally arises how localization occurs beyond a cutoff in the Born approximation of the Lyapunov exponent.

Equation (2.99) shows that the third-order term may also have a cutoff. If the support of the bispectrum $\hat{c}_3(q_1, q_2)$ is enclosed in a disk of radius $2\kappa_c'$, then $\gamma^{(3)}$ vanishes identically for $k > k_c' = \kappa_c'/\sigma_{\rm R}$. This result is relevant for potentials which do not have a symmetric probability distribution (or are invariant with respect to an overall change of sign $V_{\rm R} \to -V_{\rm R}$). Such a symmetry is often assumed for simplicity, and then $\gamma^{(3)}$ is simply zero. Expression (2.99) shows that cutoffs in the leading orders arise for a larger class of random potentials, and that the fourth-order term $\gamma^{(4)}$ may be the first non-vanishing order for some values of k, whether the potential is symmetric or not.

The formulas derived above for the fourth-order term $\gamma^{(4)}$ allow a calculation of the Lyapunov exponent in the event that the two leading orders both have a high-momentum cutoff. In the following section, we analyze the behavior of $\gamma^{(4)}$ for a class of random potentials where such is the case.

2.3 Localization in weak speckle potentials

In this section we study the Lyapunov exponent of non-interacting particles in weak speckle potentials, such as those used in current experiments with ultracold atoms. Speckle potentials have a cutoff at a certain value $2k_c$ in their spatial (power) spectrum, and have been shown to give rise to an effective mobility edge in 1D, associated with the fact that the Lyapunov exponent vanishes in the Born approximation for particles with momenta $\hbar k > \hbar k_c$ [29,34,183]. We apply here the results of the previous section to characterize localization around the effective mobility edge at k_c and beyond.

Localization beyond a high-momentum cutoff $\hbar k_c$ in the Born approximation was also addressed in Ref. [219]. In this reference, models of disorder with symmetric probability distribution were studied, and fourth-order terms for the exponent $\lim_{|z-z_0|\to\infty} \ln[\langle r(z)/r_0\rangle]/|z - z_0|$ were calculated. Examples were exhibited for which localization occurs even for $k > k_c$, but on much longer length scales than for $k < k_c$. It was also concluded that for Gaussian disorder, there is a second mobility edge at $2k_c$, while for non-Gaussian disorder, it is generally not so. These results do not apply to speckle potentials, the probability distribution of which is asymmetric (see section 1.3.3). Moreover, although speckle potentials are not Gaussian, they derive from the squared modulus of a Gaussian field and, as shown below, the conclusions of Ref. [219] regarding higher-order cutoffs needs to be re-examined. Finally, the exponent used in Ref. [219] is not a self-averaging quantity [87]. It can be used as an indicator of localization, but its precise quantitative relationship with the localization length is unclear beyond the second-order perturbation theory [219,220].[23] The formulas derived in the previous section for the Lyapunov exponent $\gamma = \lim_{|z-z_0|\to\infty} \langle \ln[r(z)/r_0]\rangle/(z - z_0)$, on the other hand, allow a quantitative study of the (self-averaging) localization length.

Below, we first study generic speckle potentials, and show the existence of a *series* of effective mobility edges at $k_c^{(p)} = pk_c$, with integer p, which delimit intervals $[k_c^{(p-1)}, k_c^{(p)}]$ where

[23] Note, however, that the technique of ordered cumulants used in Ref. [219] has been adapted in Ref. [220] to the calculation of the (self-averaging) Lyapunov exponent and the case of asymmetric potentials.

localization results from scattering processes of increasing order. At each effective mobility edge, the Lyapunov exponent is thus expected to experience sharp crossovers and drop by orders of magnitude in weak potentials. The existence of the first two effective mobility edges is proved by analyzing the three leading perturbation orders $\gamma^{(2)}$, $\gamma^{(3)}$ and $\gamma^{(4)}$ of the Lyapunov exponent. Arguments are given for the higher-order cutoffs. Then, the leading orders of γ are calculated explicitly for the specific model of speckle potential used in the experiments. The analytical expressions are compared to numerical transfer matrix calculations. The results of these calculations reveal how the Lyapunov exponent behaves beyond the first effective mobility edge at weak and intermediate disorder strengths.

2.3.1 Speckle potentials

Correlation functions

Speckle potentials have been introduced in section 1.3.3. The models we consider in this thesis are completely determined by the specification of an amplitude V_{R}, a correlation length σ_{R}, and the correlation function $c_a(u) = \langle a^*(0)a(u)\rangle$ of the reduced complex electric field *amplitude a* which couples to the atoms. By definition, $\hat{c}_a(q)$ has a high-q cutoff

$$\hat{c}_a(q) = 0 \quad \text{for } |q| > k_c\sigma_{\mathrm{R}} = \kappa_c = 1. \tag{2.104}$$

The speckle potential V is proportional to the squared modulus of a, and shifted so as to have zero mean (see Eq. A.5). The reduced correlation functions of V are

$$\begin{aligned}
c_2(u) &= |c_a(u)|^2 && (2.105)\\
c_3(u,v) &= c_a(u)c_a(v-u)c_a(-v) + \text{c.c.} && (2.106)\\
c_4(u,v,w) &= c_4^A(u,v,w) + c_4^B(u,v,w) + c_4^C(u,v,w) \\
&\quad + [c_4^D(u,v,w) + \text{c.c.}] + [c_4^E(u,v,w) + \text{c.c.}] + [c_4^F(u,v,w) + \text{c.c.}], && (2.107)
\end{aligned}$$

where c_4^A, c_4^B and c_4^C are the factorized ("Gaussian") components

$$\begin{aligned}
c_4^A(u,v,w) &= |c_a(u)|^2|c_a(w-v)|^2 && (2.108)\\
c_4^B(u,v,w) &= |c_a(v)|^2|c_a(u-w)|^2 && (2.109)\\
c_4^C(u,v,w) &= |c_a(w)|^2|c_a(v-u)|^2, && (2.110)
\end{aligned}$$

and c_4^D, c_4^E and c_4^F are the unfactorized parts

$$\begin{aligned}
c_4^D(u,v,w) &= c_a(u)c_a(v-u)c_a(w-v)c_a(-w) && (2.111)\\
c_4^E(u,v,w) &= c_a(v)c_a(w-v)c_a(u-w)c_a(-u) && (2.112)\\
c_4^F(u,v,w) &= c_a(w)c_a(u-w)c_a(v-u)c_a(-v). && (2.113)
\end{aligned}$$

Note that the latter come along with their complex conjugates in Eq. (2.107).

Cutoffs in the perturbation terms

Taking the Fourier transform of Eqs. (2.105) and (2.106), and using the equality $c_a^*(u) = c_a(-u)$, we derive

$$\hat{c}_2(2\kappa) = \frac{1}{\sqrt{2\pi}} \int \mathrm{d}q' \overbrace{\hat{c}_a(q')\hat{c}_a(q'-2\kappa)} \tag{2.114}$$

$$\hat{c}_3(q,2\kappa) = \frac{1}{\sqrt{2\pi}} \int \mathrm{d}q' \left[\hat{c}_a(q') \overbrace{\hat{c}_a(q'-q)\hat{c}_a(q'-q-2\kappa)} + \hat{c}_a(q') \overbrace{\hat{c}_a(q'+q)\hat{c}_a(q'+q+2\kappa)} \right]. \tag{2.115}$$

Since $\hat{c}_a(q)$ vanishes for $|q| > 1$, the supports of those $\hat{c}_a$ correlators which appear under braces in Eqs. (2.114) and (2.115) do not overlap for $\kappa > 1$, and in that case the functions $\hat{c}_2(2\kappa)$ and $\hat{c}_3(q, 2\kappa)$ vanish. Let us reproduce here Eqs. (2.98) and (2.99):

$$f_2(\kappa) = +\frac{\sqrt{2\pi}}{8}\, \hat{c}_2(2\kappa) \tag{2.116}$$

$$f_3(\kappa) = -\frac{1}{4}\, \mathcal{P} \int \mathrm{d}q \frac{\hat{c}_3(q,2\kappa) + \hat{c}_3(-q,-2\kappa)}{2\,q}. \tag{2.117}$$

As a consequence of these relations, the functions $f_2(\kappa)$ and $f_3(\kappa)$ also vanish identically for $\kappa > 1$. *In other words, we find that the Born term $\gamma^{(2)}(k)$ and the next-order term $\gamma^{(3)}(k)$ vanish for single-particle states with $k > k_c = 1/\sigma_R$.*

To calculate the function $f_4(\kappa)$, we may use formula (2.97). Because of the various parts of the four-point correlator, we end up with many integrals to calculate. Details of this lengthy task are given in appendix B. It turns out that $f_4(\kappa)$ can be expressed as the sum of a reduced number of "elementary" integrals (labeled R_κ^i below), which resemble those in Eqs. (2.114) and (2.115), and in which cutoffs are easily identified by considering the overlap of the $\hat{c}_a$ correlators. A complete list of the elementary integrals and their cutoffs is given in appendix B. Let us illustrate these cutoffs by reproducing a few of these terms:

$$R_\kappa^1 = -\frac{1}{8\pi\kappa} \int \mathrm{d}q \overbrace{\hat{c}_a(q)\hat{c}_a(q+2\kappa)} \times \iint \mathrm{d}q\, \mathrm{d}q'\, \frac{\hat{c}_a(q)\hat{c}_a(q')}{q-q'+2\kappa} \qquad (c_4^A, \kappa_c) \tag{2.118}$$

$$R_\kappa^{11} = \frac{\pi}{4} \int \mathrm{d}q \overbrace{\hat{c}_a(q)\hat{c}_a(q+4\kappa)}\, \hat{c}_a(q+2\kappa)^2 \qquad (c_4^D, c_4^E, \kappa_c/2) \tag{2.119}$$

$$R_\kappa^3 = -\frac{1}{4\pi} \iiint \mathrm{d}q\, \mathrm{d}q'\, \mathrm{d}q'' \frac{\overbrace{\hat{c}_a(q)\hat{c}_a(q')\hat{c}_a(q'')\hat{c}_a(-q+q'+q''-2\kappa)}}{(q'-q)(q-q'+2\kappa)} \qquad (c_4^B, 2\kappa_c) \tag{2.120}$$

$$R_\kappa^{17} = -\frac{1}{4\pi} \iiint \mathrm{d}q\, \mathrm{d}q'\, \mathrm{d}q'' \frac{\overbrace{\hat{c}_a(q)\hat{c}_a(q')\hat{c}_a(q'')\hat{c}_a(q-q'+q''+2\kappa)}}{(q-q'+2\kappa)(q'-q'')} \qquad (c_4^F, 2\kappa_c) \tag{2.121}$$

$$R_\kappa^5 = \int \frac{\mathrm{d}q}{2q} \left\{ \Big[\hat{c}_2(2\kappa) - \overbrace{\hat{c}_2(q+2\kappa)}\Big] \overbrace{\frac{\mathrm{d}\hat{c}_2}{\mathrm{d}q}(q)} + \Big[\frac{\mathrm{d}\hat{c}_2}{\mathrm{d}q}(2\kappa) - \overbrace{\frac{\mathrm{d}\hat{c}_2}{\mathrm{d}q}(q+2\kappa)}\Big] \hat{c}_2(q) \right\} \qquad (c_4^C, 2\kappa_c). \tag{2.122}$$

In these expressions, the integrals with quotients are understood as principal values. The

parentheses in front of the equation numbers indicate from which part of the correlator c_4 the terms originate [see Eqs. (2.108) to (2.113)], and where their cutoffs lie.[24]

The contributions to the fourth-order Lyapunov exponent in a speckle potential all have a cutoff. More precisely, these cutoffs are found at $\kappa = \kappa_c/2,\ \kappa_c,\ 2\kappa_c$. In particular, some terms extend beyond the cutoff at $\kappa = \kappa_c = 1$ found in the Born term $\gamma^{(2)}$ and the third-order term $\gamma^{(3)}$. These terms are all listed in Eqs. (2.120) to (2.122). It can be checked with specific forms of $\hat{c}_a$ that, in general, the contributions at $\kappa > 1$ do not cancel out (see section 2.3.2). For weak-enough disorder, they will not be cancelled by higher-order terms in the expansion of γ either. However, they do vanish at a cutoff $\kappa = 2\kappa_c$ imposed by the field-field correlator $\hat{c}_a$.

Localization beyond the first effective mobility edge

Equations (2.120) to (2.122) show that the single-particle states are localized beyond the cutoff k_c in the Born term. Note that contributions for $k > k_c$ arise both from the Gaussian (c_4^B, c_4^C) and the non-Gaussian (c_4^F) parts of the four-point correlator.

Higher-order cutoffs - Remarkably, all terms of $\gamma^{(4)}$ that contribute to $k > k_c$ vanish identically for $k > 2k_c$, which suggests that cutoffs might occur for every integer multiple pk_c of the first cutoff k_c. As the power-dependence of the leading-order Lyapunov exponent on the disorder amplitude V_{R} changes across each of these cutoffs, localization is expected to be dramatically reduced from one region $[k_c^{(p-1)}, k_c^{(p)}]$ to the next when the disorder is weak. The existence of several cutoffs is not specific to speckle potentials. In particular, such a series of effective mobility edges should occur in any Gaussian potential with a cutoff in the power spectrum, since higher-order correlation functions of the potential factorize into products of two-point correlators.

The occurence of a second effective mobility edge at $2k_c$ in Gaussian potentials was pointed out in Ref. [219]. An example of non-Gaussian disorder with a similar cutoff in the power-spectrum but without second effective mobility edge was also exhibited. Conversely, the above analysis shows that the non-Gaussian character of the disorder is not a sufficient criterion to conclude on the absence of higher-order effective mobility edges. In brief, higher-order effective mobility edges occur systematically in Gaussian potentials with a cutoff in the power-spectrum, but also in some classes of non-Gaussian potentials.

In any case, higher orders in the expansion of the Lyapunov exponent are expected to cover the whole positive k axis step by step and ensure localization at all energies, in agreement with the general understanding of one-dimensional systems.

Odd terms - Interestingly, speckle potentials have an asymmetric probability distribution, and bring along odd powers in the expansion of the Lyapunov exponent, as exemplified by γ_3 and f_3 in this section. Depending on the sign of V_{R}, these odd (non-Gaussian) terms might enhance or reduce localization. As the Lyapunov exponent calculated from definition (2.19) is, with probability one, a positive quantity, it is clear that odd terms cannot be the leading orders in any spectral region. This argument is consistent with the observation that $\gamma^{(3)}$ has the same cutoff than $\gamma^{(2)}$ in speckle potentials, and suggests that, in general, if $\gamma^{(2p)}$ has a cutoff and odd terms are present, then $\gamma^{(2p+1)}$ should have the same cutoff than $\gamma^{(2p)}$. For weak speckle

[24] For the analysis of Eq. (2.122), note that $\hat{c}_2$ has twice the width of $\hat{c}_a$.

potentials we thus expect the Lyapunov exponent to scale with $(\epsilon_{\rm R}/k\sigma_{\rm R})^2$ for $k < \sigma_{\rm R}$, with $(\epsilon_{\rm R}/k\sigma_{\rm R})^4$ for $\sigma_{\rm R} < k < 2\sigma_{\rm R}$, and with $(\epsilon_{\rm R}/k\sigma_{\rm R})^6$ at most for $k > 2\sigma_{\rm R}$.

2.3.2 The simplest speckle model

We now work out the exact functional dependence of the leading exponents $\gamma^{(n)}\,[n = 2, 3, 4]$, for the field-field correlator

$$c_a(u) = \mathrm{sinc}(u) \equiv \frac{\sin(u)}{u}. \tag{2.123}$$

This correlation function arises in the diffraction pattern created behind a square aperture with uniform illumination [31], which is relevant for current experiments with ultracold atoms [26, 27, 29, 31]. The Fourier transform of c_a has the simple form

$$\hat{c}_a(q) = \sqrt{\frac{\pi}{2}}\Theta(1 - |q|), \tag{2.124}$$

where Θ is the Heaviside step function.

Correlation functions - The first two correlation functions of the potential V are also simple in Fourier space:

$$\hat{c}_2(q) = \sqrt{\frac{\pi}{2}}\left(1 - \frac{|q|}{2}\right)\Theta\left(1 - \frac{|q|}{2}\right) \tag{2.125}$$

$$\hat{c}_3(q, q') = \pi\left(1 - \frac{\max(|q|, |q'|, |q + q'|)}{2}\right)\Theta\left(1 - \frac{\max(|q|, |q'|, |q + q'|)}{2}\right). \tag{2.126}$$

The last expression clearly shows that the support of the bispectrum $\hat{c}_3$ is enclosed in a disk of minimum radius 2, so that $\gamma^{(3)}$ vanishes for $\kappa > 1$.

f_n functions - The above correlators are inserted into Eqs. (2.98) and (2.99), and we find

$$f_2(\kappa) = \frac{\pi}{8}(1 - \kappa)\Theta(1 - \kappa) \tag{2.127}$$

$$f_3(\kappa) = \frac{\pi}{4}\left[\kappa \ln\left(\frac{1}{\kappa}\right) + (1 - \kappa)\ln\left(\frac{1}{1 - \kappa}\right)\right]\Theta(1 - \kappa). \tag{2.128}$$

The calculation of $f_4(\kappa)$ is detailed in appendix B. The result can be cast into the form

$$f_4(\kappa) = f_4^{[0,1/2]}(\kappa)\Theta(1/2 - \kappa) + f_4^{[0,1]}(\kappa)\Theta(1 - \kappa) + f_4^{[1,2]}(\kappa)\Theta(2 - \kappa)\Theta(\kappa - 1). \tag{2.129}$$

The functions $f_4^{[\alpha,\beta]}$ in this expression are defined on the interval $[\alpha,\beta]$ and read

$$f_4^{[0,1/2]}(\kappa) = -\frac{\pi^3}{16}(1-2\kappa) \tag{2.130}$$

$$\begin{aligned} f_4^{[0,1]}(\kappa) = \frac{\pi}{64}\Bigg\{ & 4-6\kappa-\frac{10\pi^2}{3}(1-2\kappa)-\left(\frac{5}{\kappa}-3\kappa\right)\ln(1-\kappa) \\ & +22(1-\kappa)\ln^2(1-\kappa)-16(1-\kappa)\ln(1-\kappa)\ln(\kappa) \\ & -4(1-\kappa)\ln(1-\kappa)\ln(1+\kappa)-(4-2\kappa)\ln(\kappa)-(4-8\kappa)\ln^2(\kappa) \\ & -32(1+\kappa)\ln(\kappa)\ln(1+\kappa)+\left(\frac{1}{\kappa}+\kappa\right)\ln(1+\kappa) \\ & +(18+14\kappa)\ln^2(1+\kappa)-24(1+\kappa)\mathrm{Li}_2(\kappa)+32(1+\kappa)\mathrm{Li}_2\left(\frac{\kappa}{1+\kappa}\right) \\ & -8\kappa\mathrm{Li}_2\left(\frac{2\kappa}{1+\kappa}\right)-8(1-2\kappa)\mathrm{Li}_2\left(2-\frac{1}{\kappa}\right)\Bigg\} \end{aligned} \tag{2.131}$$

$$\begin{aligned} f_4^{[1,2]}(\kappa) = \frac{\pi}{32}\Bigg\{ & -2+\left(1+\frac{\pi^2}{3}\right)\kappa-\left(\frac{2}{\kappa}-2+\kappa\right)\ln(\kappa-1) \\ & -2(\kappa-1)\ln^2(\kappa-1)+4\kappa\ln(\kappa-1)\ln(\kappa)+4\kappa\mathrm{Li}_2(1-\kappa)\Bigg\}, \end{aligned} \tag{2.132}$$

where $\mathrm{Li}_2(x)$ is the dilogarithm function [227], which is documented in appendix C.[25] The function f_4 has a quite complicated expression, but its behaviour is clear when it is plotted (see Fig. 2.4). While $f_2(\kappa)$ and $f_3(\kappa)$ vanish for $\kappa > 1$, the support of $f_4(\kappa)$ extends up to $\kappa = 2$. This result agrees with the findings of section 2.3.1, showing that there is localization (on longer length scales) beyond the cutoff in the Born term.

Let us mention a few other remarkable features of f_4. We find a kink at $\kappa = 1/2$ which originates from the terms such as (2.119), and logarithmic divergences at $\kappa = 0$ and $\kappa = 1$:

$$f_4(\kappa) \sim -\frac{\pi}{16}\ln(\kappa) \qquad [\kappa \to 0^+] \tag{2.133}$$

$$f_4(\kappa) \sim -\frac{\pi}{32}\ln|1-\kappa| \qquad [\kappa \to 1^\pm]. \tag{2.134}$$

The logarithmic divergence at $\kappa = 1$ may require further study, as it happens just at the first effective mobility edge. Numerical calculations presented in section 2.3.3 suggest that the Lyapunov exponent γ remains continuous across the cutoff at $\kappa = 1$. The divergence of $\gamma^{(4)}$ indicates that in a very narrow interval around each effective mobility edge, a non trivial summation of the entire perturbation series might be necessary.

Lyapunov exponent - The full functional dependence of the Lyapunov exponent for the simple speckle potential (2.123), evaluated two orders beyond the Born approximation, on the wavenumber k, the disorder amplitude V_{R}, and the correaltion length σ_{R} is shown in Fig. 2.5.

[25] Note that expressions (2.131) and (2.132) can be written in many equivalent ways (which may appear quite different) since the dilogarithm satisfies a number of functional identities which can be used to simplify the results (see appendix C).

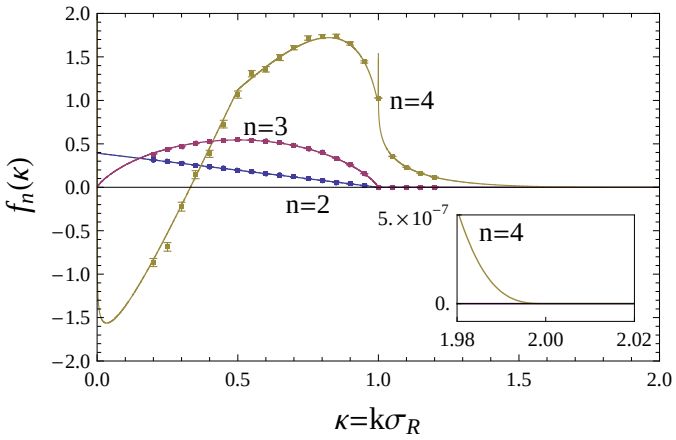


Figure 2.4: Functions f_n for $n = 2, 3, 4$ and for the simple speckle potential $\hat{c}_a(q) \propto \Theta(1 - |q|)$ created with a square aperture. The solid lines represent expressions (2.127), (2.128) and (2.129). The points with error bars correspond to numerical transfer matrix calculations (see section 2.3.3). The support of $f_4(\kappa)$ extends up to $\kappa = 2$, as shown in the inset.

A clear step, which becomes sharper with weaker disorder, separates the spectral regions $k < k_c = 1/\sigma_{\mathrm{R}}$ and $k > k_c$. The logarithmic divergence at the first effective mobility edge $k = k_c$ does not appear on the graph due to the finite resolution of the sampling grid. The drop at low energy is due to the negative tail of $f_4(\kappa)$ and the dominating behavior of $(\epsilon_{\mathrm{R}}/k\sigma_{\mathrm{R}})^4$ for small κ, and most probably signals that the truncated perturbation series $\gamma^{(2)} + \gamma^{(3)} + \gamma^{(4)}$ offers a poor approximation of γ in that regime, where the Lyapunov is expected to have a monotonous behavior (see Fig. 2.6). The spectral region where this occurs becomes narrower for weak disorder.

2.3.3 Transfer matrix calculations

In one dimension, the Lyapunov exponent can be computed numerically by means of transfer matrix calculations. The data presented in Figs. 2.4 and 2.6 has been obtained by D. Delande. Below, we outline the principle of transfer matrix calculations. We also emphasize a few points which become important with the analysis of higher-order terms in the Lyapunov exponent, and the strategy that has been used by D. Delande to obtain the data of Figs. 2.4 and 2.6.

Set-up

In transfer matrix calculations, the Schrödinger equation is discretized on a regular lattice with spacing Δz between sites, and eigenstates at energy E obey

$$-\frac{\hbar^2}{2m}\frac{\psi_{n+1} - 2\psi_n + \psi_{n-1}}{(\Delta z)^2} + V_n\psi_n = E\psi_n. \tag{2.135}$$

Solutions of this equation are completely determined by the specification of the energy E and some initial conditions ψ_0 and ψ_1.

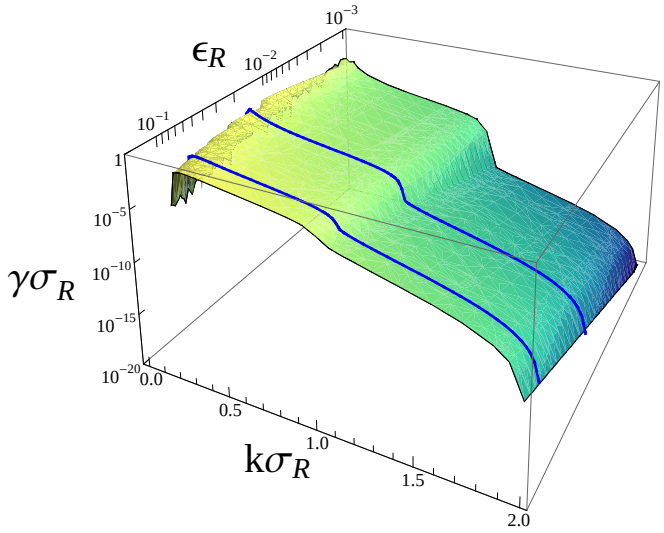


Figure 2.5: Lyapunov exponent γ calculated analytically up to two orders beyond the Born approximation for a speckle potential with field-field correlator $\hat{c}_a(q) \propto \Theta(1-|q|)$, and plotted as a function of the particle wave number k and the strength of the disorder $\epsilon_{\rm R} = 2m\sigma_{\rm R}^2 V_{\rm R}/\hbar^2$, where $V_{\rm R}$ and $\sigma_{\rm R}$ are the amplitude and the correlation length of the disorder. The blue lines correspond to $\epsilon_{\rm R} = 0.1$ and $\epsilon_{\rm R} = 0.02$, that is, experimental conditions of Ref. [29]; see text.

Transfer matrices - Equation (2.135) defines a recursion formula which allows the calculation of ψ_n for all n, given a set of initial conditions ψ_0 and ψ_1. This recursion formula is most conveniently cast into a matrix form. Here we chose the representation [59]

$$\begin{pmatrix} \psi_{n+1} \\ \psi_n \end{pmatrix} = T_n \begin{pmatrix} \psi_n \\ \psi_{n-1} \end{pmatrix} \tag{2.136}$$

where the components ψ_n are real, and T_n is a 2×2 transfer matrix defined as

$$T_n = \begin{pmatrix} 2 + \frac{V_n - E}{E_z} & -1 \\ 1 & 0 \end{pmatrix}, \tag{2.137}$$

with $E_z = \hbar^2/2m(\Delta z)^2$. For $n \to \infty$, the eigenvalues of the product $T_n \cdots T_2 T_1$ eventually converge to the set $(\mathrm{e}^{+\gamma n \Delta z}, \mathrm{e}^{-\gamma n \Delta z})$, where $\gamma > 0$ is the positive Lyapunov exponent of interest. As, with probability one, an arbitrary initial vector $v_1 = [\psi_1, \psi_0]^{\rm T}$ has a component along the direction of exponential growth, analyzing the growth of the vector $T_n \cdots T_2 T_1 v_1$ (i.e. propagating only a two-component vector v_n instead of the 2×2 matrix) suffices to determine the Lyapunov exponent. The norm of the vector can defined by

$$r_n = [\psi_n^2 + (\psi_n - \psi_{n-1})^2/(k\Delta z)^2]^{1/2} \tag{2.138}$$

as in the phase formalism [see Eq. (2.15)]. Monitoring the asymptotic growth of $|\phi|$ for a complex ϕ should yield the same result [224].

System sizes - For $n \to \infty$, the quantity $\ln[r_{n+1}/r_1]/(n\Delta z)$ approaches a limit which is independent of the initial conditions, and is equal to the Lyapunov exponent.[26] A single realization of the random potential suffices in principle for an accurate estimate of the Lyapunov exponent, provided the system is large enough. In practice, propagation over samples of large size is combined with averaging over several realizations of the random potential, in order to obtain a good estimate of the Lyapunov exponent at the smallest possible computational cost. How large should the system size n be in each realization ? The analysis of the fluctuations of the logarithmic growth of the wave function around the Lyapunov exponent (see Eq. 1.13) shows that ψ should be propagated on a large number of localization lengths, which here translates into

$$n \gg 1/(\gamma \Delta z). \tag{2.139}$$

Additionally, the conditions

$$\Delta z \ll \sigma_{\rm R}, \qquad \Delta z \ll \frac{1}{k} \tag{2.140}$$

must be satisfied to ensure that the details of the correlation function are reproduced accurately, and that the discretization of the Schrödinger operator does not affect significantly the free dispersion relation $E = \hbar^2 k^2/2m$ in the regime of interest. For numerical data shown in Figs. 2.4 and 2.6, the parameters are $\Delta z/\sigma_{\rm R} = \pi/16$ and $n\Delta z/\sigma_{\rm R} = 10^8\pi$.

Generating long speckle potentials - Speckle potentials are generated numerically by computing the fast Fourier transform (FFT) of a random field (see chapter 1). Even though the FFT algorithm has complexity $\mathcal{O}(n \log n)$, generating speckle samples which are large enough to study $\gamma^{(4)}$ is expensive in terms of computation time and memory. Concatenating different speckle samples should be avoided, as the interface between two uncorrelated speckle samples produces small reflections which significantly alter the estimate of the Lyapunov exponent for small energies and small disorder amplitudes [224]. The strategy developed by D. Delande for the data presented here consists in: i) generating a random (Gaussian) delta-correlated source field, ii) applying a "short" FFT to part of this field (of size $1024\pi\sigma_{\rm R}$) to generate the corresponding sources in k space, iii) truncating the sequence in k space at the cutoff value k_c, iv) applying an inverse FFT to obtain a speckle field with the required correlation functions, and v) choosing a sufficient overlap (typically $64\pi\sigma_{\rm R}$) between successive source field in step (i) so that discontinuity effects are negligible. The results were checked not to depend on the length of the overlaps. The Lyapunov exponent was extracted by fitting $\log[r_{n+1}/r_1]$ by an affine law $an + b$, rather than just retrieving the value $\log[r_{N+1}/r_1]/N\Delta z$, where N is the size of the system. Additionally, averaging was performed over 8 potential samples for the data in the figures.

Application to the simple speckle potential

Lyapunov exponent - Results of such transfer matrix calculations for the speckle potential (2.124) are shown in Fig. 2.6 and compared to analytical expressions of the Lyapunov exponent in the Born approximation and two orders beyond. The numerical curves are obtained from series of calculations at variable $k\sigma_{\rm R}$ values and fixed $\epsilon_{\rm R}$ parameter. The values $\epsilon_{\rm R} = 0.02$ and $\epsilon_{\rm R} = 0.10$ correspond to $V_{\rm R}/\hbar = 2\pi \times 16$Hz in Fig. 3 of Ref. [29], and $V_{\rm R}/\hbar = 2\pi \times 80$Hz

[26] This is a consequence of the self-averaging properties of $\langle \ln[r(z)/r_0] \rangle / |z - z_0|$. See section 1.1.3

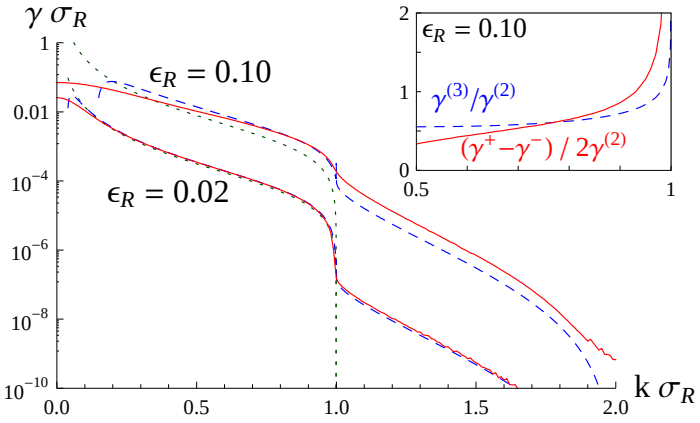


Figure 2.6: Lyapunov exponent as a function of the momentum k in the speckle potential (2.124), as obtained from numerical transfer matrix calculations (red line), the Born approximation $\gamma^{(2)}$ (green dotted line), and the fourth-order approximation $\gamma^{(2)}+\gamma^{(3)}+\gamma^{(4)}$ of the Lyapunov exponent (dashed blue line). The values of $\epsilon_{\rm R} = V_{\rm R}/E_\sigma$ correspond to experimental conditions of Ref. [29]. Inset: contribution of odd terms, normalized by the Born approximation, for $\epsilon_{\rm R} = 0.1$ (red solid line: numerical calculations; dashed blue line: third-order analytical result).

in Figs. 3 and 4 of Ref. [29], respectively. For sufficiently weak disorder ($\epsilon_{\rm R} = 0.02$), we find an excellent agreement of the numerical data with the analytical expression $\gamma^{(2)} + \gamma^{(3)} + \gamma^{(4)}$ down to $k\sigma_{\rm R} \simeq 0.1$. In particular, the drop of γ by about two orders of magnitude at the first effective mobility edge is reproduced, and $\gamma^{(4)}$ is found to provide an accurate description of γ beyond the first effective mobility edge. For larger disorder (here $\epsilon_{\rm R} = 0.1$), the numerical data confirm the trend announced by the analytical approximation, but the truncated weak-disorder expansion breaks down sooner at low energy, and a discrepancy by a factor of roughly two is observed beyond the first effective mobility edge. This signals that, while the three leading orders indeed provide a reasonable estimate of γ, higher-order terms (e.g. $\gamma^{(5)}$) start contributing significantly for such values of $\epsilon_{\rm R}$.

Odd terms - Experimentally and numerically, the odd terms in the weak-disorder expansion of γ can be evaluated by forming $(\gamma^+ - \gamma^-)/2$, where γ^+ and γ^- are the values of γ obtained for $V_{\rm R} > 0$ and $V_{\rm R} < 0$, respectively, with the same k and $\sigma_{\rm R}$. The inset of Fig. 2.6 emphasizes the role of these odd terms. For $\epsilon_{\rm R} = 0.1$ and $k\sigma_{\rm R}$ values ranging from 0.6 to 0.9, the odd terms amount to 30 to 70% of the Born term. The contribution of odd terms can therefore be significant in current experiments with speckle potentials. For weak disorder and away from the divergence at $k\sigma_{\rm R} = 1$, the odd terms are well approximated by the sole third-order contribution $\gamma^{(3)}$.

f_n functions - The f_n functions can be obtained numerically by computing the Lyapunov exponent at fixed $k\sigma_{\rm R}$ and for various potential strength $\epsilon_{\rm R}$, and fitting the result by a polyno-

mial law of $\epsilon_{\rm R}$. The coefficients of the fit are the f_n functions evaluated at point $k\sigma_{\rm R}$:

$$\gamma\sigma_{\rm R} = \sum f_n(k\sigma_{\rm R}) \left(\frac{\epsilon_{\rm R}}{k\sigma_{\rm R}}\right)^n . \tag{2.141}$$

For the fitting procedure to be accurate, the number of free parameters in the fit, i.e. the number of terms in the sum (2.141), has to be kept low. This imposes to perform calculations at very low $V_{\rm R}$ to avoid contributions from higher-order terms, especially at low energy. The procedure is straightforward for the two leading orders f_2 and f_3. The fourth order f_4 is more difficult to extract. For each value of $k\sigma_{\rm R}$, the Lyapunov exponent was computed for $\epsilon_{\rm R}$ in the range $[-0.03k\sigma_{\rm R}, +0.03k\sigma_{\rm R}]$, and a polynomial fit of degree 8 was used to extract the $f_n(k\sigma_{\rm R})$ coefficients. To improve the procedure and discriminate better between the contributions of successive terms, even terms can be extracted from $(\gamma^+ + \gamma^-)/2$, while odd terms are extracted from $(\gamma^+ - \gamma^-)/2$.

The terms f_2, f_3 and f_4 extracted with the above scheme for the speckle model (2.123) are displayed as data points in Fig. 2.4. The agreement with the analytical formulas (2.127) to (2.129) proves to be excellent. In particular, the numerical calculations reproduce the predicted kink at $k\sigma_{\rm R} = 1/2$. These calculations corroborate the analytical expressions found for speckle potentials and, more generally, the expressions derived for the third- and fourth-order Lyapunov exponents in generic random potentials.

2.3.4 Anderson localization of matter waves in speckle potentials

First experiments aiming at the observation of Anderson localization in coordinate space with ultracold atoms were carried out in 2005 [26–28]. In these experiments, the expansion of interacting BECs through speckle potentials was monitored to observe localization effects. However, the experiments were performed in a regime of strong disorder, which prevented the observation of Anderson localization [183]. Subsequently, an experimental scheme was proposed in Ref. [34] in which *weak* speckle potentials are used in order to reach a regime of Anderson localization of non-interacting particles. The theoretical analysis of Ref. [34] also predicted that a signature of the first effective mobility edge of the speckle potential (at $k = k_c = 1/\sigma_{\rm R}$) should be found in the crossover from a regime of exponential localization of the wave packet to a regime where the density profile decays according to a power law. The experiments of Ref. [29] provided evidence of Anderson localization, and confirmed this scenario. They also raised the question as to how particles localize beyond the first effective mobility edge. As we shall see below, the results of this chapter provide an answer to this question.

Let us first summarize the experimental scheme, the theoretical model describing the localization process, and the experimental results. Details can be found in Refs. [29, 34, 183, 203].

Theoretical model

In the experiment envisioned in Ref. [34], an interacting BEC is released from a harmonic trap and left to expand in a 1D geometry, in the presence of a speckle potential (see Fig. 2.7). The amplitude of the speckle potential is chosen to be much smaller than the chemical potential of the BEC initially at rest in the trap. This choice ensures a conversion of the initial interaction energy into kinetic energy before localization in the random potential.

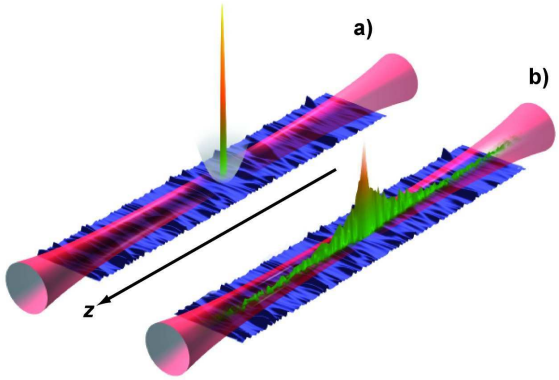


Figure 2.7: Experimental scheme of Ref. [29], where the 1D Anderson localization of matter waves in a speckle potential was observed. (a) Atomic Bose-Einstein condensate initially held at rest in the combined potential formed by a magnetic trap (gray), a 1D speckle potential created by a blue-detuned laser, and a 1D wave guide created by a red-detuned laser. (b) Stationary, localized density profile observed after expansion of the BEC in the wave guide.

Expansion - A two-stage model is adopted to describe the expansion. The disorder is assumed to play no role during the onset of the expansion, as its amplitude is much smaller than the interaction energy per atom in the initial trap. At the end of this first stage, the wave packet has a momentum distribution $\mathcal{D}(k)$ known from the analysis of the expansion without disorder. The distribution $\mathcal{D}(k)$ has a high-k cutoff $k_{\max}$ set by the chemical potential of the initial (trapped) cloud. In the second stage, the gas has become dilute and the interaction energy is much smaller than the typical kinetic energy. The wave packet is described by a collection of non-interacting waves ϕ_k which are scattered elastically by the random potential and localize. Assuming that the relative phases of the wave-packet components ϕ_k have been scrambled by the random potential, the total density writes

$$n_0(z) = 2\int_0^\infty \mathrm{d}k\mathcal{D}(k)\langle|\phi_k(z)|^2\rangle. \tag{2.142}$$

The behavior of the densities $\langle|\phi_k(z)|^2\rangle$ is analyzed at the level of the Born approximation [228, 229]. Thus, for $k < k_c$, the $\langle|\phi_k(z)|^2\rangle$ are exponentially localized with a Lyapunov exponent determined in the Born approximation. For $k > k_c$, on the other hand, the ϕ_k components are assumed not to localize on the length scale of the system[27] and not to contribute to the localized profile of the wave packet. The integration is therefore truncated at k_c in Eq. (2.142). As the distribution $\mathcal{D}(k)$ has a high-k cutoff $k_{\max}$, Eq. (2.142) rewrites

$$n_0(z) = 2\int_0^{\min(k_c,k_{\max})} \mathrm{d}k\mathcal{D}(k)\langle|\phi_k(z)|^2\rangle. \tag{2.143}$$

The asymptotic behavior of $n_0(z)$ at large z is dominated by the ϕ_k components close to the cutoff set by k_c or $k_{\max}$, as those states have the longest localization lengths [34, 183].

[27] It has been checked numerically in Ref. [34] that, for parameters which are close to those of the experiment of Ref. [29], the localization lengths for $k > k_c$ exceeds the system sizes achievable in current experiments.

Localization regimes - The analysis of Eq. (2.143) shows that the asymptotic behavior of $n_0(z)$ depends qualitatively on which of the two cutoffs k_c and $k_{\max}$ is the limiting one. For $k_{\max} < k_c$, an exponential localization of $n_0(z)$ is found. For $k_{\max} > k_c$, on the other hand, the asymptotic decay of $n_0(z)$ follows a power law $n_0(z) \propto |z|^{-2}$. In that case, the components ϕ_k with $k < k_c$ are (individually) exponentially localized, but their contributions sum up to an algebraic (power-law) density profile.

Experiment

Figure 2.7 shows a schematic of the experiment performed in Ref. [29]. A Bose-Einstein condensate is initially held at rest in a magnetic trap [in gray in Fig. 2.7(a)] in the presence of a blue-detuned speckle potential. A red-detuned laser beam additionally creates a wave guide to restrict the subsequent motion of the atoms to the direction along the z-axis. The speckle potential is created behind a rectangular aperture, and therefore follows model (2.123), with a correlation length $\sigma_{\mathrm{R}} = 0.26\,\mu$m in the z-direction. At time $t = 0$, the harmonic trap is switched off, and the cloud starts expanding in the 1D wave guide as the interaction energy of the atoms present in the trap is converted into kinetic energy. Absorption images reveal that the atomic wave packet reaches a stationary density profile after an expansion time of the order of one second [Fig. 2.7(b)]. In the tails of the stationary profile, the gas is very dilute, and the kinetic energy by far exceeds the interaction energy. Localization is characterized by fitting the density $n_0(z)$ in the wings of the stationary profile (see Fig. 2.8).

Results - Evidence for both the exponential localization and the algebraic regime was found in the experiments of Ref. [29]. Figure 2.8 shows stationary density profiles obtained in the experiment. The density profile in Fig. 2.8(a) is obtained for $k_{\max} > k_c = 1/\sigma_{\mathrm{R}}$, and decays with a power law, as shown by the double-logarithmic plot (main graph). In Fig. 2.8(b), the data is obtained for $k_{\max} > k_c = 1/\sigma_{\mathrm{R}}$, and the density profile decays exponentially, as shown by the log-linear plot in the inset. These findings demonstrate the consequences an effective mobility edge may have on the localization properties of non-interacting particles.

Beyond the first effective mobility edge

The algebraic regime for $k_{\max} > k_c$ arises because of the drop of the Lyapunov exponent at the effective mobility edge and the fact that the atoms with $k > k_c = 1/\sigma_{\mathrm{R}}$ are not localized within the system size. The results of this chapter allow a more precise description of the regime $k_{\max} > k_c$ as i) they provide an precise estimate of the localization lengths of wave-packet components with $k > 1/\sigma_{\mathrm{R}}$, ii) they can be used to discuss when the contribution of these components can be neglected, and iii) conversely, they can form the basis of an analysis beyond the algebraic regime.

In Fig. 2.9, we plot the analytical expression $\gamma^{(2)} + \gamma^{(3)} + \gamma^{(4)}$ for the same parameters as in Figs. 2.8(a) and 2.8(b), and we indicate in thick lines those momentum classes that are populated. The vertical lines correspond to the cutoffs $k_{\max}$ imposed by the momentum distribution of the cloud. The typical system size (i.e. the size of the experimentally-accessible region) is indicated by a horizontal line (see caption of Fig. 2.8). For $k_{\max}\sigma_{\mathrm{R}} = 0.65$, which corresponds to the exponential regime, all k components are well localized within the system. In the case $k_{\max}\sigma_{\mathrm{R}} = 1.15$, which corresponds to the algebraic regime, the Lyapunov exponent

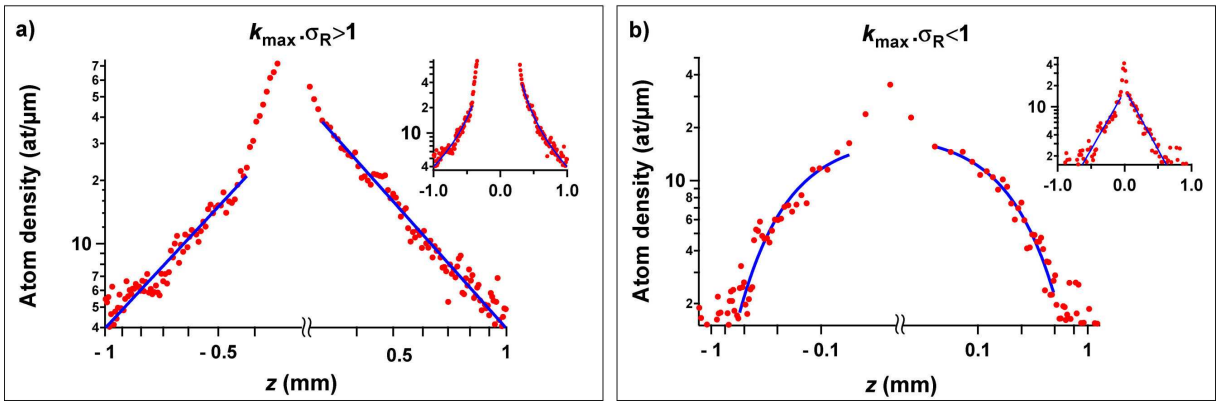


Figure 2.8: Stationary density profiles of a matter wave in a 1D speckle potential. The scales (log-log in the main graphs, semi-log in the insets) reveal the difference between the algebraic ($k_{\max}\sigma_{\rm R} > 1$) and exponential ($k_{\max}\sigma_{\rm R} < 1$) regimes. Here $k_{\max}$ corresponds to a cutoff in the momentum distribution of the cloud, and $\sigma_{\rm R}$ is the correlation length of the speckle potential ($\sigma_{\rm R} = 0.26\,\mu$m, $E_\sigma/h = 860\,$Hz). (a) Algebraic regime observed for $k_{\max}\sigma_{\rm R} = 1.16$. The wings are fitted with a power law $1/|z|^\beta$ which yields values of β close to 2 [29]. (b) Exponential regime observed for $k_{\max}\sigma_{\rm R} = 0.65$. The wings are fitted with exponentials. The potential amplitudes in (a) and (b) are $V_{\rm R}/E_\sigma = 0.09$ and $V_{\rm R}/E_\sigma = 0.04$, respectively.

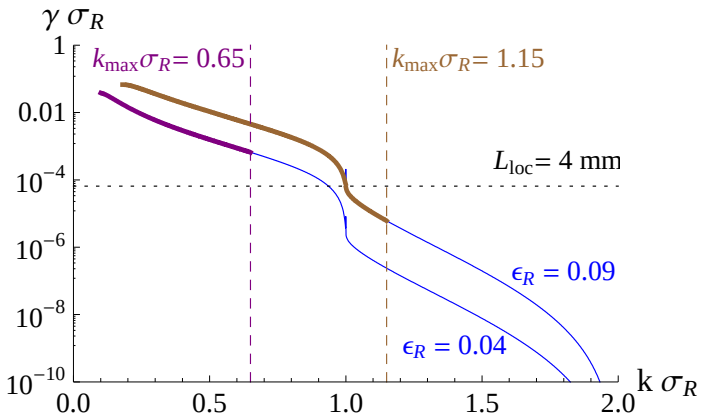


Figure 2.9: Effect of the first effective mobility edge in a speckle potential on the localization of an expanding wave packet. The thin blue lines correspond the Lyapunov exponent of single particles with energy $E = \hbar^2k^2/2m$, calculated two orders beyond the Born approximation (see section 2.3.2 and Fig. 2.6), for the values of $\epsilon_{\rm R} = V_{\rm R}/E_\sigma$ in Fig. 2.8. The thick lines on top indicate which momentum classes are populated in the expanding BECs of Fig. 2.8 (the lowest momentum classes are not shown). The cutoffs of the momentum distributions appear as dashed lines. The horizontal line indicates the localization length which corresponds to half the system size, defined by both the field width of the absorption images which are taken of the cloud and the $1/e$ extent of the 1D speckle field along z. Localization lengths of up to 2 mm have been measured in Ref. [29].

of the k components beyond the effective mobility edge drop well below the inverse system size. These components are therefore effectively extended on the length scale of the system. Physically, this most probably means that the associated wave packet leaves the system.

Hence, Fig. 2.9 shows that the contribution of the atoms beyond the first effective mobility in the case $k_{\max}\sigma_{\mathrm{R}} = 1.15$ can be neglected. The analysis carried out in this section thereby corroborates the findings of Refs. [29,34], and confirms the relevance of effective mobility edges in speckle potentials.

Finally, our analysis shows that exponential localization of the wave packet can be expected even in the regime $k_{\max} > 1/\sigma_{\mathrm{R}}$. To observe this regime, however, much longer systems and an accurate measurement of very low atom densities would be required.

2.4 Conclusion

In this chapter we studied one-dimensional Anderson localization of non-interacting particles in correlated random potentials. A weak-disorder perturbative expansion of the Lyapunov exponent (inverse localization length) was carried out two orders beyond the usual Born approximation to describe the localization caused by higher-order scattering processes in the potential.

The phase formalism used in the expansion directly leads to a perturbation series for the exact Lyapunov exponent, without any additional approximation, such as the diffusion approximation used in higher dimensions [40,41]. Moreover, the Lyapunov exponent calculated in the expansion is a self-averaging quantity [86], and therefore describes the typical behavior of large disordered systems.

We found simple expressions for the three leading orders of the Lyapunov exponent as a function of the single-particle energy and the correlation functions of the random potential. These results apply to potentials which need not be delta-correlated, Gaussian, or symmetric.

We examined models of random potentials whose spatial power spectra have a finite support, limited e.g. by a high momentum cutoff. For these models, the Lyapunov exponent calculated in the Born approximation vanishes identically over an extended region of the single-particle spectrum. An inspection of the higher-order terms in the perturbation series shows that, quite generally, higher-order terms extend the region of localization. However, higher orders may also have cutoffs. This is systematically the case for Gaussian potentials which have a cutoff in their power spectrum. We showed that this can also be the case in non-Gaussian potentials, for instance in the speckle potentials used in current experiments with ultracold atoms.

Each of the cutoffs found in the perturbation orders defines an *effective mobility edge*, which separates regions of the single-particle spectrum where localization is caused by scattering processes of increasing order. In weak potentials, these effective mobility edges thus correspond to sharp drops in the magnitude of the Lyapunov exponent. Experiments with ultracold atoms in speckle potentials have shown that an effective mobility edge might affect significantly the transport and localization properties of non-interacting wave packets. We provided an quantitative answer to the question of how the single-particle states beyond such an effective mobility edge localize.

In higher-dimensions, elastic scattering is possible at various deflection angles, and the random potential can transfer a continuum of momentum values to the particles. As a consequence, the effects associated with cutoffs in 1D are expected to be washed out. It would nevertheless

be interesting to study whether such special long-range correlations have a non-trivial effect on localization in 2D and 3D.

CHAPTER 3

Weakly-interacting Bose gas in a correlated 1D random potential

In his seminal publication, Anderson showed that disorder could have dramatic effects on the transport of non-interacting particles [1], and subsequent work lead to the astounding conclusion that, generally, an infinitesimal amount of disorder leads to an exponential localization of all single-particle states in one and two dimensions [53]. In chapter 2, we showed that the strength of localization in 1D could depend crucially on the statistical properties of the disorder. Localization was nevertheless found to occur. However, an important challenge arises with the description of interacting systems, as there is no simple theoretical answer on the interplay of disorder, interactions and kinetic energy, even in the ground state of a many-body system. In particular, it is known that interactions may compete or cooperate with disorder to localize the particles, depending on the regime of interactions (see section 1.2.2 and below). Elucidating this interplay is central to the understanding of metal-insulator or superfluid-insulator transition in the presence of disorder.

In this chapter, we study the ground-state of a disordered Bose gas with weak repulsive interactions. We assume that the disorder is one-dimensional, but allow for transverse degrees of freedom of the Bose gas. We discuss the quantum states of the Bose gas as a function of the strength of interactions and disorder, focusing on localization properties from the point of view of the boson density distribution and on a microscopic description of the underlying states.[1] For interactions which are strong enough, while remaining compatible with mean-field approaches (see below), the Bose gas forms a delocalized, disordered Bose-Einstein condensate (BEC) phase. For weaker interactions, the BEC is fragmented under the influence of the random potential. For very weak interactions, on the other hand, the Bose gas populates a small number of low-energy single-particle states called Lifshits states. The range of parameters for which this microscopic description of the many-body state applies is called Lifshits glass regime.

This chapter is organized as follows. In section 3.1, we emphasize the relevance of a microscopic description of the weakly-interacting regime of disordered 1D bosons. In section 3.2, we precisely define the framework of our study. In section 3.3 we describe the BEC phase, starting from the limit without disorder. The Lishits glass regime, on the other hand, is described in section 3.4, starting from the non-interacting case. Finally, section 3.5 provides a discussion of the quantum-state boundaries. This discussion is based both on scaling arguments and explicit results derived in this chapter.

[1] Our findings are summarized in the quantum-state diagram of Fig. 3.10 on page 122. In this diagram, the interactions increase from left to right and the amplitude of disorder from bottom to top.

3.1 Introduction

Initially triggered by experiments on liquid helium in porous media [10], the "dirty boson" problem [6–8, 128] has attracted a lot of attention since the eighties, as it raises the question of the possible destruction of superfluidity by disorder and disorder-induced localization phenomena. These localization effects are determined by the complex interplay of disorder and interactions, the understanding of which is probably the most advanced in the one-dimensional geometry.

Figure 3.1(a) displays the result of a numerical study of the ground-state quantum-phase diagram of disordered 1D bosons in the presence of a lattice. The average number of bosons per lattice site in this figure (filling 0.5) is such that, qualitatively, the conclusions apply to the continuous case (without lattice potential).[2] For moderate interactions and weak disorder, the bosons form a delocalized superfluid phase, as in a disorder-free Bose system. For strong disorder, a disordered, gapless insulating phase is found, which is called Bose glass [8, 128]. Interestingly, this phase extends to the range of weak disorder for both weak and strong interactions, and encloses the superfluid regime.

The insulating regime depicted close to the left axis in Fig. 3.1(a) is consistent with the behavior expected on the line of vanishing interactions. On that line, the bosons are all localized, according to general results on the localization of non-interacting particles in 1D. However, as pointed out in Ref. [128], this does not guarantee an easy description of the region for very weak but non-vanishing repulsion between the bosons. The situation where all the bosons populate the localized single-particle ground-state is often said to be unstable with respect to the introduction of a small amount of interactions. This point will be addressed in section 3.4.

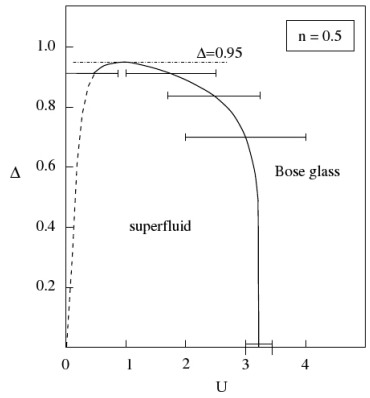
As for the presence of the Bose glass phase both for weak and strong disorder, it is explained by two different effects depending on the disorder strength. This twofold effects of interactions were explicitly put forward by Scalettar *et al.* [130]. Figure 3.1(b) reproduces their observation of the non-monotonous behavior of the superfluid density ρ_s as a function of the interaction strength. In lattice systems without disorder, ρ_s is maximum at low V/t, and decreases monotonously as V/t increases. In the presence of disorder, however, the superfluid density vanishes for the lowest values of V/t.[3] This destruction of superfluidity is attributed to an Anderson-like localization of the bosons [130]. The increase of ρ_s observed in Fig. 3.1(b) for slightly larger V/t ratios, on the other hand, is interpreted as a manifestation of the fact that *weak* interactions *compete* with the disorder, and favor a *delocalization* of the bosons.[4]

In contrast, it is recognized that *strong* interactions *cooperate* with the disorder to *localize* the particles, reduce the number fluctuations and destroy the phase coherence of the many-body systems [128, 130, 148]. This behavior is consistent with the propensity of strongly-interacting bosons to form a localized Mott insulator in the presence of a disorder-free lattice potential [136, 146, 147]. Let us emphasize that, in such a regime of strong interactions, the term of "localization" takes a different meaning than in the Anderson case. In the case of Anderson localization, the density profile of the gas is highly inhomogeneous on long length scales. For strong interactions, this term is used to characterize the many-body system from the point of

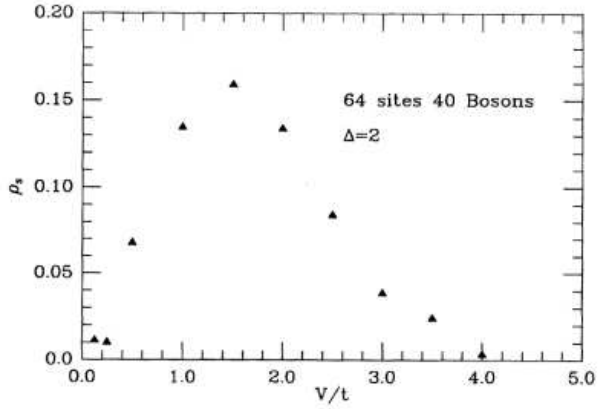
[2] Diagram 3.1(a) agrees qualitatively with the analytical results of Ref. [8] for the continuous 1D case.

[3] Scalettar *et al.* emphasize that for the parameters of Fig. 3.1(b) the superfluid fraction vanishes identically below a threshold interaction strength, which is small, but strictly positive.

[4] This behavior is understood at the mean-field level (see sections 3.3.2 and appendix D) as a penalty imposed by interactions on highly inhomogeneous, localized density profiles.



(a) DMRG, filling 0.5, hopping $t/2 = 1/2$ (Fig. 2 of Ref. [148]).



(b) Monte Carlo, filling 0.625, hopping t, disorder $\Delta/t = 10$ (?) (Fig. 4 of Ref. [130]).

Figure 3.1: Phases of disordered 1D lattice Bose gases. (a) Quantum phase diagram of the 1D disordered Bose Hubbard with random on-site energies $\epsilon_i \in [-\Delta, \Delta]$, at filling 0.5, obtained by DMRG calculations in Ref. [148]. (b) Superfluid fraction ρ_s of a disorder 1D lattice Bose gas as a function of the ratio of on-site repulsion V to tunneling energy t. The data was obtained by Scalettar *et al.* in a Monte-Carlo study of the disorder Bose-Hubbard model with random on-site energies $\epsilon_i \in [-\Delta, \Delta]$, for $\Delta/t = 10$ (?), at incommensurate filling 0.625.

view of correlation functions, and the density profile of the gas is globally delocalized [8].

Numerical calculations support the conclusion that the weakly- and strongly-interacting regimes surrounding the superfluid phase form a unique Bose glass phase [148]. This phase is characterized by a gapless excitation spectrum, a vanishing superfluid fraction and a non-vanishing compressibility, following the definition by Fisher *et al.* [128]. In the numerical calculations of Ref. [148], no abrupt change in macroscopic observables such as the compressibility and the superfluid fraction (indicating a phase transition) was found between the weakly- and strongly-interacting regimes of the insulator. However, as explained above, the effect of interactions is different in those two regimes, and providing physically-transparent pictures of the microscopic processes at work in both regimes is of considerable interest. For the regime of strong interactions, analytical results describing the superfluid-insulator transition at weak disorder were derived in Ref. [8] (see Fig. 1.7(c) on page 29).

In this chapter, we address the weakly-interacting part of the zero-temperature quantum-phase diagram.[5] The subject of disordered, weakly-interacting bosons itself has seen a surge of interest in recent years. Theoretical studies have focused so far on the effect of disorder on the condensate and superfluid fractions as a function of disorder strength [132, 230–233], thermodynamics and the normal-superfluid transition [132,234,235], collective oscillations [236, 237], transport [238–241], sound propagation [231, 233], density modulations [171, 242] and elementary excitations (see chapter 4) in the (quasi-) BEC regime. Here, we concentrate on the description of the zero-temperature quantum states of the system, in order to characterize

[5] In the quantum phase diagrams of Figs. 3.1(a) and 3.1(b), this regime corresponds qualitatively to the part found left of the tip of the superfluid lobe, both in the superfluid and in the Bose-glass regimes. Thus, as far as the (Bose-glass) insulator is concerned, it corresponds entirely to the regime called Anderson glass by Scalettar *et al.* [130].

the superfluid (quasi-BEC) and insulator phases from the point of view of localization, and to locate quantum-state boundaries [243]. We examine the disordered (quasi-) BEC phase and the crossover to the (insulating) regime of fragmented BEC, as well as the deep insulating regime found for very weak interactions or strong disorder.

Related and complementary studies appeared in Refs. [28, 244–247]. In Refs. [28, 244], the destruction of localization by a weak non-linearity and the superfluid-insulator transition, respectively, were studied numerically. Recently, the deep fragmentated regime at very weak interactions and strong disorder has also been addressed in Refs. [245–247].

3.2 Framework of the analysis

3.2.1 Weakly-interacting Bose gases

Many-body Hamiltonian

We consider in this chapter d-dimensional ultracold Bose gases, with weak repulsive interactions.[6] These interactions are modeled by a contact interaction potential

$$V_{\rm int}(\mathbf{r}-\mathbf{r}') = g\delta(\mathbf{r}-\mathbf{r}'), \tag{3.1}$$

where g is a positive coupling constant. The many-body Hamiltonian describing the system then takes the form [248, 249]

$$\hat{H} = \int \mathrm{d}\mathbf{r} \left\{ \hat{\Psi}^\dagger(\mathbf{r}) \left[-\frac{\hbar^2\nabla^2}{2m} + V_{\rm ext}(\mathbf{r}) \right] \hat{\Psi}(\mathbf{r}) + \frac{g}{2}\hat{\Psi}^\dagger(\mathbf{r})\hat{\Psi}^\dagger(\mathbf{r})\hat{\Psi}(\mathbf{r})\hat{\Psi}(\mathbf{r}) \right\}, \tag{3.2}$$

where $\hat{\Psi}$ and $\hat{\Psi}^\dagger$ are field operators which satisfy bosonic commutation relations

$$[\hat{\Psi}(\mathbf{r}), \hat{\Psi}^\dagger(\mathbf{r}')] = \delta(\mathbf{r}-\mathbf{r}'), \qquad [\hat{\Psi}(\mathbf{r}), \hat{\Psi}(\mathbf{r}')] = 0, \tag{3.3}$$

m is the mass of the particles, and $V_{\rm ext}$ is an external potential acting on them.

The assumption of weak interactions implies

$$n^{1-2/d} \ll \frac{\hbar^2}{mg}, \tag{3.4}$$

where n is the d-dimensional gas density. In 3D, the coupling constant reads [32]

$$g = \frac{4\pi\hbar^2 a_s}{m}, \tag{3.5}$$

where a_s is the 3D s-wave scattering length [111]. Hence, weak interactions are achieved for

$$n a_s^3 \ll 1 \tag{3.6}$$

[6] Low-dimensional systems ($d < 3$) are achieved by using strongly confining potentials. Such potentials create an energy splitting for "transverse" single-particle excitations (i.e. excitations out of the "longitudinal" d-dimensional geometry) by a mere finite-size effect. If this splitting is larger than any relevant energy scale of the d-dimensional problem, the particles are frozen into the transverse single-particle ground state, and the system is effectively d-dimensional.

in 3D. For lower-dimensional geometries, effective coupling constants are obtained from the 3D case [250–252].

The density n is related to the quantum state $|\Psi\rangle$ under consideration through

$$n(\mathbf{r}) = \langle\Psi|\hat{\Psi}(\mathbf{r})^\dagger\hat{\Psi}(\mathbf{r})|\Psi\rangle, \tag{3.7}$$

and to the number N of atoms in the system via

$$N = \int \mathrm{d}\mathbf{r}\, n(\mathbf{r}). \tag{3.8}$$

Criterion (3.4) is derived from the requirement that the interaction energy gn be much smaller than the kinetic energy $\hbar^2/2ma^2$ associated with the mean interparticle spacing $a = n^{-1/d}$, so that forming a crystal of regularly spaced particles costs the system more kinetic energy than the interaction energy gained by such a localization. In that case, the correlations induced by interactions between particles are assumed to be small or negligible. This distinguishes weakly-interacting Bose gases from strongly correlated systems. Note that inequality (3.4) is satisfied for dilute systems in 3D [253], and for high densities in 1D [251, 254, 255]. The 2D geometry is the marginal case, and the criterion for weak interactions has no dependence, or only a weak logarithmic dependence, on the density [252, 256].

What determines the properties of the Bose gas ?

We work here in the grand canonical ensemble, where the system is assumed to exchange both energy and particles with a reservoir. Then, the system is described by the grand-canonical Hamiltonian

$$\hat{K} = \hat{H} - \mu\hat{N} = \int \mathrm{d}\mathbf{r} \left\{ \hat{\Psi}^\dagger(\mathbf{r}) \left[-\frac{\hbar^2\nabla^2}{2m} + V_{\mathrm{ext}}(\mathbf{r}) - \mu \right] \hat{\Psi}(\mathbf{r}) + \frac{g}{2}\hat{\Psi}^\dagger(\mathbf{r})\hat{\Psi}^\dagger(\mathbf{r})\hat{\Psi}(\mathbf{r})\hat{\Psi}(\mathbf{r}) \right\}, \tag{3.9}$$

where μ is the chemical potential of the Bose gas, and $\hat{N}$ is the number operator

$$\hat{N} = \int \mathrm{d}\mathbf{r}\hat{\Psi}^\dagger(\mathbf{r})\hat{\Psi}(\mathbf{r}). \tag{3.10}$$

In the grand-canonical Hamiltonian, the number of particles is allowed to have statistical fluctuations,[7] but the average number of particles $N = \langle\Psi|\hat{N}|\Psi\rangle$ is imposed by μ.[8] Physically, the chemical potential corresponds to the energy gained by the system upon addition of one particle. Hence, we can think of μ as a typical energy per particle, although it differs from the average energy per particle because of interactions.

[7] Then, the density matrix of the system necessarily has entries corresponding to Fock states with various numbers of particles. This is *also* the case when the quantum field $\hat{\Psi}$ is assumed to be in a coherent state, as in descriptions of a Bose condensate by a classical field with well-defined phase [257].

[8] The choice of the grand-canonical ensemble can be motivated on physical grounds, or by technical reasons. The introduction of a chemical potential proves convenient when seeking a ground state of $\hat{H}$, i.e. a quantum state $|\Psi\rangle$ minimizing $\langle\Psi|\hat{H}|\Psi\rangle$, under the constraint of a given average number of particles $N = \langle\Psi|\hat{N}|\Psi\rangle$. In the grand-canonical ensemble, μ is a Lagrange multiplier used to solve this problem of constrained optimization (see section 3.3.2). Such a Lagrange multiplier is systematically used in descriptions of the Bose gas where the number of particles is not known *a priori*, such as the non-conserving Bogolyubov approach [258].

In equation (3.9) we identify the various forms of energy whose interplay determines the properties of the Bose gas: a term of kinetic energy, the external potential $V_{\rm ext}$, the chemical potential μ, and an interaction term of magnitude gn. In this chapter, we study the ground state of a weakly-interacting Bose gas in a 1D random potential, described below.

3.2.2 Trap geometry and disorder

For the discussion of the combined effect of disorder and weak interactions on a Bose gas, we consider a 3D Bose gas confined to a box of length $2L$ in the longitudinal z-direction, in the presence of a 1D random potential $V(z)$. We assume that the gas is trapped in the transverse directions by a two-dimensional harmonic potential $V_\perp$ with homogeneous frequency $\omega_\perp$:

$$V_{\rm ext}(\rho, z) = V_\perp(\rho) + V(z) \tag{3.11}$$

$$V_\perp(\rho) = \frac{1}{2} m\omega_\perp^2 \rho^2, \tag{3.12}$$

where $\rho = \sqrt{x^2+y^2}$ is the radial coordinate in the plane perpendicular to the z-axis. Note that the random potential is translation-invariant in that transverse plane. When the harmonic confinement is so tight that the energy splitting $\hbar\omega_\perp$ between the oscillator levels exceeds any other energy scale in the problem (in particular the chemical potential μ), the particles are frozen into the ground state of the radial oscillator, and the system is kinematically 1D. Then, the analysis can be carried out in the framework of Eqs. (3.1) to (3.10) with $d = 1$ and the sole random potential $V(z)$. Conversely, if the trapping is shallow, transverse degrees of freedom need to be considered explicitly.

The disorder is assumed to have a vanishing average ($\langle V\rangle = 0$) and to be homogeneous in the sense that its statistical properties are independent of *absolute* coordinates along z (see section 1.3.1). We write

$$V(z) = V_{\rm R} v(z/\sigma_{\rm R}), \tag{3.13}$$

where $|V_{\rm R}| = \sqrt{\langle V\rangle}$ is the root-mean-square amplitude of the potential, and $\sigma_{\rm R}$ its correlation length.[9] As in chapter 2, the model of disorder is then characterized by a set of reduced n-point correlation functions

$$\langle v(u_0)v(u_1)\cdots v(u_{n-1})\rangle = c_n(u_1-u_0,\cdots,u_{n-1}-u_0) \tag{3.14}$$

with, in particular, a reduced autocorrelation function

$$c_2(u) = \langle v(u_0)v(u_0+u)\rangle \tag{3.15}$$

which has amplitude $c_2(0) = \langle v^2\rangle = 1$ at the origin, and typical width unity. The ratio of the potential amplitude $V_{\rm R}$ and the energy scale $E_\sigma = \hbar^2/2m\sigma_{\rm R}^2$ associated with the correlation length appears either as

$$\epsilon_{\rm R} = \frac{V_{\rm R}}{E_\sigma} \tag{3.16}$$

or as

$$\alpha_{\rm R} = \frac{1}{\epsilon_{\rm R}} \tag{3.17}$$

[9] A definition of the correlation length may depend on the precise model of disorder. See the discussion of section 1.3.1.

to comply with the notations of chapter 2 and Ref. [243]. Neither $\epsilon_{\rm R}$ nor $\alpha_{\rm R}$ need be small.

As an illustration of our approach, we will consider a repulsive ("blue-detuned") 1D speckle potential, which in the present context means that v has the single-point probability distribution

$$P[v(u)] = \begin{cases} \mathrm{e}^{-[v(u)+1]} & \text{if } v(u) \geq -1 \\ 0 & \text{otherwise} \end{cases} . \tag{3.18}$$

The reduced autocorrelation function assumes the form

$$c_2(u) = \mathrm{sinc}(u)^2 \equiv \frac{\sin(u)^2}{u^2}, \tag{3.19}$$

as for a speckle pattern created from a square diffusive plate with uniform illumination [31].

3.3 Delocalized BEC regime

The present chapter aims at developping a microscopic description of disordered, weakly-interacting Bose gases, and at characterizing the density profile of the gas from the point of view of localization. In this section we examine the case where the disorder is weaker than the interactions. A priori, this means that the amplitude of the random potential should be smaller than the chemical potential ($V_{\rm R} \ll \mu$). This turns out to be a sufficient criterion. A more accurate criterion, which involves the detailed correlations of the random potential, is derived in our analysis. In this regime of weak disorder, the Bose gas forms a delocalized Bose-Einstein condensate, or a quasi-BEC in elongated geometries (see below). The density profile of the Bose gas is described starting from the homogeneous case, where the random potential is absent, and the weak potential is introduced as a perturbation.

This section is organized as follows. We briefly present the standard field theory and mean-field description of weakly-interacting Bose gases. Then, a perturbation expansion is presented which allows for a precise description of the ground-state density profile in (arbitrary) weak potentials. Finally, these results are applied to the study a trapped Bose gas in correlated 1D disorder. In this last part, in particular, we discuss the regime of parameters for which the Bose gas indeed forms a single delocalized phase.

3.3.1 Quantum field for condensates and quasi-condensates

Condensates and quasi-condensates

Weakly-interacting 3D Bose gases undergo Bose-Einstein condensation at low temperatures, when they reach a phase-space density $n\lambda_{\rm dB}^3$ larger than one, where $\lambda_{\rm dB} = (\hbar^2/2\pi m k_B T)^{1/2}$ is the thermal de Broglie wavelength of the atoms at temperature T. Following the criterion of Penrose and Onsager [154, 155] and the subsequent work of C. N. Yang [156],[10] condensation is characterized by off-diagonal long-range order in the one-body density matrix $\rho_1(\mathbf{r}, \mathbf{r}') = \langle \Psi | \hat{\Psi}^\dagger(\mathbf{r}) \hat{\Psi}(\mathbf{r}') | \Psi \rangle$, which essentially means that $\rho_1(\mathbf{r}, \mathbf{r}')$ does not decay to zero for large separation of $\mathbf{r}$ and $\mathbf{r}'$ [259, 260].

[10] Yang showed the equivalence of the criterion of a large eigenvalue of the one-body density matrix $\hat{\rho}_1$ with the presence of off-diagonal long-range order in $\hat{\rho}_1$ and higher-order density matrices.

Under certain circumstances, which we touch upon below, the field operator can be written $\hat{\Psi}(\mathbf{r}) = \mathrm{Exp}[\mathrm{i}\hat{\theta}(\mathbf{r})]\sqrt{\hat{n}(\mathbf{r})}$, where $\hat{n}$ and $\hat{\theta}$ are density and phase operators, respectively. It is known that in infinite homogeneous 1D and 2D systems, no condensate exists at any temperature $T > 0$, due to long-wavelength phase fluctuations [261–263]. In 1D, the absence of true condensate persists down to zero temperature, where a power-law decay of the one-body density matrix ρ_1 is found as a function of the separation $|r - r'|$ [139, 147].[11] Remarkably, however, a weakly-interacting 1D Bose gas close to the ground state has reduced density fluctuations, as in the case of BEC [251, 263, 264]. Therefore, such a 1D Bose gas with fluctuating phase and reduced density fluctuations is called quasi-condensate, or quasi-BEC.[12] It turns out that BEC and quasi-BEC can be treated on the same footing (see Ref. [256] and below) and, as long as one is interested in the properties of the gas density, as is the case here, the distinction between BEC and quasi-BEC is not crucial. In the following, we shall not systematically distinguish between the two.

Hamiltonian in the density-phase picture

In fact, the weak density fluctuations also allow for the above representation of the field operator as

$$\hat{\Psi}(\mathbf{r}) = \mathrm{e}^{\mathrm{i}\hat{\theta}(\mathbf{r})}\sqrt{\hat{n}(\mathbf{r})}, \tag{3.20}$$

where

$$\hat{n}(\mathbf{r}) = \hat{\Psi}^\dagger(\mathbf{r})\hat{\Psi}(\mathbf{r}). \tag{3.21}$$

In these expressions, $\hat{\theta}(\mathbf{r})$ and $\hat{n}(\mathbf{r})$ are Hermitian phase and density operators [256,264,269,270], which satisfy the commutation relation[13]

$$[\hat{n}(\mathbf{r}), \hat{\theta}(\mathbf{r}')] = \mathrm{i}\delta(\mathbf{r} - \mathbf{r}'). \tag{3.22}$$

Then, in terms of the phase and density operators, Hamiltonian (3.2) and the number operator are rewritten as

$$\begin{aligned}\hat{H} &= \int \mathrm{d}\mathbf{r} \left\{ \frac{\hbar^2}{2m} \left[(\nabla\sqrt{\hat{n}})^2 + \sqrt{\hat{n}}(\nabla\hat{\theta})^2\sqrt{\hat{n}} + \mathrm{i}\nabla\sqrt{\hat{n}}\nabla\hat{\theta}\sqrt{\hat{n}} - \mathrm{i}\sqrt{\hat{n}}\nabla\hat{\theta}\nabla\sqrt{\hat{n}} \right] + V_{\mathrm{ext}}(\mathbf{r})\hat{n} \right\} \\ &\quad + \frac{g}{2}\int \mathrm{d}\mathbf{r}\sqrt{\hat{n}}\,\mathrm{e}^{-\mathrm{i}\hat{\theta}}\hat{n}\,\mathrm{e}^{\mathrm{i}\hat{\theta}}\sqrt{\hat{n}}\end{aligned} \tag{3.23}$$

[11] Systems with power-law decay of correlation functions are sometimes said to display quasi-long-range order.

[12] Phase fluctuations are important for elongated systems. In the presence of a trapping potential, a low-energy (long-wavelength) cutoff is imposed on excitations carrying phase fluctuations [265]. This leads to the formation of partial phase coherence across the system, characterized by a phase coherence-length. Depending on the system size, a crossover is observed between a quasi-BEC regime, where the phase coherence-length is smaller than the system size, and a BEC in the opposite case where the phase coherence-length exceeds the system size [251, 252, 266–268], and the gas displays global phase coherence. In our model, the Bose gas is expected to be qualitatively close to the one-dimensional quasi-BEC regime if the radial oscillator energy $\hbar\omega_\perp$ exceeds μ, and μ itself exceeds by far a finite-size cutoff of the form $\hbar^2/mL^2$ [251].

[13] The definition of a phase operator with those desired properties is a standard problem of quantum optics (see e.g. Refs. [271], [272] and references therein). For non-zero but small fluctuations of the associated density operator $\hat{n}$ around a large expectation value n, however, it is admitted that the phase and density operators are well behaved and satisfy relation (3.22).

and

$$\hat{N} = \int \mathrm{d}\mathbf{r}\, \hat{n}(\mathbf{r}). \tag{3.24}$$

In this formulation, the Bogolyubov approach leading to Eq. (1.20) is generalized, and the density operator $\hat{n}(\mathbf{r})$ is expanded as

$$\hat{n}(\mathbf{r}) = n(\mathbf{r}) + \delta\hat{n}(\mathbf{r}), \tag{3.25}$$

where $n(\mathbf{r})$ is a classical field, and $\delta\hat{n}(\mathbf{r})$ is a small fluctuation field: $||\delta\hat{n}(\mathbf{r})|| \ll n(\mathbf{r})$. To zeroth order in $\delta\hat{n}(\mathbf{r})/n(\mathbf{r})$, i.e. when the density fluctuations are completely neglected, the second line of Eq. (3.23) simplifies, as the classical field $n(\mathbf{r})$ commutes with the phase operator $\hat{\theta}(\mathbf{r})$. Then, the Hamiltonian contains only phase gradients $\nabla\hat{\theta}$, and no reference to the phase $\hat{\theta}$ itself. This observation holds in careful expansions of the Hamiltonian beyond the zeroth-order term,[14] as expected from the symmetry of the exact Hamiltonian. This fact is appreciated in the study of low-dimensional systems, where phase fluctuations are important [256, 264, 269, 270], and when ones wants to avoid the symmetry-breaking point of view where the perturbation expansion of the field operator is carried out around a classical field with well-defined phase.

Phase gradients, on the other hand, can also be expanded as

$$\nabla\hat{\theta}(\mathbf{r}) = \nabla\theta(\mathbf{r}) + [\nabla\hat{\theta}(\mathbf{r}) - \nabla\theta(\mathbf{r})], \tag{3.26}$$

where $\nabla\hat{\theta}(\mathbf{r}) - \nabla\theta(\mathbf{r})$ is a small fluctuations field. It is readily checked that a non-zero phase gradient $\nabla\theta$, which corresponds to a superfluid current associated with the motion of the condensate, only increases the kinetic energy of the quantum state. As we are generally interested in the ground state and the fluctuations around the ground state of the Hamiltonian, we can set $\nabla\theta(\mathbf{r}) = 0$.

Form (3.23) proves to be a convenient starting point to derive equations for the density n and the fluctuations $\delta\hat{n}$ and $\nabla\hat{\theta}$. Here we use the density-phase picture to derive a mean-field equation for the ground-state density profile without resorting to the symmetry-breaking approximation (1.20).

3.3.2 Mean-field description of the ground state

In the mean-field description of the ground state, the fluctuations $\nabla\hat{\theta}$ and $\delta\hat{n}$ are neglected altogether. Then, the ground-state density profile $n_0(\mathbf{r})$ is found by minimizing the energy functional

$$H[n] = \int \mathrm{d}\mathbf{r} \sqrt{n(\mathbf{r})} \left\{ -\frac{\hbar^2\nabla^2}{2m} + V_{\mathrm{ext}}(\mathbf{r}) + \frac{g}{2} n(\mathbf{r}) \right\} \sqrt{n(\mathbf{r})} \tag{3.27}$$

associated with Hamiltonian (3.23), under the constraint

$$N[n] = \int \mathrm{d}\mathbf{r}\, n(\mathbf{r}) = N. \tag{3.28}$$

Here $N[.]$ is a functional counting the particles, and N is the total number of atoms in the system. The existence and unicity of such a ground-state solution in a harmonic trap has been proved by Lieb *et al.* [273].

[14] See Eq. (40) of Ref. [256]. The interaction term on the second line of Eq. (3.23) generates infinities when the operators are reordered so as to eliminate $\hat{\theta}$: $\hat{\Psi}^\dagger(\mathbf{r})\hat{\Psi}^\dagger(\mathbf{r})\hat{\Psi}(\mathbf{r})\hat{\Psi}(\mathbf{r}) = \hat{n}(\mathbf{r})^2 - \hat{n}(\mathbf{r})[\hat{\Psi}(\mathbf{r}), \hat{\Psi}^\dagger(\mathbf{r})]$, where the commutator evaluates to $\delta(0)$. The technicalities involved in dealing with this term are naturally avoided at the level of the mean-field.

Gross-Pitaevskii equation

It can be shown that the ground-state solution of (3.27) with constraint (3.28) should minimize

$$K[n,\mu] = \int \mathrm{d}\mathbf{r}\sqrt{n(\mathbf{r})}\left\{-\frac{\hbar^2\nabla^2}{2m} + V_{\mathrm{ext}}(\mathbf{r}) + \frac{g}{2}n(\mathbf{r}) - \mu\right\}\sqrt{n(\mathbf{r})} \tag{3.29}$$

with respect to variations of $n(\mathbf{r})$, i.e. satisfy

$$\left.\frac{\delta K}{\delta n}\right|_{(n_0,\mu)} = 0. \tag{3.30}$$

Functional derivation of Eq. (3.29) with the condition $\delta K/\delta n = 0$ yields the Gross-Pitaevskii equation (GPE) [274, 275]

$$\left[-\frac{\hbar^2\nabla^2}{2m} + V_{\mathrm{ext}}(\mathbf{r}) + gn_0(\mathbf{r}) - \mu\right]\sqrt{n_0}(\mathbf{r}) = 0. \tag{3.31}$$

In this equation, the constraint of the number of bosons is replaced by the specification of μ. For a each μ, several solutions $n_0(\mathbf{r})$ may coexist, and a ground state is found among those solutions as a minimizer of H.[15] We assume that such a ground state is unique. Then, $n_0(\mathbf{r})$ and $N = \int \mathrm{d}\mathbf{r}\, n_0(\mathbf{r})$ are uniquely defined by μ. Conversely, the number of atoms uniquely defines the ground-state value of μ.

This approach completely determines the ground-state density profile of a weakly-interacting Bose gas, at the level of the mean field.

Chemical potential and healing length

Differentiation of (3.27) shows that $\mu = \mathrm{d}H[n_0^{(N)}]/\mathrm{d}N$, where $H[n_0^{(N)}]$ is the energy of the mean-field ground-state, calculated for N particles [253]. Therefore, μ is identified with a chemical potential, i.e. the energy gained by the system upon addition of one particle.

It proves convenient to associate a length scale to the chemical potential. This is done by defining the *healing length*

$$\xi = \frac{\hbar}{\sqrt{4m\mu}} \tag{3.32}$$

such that

$$\mu = \frac{\hbar^2}{4m\xi^2}. \tag{3.33}$$

[15] The minimization of Hamiltonian (3.27) under the constraint (3.28) is achieved by introducing the functional

$$L[n,\lambda] = H[n] - \lambda\left(N[n] - N\right),$$

where λ acts as a Lagrange multiplier. If n_0 minimizes H under the constraint $N[n_0] = N$, then n_0 is to be found among the stationary points of L, i.e. the points $(n,\lambda) = (n_0,\mu)$ where $\delta L/\delta n|_{(n_0,\mu)} = 0$ and $\partial L/\partial\lambda|_{(n_0,\mu)} = 0$. Observing that $L[n,\mu] = K[n] + \mu N$, where $K[.]$ is the grand-canonical energy functional (3.29) and N the number of atoms, it is established that the ground-state solution should satisfy $\delta K/\delta n|_{(n_0,\mu)} = 0$. This, however, provides only a necessary condition for n_0 to be a ground state of H. Equation (3.31) may have several solutions corresponding to non-ground-state stationary states of the GPE [276, 277].

The factor of four, which differs from definitions found elsewhere, is introduced for later convenience. The GPE then eventually rewrites

$$\left[-2\xi^2\nabla^2 + \frac{V_{\rm ext}(\mathbf{r})}{\mu} + \frac{gn_0(\mathbf{r})}{\mu} - 1\right]\sqrt{n_0}(\mathbf{r}) = 0. \tag{3.34}$$

This expression allows for a discussion of the relative weights of the various forms of energy (kinetic energy, external potential, mean-field interactions) which contribute to shaping the ground-state density profile.

The ground-state solutions of the GPE are well known in standard geometries and potentials (free space, harmonic traps, isolated delta impurities [278], 1D piece-wise continuous potentials [277, 279],...). Those standard potentials which are relevant to our study are detailed in appendix D. We now address the case of generic potentials of small amplitude, with application to random potentials.

3.3.3 Perturbation of the density profile by a weak potential

Motivation

In the absence of interactions, an infinitesimal amount of disorder can have dramatic effects. In particular, in 1D and 2D all single-particle states undergo Anderson localization irrespective of their energy. We have seen in chapter 2 that the asymptotic decay of the single-particle wave functions originates from a process which is independent of the absolute amplitude of those wave functions, in agreement with the linearity of the Schrödinger equation. It was also argued that conventional perturbation theory on the wave function was ascertained to run into trouble. In the non-linear GPE, on the contrary, the absolute magnitude of the density enters the balance of energies via the mean-field term $gn_0(\mathbf{r})$, and the homogeneous properties of the potential can be used in a hand-waving argument to rule out localization of the density profile *on asymptotically long length scales*.

The intuitive argument goes as follows. We consider the ground state of an interacting gas in a random potential, in an infinite system. We choose two finite subsystems A and B such that the variations of the random potential in B closely resemble those found in A, to the extent at least that the average value of the potential is roughly the same in both subsystems. We now assume *ad absurdum* that the density profile is localized on long length scales, and that we can still pick A and B with closely similar potentials, with now significantly different average densities, as shown in Fig. 3.2. In both subsystems, the density profile solves a local GPE which involves the kinetic energy and the mean-field interaction energy of the Bose gas, the potential and a chemical potential. Assuming, for simplicity, that the kinetic energy associated with the modulations of the density profile is roughly the same in A and B, the typical kinetic energy, interaction energy, and average potential amplitude sum up to different chemical potentials in A and B, in contradiction with the equilibrium required in the ground state.

The above reasoning can be rephrased by saying that, in the interacting system, the mean-field energy term balances out the chemical potential, the external potential and the kinetic energy in the GPE. If the potential has homogeneous properties on long length scales, the density cannot drop on those length scales. This applies to random and non-random potentials. The argument does not rule out localization in the Schrödinger case, as the absolute amplitude of the wave function plays no role in the Schrödinger equation. And neither does the argument

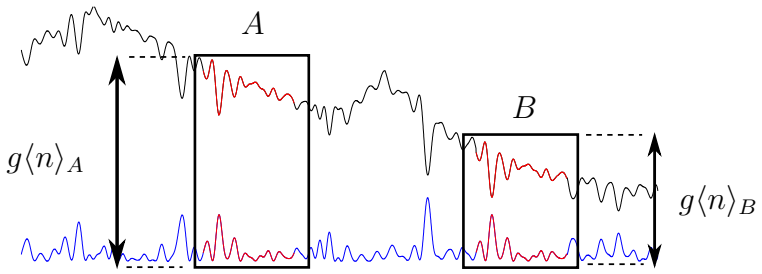


Figure 3.2: Hand-waving argument for the absence of localization of the ground-state density profile in the interacting Bose gas. The blue line (bottom) represents the external potential, and the black line (top) the density profile. The potential variations in subsystems A and B are closely similar. Significant differences between the average densities in A and B are incompatible with a unique chemical potential, i.e. with equilibrium, because of the mean-field interaction terms.

rule out strong modulations of the density of the interacting gas on *short length scales* if the external potential is strong. Note also that the argument applies to the density profile, and not to the correlation functions of the many-body system.

In the absence of localization, the density profile of the interacting gas in a weak potential can be sought in a perturbation expansion around the homogeneous case ($V = 0$).

Assumptions

In this section we analyze the ground-state solutions of the Gross-Pitaevskii equation

$$\left[-\frac{\hbar^2\nabla^2}{2m} + V(\mathbf{r}) + gn_0(\mathbf{r}) - \mu\right]\sqrt{n_0}(\mathbf{r}) = 0 \tag{3.35}$$

when no trapping potential is present, and $V(\mathbf{r})$ is a weak potential. This notion of weakness is stated more precisely below. To begin with, we require the potential to be everywhere much smaller than the chemical potential: $|V(\mathbf{r})| \ll \mu$. Calling V_{R} a typical amplitude of the potential, this condition reads

$$|V_{\mathrm{R}}| \ll \mu. \tag{3.36}$$

We will see below that a less stringent criterion on the amplitude of the potential can be derived.[16] Without loss of generality, we assume that V has a vanishing spatial average:

$$\langle V\rangle = 0. \tag{3.37}$$

The potential V might be either deterministic or random, and mean values are here understood as spatial averages. The spatial variations of the potential are characterized by a minimal length

[16] See the discussions following Eqs. (3.52) and (3.70).

scale σ_{R}. If V is a random potential with homogeneous statistical properties,[17] σ_{R} is chosen as a typical width of the autocorrelation function $C_2(\mathbf{r}) = \langle V(\mathbf{r}'+\mathbf{r})V(\mathbf{r})\rangle$. If V is periodic, σ_{R} is chosen as the smallest period of the d-dimensional lattice. In any case, σ_{R} serves as a scale for the smallest spatial features of V.

In the absence of potential ($V_{\mathrm{R}} = 0$), the density profile is homogeneous:

$$n_0^{(0)}(\mathbf{r}) = \langle n_0^{(0)}\rangle = \frac{\mu}{g}. \tag{3.38}$$

In the presence of a weak potential, the density profile n_0 is only weakly perturbed around the homogeneous solution $n_0^{(0)}$ and an exact solution of the GPE (3.35) can be sought in the form of a perturbation series of $\sqrt{n_0}$ in powers of V_{R}/μ. The density profile then follows as

$$n_0(\mathbf{r}) = n_0^{(0)} + n_0^{(1)}(\mathbf{r}) + n_0^{(2)}(\mathbf{r}) + \cdots \tag{3.39}$$

Details of the expansion can be found in appendix E and Ref. [242], where this approach was developed. The main results are reviewed below.

Smoothing solution of the Gross-Pitaevskii equation

Most generally, the density profile can be cast into

$$n_0(\mathbf{r}) = \frac{\mu - \widetilde{V}(\mathbf{r}) + \Delta}{g}, \tag{3.40}$$

where $\widetilde{V}$ is a fluctuation with zero average, i.e. such that

$$\langle \widetilde{V}\rangle = 0, \tag{3.41}$$

and the quantity

$$\Delta = g\langle n_0\rangle - \mu \tag{3.42}$$

measures a deviation from the homogeneous equation of state ($\mu = g\langle n_0\rangle$). Both $\widetilde{V}$ and Δ vanish for $V_{\mathrm{R}} = 0$. In the presence of a weak potential, they remain small compared to μ and admit expansions of the form

$$\widetilde{V}(\mathbf{r}) = \sum_{i\geq 1} \widetilde{V}^{(i)}(\mathbf{r}) \tag{3.43}$$

$$\Delta = \sum_{i\geq 1} \Delta^{(i)}, \tag{3.44}$$

where the superscripts indicate increasing powers of V_{R}/μ. It turns out that Δ vanishes at first order:

$$\Delta^{(1)} = 0. \tag{3.45}$$

[17] Statistical properties of a random potential are said to be homogeneous when they do not depend on absolute position in the system. Unless stated otherwise, the random potentials studied here always have homogeneous statistical properties. Averages like $\langle V\rangle$ or $\langle V^2\rangle$ and other correlation functions then coincide with spatial averages.

Therefore, the leading-order expansion of the density profile reads

$$n_0(\mathbf{r}) \simeq \frac{\mu - \widetilde{V}^{(1)}(\mathbf{r})}{g}. \tag{3.46}$$

The first-order fluctuation term is found as

$$\widetilde{V}^{(1)}(\mathbf{r}) = \int \mathrm{d}\mathbf{r}'\; G_\xi(\mathbf{r}-\mathbf{r}')V(\mathbf{r}'), \tag{3.47}$$

where $G_\xi(\mathbf{r})$ is a Green function which depends on the healing length ξ and is most conveniently written in Fourier space:[18]

$$G_\xi(\mathbf{q}) = \frac{(2\pi)^{-d/2}}{1+(|\mathbf{q}|\xi)^2}. \tag{3.48}$$

The function G_ξ acts as a positive convolution kernel with unit sum ($\int \mathrm{d}\mathbf{r} G_\xi(\mathbf{r}) = 1$) and width ξ in coordinate space. Therefore, the amplitude and the shape of the density modulations depend not only on the amplitude of the external potential, but also crucially on the competition of two length scales, namely the *scale of potential variations* σ_{R} and the *healing length* ξ [242].

Thomas-Fermi limit - If $\xi \ll \sigma_{\mathrm{R}}$, the potential V varies on length scales much longer than ξ, and we obtain

$$\widetilde{V}^{(1)}(\mathbf{r}) \simeq V(\mathbf{r}) \qquad (\xi \ll \sigma_{\mathrm{R}}) \tag{3.49}$$

in Eq. (3.47). In other words, the density profile almost exactly follows the shape of the external potential:

$$n_0(\mathbf{r}) \simeq \frac{\mu - V(\mathbf{r})}{g} \qquad (\xi \ll \sigma_{\mathrm{R}}). \tag{3.50}$$

Expression (3.50) coincides with the result obtained from the Thomas-Fermi approximation, which consists in discarding the Laplacian term in the GPE (3.35). As in the cases studied in appendix D, the Thomas-Fermi approximation is valid in the regime where the mean-field interaction $gn_0 \simeq \mu$ is much larger than the kinetic energy E_σ associated with the variations of the external potential:

$$E_\sigma = \frac{\hbar^2}{2m\sigma_{\mathrm{R}}^2}. \tag{3.51}$$

While this approximation generally applies irrespective of the potential strength, it is recovered here as a limiting case for a weak potential.

Smoothing - If, on the other hand, we have $\xi \gtrsim \sigma_{\mathrm{R}}$ (or, equivalently, $\mu \lesssim E_\sigma$), the short-wavelength variations of the external potential $V(\mathbf{r})$ are smoothed out in the convolution product (3.47). Turning to Fourier space, we obtain

$$\widetilde{V}^{(1)}(\mathbf{q}) = \frac{V(\mathbf{q})}{1+(|\mathbf{q}|\xi)^2}, \tag{3.52}$$

[18] Throughout this thesis, the Fourier transform is defined with the normalization $f(\mathbf{q}) = (2\pi)^{-d/2}\int \mathrm{d}\mathbf{r} f(\mathbf{r})\mathrm{e}^{-\mathrm{i}\mathbf{q}\cdot\mathbf{r}}$, where d is the dimension of space. From now on, we add hats to the Fourier transforms only when there is ambiguity between a function and its transform, as e.g. for adimensional arguments.

which shows that the imprint of *all* spatial frequencies of V on the density profile is reduced, but that Fourier components with $\mathbf{q}$ larger $1/\xi$ tend to be particularly suppressed. In the case $\xi \gtrsim \sigma_{\rm R}$, this affects a considerable part of the spatial spectrum of V.

In general, the density thus follows the smoothed variations of the external potential V, and $\widetilde{V}^{(1)}$ is therefore called a *smoothed potential* [242]. An inspection of higher-order terms suggests that such a smoothing occurs at all orders of the perturbation theory [see e.g. Eq. (E.19) in appendix E].

Finally, let us emphasize the relevance of a description which goes beyond the Thomas-Fermi approximation. Experiments now implement ordered and disordered potentials with submicron length scales, which brings $\sigma_{\rm R}$ close to the healing ξ and invalidates the Thomas-Fermi approximation. Chapter 4 will also provide an example where the precise description of the ground state is required for the study of elementary excitations of the condensate.

Application to random potentials

In the context of the present chapter, we wish to understand the properties of n_0 in the case where V is a random potential, with a special focus on localization properties.

We now assume that V is a random potential with homogeneous statistical properties, an amplitude $V_{\rm R}$ such that

$$|V_{\rm R}| = \sqrt{\langle V^2 \rangle}, \tag{3.53}$$

and an autocorrelation function

$$C_2(\mathbf{r}) = \langle V(\mathbf{r}')V(\mathbf{r}'+\mathbf{r})\rangle = V_{\rm R}^2 c_2(\mathbf{r}/\sigma_{\rm R}), \tag{3.54}$$

where $\sigma_{\rm R}$ is the correlation length.

Smoothed potential - Applying the results of the previous paragraphs, we find that the density profile is extended and that, up to first order in the disorder strength $V_{\rm R}$, it follows [see Eqs. (3.46) and (3.47)]

$$n_0(\mathbf{r}) \simeq \frac{\mu - \widetilde{V}^{(1)}(\mathbf{r})}{g} \tag{3.55}$$

where

$$\widetilde{V}^{(1)}(\mathbf{r}) = \int \mathrm{d}\mathbf{r}'\; G_\xi(\mathbf{r}-\mathbf{r}')V(\mathbf{r}') \tag{3.56}$$

is a *smoothed random potential* with zero mean. Figure 3.3 displays the density profile and the smoothed random potential computed numerically for a 1D Bose gas in a weak speckle potential. The agreement of expression (3.55) with the exact density profile is excellent, especially when compared to the Thomas-Fermi approximation. In Fig. 3.3, differences between the exact density profile and the first-order approximation (3.55) are visible only in the deep dip close to the origin, which is caused by a peak of large amplitude in the potential. The response of the density profile to such large potential variations is captured by higher orders in the perturbation expansion.

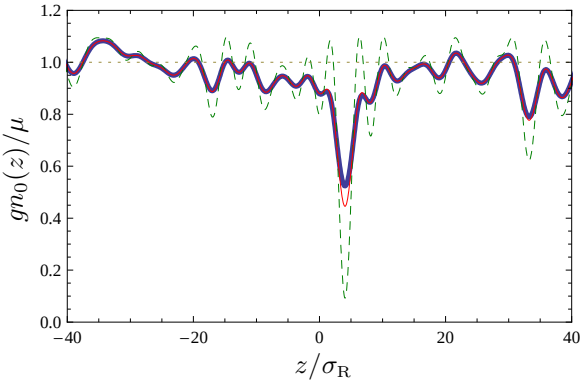


Figure 3.3: Density profile of a 1D Bose gas placed in a speckle potential with autocorrelation $C_2(z) = V_R^2 \mathrm{sinc}(z/\sigma_R)^2$ with $V_R/\mu = 0.1$ and $\sigma_R = \xi$. The exact density profile (thick blue line), obtained numerically by propagation in imaginary time, is compared to the first order smoothing solution (thin red line) given by Eq. (3.56). Differences are visible only at the location of the deepest density dip. The Thomas-Fermi approximation (green dashed line) defined by Eq. (3.50) and the homogeneous density profile in the absence of disorder (brown dotted line) are shown for comparison.

Autocorrelation and power-spectrum of the density modulations - Expressions (3.55) and (3.56) allow an explicit calculation of the statistical properties of the modulations of the density profile n_0. By construction of the $\widetilde{V}^{(n)}$ functions [see Eqs.(3.40) to (3.42)], and in agreement with Eq. (3.56), we have $\langle \widetilde{V}^{(1)} \rangle = 0$, that is, $\langle n_0 \rangle \simeq \mu/g$ to first order in the perturbation theory. To analyze the modulations of n_0 around the average, we define the autocorrelation function of the smoothed potential $\widetilde{V}^{(1)}$ as

$$\widetilde{C}_2^{(1)}(\mathbf{r}) = \langle \widetilde{V}^{(1)}(\mathbf{r}')\widetilde{V}^{(1)}(\mathbf{r}'+\mathbf{r}) \rangle. \tag{3.57}$$

In Fourier space, this autocorrelation function has a simple expression in terms of the autocorrelation function C_2 of the bare potential V:

$$\widetilde{C}_2^{(1)}(\mathbf{q}) = \frac{C_2(\mathbf{q})}{\left[1 + (|\mathbf{q}|\xi)^2\right]^2}. \tag{3.58}$$

By virtue of the Wiener-Khintchin theorem, the Fourier transforms in equality (3.58) are the power spectra of V and $\widetilde{V}^{(1)}$:

$$\langle V(\mathbf{q})V(\mathbf{q}')^* \rangle = (2\pi)^{d/2} C_2(\mathbf{q})\delta(\mathbf{q}'-\mathbf{q}) \tag{3.59}$$

$$\langle \widetilde{V}^{(1)}(\mathbf{q})\widetilde{V}^{(1)}(\mathbf{q}')^* \rangle = (2\pi)^{d/2} \widetilde{C}_2^{(1)}(\mathbf{q})\delta(\mathbf{q}'-\mathbf{q}). \tag{3.60}$$

Amplitude of the density modulations - Integrating Eq. (3.58) over $\mathbf{q}$, we obtain the average quadratic amplitude (variance) of the density modulations

$$\langle \widetilde{V}^{(1)}(\mathbf{r})^2 \rangle = (2\pi)^{-d/2} \int \mathrm{d}\mathbf{q} \frac{C_2(\mathbf{q})}{\left[1 + (|\mathbf{q}|\xi)^2\right]^2}. \tag{3.61}$$

This result can be written in a rescaled form with the help of the reduced correlator introduced in Eq. (3.54):

$$C_2(\mathbf{q}) = V_{\mathrm{R}}^2 \sigma_{\mathrm{R}}^d \hat{c}_2(\mathbf{q}\sigma_{\mathrm{R}}). \tag{3.62}$$

The root-mean-square amplitude of density modulations follows as

$$|\widetilde{V}_{\mathrm{R}}^{(1)}| = \sqrt{\langle \widetilde{V}^{(1)^2} \rangle} = |V_{\mathrm{R}}| \sqrt{I_2(\xi/\sigma_{\mathrm{R}})} \tag{3.63}$$

where, for all $n \geq 0$, we define

$$I_n\left(\frac{\xi}{\sigma_{\mathrm{R}}}\right) = \frac{\sigma_{\mathrm{R}}^d}{(2\pi)^{d/2}} \int \mathrm{d}\mathbf{q} \frac{\hat{c}_2(\mathbf{q}\sigma_{\mathrm{R}})}{[1 + (|\mathbf{q}|\xi)^2]^n}. \tag{3.64}$$

Note that integral I_n depends only on the model of disorder and the ratio ξ/σ_{R}. For small or large ξ/σ_{R} ratio, we obtain

$$I_n\left(\frac{\xi}{\sigma_{\mathrm{R}}}\right) \simeq 1 - \left(\frac{\xi}{\sigma_{\mathrm{R}}}\right)^2 \frac{n}{(2\pi)^{d/2}} \int \mathrm{d}\boldsymbol{\kappa} |\boldsymbol{\kappa}|^2 \hat{c}_2(\boldsymbol{\kappa}) \qquad \text{for } \xi \ll \sigma_{\mathrm{R}} \tag{3.65}$$

$$I_n\left(\frac{\xi}{\sigma_{\mathrm{R}}}\right) \simeq \left(\frac{\sigma_{\mathrm{R}}}{\xi}\right)^d \frac{\Gamma(n - d/2)}{2^{d/2}\Gamma(n)} \hat{c}_2(\mathbf{0}) \qquad \text{for } \sigma_{\mathrm{R}} \ll \xi,\ n > d/2, \tag{3.66}$$

where Γ is the gamma function.[19]

Since $\hat{c}_2$ is a positive function [see Eqs. (3.59) and (3.62)], the functions defined in Eq. (3.64) satisfy $0 < \cdots \leq I_{n+1} \leq I_n \leq \cdots \leq I_0$. As c_2 is normalized so that

$$I_0 = \frac{\sigma_{\mathrm{R}}^d}{(2\pi)^{d/2}} \int \mathrm{d}\mathbf{q}\, \hat{c}_2(\mathbf{q}\sigma_{\mathrm{R}}) = c_2(\mathbf{0}) = 1, \tag{3.67}$$

we obtain the following ordering, valid for all ξ/σ_{R} and in any dimension d:

$$0 < \cdots \leq I_2 \leq I_1 \leq 1. \tag{3.68}$$

In particular, the inequality

$$I_2\left(\frac{\xi}{\sigma_{\mathrm{R}}}\right) \leq 1, \tag{3.69}$$

combined with result (3.63), shows that the amplitude of the smoothed random potential is always smaller than the amplitude of the bare potential V:

$$|\widetilde{V}_{\mathrm{R}}^{(1)}| \leq |V_{\mathrm{R}}|. \tag{3.70}$$

This reduction of the modulations of the density profile originates from the smoothing effect discussed above. The magnitude of the smoothing effect depends crucially on the competition

[19] The gamma function is defined by $\Gamma(z) = \int_0^\infty t^{z-1} \mathrm{e}^{-t}$ for complex numbers z with positive real part [280]. Here, the relevant values are obtained from the recursion relation $\Gamma(z+1) = z\Gamma(z)$ with $\Gamma(1/2) = \sqrt{\pi}$, $\Gamma(1) = 1$.

of the correlation length $\sigma_{\rm R}$ and the healing length ξ [242]. Limiting behaviors are obtained from the expansions (3.65) and (3.66):

$$\left|\frac{\widetilde{V}_{\rm R}^{(1)}}{V_{\rm R}}\right| \simeq 1-\left(\frac{\xi}{\sigma_{\rm R}}\right)^2 (2\pi)^{-d/2}\int {\rm d}\boldsymbol{\kappa}|\boldsymbol{\kappa}|^2\hat{c}_2(\boldsymbol{\kappa}) \qquad \text{for } \xi\ll\sigma_{\rm R} \tag{3.71}$$

$$\left|\frac{\widetilde{V}_{\rm R}^{(1)}}{V_{\rm R}}\right| \simeq \left(\frac{\sigma_{\rm R}}{\xi}\right)^{d/2}\sqrt{2^{-d/2}\Gamma(2-d/2)\hat{c}_2(\mathbf{0})} \qquad \text{for } \sigma_{\rm R}\ll\xi. \tag{3.72}$$

In the Thomas-Fermi limit $\xi\ll\sigma_{\rm R}$, the variations of the density profile have the same amplitude as the random potential. For $\xi\gtrsim\sigma_{\rm R}$, however, they tend to be smoothed out. The example in Fig. 3.3 shows that a significant reduction of the amplitude of the density modulations is already obtained when ξ is of the order of $\sigma_{\rm R}$.

Criterion for weak disorder - The density profile is weakly perturbed around the homogeneous solution μ/g as long as

$$|\widetilde{V}_{\rm R}^{(1)}|\ll\mu. \tag{3.73}$$

Note that this provides us with a criterion of validity for the perturbation expansion which is somewhat looser than the naive assumption $|V_{\rm R}|\ll\mu$.[20]

In the opposite case where $|\widetilde{V}_{\rm R}^{(1)}|\gtrsim\mu$, the density profile is no longer weakly perturbed by the random potential. While it is reasonable to assume that the density profile retains homogeneous statistics on length scales much larger than the correlation length (and that, in this sense, the density profile is not *asymptotically* localized), large local fluctuations of the random potential eventually cause the density to drop to zero in some regions of the system and the gas to fragment into disconnected volumes.[21]

Leading-order deviation from the homogeneous equation of state

The variations $\widetilde{V}$ of the density profile are well captured by the smoothed potential at first order in $V_{\rm R}$. The first correction to the homogeneous equation of state, on the other hand, requires an expansion at second order, which is carried out in appendix E. The result reads

$$g\langle n_0\rangle-\mu\simeq\Delta^{(2)} \tag{3.74}$$

with

$$\Delta^{(2)}=\frac{V_{\rm R}^2\sigma_{\rm R}^d}{2(2\pi)^{d/2}\mu}\int {\rm d}\mathbf{q}\,\frac{(|\mathbf{q}|\xi)^2}{\left[1+(|\mathbf{q}|\xi)^2\right]^2}\hat{c}_2(\mathbf{q}\sigma_{\rm R}) \tag{3.75}$$

or, equivalently,

$$\Delta^{(2)}=\frac{V_{\rm R}^2}{2\mu}\left[I_1-I_2\right]. \tag{3.76}$$

[20] The results found for the first couple of terms $\widetilde{V}^{(1)}$ and $\widetilde{V}^{(2)}$ [see Eq. (E.29 in appendix E] suggest that smoothing indeed extends to all perturbation orders $V^{(n)}$. Therefore, criterion (3.73) probably holds beyond the first-order approximation (3.55).

[21] Strictly speaking, there is always residual tunneling unless the potential takes on infinite values.

With the ordering (3.68), we find

$$0 < \Delta^{(2)} \leq \frac{V_{\mathrm{R}}^2}{2\mu}. \tag{3.77}$$

The first inequality is consistent with the fact that the chemical potential μ of weakly-repulsive bosons in a potential with zero mean is smaller than the average mean-field energy $g\langle n_0 \rangle$, as argued in Ref. [129]:

$$\mu < g\langle n_0 \rangle. \tag{3.78}$$

Note that these results are general, and V need not be random.[22]

Limiting cases - In the Thomas-Fermi limit $\xi \ll \sigma_{\mathrm{R}}$, the deviation $\Delta^{(2)}$ behaves as

$$\Delta^{(2)} \simeq \frac{V_{\mathrm{R}}^2}{2\mu} \left(\frac{\xi}{\sigma_{\mathrm{R}}}\right)^2 (2\pi)^{-d/2} \int \mathrm{d}\boldsymbol{\kappa} |\boldsymbol{\kappa}|^2 \hat{c}_2(\boldsymbol{\kappa}) \qquad (\xi \ll \sigma_{\mathrm{R}}), \tag{3.79}$$

so that

$$\Delta^{(2)}/\mu \propto (V_{\mathrm{R}}/\mu)^2 (\xi/\sigma_{\mathrm{R}})^2 \ll (V_{\mathrm{R}}/\mu)^2 \ll 1. \tag{3.80}$$

Let us now discuss the opposite limit when V is random, and $C_2(\mathbf{q})$ has a limit when $\mathbf{q} \to \mathbf{0}$. In the regime $\sigma_{\mathrm{R}} \ll \xi$, we approach in principle the white-noise limit, where the correlation length is set to zero: $C_2^{\mathrm{w.n.}}(\mathbf{r}) = D\delta(\mathbf{r})$. Starting from any model of disorder, this limit is usually obtained by letting σ_{R} vanish while keeping the product $V_{\mathrm{R}}^2 \sigma_{\mathrm{R}}^d$ constant.[23] At the end of the process, the properties of the system are expected not to depend on the details of the autocorrelation function originally used. Carried out at fixed μ and ξ, this procedure should amount here to letting the ratio σ_{R}/ξ tend to zero at fixed $V_{\mathrm{R}}^2 \sigma_{\mathrm{R}}^d$, and legitimize the replacement of the rescaled power spectrum $\hat{c}_2$ in Eqs. (3.62) and (3.75) by a constant: $\hat{c}_2(\mathbf{q}\sigma_{\mathrm{R}}) \simeq \hat{c}_2(\mathbf{0})$. In fact, the integrand $\mathrm{d}\mathbf{q}(|\mathbf{q}|\xi)^2/\left[1 + (|\mathbf{q}|\xi)^2\right]^2$ in Eq. (3.75) scales as $q^{d-3}\mathrm{d}q$ for high momenta ($q \gg 1/\xi$), and such a white-noise limit is correctly defined only for $d = 1$. In one dimension, we then obtain

$$\Delta^{(2)} \simeq \frac{\sqrt{\pi} V_{\mathrm{R}}^2 \sigma_{\mathrm{R}}}{4\sqrt{2}\mu\xi} \hat{c}_2(0) \qquad (\sigma_{\mathrm{R}} \ll \xi;\, d = 1), \tag{3.81}$$

so that

$$\Delta^{(2)}/\mu \propto (V_{\mathrm{R}}/\mu)^2 (\sigma_{\mathrm{R}}/\xi) \ll (V_{\mathrm{R}}/\mu)^2 \ll 1. \tag{3.82}$$

For $d \geq 2$, the limit $\sigma_{\mathrm{R}} \to 0$ cannot be taken in the correlator $\hat{c}_2$ without causing an ultraviolet divergence of the integral. This shows that in dimensions higher than one the exact result for $\Delta^{(2)}$ depends on the detailed form of the autocorrelation function and the decay of $\hat{c}_2(\boldsymbol{\kappa})$ as a function of $\boldsymbol{\kappa}$.

Application to lattice and speckle potentials - In figure 3.4, expression (3.75) is compared to exact numerical calculations of Δ at various σ_{R}/ξ ratios, for a speckle random potential

[22] It might be worth pointing out that this result stands in contrast with the typical *increase* in chemical potential caused by boundary effects (see appendix D).

[23] See the discussion preceding Eq. (2.45).

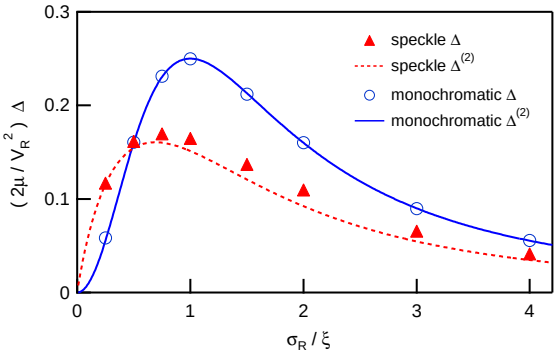


Figure 3.4: Correction to the homogeneous equation of state for a 1D speckle potential with auto-correlation function $C_2(z) = V_{\rm R}^2 \mathrm{sinc}(z/\sigma_{\rm R})^2$ and a 1D lattice $V(z) = V_{\rm R}\sqrt{2}\,\cos(z/\sigma_{\rm R})$. The analytical result for the leading-order correction $\Delta^{(2)}$ [lines defined by Eq. (3.75)] is compared to numerical calculations of Δ [circles and triangles] for $V_{\rm R} = 0.1\mu$. The calculations were performed in a 1D box with periodic boundary conditions to avoid kinetic terms arising from the boundaries.

and a monochromatic lattice in a 1D geometry. The reduced autocorrelation functions of the speckle potential used here are

$$c_2(u) = \mathrm{sinc}(u)^2 \tag{3.83}$$

$$\hat{c}_2(\kappa) = \sqrt{\frac{\pi}{2}}(1 - |\kappa|/2)\Theta(1 - |\kappa|/2), \tag{3.84}$$

where $\mathrm{sinc}(u) \equiv \sin(u)/u$ and Θ is the Heaviside step function [see Eq. (2.125)]. The corresponding deviation reads

$$\Delta^{(2)} = \frac{V_{\rm R}^2}{2\mu}\left[\frac{\sigma_{\rm R}}{2\xi}\arctan\left(\frac{2\xi}{\sigma_{\rm R}}\right) - \frac{\sigma_{\rm R}^2}{4\xi^2}\ln\left(1 + \frac{4\xi^2}{\sigma_{\rm R}^2}\right)\right]. \tag{3.85}$$

The lattice potential is defined as

$$V(z) = \sqrt{2}V_{\rm R}\cos(z/\sigma_{\rm R}), \tag{3.86}$$

which translates into

$$c_2(u) = \cos(u) \tag{3.87}$$

$$\Delta^{(2)} = \frac{V_{\rm R}^2(\xi/\sigma_{\rm R})^2}{4\mu\left[1 + (\xi/\sigma_{\rm R})^2\right]^2}. \tag{3.88}$$

As expected, the agreement is good for values of $V_{\rm R}/\mu$ as small as the one chosen in the figure. We checked that the small discrepancy between $\Delta^{(2)}$ and Δ in the random case agrees well with the contributions of order $V_{\rm R}^3$ (not detailed here), which are absent in a monochromatic lattice.

3.3.4 Trapped Bose gas in one-dimensional disorder

We now consider the situation of section 3.2.2, where the bosons are confined to a box of size $2L$ along one direction, and trapped harmonically in the two-dimensional transverse plane. A random potential V with amplitude $V_{\rm R}$ and correlation length $\sigma_{\rm R}$ is added along the main direction. The GPE then reads

$$\left[-\frac{\hbar^2\nabla^2}{2m}+\frac{1}{2}m\omega_\perp^2\rho^2+V(z)+gn_0(\rho,z)-\mu\right]\sqrt{n_0(\rho,z)}=0 \tag{3.89}$$

where ρ is the radial coordinate in the transverse plane. We can now apply the results of the preceding sections.

Assuming that the box size is large enough ($\hbar^2/2mL^2 \ll \mu, \hbar\omega_\perp$) so that the boundaries of the box play no role, the system can be considered homogeneous along the z-direction in the absence of disorder[24]. Note that in this configuration, the smallest possible value of μ is the ground-state energy $\hbar\omega_\perp$ of the 2D radial oscillator. We therefore introduce

$$\mu' = \mu - \hbar\omega_\perp, \tag{3.90}$$

which measures the chemical potential from the ground-state energy of the harmonic trap.

Tight harmonic trapping

For a tight harmonic trapping, i.e. $\mu' \ll \hbar\omega_\perp$, the transverse motion of the atoms is frozen in the radial oscillator ground-state. The density profile then separates in longitudinal and radial components:

$$\sqrt{n_0(\rho,z)}=\phi_\perp(\rho)\sqrt{n_0^{\rm 1D}(z)}, \tag{3.91}$$

where $n_0^{\rm 1D}(z)$ is the linear density along the z-axis, and $\phi_\perp(\rho)$ is the normalized oscillator ground-state wave function

$$\phi_\perp(\rho)=\frac{{\rm e}^{-\rho^2/2a_{\rm ho}^2}}{\sqrt{\pi}a_{\rm ho}}, \tag{3.92}$$

with

$$a_{\rm ho}=\sqrt{\frac{\hbar}{m\omega_\perp}}. \tag{3.93}$$

The radial wave function solves the Schrödinger equation of the 2D harmonic oscillator with eigen-energy $\hbar\omega_\perp$:

$$\left[-\frac{\hbar^2\nabla_\rho^2}{2m}+\frac{1}{2}m\omega_\perp^2\rho^2-\hbar\omega_\perp\right]\phi_\perp(\rho)=0. \tag{3.94}$$

The problem then reduces to a 1D Gross-Pitaevskii equation for the linear density

$$\left[-\frac{\hbar^2\partial_z^2}{2m}+V(z)+g_{\rm 1D}n_0^{\rm 1D}(z)-\mu'\right]\sqrt{n_0^{\rm 1D}(z)}=0 \tag{3.95}$$

[24] Standard results on the ground-state solution of the GPE in box potentials and harmonic traps are reviewed in appendix D.

where the effective 1D coupling constant $g_{1\mathrm{D}}$ is obtained by integration over transverse degrees of freedom in Eq. (3.27) or Eq. (3.29):

$$g_{1\mathrm{D}} = g \int \mathrm{d}\boldsymbol{\rho} |\phi_\perp(\rho)|^4 = \frac{g}{2\pi a_{\mathrm{ho}}^2}, \tag{3.96}$$

that is,

$$g_{1\mathrm{D}} = \frac{2\hbar^2 a_s}{m a_{\mathrm{ho}}^2}, \tag{3.97}$$

where a_s is the 3D scattering length. These expressions are valid provided that a_{ho} is still large enough so that low-energy s-wave scattering theory applies (i.e. $a_{\mathrm{ho}} \gg r_0$, where r_0 is the effective range of the true atom-atom interaction potential) and that $a_{\mathrm{ho}} \gg a_s$ [250, 251].

For a weak potential such that $V_{\mathrm{R}} \ll \mu'$, the GPE (3.95) is solved with the approach of section 3.3.3, and we obtain the longitudinal part of expression (3.91):

$$\sqrt{n_0^{1\mathrm{D}}(z)} \simeq \sqrt{\frac{\mu'}{g_{1\mathrm{D}}}} \left[1 - \frac{\widetilde{V}^{(1)}(z)}{2\mu'} \right] \tag{3.98}$$

where

$$\widetilde{V}^{(1)}(z) = \int \mathrm{d}z' G_{\xi'}(z - z') V(z') \tag{3.99}$$

is a smoothed random potential with 1D smoothing kernel [242]

$$G_{\xi'}(z) = \frac{\mathrm{e}^{-|z|/\xi'}}{2\xi'} \tag{3.100}$$

and healing length

$$\xi' = \frac{\hbar}{\sqrt{4m\mu'}}. \tag{3.101}$$

Putting the radial and the longitudinal components together, we finally obtain

$$\sqrt{n_0(\rho, z)} \simeq \sqrt{\frac{2\mu' \mathrm{e}^{-\rho^2/a_{\mathrm{ho}}^2}}{g}} \left[1 - \frac{\widetilde{V}^{(1)}(z)}{2\mu'} \right], \tag{3.102}$$

where g is the 3D coupling constant.

The density profile is only weakly perturbed around the solution without disorder when the root-mean-square amplitude $|\widetilde{V}_{\mathrm{R}}^{(1)}|$ of the smoothed potential $\widetilde{V}^{(1)}$ is much smaller than μ'. Using relation (3.63), this condition reads

$$\mu' \gg |V_{\mathrm{R}}| \sqrt{I_2(\xi'/\sigma_{\mathrm{R}})}, \tag{3.103}$$

where

$$I_2\left(\frac{\xi'}{\sigma_{\mathrm{R}}}\right) = \frac{\sigma_{\mathrm{R}}}{\sqrt{2\pi}} \int \mathrm{d}q \frac{\hat{c}_2(q\sigma_{\mathrm{R}})}{\left[1 + (q\xi')^2\right]^2} \tag{3.104}$$

and $\hat{c}_2$ is the Fourier transform of the reduced autocorrelation function of V.

Loose harmonic trapping

Let us now consider the case of loose radial confinement: $\hbar\omega_\perp \ll \mu'$. In this case, the offset introduced by the ground-state energy $\hbar\omega_\perp$ need not be considered: $\mu' \simeq \mu$. The condition of loose radial confinement can then be written $\xi \ll a_{\rm ho}$. For $V = 0$, the density is invariant along the z-direction, and the density profile obeys the radial GPE

$$\left[-\frac{\hbar^2\nabla_\rho^2}{2m} + \frac{1}{2}m\omega_\perp^2\rho^2 + gn_0^0(\rho,z) - \mu\right]\sqrt{n_0^0(\rho,z)} = 0. \tag{3.105}$$

As the mean-field interaction energy exceeds by far the level splitting of the harmonic oscillator, the gas adopts a radial Thomas-Fermi profile, obtained by neglecting the kinetic term:

$$\left[\frac{1}{2}m\omega_\perp^2\rho^2 + gn_0^0(\rho,z) - \mu\right]\sqrt{n_0^0(\rho,z)} \simeq 0, \tag{3.106}$$

so that

$$n_0^0(\rho,z) \simeq \left\{\begin{array}{ll} \frac{\mu}{g}\left(1-\rho^2/R_\perp^2\right) & \text{if } \rho < R_\perp \\ 0 & \text{otherwise} \end{array}\right. , \tag{3.107}$$

with

$$R_\perp = \sqrt{\frac{2\mu}{m\omega_\perp^2}}. \tag{3.108}$$

In the presence of the random potential $V(z)$ with $V_{\rm R} \ll \mu$, the density profile and the chemical potential are only weakly affected. Neglecting the radial kinetic energy in the equilibrium equation for the gas is therefore still legitimate. The longitudinal kinetic energy associated with the modulations of the density profile, however, depends on the detailed form of V, which might vary on length scales smaller than ξ. We therefore write the GPE as

$$\left[-\frac{\hbar^2\partial_z^2}{2m} + \frac{1}{2}m\omega_\perp^2\rho^2 + V(z) + gn_0(\rho,z) - \mu\right]\sqrt{n_0(\rho,z)} \simeq 0. \tag{3.109}$$

For every $\rho < R_\perp$, the z-dependence of the density profile is worked out with the technique of section 3.3.3, and we obtain

$$n_0(\rho,z) \simeq \frac{\mu(\rho) - \widetilde{V}^{(1)}(\rho,z)}{g}, \tag{3.110}$$

where

$$\mu(\rho) = \mu - \frac{1}{2}m\omega_\perp^2\rho^2 = \mu\left(1 - \frac{\rho^2}{R_\perp^2}\right). \tag{3.111}$$

The smoothed random potential $\widetilde{V}^{(1)}$ derives from the bare potential V via

$$\widetilde{V}^{(1)}(\rho,z) = \int {\rm d}z\, G_{\xi(\rho)}(z-z')V(z'), \tag{3.112}$$

where

$$G_{\xi(\rho)}(z) = \frac{{\rm e}^{-|z|/\xi(\rho)}}{2\xi(\rho)} \tag{3.113}$$

$$\xi(\rho) = \frac{\hbar}{\sqrt{4m\mu(\rho)}}. \tag{3.114}$$

The effective healing length $\xi(\rho)$ increases from the center of trap, where it assumes the value $\xi(0) = \xi$, to the edge of the Thomas-Fermi parabola. In the radial regions where the correlation length $\sigma_{\rm R}$ of the potential is such that $\sigma_{\rm R} \lesssim \xi(\rho)$, the random potential $\widetilde{V}^{(1)}(\rho, z)$ follows the smoothed variations of $V(z)$. The increase of $\xi(\rho)$ from $\rho = 0$ to $\rho = R_\perp$ means that the smoothing effect becomes more important close to edge of the radial profile. The highest *absolute* amplitude of the density modulation therefore occurs at the trap center (relative amplitudes are discussed below).[25] If $\sigma_{\rm R} \ll \xi$, the smoothing effect is considerable all over the radial profile. If on the other hand we have $\xi \lesssim \sigma_{\rm R}$, then the smoothing is reduced. In particular when $\xi \ll a_{\rm ho} \lesssim \sigma_{\rm R}$, result (3.110) turns into the expected Thomas-Fermi approximation with respect to both the radial and the longitudinal components of the external potential: $g n_0(\rho, z) \simeq \mu - m\omega_\perp^2 \rho^2/2 - V(z)$.

For a weak random potential ($V_{\rm R} \ll \mu$), the typical amplitude of $\widetilde{V}^{(1)}(\rho, z)$ is much smaller than $\mu(\rho)$ on most of the radial profile. Expression (3.110) therefore expands as

$$\sqrt{n_0(\rho, z)} \simeq \sqrt{\frac{\mu(\rho)}{g}} \left(1 - \frac{\widetilde{V}^{(1)}(\rho, z)}{2\mu(\rho)} \right) \tag{3.115}$$

or, equivalently,

$$\sqrt{n_0(\rho, z)} \simeq \sqrt{\frac{\mu(1 - \rho^2/R_\perp^2)}{g}} \left(1 - \frac{\widetilde{V}^{(1)}(\rho, z)}{2\mu(\rho)} \right). \tag{3.116}$$

Note the formal analogy of this expression with the pure 1D case (obtained by setting here $\rho = 0$ and identifying g with the 1D coupling constant), and the similarity of the longitudinal dependence with the tight-confinement result (3.102).

The density profile at given distance ρ of the z-axis is weakly perturbed by the random potential if the root-mean-square amplitude $|\widetilde{V}_{\rm R}^{(1)}(\rho)|$ of the smoothed random potential is such that

$$\mu(\rho) \gg |\widetilde{V}_{\rm R}^{(1)}(\rho)|, \tag{3.117}$$

where $\mu(\rho) = \mu(1 - \rho^2/R_\perp^2)$. Adapting Eq. (3.63) as

$$|\widetilde{V}_{\rm R}^{(1)}(\rho)| = |V_{\rm R}| \sqrt{I_2 \left[\frac{\xi(\rho)}{\sigma_{\rm R}} \right]} \tag{3.118}$$

and using the fact that $\xi(\rho)^2 = \xi^2/(1 - \rho^2/R_\perp^2)$, we find that this condition rewrites

$$\mu^2 (1 - \rho^2/R_\perp^2)^2 \gg |V_{\rm R}|^2 \frac{\sigma_{\rm R}}{\sqrt{2\pi}} \int {\rm d}q \frac{\hat{c}_2(q\sigma_{\rm R})}{[1 + (q\xi)^2/(1 - \rho^2/R_\perp^2)]^2}. \tag{3.119}$$

[25] The formal divergence of $\xi(\rho)$ when ρ approaches $R_\perp$ can be disregarded as the description in terms of a Thomas-Fermi profile breaks down anyway in the region where $\mu(\rho)$ becomes smaller than $\hbar\omega_\perp$ (i.e. when $\xi(\rho)$ becomes larger than $a_{\rm ho}$). This region is very small as soon as loose trapping ($\xi \ll a_{\rm ho}$) is guaranteed. The considerations developed within the radial domain of validity of the Thomas-Fermi approximation also show that the largest absolute amplitude of the density modulations occurs at the trap center, while their relative amplitude grows with the distance from the z-axis. Qualitatively, these results can be extrapolated to the edge of the radial profile.

Finally, we obtain the condition

$$\mu^2 \gg |V_{\rm R}|^2 \frac{\sigma_{\rm R}}{\sqrt{2\pi}} \int \mathrm{d}q \frac{\hat{c}_2(q\sigma_{\rm R})}{\left[1-\rho^2/R_\perp^2+(q\xi)^2\right]^2}. \tag{3.120}$$

As $\hat{c}$ is a positive function, the right-hand-side grows with the distance ρ. In other words, *relative* density modulations increase from the trap center to the edges of the radial profile and the less stringent criterion on the potential strength is met at the trap center ($\rho = 0$).

If the potential is not weak enough, fragmentation enters the gas from the edges of the radial Thomas-Fermi profile, and a complete disconnection under the influence of a potential fluctuation is achieved when the density drops to zero on the z-axis. As in the pure 1D case, we end up with the condition

$$\mu \gg |V_{\rm R}| \sqrt{I_2(\xi/\sigma_{\rm R})}, \tag{3.121}$$

with

$$I_2\left(\frac{\xi}{\sigma_{\rm R}}\right) = \frac{\sigma_{\rm R}}{\sqrt{2\pi}} \int \mathrm{d}q \frac{\hat{c}_2(q\sigma_{\rm R})}{\left[1+(q\xi)^2\right]^2}. \tag{3.122}$$

If condition (3.121) is not satisfied, the Bose gas forms a fragmented BEC.

3.4 Lifshits glass regime

Let us now examine the case where interactions are vanishingly small. We assume that the random potential has a lower bound $V_{\rm min} = \min(V)$. Then, the single-particle spectrum is also bounded below, and we assume that a single-particle ground state can be isolated. In the absence of interactions, the bosons all populate this single-particle ground state.

The non-interacting limit of disordered bosons is often said to be pathological as the situation where a large number of bosons populates the sole single-particle ground state is unstable with respect to the introduction of a finite repulsion between the particles. In turn, we show here how the *set* of lowest-energy eigenstates of the disordered single-particle problem offers a good basis to describe the redistribution of bosons as very weak interactions are turned on.

3.4.1 Non-interacting case: the Lifshits tail

The non-interacting system is described by the 1D single-particle Hamiltonian

$$\hat{h} = -\frac{\hbar^2\nabla_\rho^2}{2m} - \frac{\hbar^2\partial_z^2}{2m} + \frac{1}{2}m\omega_\perp^2\rho^2 + V(z) \tag{3.123}$$

which, given the cylindrical geometry, separates into radial and longitudinal components. In the ground-state of the system, or for excitation energies which are much smaller than the radial oscillator splitting $\hbar\omega_\perp$, the radial wave function is constrained to the harmonic oscillator ground state (3.92). We are then left to study the 1D Schrödinger problem

$$\left[-\frac{\hbar^2}{2m}\frac{\mathrm{d}^2}{\mathrm{d}z^2} + V(z)\right]\chi_\nu = E_\nu\chi_\nu, \tag{3.124}$$

where $\chi_\nu(z)$ accounts for the longitudinal motion of the atoms. The eigenstates of the 1D disordered Schrödinger operator are generally all localized in the sense of Anderson, irrespective

of their energy. However, it turns out that the processes which give rise to localization in the random potential are of somewhat different nature in the high- and in the low-energy regimes. In order to describe the low-energy eigenstates, let us therefore start by reviewing some ways to characterize localization.

Measures of localization

Localization is characterized by properties of both the wave functions χ_ν and the eigenvalues E_ν.

Localization length - The eigenfunctions of the disordered 1D Schrödinger operator undergo Anderson localization, which means that they decay exponentially with the distance from a center (randomly) located somewhere in the system. In infinite systems, the landmark of Anderson-localized wave functions is therefore a finite *localization length*. This characteristic length scale is defined as the inverse of the Lyapunov exponent γ, which measures the rate of exponential decay of $\chi_\nu(z)$ at asymptotically large distances:

$$\gamma = -\lim_{|z|\to\infty} \frac{\langle \ln \|\chi(z)\| \rangle}{|z|}. \tag{3.125}$$

In this expression, $\langle . \rangle$ denotes statistical averaging, and $\|.\|$ stands for a suitably chosen norm.[26] The Lyapunov exponent is a non-random quantity which depends on the statisitical properties of the random potential, as well as the energy E of the particle (see chapter 2).

Participation length - Strictly speaking, a positive Lyapunov exponent is all is needed to define Anderson-localized eigenfunctions. Note, however, that the Lyapunov exponent only captures exponential decay and *asymptotic* properties of the wave functions. As an alternative measure of localization, it is possible to introduce the *participation length*

$$P_\nu = \frac{1}{\int \mathrm{d}z |\chi_\nu(z)|^4} \tag{3.126}$$

which, for an eigenfunction χ_ν normalized to unity, estimates the size of the region where the amplitude of χ_ν is significant. As the weighting of the integral favors high densities, the participation length is related to the typical width of a localized state around its center, rather than the length scales of decay in the wings. As P_ν measures the typical width of a state, it decreases for localization on shorter length scales.

The participation length defined in Eq. (3.126) is often divided by the system size (in finite systems). In that case it is called participation ratio. The participation ratio and the participation length are often used in numerical studies where their scaling with the system size is analyzed to locate possible delocalization transitions or estimate the localization length of localized states [81]. A participation ratio which remains close to one despite of the scaling of the system size indicates the possibility of a delocalized state. Conversely, the participation ratio of a localized state starts dropping as soon as the system size exceeds the localization length. In the Lifshits tail studied below, however, the participation length and the localization length are seen to have different meanings.

[26] See e.g. definition (2.15) for excitations of positive energy.

Spectral properties - From the point of view of the eigenvalues E_ν, localization manifests itself in a dense pure-point spectrum of eigenvalues E_ν. The pure-point nature of the spectrum can be associated with the fact that the χ_ν are square-integrable bound states. The dense character of the spectrum means that, with probability one, the vicinity of a given point E of the spectrum contains either zero or an infinity of eigenvalues [86]. It is possible to define the density of states (DoS) $\mathcal{D}(E)$, which counts the number $\mathrm{d}\mathcal{N}$ of eigenvalues in an interval $\mathrm{d}E$ around the energy E, per unit of system length. Most importantly, as the Lyapunov exponent, the density of states is a self-averaging quantity in the case of homogeneous disorder. In other words, the calculation of $\mathcal{D}$ in a system whose size tends to infinity and statistical averaging yield the same non-random limit [86, 281]. Similarly, the cumulative (or *integrated*) density of states (CDoS)

$$\mathcal{N}(E) = \int_{-\infty}^{E} \mathrm{d}E' \mathcal{D}(E'), \tag{3.127}$$

which counts the number of eigenvalues up to energy E (per unit length), converges to a non-random limit for large system sizes. In the following, we denote by $\mathcal{D}_{2L}$ ($\mathcal{N}_{2L}$) the DoS (CDoS) integrated on the length $2L$ of the box which confines our system, and assume that $2L$ is large enough so that $\mathcal{D}_{2L}/2L$ ($\mathcal{N}_{2L}/2L$) is representative of $\mathcal{D}$ ($\mathcal{N}$). Then, both $\mathcal{D}_{2L}$ and $\mathcal{N}_{2L}$ are bound to grow linearly with L.

The reference cumulative density for the 1D Schrödinger operator without disorder is

$$\mathcal{N}_0(E) = \begin{cases} \frac{1}{\pi}\sqrt{2mE/\hbar^2} & \text{if } E \geq 0 \\ 0 & \text{otherwise} \end{cases}, \tag{3.128}$$

and the density is obtained as $\mathcal{D}_0(E) = \mathrm{d}\mathcal{N}_0(E)/\mathrm{d}E$. In the presence of disorder, the leading high-energy dependence of the cumulative density of states generally retains the form of the free particle case [197], that is

$$\mathcal{N}(E) \sim \frac{1}{\pi}\sqrt{2mE/\hbar^2} \qquad [E \to +\infty]. \tag{3.129}$$

In contrast, the low-energy behavior is strongly affected by the presence of disorder.

The Lifshits tail

Particles of moderate and high energy E localize because of repeated scattering events on the random potential. Let us take the average value of the potential as zero-energy reference. Then, particles with positive energy tend to accumulate phase, and the destructive interference caused by the scattering events eventually leads to an exponential decay of the wave function on rather long length scales (see chapter 2). Therefore, those localized states are best described by the asymptotic properties captured in the Lyapunov exponent (or inverse localization length).

Eigenstates with negative energy, on the other hand, tend to be trapped by fluctuations of the random potential. They decay exponentially because they lack, on average, the kinetic energy to escape potential wells created by those fluctuations.[27] In particular, if the potential

[27] In the case of a perfect lattice, tunneling creates extended Bloch states even for $E = V_{\min}$ i.e. at the band bottom. While the states at the band bottom are extended, they nevertheless essentially grow and decay exponentially between two adjacent sites of the lattice. This reflects the fact that their energy lies below the

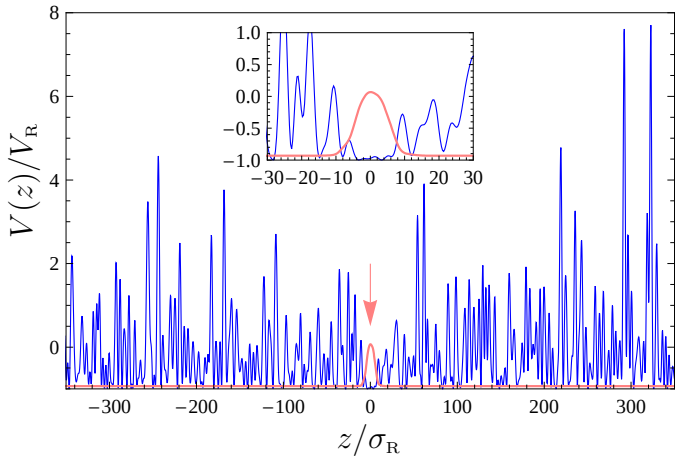


Figure 3.5: Lifshits state in a 1D speckle potential. The eigenstate represented in light red line (indicated by an arrow) on top of a random potential landscape is the single-particle ground state computed in a box of size roughly $10^5\sigma_R$, for a realization of a speckle potential (solid blue line) such that $V_R/E_\sigma = 1$. This state has eigen-energy E close to the potential minimum $V_{\min} = -V_R$ ($E/V_R + 1 \simeq 0.07$), and is created by a rare event where the random potential assumes nearly its minimum value (within 10% of V_R) on twelve correlation lengths. This was checked to be the longest such span in the sample. We also checked that the probability of such spans of size w decreases exponentially with w. The inset shows a magnification of the vicinity of the localization center, around which the z-axis is centered artificially. The eigenfunction is normalized arbitrarily and placed so that the values in the far wings correspond to the eigenvalue E on the potential scale.

is bounded below by some constant

$$V_{\min} = \min(V), \tag{3.130}$$

then the spectrum is also bounded below by $V_{\min}$, and the eigenstates close the spectrum boundary are created by rare fluctuations of the random potential where V assumes values close to $V_{\min}$ on a large region of space, bordered by less exceptional fluctuations. Figure 3.5 shows the occurence of such a rare fluctuation in a blue-detuned speckle potential and the subsequent creation of a deep eigenstate. If we call w the width of such a potential well, $E_w = \hbar^2/2mw^2$ the associated kinetic energy, and if we assume that the walls of the well are steep enough, the energy of the lowest trapped state is $E \simeq V_{\min} + E_w$. Statistically, or in an infinite system, it is always possible to find a fluctuation with larger w and, hence, states closer to $V_{\min}$. The probability of finding such a fluctuation, however, decreases exponentially with the width $w = \sqrt{\hbar^2/2mE_w}$ of the well.[28] Therefore, the probability of finding states up to energy $E = V_{\min} + E_w$ is argued to scale as $\exp(-C''/\sqrt{E - V_{\min}})$, where C'' is a positive

average of the potential. In a sinusoidal lattice with amplitude V_0 and period λ, the effect is pronounced if V_0 and λ are large ($V_0 \gg \hbar^2/2m\lambda^2$). Because of the perfect order in the lattice, the sequence of growth and decay does not lead to an asymptotic decay. Hence, and in order to resort to a physical picture, the localization of low-energy eigenstates in a random potential might be attributed to the absence of resonant tunneling [197].

[28] In higher dimensions, this probability decreases exponentially with the volume $(\hbar^2/2mE_w)^{d/2}$.

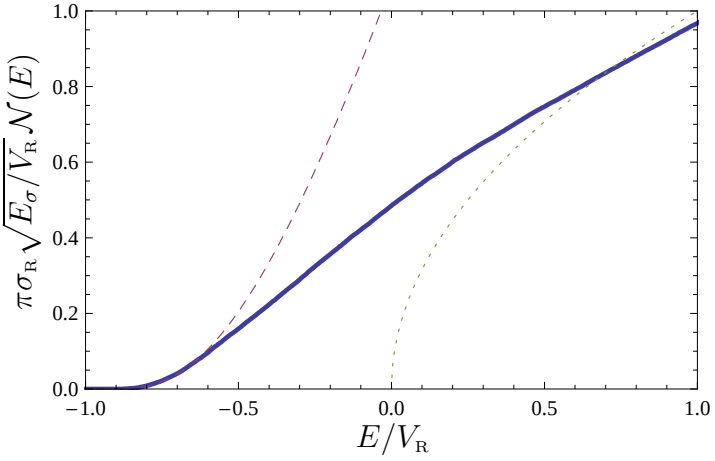


Figure 3.6: Cumulative density of state $\mathcal{N}(E)$ of Schrödinger particles in a speckle potential with autocorrelation function $C_2(z) = V_{\rm R}^2 \mathrm{sinc}(z/\sigma_{\rm R})^2$, bounded below by $V_{\rm min} = -V_{\rm R}$, and such that $V_{\rm R}/E_\sigma = 1$. The numerical data (thick blue line) was obtained by direct diagonalization and averaging over 100 samples of size roughly $10^3\sigma_{\rm R}$. The dashed purple line is a fit by a stretched exponential of the form (3.132) with $\beta = 1/2$, and the brown dotted line represents the free-particle cumulative density of state (3.128).

constant, in 1D. According to this qualitative argument, the cumulative density of state should take the form of a stretched exponential

$$\mathcal{N}(E) \sim C' \mathrm{e}^{-C''/\sqrt{E-V_{\rm min}}} \qquad [E \to V_{\rm min}^+], \tag{3.131}$$

with constant C' and C'', when E approaches $V_{\rm min}$ from above. This form of the cumulative density of states in disordered systems was first proposed and studied by I.M. Lifshits, and is therefore called the Lifshits tail of the spectrum [282, 283]. Eigenstates which belong to the Lifshits tail are termed Lifshits states. Figure 3.6 displays the cumulative density of states computed for a 1D speckle potential. The CDoS assumes a form compatible with a stretched exponential at low energy,[29] and crosses over to the free-particle limit (3.129) at high energy.

Interestingly, the precise form of the stretched exponential generally depends on the statistical properties of the random potential [197, 281]. For simplicity, and without loss of generality in the ensuing discussion of the very-weakly-interacting many-body problem, we assume that the cumulative density of states near the bottom of the spectrum takes the form

$$\mathcal{N}(E) \sim C' \mathrm{e}^{-c\left(\frac{V_{\rm R}}{E-V_{\rm min}}\right)^\beta}, \qquad [E \to V_{\rm min}^+] \tag{3.132}$$

with $\beta > 0$. We have here introduced the typical amplitude $V_{\rm R}$ of the random potential, which is assumed to be positive. In the case of a blue-detuned speckle potential, we have $V_{\rm min} = -V_{\rm R}$ owing to the exponential single-point probability distribution (3.18). Numerical calculations performed for such a speckle potential show a reasonable agreement with law (3.132).

[29] We briefly discuss this point in appendix F. A rigorous proof lies beyond the scope of our study.

Localization and participation lengths

For single particles in standard models of disorder, the strength of localization increases with decreasing energy.[30] The Lifshits states at the bottom of the spectrum tunnel across a potential landscape of average height $-V_{\rm min}$. Hence, those states decay asymptotically with a Lyapunov exponent of the order of $\sqrt{-2mV_{\rm min}/\hbar^2}$. As soon as the system is large enough, i.e. such that $-V_{\rm min} \gg E_L = \hbar^2/2mL^2$, the tails of the Lifshits states decay on length scales much shorter than the system size. For a correlated speckle potential, we find localization lengths of the order of $\sqrt{\hbar^2/2mV_{\rm R}} = \sigma_{\rm R}\sqrt{E_\sigma/V_{\rm R}}$ at the bottom of the spectrum, that is, a few correlation lengths for $V_{\rm R}/E_\sigma$ of the order of one.[31]

The typical size of the localized states around their localization center is measured by the participation length P. In every energy interval, P assumes a whole distribution of values, corresponding to different local configurations of the potentials which give rise to eigenstates in that interval. We denote by $\bar{P}(E)$ the average of the distribution of P at energy E. Figure 3.7 shows the probability distribution of P obtained for a speckle potential. The average participation length $\bar{P}(E)$ is seen to decrease from the high-energy region of the spectrum to the regime of negative energies. Deep in the Lifshits tail, the average participation ratio increases again due to the growing size of the potential wells which support the states of lowest energy. This regrowth, however, appears significant only in a region very close to the lower boundary of the spectrum. As shown in Fig. 3.7, the regime of intermediate negative energies is characterized by an almost constant average participation length of a few correlation lengths.

Low-energy eigenstates in a system of finite but large size

As the deepest states in the Lifshits tail are created only by very rare events in the random potential, let us now examine the relevant features which characterize the eigenstates of lowest-energy for a typical realization of the random potential in a system of finite but large size.

Figure 3.8 shows the results obtained for such a realization of a speckle potential in a box of size $2L$. Note that the ratio of L and $\sigma_{\rm R}$ chosen in this example corresponds to realistic experimental conditions [26, 29, 31, 171, 172]. The reference energy $E_L = \hbar^2/2mL^2$ chosen here corresponds roughly to the low-energy cutoff for longitudinal single-particle excitations in the absence of disorder.

The main graph in Fig. 3.8(a) represents the number $\mathcal{N}_{2L}(E)$ of eigenstates up to energy E, and shows that the cumulative density of states takes the form of a Lifshits tail at low energy, whereas it approaches the free-particle expression for high energies. The participation ratio displayed in the inset fluctuates around the average value shown in Fig. 3.7, and globally decreases with decreasing energy, due to stronger localization. Because of the finite size of the sample, no eigenstates are found arbitrarily close to the bottom of the spectrum (the ground state has here an energy around $-V_{\rm min}/2$), as the necessary fluctuations of the random potential have an exponentially small probability to occur in a single sample. Accordingly, no regrowth

[30] This statement holds for white-noise potentials, and the speckle potential examined here. A very different behavior may be observed with quasi-particles in an interacting system, such as the Bogoyubov quasi-particles studied in chapter 4.

[31] The estimate $\sigma_{\rm R}\sqrt{E_\sigma/V_{\rm R}}$ for the limiting value of the localization length was checked to be accurate within 10% in numerical calculations for $V_{\rm R}/E_\sigma = 0.1, 1, 10$. This confirms the assumption that the dominant mechanism in the localization of the eigenstates of lowest energy is decay through tunneling (trapping). Interference effects are expected to produce only marginal corrections at the bottom of the spectrum.

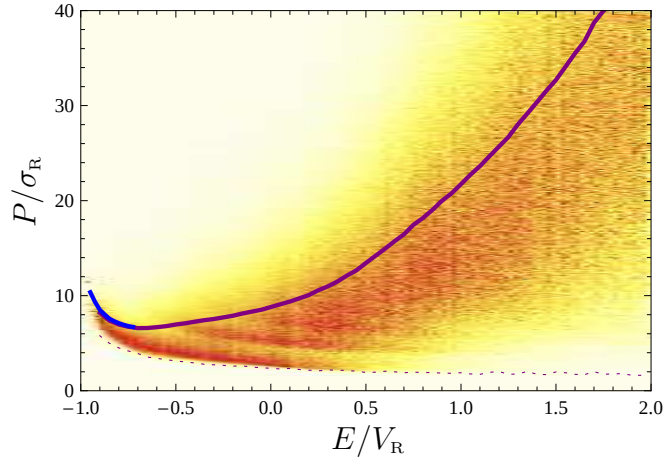


Figure 3.7: Distribution of participation lengths P as a function of the single-particle energy E in a speckle potential with $V_R/E_\sigma = 1$. The solid curves represent the average participation length $\bar{P}(E)$ obtained by direct diagonalization (purple: $2L/\sigma_R = 10^4$; blue: additional data for $2L/\sigma_R = 10^5$). The data was averaged over spectral intervals of width $0.025V_R$ and over 500 to 5000 realizations of the potential depending on the system size. The background color indicates the probability density of P, normalized to the maximum in each energy interval (white: zero; red: one). The minimum participation length appears as a dotted line.

of the participation length is observed, and the eigenstates of lowest energy are characterized by a small, almost constant participation length $P(E)$ of a few correlation lengths ($P(E) \ll L$).

Figure 3.8(b) shows the wave functions $\chi_0, \chi_1, \ldots$ of the ground state and the first few excited states, indexed in order of increasing energy. These states are all strongly localized and have a typical size of a few correlation lengths, in agreement with the computed participation ratios. Most importantly, they appear to be distributed randomly in the box, and hardly overlap due to the (very fast) decay of their wings on the length scale of a few correlation lengths.

3.4.2 Lifshits regime

We now address the regime of finite but very weak interactions. The exact ground state of the interacting system is delicate to derive. However, when the chemical potential μ lies in the Lifshits tail of the longitudinal single-particle spectrum, the Lifshits states χ_ν offer a convenient basis to work with. As these states hardly overlap, they can be regarded as trapping microsites, populated by a given number of bosons whose longitudinal motion is frozen to χ_ν. This picture is discussed below from a many-body point of view. We then derive equations for the associated mean-field density profile.

Many-body description

The solutions $\{\chi_\nu, \nu \in \mathbb{N}\}$ of the Schrödinger equation (3.124) form a complete set which can be used to describe the longitudinal distribution of the atoms. When the chemical potential of the interacting Bose gas lies in the Lifshits tail of the single-particle spectrum, the atoms lack

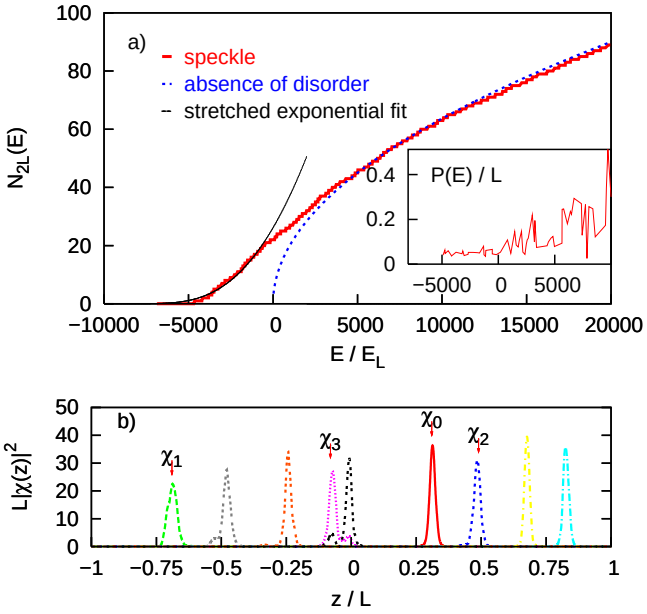


Figure 3.8: Low-energy single-particle states in a typical realization of a speckle random potential. The correlation length is here $\sigma_{\rm R} = 2\times10^{-3}L$, where L is half the box size. The amplitude of the disorder is $V_{\rm R} = 10^4 E_L$, with $E_L = \hbar^2/2mL^2$ ($\epsilon_{\rm R} = 0.04$, $\alpha_{\rm R} = 25$). (a) Integrated cumulative density of states $\mathcal{N}_{2L}$ (red solid line) crossing over from a stretched exponential (black solid line) to the free-particle expression (blue dotted line) with increasing energy. Inset: participation length normalized by the system size. (b) Wave functions of the first few low-energy Lifshits states.

energy to populate high-energy single-particle orbitals. Hence, their longitudinal distribution can be expanded on the set of low-lying Lifshits states. We show here that the set of Lifshits states indeed offers a convenient representation of the interacting many-body states of the Bose gas.

The Lifshits states χ_ν are strongly localized eigenstates of the single-particle problem. Their wave functions decay exponentially beyond a few correlation length from the localization center. Strictly speaking, we may call microsite ν the location of the corresponding χ_ν or the "central part" of the wave function χ_ν. In Fig. 3.8(b), the microsites correspond to the visible part of the wave functions χ_ν.[32] The difference only lies in the tails of the Lifshits states, which fall off exponentially fast. In the following description of the very-weakly-interacting Bose gas, however, we shall completely neglect the role of the tails of the Lifshits states. Then, Lifshits states and microsites can be identified.

When the chemical potential lies deep in the Lifshits tail of the spectrum, only a few distant Lifshits states are populated (see below). Then, interaction-induced couplings between the microsites can be neglected, and the Lifshits states can be regarded as trapping microsites

[32]This definition is, of course, only qualitative. For a rigorous analysis, e.g. in terms of coupled Josephson junctions, the microsites wave functions should be chosen as an orthogonal set.

with *on-site* interaction only.

An important question is to know *how* the bosons populate the various microsites. In the presence of interactions, we expect that mean-field energy shifts will bring distant microsites to resonance, and it is natural to ask whether the best approximate single-particle basis consists of linear combinations of the Lifshits states, or if the bosons form number states localized on individual microsites.

If the overlap (coupling) of the Lifshits states with the surrounding microsites is not completely neglected, the ground state and dynamics of the interacting bosons populating the microsites can be described by the physics of Josephson junctions [111, 284–288]. Such an analysis shows that, in the regime where the on-site mean-field interaction energy (also called *charging* energy E_c) exceeds the coupling energy (often labelled E_J), the system enters a Fock regime, where the fluctuations of the number of particles on each site are suppressed [287]. In that case, the relative phase between sites is undefined. One might say that phase-locking mechanisms between the sites vanish along with the amplitude of the couplings.

Here, we neglect couplings between microsites. Then, each microsite ν contains exactly N_ν bosons. These bosons interact weakly and occupy the same ground-state radial Hartree-Fock orbital $\phi_\nu(\rho)$. The corresponding N-body states take the form

$$|\Psi\rangle = \prod_\nu \frac{1}{\sqrt{N_\nu!}} (b_\nu^\dagger)^{N_\nu} |0\rangle, \tag{3.133}$$

where $|0\rangle$ is the vacuum, the occupation numbers N_ν sum up to N,

$$\sum_\nu N_\nu = N, \tag{3.134}$$

and $b_\nu^\dagger$ is the bosonic creation operator in state $\phi_\nu(\rho)\chi_\nu(z)$,

$$b_\nu^\dagger = \int \mathrm{d}\boldsymbol{\rho} \int \mathrm{d}z\, \phi_\nu(\rho)\chi_\nu(z)\hat{\Psi}^\dagger(\boldsymbol{\rho}, z). \tag{3.135}$$

Each microsite with large N_ν contains a BEC. The entire system, however, is not phase-coherent because of the fragmentation along the z-axis [111].

Ground-state density

The energy of state (3.133) is evaluated from $\langle\Psi|\hat{H}|\Psi\rangle$, where $\hat{H}$ is the many-body Hamiltonian

$$\hat{H} = \int \mathrm{d}\mathbf{r} \left\{ \hat{\Psi}^\dagger(\mathbf{r}) \left[-\frac{\hbar^2\nabla^2}{2m} + V_{\mathrm{ext}}(\mathbf{r}) \right] \hat{\Psi}(\mathbf{r}) + \frac{g}{2}\hat{\Psi}^\dagger(\mathbf{r})\hat{\Psi}^\dagger(\mathbf{r})\hat{\Psi}(\mathbf{r})\hat{\Psi}(\mathbf{r}) \right\}. \tag{3.136}$$

Taking advantage of the fact that the χ_ν form an orthonormalized set of functions which solve

$$\left[-\frac{\hbar^2}{2m}\frac{\mathrm{d}^2}{\mathrm{d}z^2} + V(z) \right] \chi_\nu = E_\nu \chi_\nu, \tag{3.137}$$

we expand the Hamiltonian as

$$\begin{aligned} H &= \sum_\nu \int \mathrm{d}\boldsymbol{\rho} \left\{ N_\nu \phi_\nu^*(\rho) \left[-\frac{\hbar^2\nabla_\rho^2}{2m} + \frac{1}{2}m\omega_\perp^2\rho^2 + E_\nu \right] \phi_\nu(\rho) + \frac{g_{2\mathrm{D}}^\nu}{2} N_\nu(N_\nu - 1)|\phi_\nu(\rho)|^4 \right\} \\ &\quad + 2\sum_{\nu\neq\nu'} \int \mathrm{d}\boldsymbol{\rho} \left\{ \frac{g}{2} \left(\int \mathrm{d}z |\chi_\nu(z)|^2 |\chi_{\nu'}(z)|^2 \right) N_\nu N_{\nu'} |\phi_\nu(\rho)|^2 |\phi_{\nu'}(\rho)|^2 \right\}, \end{aligned} \tag{3.138}$$

where g_{2D}^{ν} is an effective on-site coupling constant, defined as

$$g_{2D}^{\nu} = g \int \mathrm{d}z |\chi_\nu(z)|^4 = \frac{g}{P_\nu}. \tag{3.139}$$

In this expression, P_ν is the participation length of eigenstate ν. An effective low-energy Hamiltonian is derived by restricting the expansion over microsites to the lowest Lifshits states χ_ν. As those low-lying states have a negligible overlap, characterized by

$$\sqrt{P_\nu P_{\nu'}} \int \mathrm{d}z |\chi_\nu(z)|^2 |\chi_{\nu'}(z)|^2 \ll 1 \qquad \text{for } \nu \neq \nu', \tag{3.140}$$

the second line of expression (3.138) can be neglected. We finally obtain

$$H \simeq \sum_\nu \int \mathrm{d}\boldsymbol{\rho} \left\{ N_\nu \phi_\nu^*(\rho) \left[-\frac{\hbar^2 \nabla_\rho^2}{2m} + \frac{1}{2} m\omega_\perp^2 \rho^2 + E_\nu \right] \phi_\nu(\rho) + \frac{g_{2D}^{\nu}}{2} N_\nu^2 |\phi_\nu(\rho)|^4 \right\}, \tag{3.141}$$

where, assuming a large occupation of the microsites, $N_\nu(N_\nu - 1)$ is approximated by N_ν^2.

To find the ground-state occupation numbers N_ν and wave functions ϕ_ν, the energy H is minimized under the constraint of a total number of bosons $N = \sum_\nu N_\nu$. As in section 3.3.2, the constraint is embedded by using a Lagrange multiplier in the form of the chemical potential μ. Rather than working with the two degrees of freedom N_ν and ϕ_ν on each microsite, let us introduce the radial densities

$$n_\nu^{2D}(\rho) = N_\nu |\phi_\nu(\rho)|^2. \tag{3.142}$$

We can, of course, restrain ourselves to positive, real-valued $\phi_\nu(\rho)$, as phase gradients along ρ would introduce kinetic energy. Then, the ground state is found among the stationary points of

$$L[\{n_\nu^{2D}\}, \lambda] = H[\{n_\nu^{2D}\}] - \lambda(N[\{n_\nu^{2D}\}] - N) \tag{3.143}$$

with respect to $\{n_\nu^{2D}\}$ and λ. Here, the energy and atom-number functionals $H[.]$ and $N[.]$ are defined as

$$H[\{n_\nu^{2D}\}] = \sum_\nu \int \mathrm{d}\boldsymbol{\rho} \left\{ \sqrt{n_\nu^{2D}(\rho)} \left[-\frac{\hbar^2 \nabla_\rho^2}{2m} + \frac{1}{2} m\omega_\perp^2 \rho^2 + E_\nu \right] \sqrt{n_\nu^{2D}(\rho)} + \frac{g_{2D}^{\nu}}{2} n_\nu^{2D}(\rho)^2 \right\} \tag{3.144}$$

and

$$N[\{n_\nu^{2D}\}] = \sum_\nu \int \mathrm{d}\boldsymbol{\rho}\, n_\nu^{2D}(\rho). \tag{3.145}$$

Evaluating the functional derivatives of Eq. (3.143), and imposing $\delta L / \delta n_\nu^{2D}|_{(n_\nu^{2D}, \lambda)} = 0$, we find a set of Gross-Pitaevskii equations for the radial profiles:

$$\left[-\frac{\hbar^2 \nabla_\rho^2}{2m} + \frac{1}{2} m\omega_\perp^2 \rho^2 + g_{2D}^{\nu} n_\nu^{2D}(\rho) + E_\nu - \mu \right] \sqrt{n_\nu^{2D}(\rho)} = 0. \tag{3.146}$$

Solving the radial GPEs in each microsite for the same chemical potential μ gives access to the 2D densities $n_\nu^{2D}(\rho)$, the microsite populations

$$N_\nu = \int \mathrm{d}\boldsymbol{\rho}\, n_\nu^{2D}(\rho), \tag{3.147}$$

and the normalized wave functions

$$\phi_\nu(\rho) = \sqrt{\frac{n_\nu^{2\mathrm{D}}(\rho)}{N_\nu}} \qquad \text{for } N_\nu > 0. \tag{3.148}$$

In Eq. (3.146), the quantity $\mu - E_\nu$ plays the role of an effective on-site chemical potential, which determines the level of filling of the microsites. Atoms populate microsite ν under the condition

$$\mu' - E_\nu = \mu - \hbar\omega_\perp - E_\nu > 0, \tag{3.149}$$

where $\hbar\omega_\perp$ is the ground state energy of the radial oscillator. Note also that, in general, the above procedure does not yield integer populations N_ν, as imposed in the Fock state (3.133). For large-enough fillings N_ν, however, the difference of ground-state energy, microsite populations and radial wave functions introduced by the fact that these fillings should be integers is negligible.[33] For increasing $\mu' - E_\nu$, the radial profile $n_\nu^{2\mathrm{D}}(\rho)$ continuously turns from a Gaussian ($\mu' - E_\nu \ll \hbar\omega_\perp$) into a Thomas-Fermi inverted parabola ($\mu' - E_\nu \gg \hbar\omega_\perp$).

3.4.3 Domain of validity

The description of the system in terms of Lifshits states is based on a few assumptions. Let us recapitulate them here. First of all, the atoms populate micro-sites centered at the location of the lowest-lying Lifshits states χ_ν. Then, the longitudinal motion of the atoms in each of these trapping sites is assumed to be frozen in the state $\chi_\nu(z)$. Finally, the overlap of the Lifshits state is small enough so that interactions can be considered local i.e. restricted to the atoms *within* the individual microsites. Let us now discuss the conditions under which these assumptions are expected to be appropriate.

As explained above, the location of the microsites is robust against the presence of interactions. As the Lifshits states originate from energetically favorable fluctuations of the potential, it remains advantageous to distribute the atoms among those locations in the first place. Since the shape and position of the Lifshits states is determined by important *local* fluctuations of the potential, and the Lifshits states are strongly localized, they are immune to the particles placed elsewhere in the system. This justifies the use of the Lifshits states as a basis of microsites. As mean-field interactions increase on a given site, either because particles are added or because interactions are turned on, one might expect the density profile to buldge. This, in particular, might be the case in the radial direction, if the trapping is very loose ($\mu' - E_\nu \gtrsim \hbar\omega_\perp$). Before the cloud located on a microsite starts buldging in the *longitudinal* direction, however, it will become favorable to populate another Lifshits state, possibly located far away in the system, and very close in energy if the system is large enough. The relevant energy scales for such

[33] From a purely technical point of view, note that it is not necessary to start from a Fock state in the first place to derive the mean-field equations (3.146). As the eigenstates χ_ν form a complete basis, the field operator can be written $\hat\Psi(\boldsymbol{\rho}, z) = \sum_\nu \chi_\nu(z)\hat\Psi_\nu(\boldsymbol{\rho})$. In the low-energy Hamiltonian, the sum runs only over the lowest Lifshits states, whose spatial overlap can neglected, so that

$$\hat H \simeq \sum_\nu \int \mathrm{d}\boldsymbol{\rho} \left\{ \hat\Psi_\nu^\dagger(\boldsymbol{\rho}) \left[-\frac{\hbar^2\nabla_\rho^2}{2m} + \frac{1}{2}m\omega_\perp^2\rho^2 + E_\nu \right] \hat\Psi_\nu(\boldsymbol{\rho}) + \frac{g_{2\mathrm{D}}^\nu}{2}\hat\Psi_\nu^\dagger(\boldsymbol{\rho})\hat\Psi_\nu^\dagger(\boldsymbol{\rho})\hat\Psi_\nu(\boldsymbol{\rho})\hat\Psi_\nu(\boldsymbol{\rho}) \right\}.$$

Then, replacing the field operators $\hat\Psi_\nu^\dagger(\boldsymbol{\rho})$ by a classical field $\sqrt{n_\nu^{2\mathrm{D}}(\rho)}$ directly leads to expression (3.144).

a redistribution are likely to be the energy of the first longitudinal single-particle excitation in the potential well associated with a given Lifshits state, and the energy splitting between this Lifshits state and another distant one. For a large system and weak interactions, it is reasonable to assume that the particles distribute among microsites whose longitudinal shape remains unaffected.

In such a picture, a breakdown of the description in terms of Lifshits states occurs primarily when atoms start populating nearby sites whose overlap cannot be neglected. As filling microsite ν requires inequality (3.149) to hold, the number of populated microsite is directly controled by the chemical potential. Precisely, the number of Lifshits states which are populated in the box of size $2L$ is $\mathcal{N}_{2L}(\mu')$. This number should be smaller than the index $\nu_{2L}^{\max}$ of the highest Lifshits state such that all lower Lifshits states hardly overlap:

$$\mathcal{N}_{2L}(\mu') \leq \nu_{2L}^{\max}. \tag{3.150}$$

If the tails of the χ_ν are neglected, $\nu_{2L}^{\max}$ should roughly be equal to the system size over the typical participation length in the Lifshits tail. A precise definition of $\nu_{2L}^{\max}$, based e.g. on the evaluation of terms such as the left-hand-side of (3.140), might involve another characteristic length scale in the Lifshits tail. In any case, both $\mathcal{N}_{2L}$ and the index $\nu_{2L}^{\max}$ derive from the properties of the single-particle problem, and grow linearly with the system size for large enough L.[34] This allows for the formulation of a criterion of validity which is independent of the system size, as shown below.

In general, $\mathcal{N}_{2L}(E)$ and $\nu_{2L}^{\max}$ have complex dependencies on the single-particle energy E, the potential amplitude $V_{\rm R}$, the correlation length $\sigma_{\rm R}$, and the model of disorder. General properties can nevertheless be discussed on the basis of a rescaled form of the single-particle problem (3.124):

$$\left[-\alpha_{\rm R}\frac{{\rm d}^2}{{\rm d}u^2} + v(u)\right]\varphi_\nu(u) = \frac{E_\nu}{V_{\rm R}}\varphi_\nu(u), \tag{3.151}$$

where

$$u = z/\sigma_{\rm R} \tag{3.152}$$
$$v(u) = V(z)/V_{\rm R} \tag{3.153}$$
$$\varphi_\nu(u) = \sqrt{\sigma_{\rm R}}\,\chi_\nu(z) \tag{3.154}$$

and

$$\alpha_{\rm R} = \frac{E_\sigma}{V_{\rm R}} = \frac{\hbar^2}{2m\sigma_{\rm R}^2 V_{\rm R}}. \tag{3.155}$$

For $L \gg \sigma_{\rm R}$, the boundaries on u play no role, and the properties of eigenvalues and eigenfunctions are seen to depend only on the parameter $\alpha_{\rm R}$ after renormalization of energies and lengths. As $\mathcal{N}_{2L}(E)$ and $\nu_{2L}^{\max}$ become extensive in this limit, we can write

$$\mathcal{N}_{2L}(E) = \frac{2L}{\sigma_{\rm R}}\zeta(\alpha_{\rm R}, E/V_{\rm R}) \tag{3.156}$$
$$\nu_{2L}^{\max} = \frac{2L}{\sigma_{\rm R}}\eta(\alpha_{\rm R}), \tag{3.157}$$

[34] Recall that $\mathcal{N}_{2L}(E)/2L$ converges to the non-random limit $\mathcal{N}(E)$. For large enough L, doubling the system size amounts to creating a copy with identical statistical properties.

where ζ and η are functions which depend only on the model of disorder v. Then, condition (3.150) rewrites

$$\zeta(\alpha_{\rm R}, \mu'/V_{\rm R}) \leq \eta(\alpha_{\rm R}). \tag{3.158}$$

As ζ is an increasing function of its second argument, expression (3.158) defines an upper bound on the chemical potential. This bound has the form

$$\mu' \leq V_{\rm R} F(\alpha_{\rm R}), \tag{3.159}$$

where the function F is defined by the solution of $\eta(\alpha_{\rm R}, F(\alpha_{\rm R})) = \eta(\alpha_{\rm R})$, and depends only on the model of disorder v.

If condition (3.159) is not satisfied, several populated Lifshits state will overlap, and the Bose gas will start forming a fragmented BEC. Each fragment will be a superposition of Lifshits states, and its shape will be modified by the interactions. The sensitivity of the shape of the fragments to interactions is expected to increase as the size of the puddles formed by overlapping Lifshits grows, and the kinetic energy associated with their boundaries decreases. The crossover from the Lifshits regime to the regime of fragmented BEC should therefore come along with variations in the compressibility of the gas.

Note also that the description we have given above in terms of Fock states of Lifshits states *completely* neglects the coupling between Lifshits states or microsites. To approach the crossover between the Lifshits regime and what we call the fragmented BEC regime, a description e.g. in terms of an array of Josephson junctions might be developed where these couplings are considered. A complication in this approach lies in the statistical nature of on-site energies and coupling elements.

3.4.4 Mean-field equation of state

We now derive the equation of state which relates the chemical potential μ to the number of bosons. The "thermodynamic limit" is obtained by relating μ to the average linear density of bosons $\langle n_0^{\rm 1D}\rangle = N/2L$ in the longitudinal direction.[35]

The starting point of the analysis is formed by the set of GPEs derived in section 3.4.2 for the radial densities $n_\nu^{\rm 2D}(\rho)$ on each microsite ν:

$$\left[-\frac{\hbar^2\nabla_\rho^2}{2m} + \frac{1}{2}m\omega_\perp^2\rho^2 + \frac{g}{P_\nu}n_\nu^{\rm 2D}(\rho) + E_\nu - \mu\right]\sqrt{n_\nu^{\rm 2D}(\rho)} = 0. \tag{3.160}$$

In terms of the associated populations and normalized wave functions

$$N_\nu = \int {\rm d}\boldsymbol{\rho}\, n_\nu^{\rm 2D}(\rho) \tag{3.161}$$

$$\phi_\nu(\rho) = \sqrt{\frac{n_\nu^{\rm 2D}(\rho)}{N_\nu}} \qquad \text{for } N_\nu > 0, \tag{3.162}$$

the radial GPEs also write

$$\left[-\frac{\hbar^2\nabla_\rho^2}{2m} + \frac{1}{2}m\omega_\perp^2\rho^2 + \frac{g}{P_\nu}N_\nu|\phi_\nu(\rho)|^2\right]\phi_\nu(\rho) = (\mu - E_\nu)\phi_\nu(\rho). \tag{3.163}$$

[35] It might be useful to stress that in the Lifshits regime, and in contrast to the delocalized BEC regime, the local density $n_0^{\rm 1D}(z)$ is very different from the average value $\langle n_0^{\rm 1D}\rangle = N/2L$.

Note that, while P_ν might assume a range of different values for the same single-particle energy E_ν (see Fig. 3.7), the quantities $n_\nu^{\rm 2D}(\rho)/P_\nu$, N_ν/P_ν and $\phi_\nu(\rho)$ in Eqs. (3.160) and (3.163) are uniquely determined by the interplay of μ, $\hbar\omega_\perp$ and E_ν. In particular, only those microsites with

$$\mu' = \mu - \hbar\omega_\perp > E_\nu \tag{3.164}$$

are populated.

General case

We define a function $f_g(\mu, \hbar\omega_\perp, E)$ such that, for all N_ν and P_ν,

$$\frac{N_\nu}{P_\nu} = f_g(\mu, \hbar\omega_\perp, E_\nu). \tag{3.165}$$

As explained above, f_g is uniquely defined by the ground-state solution of a 2D Gross-Pitaevskii equation, it increases with μ, and vanishes for $\mu - \hbar\omega_\perp < E$. Note also that f_g is homogeneous to a linear density. Let now $\bar{N}(\mu, \hbar\omega_\perp, E)$ be the number of bosons *per microsite at energy* E, averaged over the distribution of participation lengths. From the definition of f_g, we obtain

$$\bar{N}(\mu, \hbar\omega_\perp, E) = \bar{P}(E) f_g(\mu, \hbar\omega_\perp, E). \tag{3.166}$$

The total number of atoms in the system is obtained by summing the populations over Lifshits states, in a continuous formulation with level density $\mathcal{D}_{2L}$:

$$N = \int \mathrm{d}E \mathcal{D}_{2L}(E) \bar{N}(\mu, \hbar\omega_\perp, E). \tag{3.167}$$

Dividing by the system size, we find

$$\langle n_0^{\rm 1D} \rangle = \int_{V_{\rm min}}^{\mu - \hbar\omega_\perp} \mathrm{d}E \mathcal{D}(E) \bar{P}(E) f_g(\mu, \hbar\omega_\perp, E), \tag{3.168}$$

where $\mathcal{D}$ and $\bar{P}$ are determined from the properties of the 1D single-particle Lifshits states, and f_g accounts for the 2D problem with mean-field interactions.

As in the BEC regime, we now examine explicitly the cases of tight and loose radial confinement.

Tight harmonic trapping

We assume here that the chemical potential and the radial trapping frequency are such that $\mu' - V_{\rm min} \ll \hbar\omega_\perp$. Then, the inequality

$$\mu' - E_\nu \ll \hbar\omega_\perp \tag{3.169}$$

is satisfied for all populated Lifshits states, and the atoms in each microsite are confined to the ground state of the radial oscillator,

$$\phi_\nu(\rho) \simeq \frac{\mathrm{e}^{-\rho^2/2a_{\rm ho}^2}}{\sqrt{\pi} a_{\rm ho}}. \tag{3.170}$$

The populations are obtained from the radial integration of Eq. (3.163):

$$\hbar\omega_\perp + \frac{gN_\nu}{P_\nu}\int \mathrm{d}\boldsymbol{\rho}|\phi_\nu(\rho)|^4 \simeq \mu - E_\nu, \tag{3.171}$$

which yields

$$N_\nu \simeq \begin{cases} \frac{2\pi a_{\mathrm{ho}}^2 P_\nu(\mu'-E_\nu)}{g} & \text{if } \mu' > E_\nu \\ 0 & \text{otherwise} \end{cases}. \tag{3.172}$$

From (3.168), we deduce

$$\langle n_0^{1\mathrm{D}}\rangle \simeq \int_{V_{\min}}^{\mu'} \mathrm{d}E\mathcal{D}(E)\bar{P}(E)\frac{2\pi a_{\mathrm{ho}}^2}{g}(\mu'-E). \tag{3.173}$$

In this expression we recognize an effective 1D coupling constant

$$g_{1\mathrm{D}} = \frac{g}{2\pi a_{\mathrm{ho}}^2} \tag{3.174}$$

for the case of tight harmonic confinement (see Eq. 3.96). This result has a straightforward generalization in the sense that the equation of state for *any* tight transverse confinement obeys

$$g_{1\mathrm{D}}\langle n_0^{1\mathrm{D}}\rangle \simeq \int_{V_{\min}}^{\mu'} \mathrm{d}E\mathcal{D}(E)\bar{P}(E)(\mu'-E), \tag{3.175}$$

where $g_{1\mathrm{D}}$ is the suitable 1D coupling constant, obtained from the transverse ground-state wave function $\phi_\perp$ as $g_{1\mathrm{D}} = g\int \mathrm{d}\boldsymbol{\rho}|\phi_\perp(\boldsymbol{\rho})|^4$.

If we assume that the average participation length is almost constant in the Lifshits tail, i.e. that

$$\bar{P}(E) \simeq \sigma_{\mathrm{R}} p_0(\alpha_{\mathrm{R}}), \tag{3.176}$$

where p_0 is a dimensionless quantity which depends only on the model of disorder and $\alpha_{\mathrm{R}} = E_\sigma/V_{\mathrm{R}}$, then Eq. (3.175) can be integrated by part:

$$g_{1\mathrm{D}}\langle n_0^{1\mathrm{D}}\rangle \simeq \sigma_{\mathrm{R}} p_0(\alpha_{\mathrm{R}}) \int_{V_{\min}}^{\mu'} \mathrm{d}E\mathcal{N}(E). \tag{3.177}$$

We now also assume that the cumulative density of state in the Lifshits tail follows Eq. (3.132), and cast it into the form

$$\mathcal{N}(E) = \sigma_{\mathrm{R}}^{-1} b(\alpha_{\mathrm{R}})\mathrm{e}^{-c(\alpha_{\mathrm{R}})(E/V_{\mathrm{R}}-v_{\min})^{-\beta}} \tag{3.178}$$

with $v_{\min} = V_{\min}/V_{\mathrm{R}}$. Then, Eq. (3.177) evaluates to

$$g_{1\mathrm{D}}\langle n_0^{1\mathrm{D}}\rangle \simeq V_{\mathrm{R}} p_0(\alpha_{\mathrm{R}}) b(\alpha_{\mathrm{R}})\frac{c(\alpha_{\mathrm{R}})^{1/\beta}}{\beta}\Gamma\left(-\frac{1}{\beta}, c(\alpha_{\mathrm{R}})\left[\frac{\mu'}{V_{\mathrm{R}}} - v_{\min}\right]^{-\beta}\right), \tag{3.179}$$

where the functions p_0, b and c are determined by the model of disorder, and

$$\Gamma(s,x) = \int_x^{+\infty} t^{s-1}\mathrm{e}^{-t}\mathrm{d}t \tag{3.180}$$

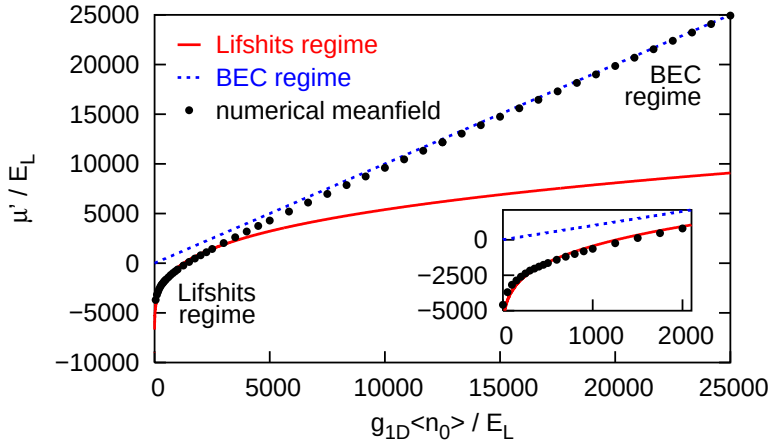


Figure 3.9: Chemical potential of a Bose gas in a speckle potential with the same parameters as in Fig. 3.8, in the case of tight radial confinement ($\mu' - E_\nu \ll \hbar\omega_\perp$). The black dots are obtained from the numerical resolution of a 1D Gross-Pitaevskii equation. The limiting form of the equation of state in the Lifshits regime (solid red line) is given by Eq. (3.179). The asymptote $\mu' \simeq g_{1D}\langle n_0^{1D}\rangle$ for the BEC regime (blue dotted line) appears here without inclusion of the leading order correction (3.74), which has been studied in Fig. 3.4.

is the incomplete gamma function. For speckle potentials, we have $v_{\min} = -1$. As $\Gamma(s,x) \sim x^{s-1}\mathrm{e}^{-x}$ for $x \to +\infty$, it is easily checked that in the limit $\mu' \to V_{\min}^+$, the product $g_{1D}\langle n_0^{1D}\rangle$ itself follows a stretched exponential with the same exponent $-\beta$ as the cumulative density of states.

Figure 3.9 shows the result of numerical computations of the chemical potential as a function of the interaction strength, for a speckle potential in the regime of tight trapping. The data was obtained by solving the GPE in a 1D box through propagation in imaginary time. The same disorder sample was used as in Fig. 3.8, and the parameters $p_0(\alpha_R)$, $b(\alpha_R)$, and $c(\alpha_R)$ were extracted from the latter study assuming $\beta = 1/2$. These parameters were plugged into the equation of state (3.179), represented by the red asymptote in Fig. 3.9. The crossover between the Lifshits and BEC regimes is clearly visible, and the chemical potential obtained numerically agrees well with formula (3.179) in the Lifshits regime.

Loose harmonic trapping

Let us now assume that the harmonic trapping is loose ($\mu' - V_{\min} \gg \hbar\omega_\perp$) so that for most populated Lifshits states

$$\mu' - E_\nu \gg \hbar\omega_\perp. \tag{3.181}$$

Then the radial density profile are inverted Thomas-Fermi parabolas

$$n_\nu^{2D}(\rho) \simeq \begin{cases} \frac{P_\nu}{g}(\mu - E_\nu)(1 - \rho^2/R_\nu^2) & \text{if } \rho < R_\nu \\ 0 & \text{otherwise} \end{cases} \tag{3.182}$$

with

$$R_\nu = \sqrt{\frac{2(\mu - E_\nu)}{m\omega_\perp^2}}, \tag{3.183}$$

and the populations are

$$N_\nu \simeq \begin{cases} \frac{\pi P_\nu (\mu - E_\nu)^2}{gm\omega_\perp^2} & \text{if } \mu > E_\nu \\ 0 & \text{otherwise} \end{cases} . \tag{3.184}$$

The linear density follows as

$$\langle n_0^{\rm 1D} \rangle \simeq \int_{V_{\rm min}}^{\mu} {\rm d}E \mathcal{D}(E) \bar{P}(E) \frac{\pi}{gm\omega_\perp^2} (\mu - E)^2. \tag{3.185}$$

An explicit expression is again readily derived under the assumption that $\bar{P}$ does not depend on the energy in the Lifshits tail.

3.5 Quantum state diagram

The results of sections 3.3 and 3.4 allow us to draw a schematic quantum-state diagram of the zero-temperature weakly-interacting Bose gas placed in 1D disorder, as a function of the chemical potential μ and the disorder strength $V_{\rm R}$.[36] Such a diagram is displayed in Fig. 3.10. Below, we recapitulate the various quantum states, and derive equations for the crossover boundaries which appear in Fig. 3.10.

We have in this chapter explicitly taken account of the possibility and consequences of a non-zero disorder correlation length $\sigma_{\rm R}$. It should be stressed that the cut through parameter space in Fig. 3.10 is performed at constant $\alpha_{\rm R} = E_\sigma / V_{\rm R}$, where $E_\sigma = \hbar^2 / 2m\sigma_{\rm R}^2$. Therefore, when $V_{\rm R}$ varies in the figure, the correlation length $\sigma_{\rm R}$ changes along too. This representation is motivated by the fact that, upon adequate rescaling, the properties of the single-particle problem depend on a single parameter ($\alpha_{\rm R}$) instead of two ($V_{\rm R}$ and $\sigma_{\rm R}$). Keeping $\sigma_{\rm R}$ fixed in diagram 3.10 would require the explicit knowledge of the properties of the single-particle problem on $\alpha_{\rm R}$. Our result is here general, and applies to any random potential which is bounded below.

The chemical potential μ is related to the average interaction term $g_{\rm 1D} \langle n_0^{\rm 1D} \rangle$ by the equation of state, which is illustrated in Fig. 3.9, and for which we have derived asymptotic forms in the various regimes [see Eqs. (3.74) and (3.175)]. Through this equation of state, Fig. 3.10 translates into a quantum state diagram as a function of disorder amplitude $V_{\rm R}$ and interaction strength $g_{\rm 1D} \langle n_0^{\rm 1D} \rangle$. The shape of the crossover boundaries will, of course, be modified when trading μ for $g_{\rm 1D} \langle n_0^{\rm 1D} \rangle$.

Experimentally, the value of the mean-field interaction term $g_{\rm 1D} \langle n_0^{\rm 1D} \rangle$ can be changed by adjusting the density of the Bose gas [26, 29, 183], or by tuning the scattering length a_s in Eq. (3.5) with so-called Feshbach resonances.[37]

3.5.1 Quantum states

Let us summarize here the findings of the previous sections.

[36] For the sake of simplicity, we set here $\mu = \mu'$. It turns out that, in the framework of our study, the identified quantum states and their boundaries in the quantum state diagram arise essentially from the characteristics of the 1D problem on the z-axis, and depend very little on the radial degrees of freedom. In the discussion of the crossover boundaries below, we refer to the results of the previous sections, where the radial degrees of freedom were examined explicitly.

[37] See Ref. [17] and references therein.

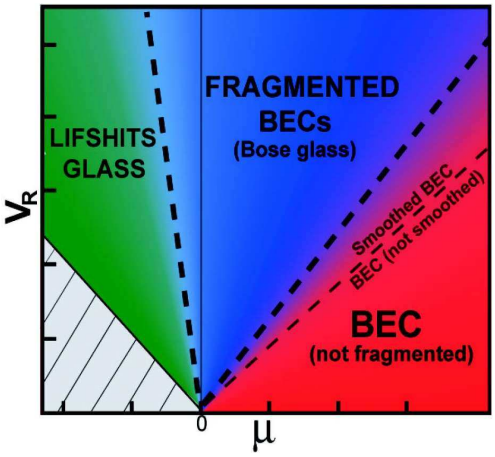


Figure 3.10: Schematic ground-state quantum-state diagram of a weakly repulsive Bose gas in 1D disorder. The variable $V_{\rm R}$ denotes the root-mean-square amplitude of the disorder, and μ is the chemical potential of the Bose gas. Interactions therefore increase from left to right in the diagram. The boundaries in the diagram (corresponding to crossovers) are controlled by the parameter $\alpha_{\rm R} = \hbar^2/2m\sigma_{\rm R}^2 V_{\rm R}$, where $\sigma_{\rm R}$ is the correlation length of the random potential. The parameter $\alpha_{\rm R}$ is kept constant as μ and $V_{\rm R}$ vary in the figure. The random potential is assumed to have a lower bound $V_{\rm min}$, and the hatched part corresponds to the unphysical case $\mu < V_{\rm min}$.

For strong mean-field interactions (large chemical potential μ) or weak disorder, the Bose gas forms a delocalized (quasi-) BEC whose density profile follows almost exactly the modulations of the random potential. This regime appears in red in Fig. 3.10, under the label **BEC**. When the strength of disorder $V_{\rm R}$ increases or μ decreases, the relative fluctuations of the density profile generally grow. Due to a larger healing length, however, this growth is possibly affected by the smoothing of the short length-scale fluctuations. In that case, the BEC is said to be smoothed to distinguish it from the Thomas-Fermi regime.

For stronger disorder or weaker interactions, the Bose gas eventually fragments, that is, breaks up into localized islands with negligible tunneling. Each of these islands might retain superfluid properties and be compressible, but the entire system is expected to be an insulator. As such, the regime which appears in blue under the label of **fragmented BECs** can be identified with a Bose glass [128]. We derive below an equation for the boundary between the BEC and the fragmented BEC regime which is based on a fragmentation criterion for the ground-state density profile. This criterion is developed at the level of the linear response (first-order perturbation theory) of the density profile to the external potential, and determines the locus of a crossover region between regimes where the density is weakly or strongly affected by the random potential.

For even weaker interactions, the fragments are well separated and their shape is mostly determined by the variations of the random potential. In particular, when the chemical potential drops below the average of the potential and enters the Lifshits tail of the single-particle spectrum, close to the minimum value $V_{\rm min}$, a description in terms of Lifshits states applies. In this limiting regime, shown in green under the label of **Lifshits glass**, the bosons populate strongly localized single-particle orbitals, the longitudinal shape of which remains unaffected

by interactions. As the fragmented Bose gas is expected to turn continuously into a Lifshits glass, the boundary between the two regime corresponds to a crossover.

3.5.2 Crossover boundaries

Building on the results of the previous sections, we now briefly discuss the crossover boundaries. Recall that diagram 3.10 is drawn for constant $\alpha_{\rm R} = E_\sigma/V_{\rm R}$.

Lifshits glass to fragmented BEC - In section 3.4.3, the description of the disordered Bose gas in terms of a Lifshits glass was shown to cover the parameter space

$$\mu \leq V_{\rm R} F(\alpha_{\rm R}) \qquad \text{[Lifshits glass]}, \tag{3.186}$$

where F is a function which accounts for the properties of both the density of states and the eigenfunctions in the Lifshits tail of the single-particle problem (3.151), and which depends only on the model of disorder. In diagram 3.10, this defines a straight boundary, the slope of which is set by the dependence of F on $\alpha_{\rm R}$.

Thomas-Fermi BEC to smoothed BEC - On the delocalized BEC side, the condition for a Thomas-Fermi profile and the absence of smoothing was discussed around Eqs. (3.50), (3.71) and (3.114), and worked out to be $\xi \ll \sigma_{\rm R}$ or, equivalently, $\mu \gg E_\sigma = \alpha_{\rm R} V_{\rm R}$. Conversely, smoothing occurs for

$$\mu \lesssim \alpha_{\rm R} V_{\rm R} \qquad \text{[smoothed BEC]}, \tag{3.187}$$

which defines another straight boundary.

BEC to fragmented BEC - From Eqs. (3.73), (3.103) or (3.121), we recall that a weak perturbation of the density profile in the BEC regime requires $\mu \gg \widetilde{V}_{\rm R}^{(1)}$, where $\widetilde{V}_{\rm R}^{(1)} = V_{\rm R}\sqrt{I_2(\xi/\sigma_{\rm R})}$ is the amplitude of the smoothed potential, evaluated at first order, and $\xi/\sigma_{\rm R} = \sqrt{\alpha_{\rm R} V_{\rm R}/\mu}$. The function I_2 is defined by

$$I_2\left(\frac{\xi}{\sigma_{\rm R}}\right) = \frac{\sigma_{\rm R}}{\sqrt{2\pi}} \int {\rm d}q \frac{\hat{c}_2(q\sigma_{\rm R})}{[1+(q\xi)^2]^2} \tag{3.188}$$

in 1D. Fragmentation, on the other hand, occurs for a strong perturbation around the homogeneous density profile. We may say that fragmentation of the density profile occurs when the relative (r.m.s.) amplitude of density modulations exceed a certain threshold t, i.e. when $t \leq \widetilde{V}_{\rm R}/\mu$. At the level of the first-order approximation $\widetilde{V}_{\rm R} \simeq \widetilde{V}_{\rm R}^{(1)}$, this criterion rewrites

$$t \leq \frac{V_{\rm R}}{\mu}\sqrt{I_2\left(\sqrt{\alpha_{\rm R}\frac{V_{\rm R}}{\mu}}\right)} \qquad \text{[fragmented BEC]}. \tag{3.189}$$

Since the inequality is saturated for $(V_{\rm R}, \mu)$ pairs with constant $V_{\rm R}/\mu$ ratio, we obtain a straight boundary as well. While the first-order estimate $\widetilde{V}_{\rm R}^{(1)}$ is accurate for small values of the threshold t ($t \ll 1$), higher-order terms in the perturbation expansion of the density are in principle required for a quantitative study when the perturbation of the density profile is strong. However, the scaling analysis outlined in the next section shows that the above conclusions remain qualitatively unchanged for stronger disorder, as far as the density profile is concerned.

Fragmentation with and without smoothing - If we start from the Thomas-Fermi BEC sector of the quantum state diagram 3.10, i.e. from a regime where the chemical potential by far exceeds the amplitude $V_{\rm R}$ and the "correlation energy" $E_\sigma = \hbar^2/2m\sigma_{\rm R}^2 = \alpha_{\rm R} V_{\rm R}$ of the random potential, and if we keep $V_{\rm R}$ and $\alpha_{\rm R}$ fixed, and start reducing the chemical potential, two effects occur. On the one hand, smoothing arises when the healing length $\xi = \hbar/\sqrt{2m\mu}$ exceeds $\sigma_{\rm R}$ (and the imprint of the random potential on the density profile is then somewhat reduced). On the other hand, fragmentation occurs when the strength of the potential becomes strong compared to the chemical potential. The onset of these two effects is described by Eqs. (3.189) and (3.187). The slopes determined by these equations allow for two scenarios. In the first case, which is depicted in the quantum state diagram 3.10, smoothing is significant before fragmentation occurs. In the second case, the fragmentation threshold is reached before smoothing becomes significant. Let us check for which parameters these scenarios are possible.

Smoothing We assume $1 \ll \alpha_{\rm R} V_{\rm R}/\mu$, so that smoothing is significant. Then, using expansion (3.72), the fragmentation criterion (3.189) writes

$$t \lesssim \alpha_{\rm R}^{-1/4} \left(\frac{V_{\rm R}}{\mu}\right)^{3/4} \left[2^{-1/2}\Gamma(3/2)\hat{c}_2(0)\right]^{1/2}. \tag{3.190}$$

For simplicity, we set t and the factor between square brackets to one. Then, fragmentation with smoothing occurs for

$$\frac{V_{\rm R}}{\mu} \gg \frac{1}{\alpha_{\rm R}} \qquad \text{and} \qquad \frac{V_{\rm R}}{\mu} \gtrsim \alpha_{\rm R}^{1/3}. \tag{3.191}$$

These two conditions are compatible and satisfied e.g. for $V_{\rm R}/\mu \gtrsim \alpha_{\rm R}^{1/3}$ when $\alpha_{\rm R} \gg 1$. The ensemble of $(V_{\rm R}/\mu, \alpha_{\rm R})$ pairs which satisfy (3.191) is represented by a light blue sector in Fig. 3.11.

No smoothing We assume $\alpha_{\rm R} V_{\rm R}/\mu \ll 1$, so that smoothing is negligible. This allows us to use expansion (3.71) and to rewrite the fragmentation criterion as

$$t \lesssim \frac{V_{\rm R}}{\mu}\left[1 - \frac{\alpha_{\rm R} V_{\rm R}}{\mu\sqrt{2\pi}} \int {\rm d}\kappa\, \kappa^2 \hat{c}_2(\kappa)\right] \simeq \frac{V_{\rm R}}{\mu}. \tag{3.192}$$

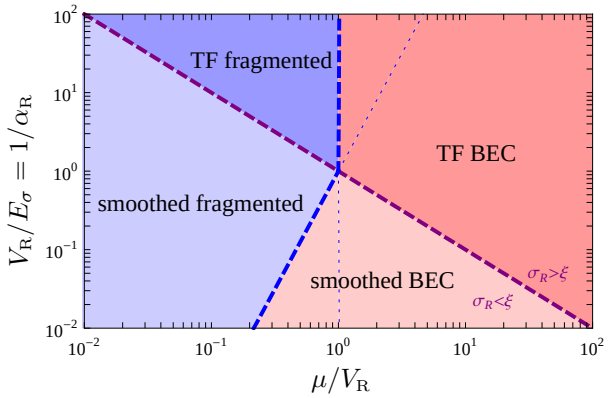
Setting $t = 1$, fragmentation without smoothing is seen to occur for

$$\frac{V_{\rm R}}{\mu} \ll \frac{1}{\alpha_{\rm R}} \qquad \text{and} \qquad \frac{V_{\rm R}}{\mu} \geq 1. \tag{3.193}$$

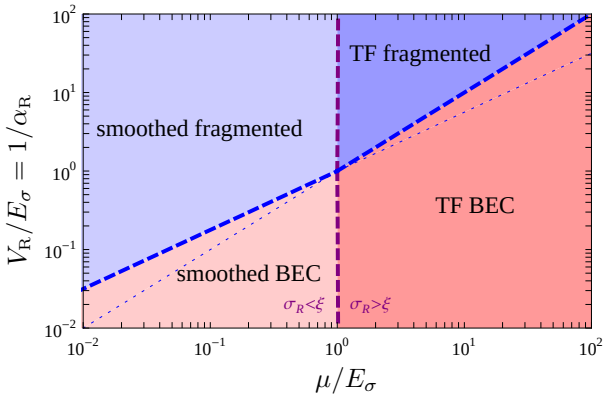
These conditions are compatible only for $\alpha_{\rm R} \ll 1$, that is, $\hbar^2/2m\sigma_{\rm R}^2 \ll V_{\rm R}$. This corresponds to potentials with large or long-length-scale variations, as expected. The range of parameters for which fragmentation occurs without smoothing is shown as a dark blue sector in Fig. 3.11.

Remark With the definition $\alpha_{\rm R} = E_\sigma/V_{\rm R}$, the criterion (3.190) for a fragmentation of the Bose gas *in the presence of smoothing* is rewritten

$$t \lesssim \frac{V_{\rm R}}{\mu^{3/4} E_\sigma^{1/4}} \left[2^{-1/2}\Gamma(3/2)\hat{c}_2(0)\right]^{1/2}. \tag{3.194}$$



(a) Slopes: -1, 3, ∞



(b) Slopes: 3/4, 1, ∞

Figure 3.11: Schematic characterization of the density profile of a disordered, weakly-repulsive Bose gas at the crossover between the regimes of (quasi-)BEC and fragmented BEC. The ground-state density profile is characterized in terms of smoothing and fragmentation, as a function of the chemical potential μ, the disorder amplitude V_R, and the energy $E_\sigma = \hbar^2/2m\sigma_R^2$ associated with the correlation length σ_R of the random potential. The boundaries (thick dashed lines) are defined by Eqs. (3.191) and (3.193). The thin dotted lines serve as guide for the eye. The difference between (a) and (b) lies in the rescaled energies chosen as coordinates. In each case, $V_R/E_\sigma = 1/\alpha_R$ is used for the vertical axis, so that a path in the quantum state diagram 3.10 corresponds to a horizontal line in both (a) and (b). The Bose gas may start crossing over to the Lifshits glass regime (not depicted here) for the lowest values of μ.

If $E_\sigma = \hbar^2/2m\sigma_R^2$ is kept constant instead of α_R when V_R and μ are left to change, this defines a boundary

$$\frac{V_R}{E_\sigma} \propto \left(\frac{\mu}{E_\sigma}\right)^{3/4}, \tag{3.195}$$

as shown in the lower left corner of Fig. 3.11(b). This result is strikingly similar to the relation $(V_R/E_\sigma) \propto (U/E_\sigma)^{0.75\pm0.03}$ found by Fontanesi *et al.* in their recent numerical study of the 1D superfluid-to-Bose-glass transition, reported in Ref. [244]. In the latter expression, U is the mean-field interaction energy. Most numerical calculations in this study have been performed for $V_R/E_\sigma \leq 1$ or, equivalently, $\alpha_R \geq 1$, i.e. a regime where smoothing is significant at the crossover from BEC to fragmented BEC. Fontanesi *et al.* observed that the exponential decay of first-order correlation functions in the Bose-glass phase was due to sudden drops and attributed the latter to the presence of "weak links" in the Bose gas. On the superfluid side, on the other hand, a rather smooth power-law decay of the first-order correlation functions was found. It would be interesting to investigate whether the (fragmentation) statistics of the ground-state density profile, as presented in this chapter, can be related to the statistics of such weak links and to the transition from power-law to exponential decay of correlation functions, as suggested by the similarity of relation (3.195) with the numerical findings of Ref. [244]. In this respect, it might be worth emphasizing that the perturbation expansions which form the basis of our analysis in the BEC regime can be carried out at fixed $g\langle n_0\rangle$ and $\bar{\xi} = \hbar/\sqrt{4mg\langle n_0\rangle}$, instead of fixed μ and $\xi = \hbar/\sqrt{4m\mu}$, as shown in appendix E. In particular, at the level of the first-order perturbation theory, μ can simply be replaced by $g\langle n_0\rangle$ in the formulas.

3.5.3 Scaling

The boundaries derived above follow from the results of section 3.3.4, where radial degrees of freedom were analyzed carefully. It turns out that identical conditions are obtained by reducing the problem of weakly-interacting bosons to the longitudinal z-axis. The boundary of the Lifshits glass regime was obtained by considering a rescaled form of a 1D Schrödinger equation. In the delocalized BEC regime, the density profile is obtained from a 1D Gross-Pitaevskii equation, and it proves equally useful to write such a GPE in a form which allows for scaling arguments. Defining

$$u = z/\sigma_{\mathrm{R}} \tag{3.196}$$
$$v(u) = V(z)/V_{\mathrm{R}} \tag{3.197}$$
$$\varrho(u) = n_0^{\mathrm{1D}}(z)/\langle n_0^{\mathrm{1D}}\rangle, \tag{3.198}$$

we obtain

$$\left[-\frac{\mathrm{d}^2}{\mathrm{d}u^2} + \frac{V_{\mathrm{R}}}{E_\sigma}v(u) + \frac{g_{\mathrm{1D}}\langle n_0^{\mathrm{1D}}\rangle}{E_\sigma}\varrho(u) - \frac{\mu}{E_\sigma}\right]\sqrt{\varrho(u)} = 0 \tag{3.199}$$

or, equivalently,

$$\left[-\alpha_{\mathrm{R}}\frac{\mathrm{d}^2}{\mathrm{d}u^2} + v(u) + \frac{g_{\mathrm{1D}}\langle n_0^{\mathrm{1D}}\rangle}{V_{\mathrm{R}}}\varrho(u) - \frac{\mu}{V_{\mathrm{R}}}\right]\sqrt{\varrho(u)} = 0. \tag{3.200}$$

The comparison of the first and last terms in the brackets, in particular, immediately provides the inequalities which define the Thomas-Fermi and the smoothed BEC regime [see expression (3.187)]. Equation (3.200) also shows that, for a constant α_{R}, the ratio V_{R}/μ uniquely determines the rescaled ground-state density ϱ, the average density $\langle n_0^{\mathrm{1D}}\rangle$ and, thereby, the relative modulations of the density profile. As a consequence, the boundary derived for the crossover to the fragmented regime is expected to remain straight even beyond the first-order perturbation expansion, for any fragmentation threshold t or any refined criterion based on the *statistics* of the density modulations.

Let us finish with a couple of remarks on the latter boundary. We wish to stress here that the scaling arguments developed above define the location of a crossover between two regimes of weak and strong fluctuations of the mean-field density profile (the quasi-BEC and fragmented BEC regimes, respectively). On the other hand, the route from the quasi-BEC regime to the Bose glass in the weakly-interacting regime is expected to involve a transition [244, 289], characterized e.g. by an abrupt change in correlation functions or response functions at critical disorder or interaction strengths. Whether a crossover boundary predicted on the basis of mean-field features of the condensate overlaps with the transition boundary, and follows a similar scaling, remains an interesting question.

Strictly speaking, fragmentation is never complete, but a Bose glass is expected to form when tunneling between the fragments is significantly reduced. This requires e.g. the upper limit t used above to be of the order of one, rather than infinitly small, and takes the mean-field approach beyond the first-order perturbation theory. The arguments developed above show that for fixed α_{R}, the statistics of the relative density modulations depend only on the ratio of V_{R} and μ, even deeply in the non-linear regime. Nevertheless, it would be interesting to determine whether other scaling laws can be worked out when the correlation length σ_{R} is kept fixed, and $\alpha_{\mathrm{R}} = E_\sigma/V_{\mathrm{R}}$ varies, or when V_{R} is plotted against the mean-field interaction energy $g_{\mathrm{1D}}\langle n_0^{\mathrm{1D}}\rangle$.

3.6 Conclusion

In this chapter we examined the ground-state properties of a weakly-interacting Bose gas in one-dimensional, correlated disorder. We discussed the quantum states resulting from the competition of the disorder and interactions, and derived analytical boundaries for the crossovers between the various regimes.

In the delocalized BEC regime found for dominating mean-field interactions, we described in detail the response of the density profile to the external potential. We discussed the impact of both the strength of disorder and its correlation length on the amplitude of the modulations imposed on the BEC density profile.

The insulating phase found for dominating disorder was approached from the non-interacting limit, and a novel description was given for the regime of very weak interactions. In this regime called Lifshits glass, the bosons were shown to populate strongly localized, spatially well separated single-particle states. A smooth crossover from this picture to the regime of fragmented BEC (or Bose glass) was argued to occur with increasing interactions as more of such states become populated and develop overlaps.

The deterministic density modulations imprinted on the density profile by the disorder in the BEC regime have been observed experimentally [171]. As now both random potentials and Feshbach resonances to tune the interactions are available on some experimental set-ups [30], the regime of very weak interactions might hopefully also be explored soon.

CHAPTER 4

Elementary excitations of disordered weakly-interacting Bose gases

In chapter 3 we examined the ground-state properties of weakly-interacting Bose gases in a 1D random potential. For weak disorder, or moderate interactions exceeding the disorder strength, the density profile of the Bose gas is extended due to the non-linearity introduced by interactions at the mean-field level. Deep in this regime the density profile is only weakly affected by the presence of the external potential and, if the density is everywhere sufficient, the Bose gas is expected to form a single Bose-Einstein condensate (or a quasi-BEC in 1D or elongated 3D Bose gases).

We now turn to the elementary excitations of the disordered Bose gas in the BEC regime. The elementary excitations we study here are small fluctuations around the ground state of the system, and take the form of quasi-particles. A description of these quasi-particles is given by the Bogolyubov theory, applied to the case of weakly-interacting spinless bosons [159]. This description goes one step beyond mean field, and takes account of correlations introduced by interactions between the particles.

At non-zero temperature, the quasi-particle modes are populated thermally, and determine the properties of the Bose gas well below the critical condensation temperature. Interestingly, however, these modes also describe the correlation and response functions of the ground state and the quantum fluctuations around the mean-field at zero temperature. Their study is therefore essential to characterize the interacting many-body state. On the one hand, the spectrum of excitations is strongly linked with macroscopic quantities like the velocity of sound [290] and superfluid properties, as emphasized by Landau's criterion for superfluidity [111, 249, 291, 292]. On the other hand, the density of states and the wave functions of the quasi-particles essentially determine the correlation functions of the Bose gas, phase coherence and long-range order [244, 256]. It is of prime importance to determine how disorder affects these quantities.

In this chapter we develop an analytical approach to describe the scattering and localization of Bogolyubov quasi-particles (BQPs) in weak, correlated random potentials. The weakness of disorder allows the set-up of a systematic perturbation expansion. We show that in the leading orders, the equations governing the Bogolyubov quasi-particles map approximately onto a Schrödinger-like problem. This is achieved by introducing a transformation which decouples some small and fast degrees of freedom from relevant ones, while covering the whole range of BQP excitation energies. The scattering and localization of Bogolyubov quasi-particles can then be described by applying results known for the non-interacting case.

The chapter is organized as follows. In section 4.1 we briefly run through the Bogolyubov theory for weakly-interacting Bose gases to set up the Boglyubov-de Gennes equations (BdGEs) which govern the elementary excitations. In section 4.2 we develop a perturbation expansion and show that in the leading orders the BdGEs can be solved by means of a Schrödinger-like

equation which accounts for the scattering properties of the BQPs. In section 4.3 we adapt the technique of chapter 2 and derive the Lyapunov exponent of BQPs in a one-dimensional geometry. In section 4.4, we discuss higher-order perturbation terms and their possible relevance for the limit of vanishingly small quasi-particle energy.

4.1 Bogolyubov quasi-particles

Here we give a brief presentation of the Bogolyubov theory of elementary excitations in the condensed phase of weakly-interacting bosons. For the sake of simplicity and following the original prescription by Bogolyubov, the derivation presented below is formulated in the grand-canonical ensemble, and the condensate wave function is assumed to have a well-defined phase (see the discussion of sections 3.2.1 and 3.3.1). The many-body system is described by the grand-canonical Hamiltonian

$$\hat{K} = \int \mathrm{d}\mathbf{r} \left\{ \hat{\Psi}^\dagger(\mathbf{r}) \left[-\frac{\hbar^2\nabla^2}{2m} + V(\mathbf{r}) - \mu \right] \hat{\Psi}(\mathbf{r}) + \frac{g}{2} \hat{\Psi}^\dagger(\mathbf{r}) \hat{\Psi}^\dagger(\mathbf{r}) \hat{\Psi}(\mathbf{r}) \hat{\Psi}(\mathbf{r}) \right\}, \tag{4.1}$$

where m is the mass of the bosons, V is the external potential, μ is the chemical potential, and $g > 0$ is the coupling constant of the two-body interaction potential $V_{\mathrm{int}}(\mathbf{r} - \mathbf{r}') = g\delta(\mathbf{r} - \mathbf{r}')$. Assuming that most atoms are condensed in a unique single-particle state ψ_0 (normalized to unity), the field operator is expanded as

$$\hat{\Psi}(\mathbf{r}) = \Psi_0(\mathbf{r}) + \delta\hat{\Psi}(\mathbf{r}), \tag{4.2}$$

with

$$\Psi_0(\mathbf{r}) = \sqrt{N_0}\,\psi_0(\mathbf{r}), \tag{4.3}$$

where ψ_0 is the condensate wave function, N_0 is the population of the condensate, and $\delta\hat{\Psi}$ is a small fluctuation field such that

$$\|\delta\hat{\Psi}(\mathbf{r})\| \ll \Psi_0(\mathbf{r}). \tag{4.4}$$

The quantum field $\delta\hat{\Psi}$ describes non-condensed particles, which can be created when the system is excited out of the ground state (e.g. at non-zero temperatures or under the effect of an external perturbation), but also exist in the ground state of the system due to the presence of interactions (this effect, which is called *quantum* depletion of the condensate, plays a marginal role for weakly-interacting gases, and is neglected here). Bogolyubov's approach assumes that such a depletion of the condensate, whether thermal or quantum, is small.

Bogolyubov's theory in its original form is often recognized as the best simple approximate theory which successfully describes essential features of the Bose-condensed system, e.g. a gapless excitation spectrum which is linear at low energy, and the slope of which coincides with the macroscopic velocity of sound [248, 293]. Some consequences and limitations of approximation (4.4) have been addressed and refined theories have been developed e.g. in Refs. [256, 293–296]. In particular, the isolation of a condensate wave function ψ_0 with well-defined phase makes *a priori* little sense in low-dimensional geometries, where phase fluctuations are known to be important. For such geometries, a phase-density representation of the field operators in the form

$$\hat{\Psi}(\mathbf{r}) = \mathrm{e}^{\mathrm{i}\hat{\theta}(\mathbf{r})}\sqrt{\hat{n}(\mathbf{r})}, \qquad \hat{\Psi}^\dagger(\mathbf{r}) = \sqrt{\hat{n}(\mathbf{r})}\mathrm{e}^{-\mathrm{i}\hat{\theta}(\mathbf{r})} \tag{4.5}$$

is preferred, and the perturbation expansion is carried out around a classical *density* field n_0, without reference to a privileged phase [251, 252, 256, 264, 297, 298]. The reformulation of the Bogolyubov theory in the phase-density picture is presented in section 4.1.2.

4.1.1 Bogolyubov theory in the symmetry-breaking approach

We review here the results obtained when the field operators are expanded around a classical field Ψ_0 with well-defined phase.

Perturbation expansion of the Hamiltonian

To find the ground state and excitations of the Bose gas, Hamiltonian (4.1) is expanded as

$$\hat{K} = \hat{K}_0 + \hat{K}_1 + \hat{K}_2 + \hat{K}_3 + \hat{K}_4, \tag{4.6}$$

where the subscripts indicate increasing powers of the small parameter $\|\delta\hat{\Psi}\|/\Psi_0$. These various orders read

$$\hat{K}_0 = \int \mathrm{d}\mathbf{r} \left\{ \Psi_0^*(\mathbf{r}) \mathcal{L}_\mu \Psi_0(\mathbf{r}) + \frac{g}{2}|\Psi_0|^4 \right\} \tag{4.7}$$

$$\hat{K}_1 = \int \mathrm{d}\mathbf{r} \left\{ \delta\hat{\Psi}^\dagger \left[\mathcal{L}_\mu + g|\Psi_0|^2\right] \Psi_0 + \delta\hat{\Psi} \left[\mathcal{L}_\mu + g|\Psi_0|^2\right] \Psi_0^* \right\} \tag{4.8}$$

$$\hat{K}_2 = \int \mathrm{d}\mathbf{r} \left\{ \delta\hat{\Psi}^\dagger \left[\mathcal{L}_\mu + 2g|\Psi_0|^2\right] \delta\hat{\Psi} + \frac{g}{2} \left[\Psi_0^2 \delta\hat{\Psi}^{\dagger 2} + \Psi_0^{*2} \delta\hat{\Psi}^2 \right] \right\} \tag{4.9}$$

$$\hat{K}_3 = \int \mathrm{d}\mathbf{r} \left\{ g \left[\Psi_0^* \delta\hat{\Psi}^\dagger \delta\hat{\Psi}^2 + \Psi_0 \delta\hat{\Psi}^{\dagger 2} \delta\hat{\Psi} \right] \right\} \tag{4.10}$$

$$\hat{K}_4 = \int \mathrm{d}\mathbf{r} \, \frac{g}{2} \delta\hat{\Psi}^{\dagger 2} \delta\hat{\Psi}^2, \tag{4.11}$$

where $\mathcal{L}_\mu$ is the operator

$$\mathcal{L}_\mu = -\frac{\hbar^2\nabla^2}{2m} + V - \mu. \tag{4.12}$$

The operators $\delta\hat{\Psi}$ and $\delta\hat{\Psi}^\dagger$ satisfy the same bosonic commutation relations as $\hat{\Psi}$ and $\hat{\Psi}^\dagger$:

$$[\delta\hat{\Psi}(\mathbf{r}), \delta\hat{\Psi}^\dagger(\mathbf{r}')] = \delta(\mathbf{r}-\mathbf{r}'), \qquad [\delta\hat{\Psi}, \delta\hat{\Psi}] = 0, \qquad [\delta\hat{\Psi}^\dagger, \delta\hat{\Psi}^\dagger] = 0. \tag{4.13}$$

Mean field

In the ground state, the classical field $\Psi_0(\mathbf{r})$ is required to minimize $\hat{K}_0 = K[\Psi_0]$. This condition yields the Gross-Pitaevskii equation (GPE)

$$\left[\mathcal{L}_\mu + g|\Psi_0|^2\right] \Psi_0 = 0, \tag{4.14}$$

which is parametrized by the chemical potential μ. If several solutions coexist for a given μ, the ground state is found as the solution minimizing $H[\Psi_0]$, where

$$H[\Psi_0] = \int \mathrm{d}\mathbf{r} \left\{ \Psi_0^*(\mathbf{r}) \left[-\frac{\hbar^2\nabla^2}{2m} + V(\mathbf{r}) \right] \Psi_0(\mathbf{r}) + \frac{g}{2}|\Psi_0|^4 \right\}. \tag{4.15}$$

We assume that this ground state solution is unique [273]. Then, the number of particles in the condensate $N_0 = \int \mathrm{d}\mathbf{r}|\Psi_0|^2$ uniquely depends on the chemical potential μ, and vice versa. For weak interactions, we have $N_0 \simeq N$, where N is the (average) number of atoms in the system. The equation of state, which relates the chemical potential to the average density or number of particles in the system, is therefore determined with reasonable accuracy by the solution of the Gross-Pitaevskii equation.[1]

Bogolyubov Hamiltonian

Since Ψ_0 solves the GPE (4.14), the first-order term $\hat{K}_1$ vanishes ($[\mathcal{L}_\mu + g|\Psi_0|^2]\Psi_0 = 0$). The third- and fourth-order terms are usually discarded as small corrections, so that the approximate Hamiltonian reads

$$\hat{K} \simeq K_0[\Psi_0] + \hat{K}_2. \tag{4.16}$$

Here $K_0[\Psi_0]$ appears as an offset which does not involve the quantum fields $\delta\hat{\Psi}$ and $\delta\hat{\Psi}^\dagger$, and hence does not contribute to the fluctuations around the classical field. Let us reproduce $\hat{K}_2$ for clarity:

$$\hat{K}_2 = \int \mathrm{d}\mathbf{r} \left\{ \delta\hat{\Psi}^\dagger \left[\mathcal{L}_\mu + 2g|\Psi_0|^2\right] \delta\hat{\Psi} + \frac{g}{2}\left[\Psi_0^2 \delta\hat{\Psi}^{\dagger 2} + \Psi_0^{*2}\delta\hat{\Psi}^2\right]\right\}. \tag{4.17}$$

This Hamiltonian forms the starting point for the analysis of the quantum fluctuations and excitations of the weakly-interacting Bose gas around the mean field Ψ_0. Its form is close to the Hamiltonian used to describe excitations around the pairing mean field in the BCS theory [300].

Canonical transformations and equations of motion

Hamiltonian $\hat{K}_2$ is often said to be "solved" by a simple canonical transformation. Let us illustrate this concept. As $\hat{K}_2$ is a Hermitian quadratic "form" of $\delta\hat{\Psi}$ and $\delta\hat{\Psi}^\dagger$, one expects to be able to bring it into a more compact form

$$\sum_\nu \epsilon_\nu \hat{b}_\nu^\dagger \hat{b}_\nu \tag{4.18}$$

by means of a suitable transformation. Because of the square terms $\delta\hat{\Psi}^2$ and $\delta\hat{\Psi}^{\dagger 2}$ in $\hat{K}_2$, the operator $\hat{b}_\nu$ should have the general form

$$\hat{b}_\nu = \int \mathrm{d}\mathbf{r} \left[\alpha_\nu(\mathbf{r})\delta\hat{\Psi}(\mathbf{r}) + \beta_\nu(\mathbf{r})\delta\hat{\Psi}^\dagger(\mathbf{r})\right], \tag{4.19}$$

and $\hat{b}_\nu^\dagger$ should follow as its Hermitian conjugate. The product of this transformation, $\hat{b}_\nu^\dagger$ and $\hat{b}_\nu$, are operators acting on the Fock basis. If they satisfy canonical commutation relations of the form

$$[\hat{b}_\nu, \hat{b}_{\nu'}^\dagger]_\eta = \delta_{\nu,\nu'}, \qquad [\hat{b}_\nu, \hat{b}_{\nu'}]_\eta = 0, \tag{4.20}$$

with $[\hat{b}_\nu, \hat{b}_{\nu'}^\dagger]_\eta \equiv \hat{b}_\nu \hat{b}_{\nu'}^\dagger - \eta \hat{b}_{\nu'}^\dagger \hat{b}_\nu$ and $\eta = \pm 1$, then $\hat{b}_\nu^\dagger$ and $\hat{b}_\nu$ are identified as the usual creation and annihilation operators, which are here seen to create or destroy an excitation of energy ϵ_ν from

[1] The first corrections to the equation of state given by the Gross-Pitaevskii equation arise with $\hat{K}_2$, and can be evaluated within the Bogolyubov theory. See e.g. Refs. [256, 299].

an excitation vacuum. Since sum (4.18) takes the shape of a Hamiltonian without interactions, such excitations of the field $\hat{\Psi}$ resemble non-interacting particles. However, because of the mixing of the field operator and its Hermitian conjugate in expression (4.19), the excitations are, by definition, quasi-particles. If the relations (4.20) are satisfied with $\eta = +1$, the excitations are bosonic, and for $\eta = -1$ they are fermionic. In the present case, the quasi-particle excitations are expected to be bosonic.[2]

In Equation (4.23), the coefficients $\alpha_\nu(\mathbf{r}) \equiv \alpha_{\nu,\mathbf{r}}$ and $\beta_\nu(\mathbf{r}) \equiv \beta_{\nu,\mathbf{r}}$ are identified as the "matrix elements" of a transformation $\mathcal{T}$ from $(\delta\hat{\Psi}, \delta\hat{\Psi}^\dagger)^{\mathrm{T}}$ to $(\hat{b}, \hat{b}^\dagger)^{\mathrm{T}}$.[3] Such a transformation is said to be canonical if it preserves the commutation relations of the field operators, which here means that the $\hat{b}_\nu$ and $\hat{b}_\nu^\dagger$ should satisfy Eq. (4.20) with $\eta = +1$. A study of the generic properties of canonical transformations can be found in Ref. [301].

The "diagonalization" of the Bogolyubov Hamiltonian $\hat{K}_2$ appears as a standard result in the literature. The procedure commonly used are nevertheless manifold. A first approach directly resorts to canonical transformations to map the Bogolyubov Hamiltonian onto an equivalent representation in a basis of quasi-particles [301]. In a second approach, which does not anticipate on the success of a quasi-particle basis, equations of evolution are written down for the field operators $\delta\hat{\Psi}$ and $\delta\hat{\Psi}^\dagger$ in the Heisenberg picture, and eigenstates of the time-evolution operator are sought for [253,296]. These eigenstates, which correspond to the excitations of the Bose gas, are then used for a modal expansion of the field operators and the Bogolyubov Hamiltonian. As a variant of the latter approach, classical equations of motion may me considered for the bosonic field variables [256, 302, 303].

The various approaches follow close paths and yield identical results, which we summarize below.

Bogolyubov Hamiltonian in canonical form

The results reported below apply whenever Ψ_0 is a local minimum of the GPE (4.14) [253, 301, 303]. This is the case here, as we consider the ground-state solution. Then, as shown in particular in Refs. [253, 294, 301, 304], the Bogolyubov Hamiltonian $\hat{K}_2$ expands as

$$\hat{K}_2 = \tilde{K}_2 + \alpha\hat{P}^2 + \sum_\nu \epsilon_\nu \hat{b}_\nu^\dagger \hat{b}_\nu, \tag{4.21}$$

where $\tilde{K}_2$ and α are scalars which we do not detail here, and the quantities ϵ_ν are real and strictly positive. The operators $\hat{b}_\nu^\dagger$ and $\hat{b}_\nu$ satisfy bosonic commutation rules:

$$[\hat{b}_\nu, \hat{b}_{\nu'}^\dagger] = \delta_{\nu,\nu'}, \qquad [\hat{b}_\nu, \hat{b}_{\nu'}] = 0. \tag{4.22}$$

They are obtained from the field operators as[4]

$$\hat{b}_\nu = \int \mathrm{d}\mathbf{r} \left[u_\nu^*(\mathbf{r})\delta\hat{\Psi}(\mathbf{r}) - v_\nu^*(\mathbf{r})\delta\hat{\Psi}^\dagger(\mathbf{r}) \right] \tag{4.23}$$

[2] The bosonic nature of the excitations need not be *assumed*, and may *emerge* naturally from the analysis of the Bogolyubov Hamiltonian (see e.g. Ref. [296]).

[3] The sign T denotes transposition.

[4] Several sign conventions coexist in the literature. If $+v_\nu^*$ is used instead of $-v_\nu^*$ in Eq. (4.23), all the subsequent formulas in this chapter apply upon replacement of (u, v) by $(u, -v)$.

and its Hermitian conjugate. The last term in Eq. (4.21) is equivalent to a free Hamiltonian, and describes non-interacting quasi-particles. The excitations described by this part of the Hamiltonian are called Bogoyubov excitations, or Bogolyubov quasi-particles. The $\hat{P}^2$ term describes the motion of a collective variable associated the condensate mode, and does not represent an elementary excitation of the Bose gas (see below).

Bogolyubov-de Gennes equations

The functions u_ν and v_ν of transformation (4.23) are the solutions for $\epsilon_\nu > 0$ of the Bogolyubov-de Gennes equations (BdGEs) [159, 300, 305]

$$\left[-\frac{\hbar^2\nabla^2}{2m} + V(\mathbf{r}) - \mu + 2g|\Psi_0(\mathbf{r})|^2\right] u_\nu(\mathbf{r}) + g\Psi_0(\mathbf{r})^2 v_\nu(\mathbf{r}) = \epsilon_\nu u_\nu(\mathbf{r}) \tag{4.24}$$

$$\left[-\frac{\hbar^2\nabla^2}{2m} + V(\mathbf{r}) - \mu + 2g|\Psi_0(\mathbf{r})|^2\right] v_\nu(\mathbf{r}) + g\Psi_0^*(\mathbf{r})^2 u_\nu(\mathbf{r}) = -\epsilon_\nu v_\nu(\mathbf{r}). \tag{4.25}$$

They naturally satisfy so-called relations of *biorthogonality*,[5] which here take the form

$$\langle u_\nu|u_{\nu'}\rangle - \langle v_\nu|v_{\nu'}\rangle = \int \mathrm{d}\mathbf{r}\,[u_\nu^*(\mathbf{r})u_{\nu'}(\mathbf{r}) - v_\nu^*(\mathbf{r})v_{\nu'}(\mathbf{r})] = 0 \qquad \text{for } \epsilon_\nu \neq \epsilon_{\nu'}, \tag{4.26}$$

$$\langle v_\nu^*|u_{\nu'}\rangle - \langle u_\nu^*|v_{\nu'}\rangle = \int \mathrm{d}\mathbf{r}\,[v_\nu(\mathbf{r})u_{\nu'}(\mathbf{r}) - u_\nu(\mathbf{r})v_{\nu'}(\mathbf{r})] = 0, \tag{4.27}$$

and are chosen and normalized so that

$$\langle u_\nu|u_{\nu'}\rangle - \langle v_\nu|v_{\nu'}\rangle = \int \mathrm{d}\mathbf{r}\,[u_\nu^*(\mathbf{r})u_{\nu'}(\mathbf{r}) - v_\nu^*(\mathbf{r})v_{\nu'}(\mathbf{r})] = \delta_{\nu,\nu'}. \tag{4.28}$$

The latter prescription is required for the commutation relations (4.22) to hold.

The BdGEs can be put in the algebraic form

$$\mathcal{B}_{\mathrm{GP}} \begin{pmatrix} u \\ v \end{pmatrix} = \hbar\omega \begin{pmatrix} u \\ v \end{pmatrix} \tag{4.29}$$

where

$$\mathcal{B}_{\mathrm{GP}} = \begin{pmatrix} \mathcal{L}_\mu + 2g|\Psi_0|^2 & g\Psi_0^2 \\ -g\Psi_0^{*2} & -\mathcal{L}_\mu - 2g|\Psi_0|^2 \end{pmatrix}. \tag{4.30}$$

We shall refer to $\mathcal{B}_{\mathrm{GP}}$ as the Bogolyubov operator. It is easily checked that each solution of Eq. (4.29) with eigenvalue $\hbar\omega$ comes along with a solution for $-\hbar\omega$. These eigenvalues are often called frequencies to distinguish them from the energy ϵ, which in the present context is always positive. It is worth stressing that the solutions of negative $\hbar\omega$ are taken into account in transformation (4.23), and that one should stick to the rule of solving the BdGEs (4.24) and (4.25) for strictly positive energies ϵ_ν in order for the $\hat{b}_\nu$ and $\hat{b}_\nu^\dagger$ to be annihilation and creation operators, respectively, and not the opposite. If the BdGEs were to be solved for negative energies ϵ_ν and transformation (4.23) was left unchanged, the Kronecker delta in

[5] The vectors $(u_\nu, v_\nu)^{\mathrm{T}}$ are eigenvectors of a non-Hermitian operator $\mathcal{B}_{\mathrm{GP}}$ (see below). The biorthogonality relations arise from the orthogonality of these eigenvectors to the eigenvectors of the Hermitian adjoint $\mathcal{B}_{\mathrm{GP}}^\dagger$ (see e.g. page 884 of Ref. [306]).

(4.22) would be affected by a minus sign, and the creation and annihilation operators would be interchanged. Physically, the positivity of ϵ_ν for the proper commutation relations (4.22) means that populating the quasi-particles modes can only increase the energy of the system. This property of *spectral* or *thermodynamical* stability follows from the assumption that Ψ_0 is a local minimum of the GPE [253, 303]. The BdGEs also have a solution of zero energy,

$$\begin{pmatrix} u_0 \\ v_0 \end{pmatrix} = \begin{pmatrix} \psi_0 \\ -\psi_0^* \end{pmatrix}. \tag{4.31}$$

This mode is commented on below.

The set of eigenvectors

The Bogolyubov operator $\mathcal{B}_{\rm GP}$ has the remarkable property of *not* being Hermitian (self-adjoint): $\mathcal{B}_{\rm GP} \neq \mathcal{B}_{\rm GP}^\dagger$. This property is a consequence of the bosonic nature of the field $\hat\Psi$,[6,7] and explains the somewhat unusual and weaker orthogonality relations (4.26) to (4.28). Unlike Hermitian operators, to which the spectral theorem applies, non-Hermitian operators are generally not diagonalizable (i.e. their eigenvectors do not span the whole vector-space), their eigenvalues may be complex, and their eigenvectors may not be orthogonal. Here, in spite of the lack of Hermiticity, the symmetries of $\mathcal{B}_{\rm GP}$ and the assumption that Ψ_0 is a local minimum of the GPE suffice to derive expansion (4.21) and the properties listed below. From Refs. [253, 301, 303] we also infer that this assumption on Ψ_0 makes $\mathcal{B}_{\rm GP}$ almost diagonalizable in the sense that one and only one eigenvector is missing to form a complete set.[8] The basis is completed by a generalized eigenvector

$$\begin{pmatrix} u_a \\ v_a \end{pmatrix} = \begin{pmatrix} \psi_a \\ \psi_a^* \end{pmatrix} \tag{4.32}$$

[6] See e.g. chapter 3 in Ref. [301] and section 6 in Ref. [253]. In the BCS theory, both the original fields and the Bogolyubov excitations are fermionic. The coefficients u and v of the Bogolyubov transformation are solutions of

$$\mathcal{B}_{\rm BCS}\begin{pmatrix} u_\nu \\ v_\nu \end{pmatrix} = \epsilon_\nu \begin{pmatrix} u_\nu \\ v_\nu \end{pmatrix}, \qquad \mathcal{B}_{\rm BCS} = \begin{pmatrix} \mathcal{L}_\mu & \Delta \\ \Delta^* & -\mathcal{L}_\mu \end{pmatrix}.$$

In this equation, Δ is diagonal in the position basis and hence symmetric, so that $\mathcal{B}_{\rm BCS}$ is Hermitian.

[7] It is well known that Eq. (4.29) is also obtained for the vector $(\delta\Psi, \delta\Psi^*)^{\rm T}$ in a perturbation expansion of the time-dependent Gross-Pitaevskii equation with $\Psi = \Psi_0 + \delta\Psi$, where Ψ_0 is some solution of the GPE, and $\delta\Psi$ is a *classical* perturbation [32, 253]. In other words, the non-Hermitian operator $\mathcal{B}_{\rm GP}$ also arises for classical fields. In that case, the non-Hermiticity of $\mathcal{B}_{\rm GP}$ originates from the structure of Hamilton's equations of motion, which describe the time evolution of conjugate variables [302]. So why refer to specific quantum statistics to explain the non-Hermiticity of $\mathcal{B}_{\rm GP}$? Complex numbers are indeed used in classical representations of bosonic fields. Hamilton's classical equations are then used instead of Heisenberg's equations of motion (which involve a commutator) for conjugate operators of a bosonic quantum field (see e.g. Ref. [256, 302]). For fermions, on the other hand, "classical" equations of motion would have to involve anticommuting Grassmann numbers instead of normal complex numbers, and Hamilton's equations cannot be used as such.

[8] We refer in particular to section III.C of Ref. [303], pages 63 and 65 of Ref. [301], and section 7.9 of Ref. [253]. If Ψ_0 is a local minimum of the GPE, the Hermitian operator $\mathcal{M}_{\rm GP}$ defined by

$$\mathcal{M}_{\rm GP} = \sigma_3 \mathcal{B}_{\rm GP} = \begin{pmatrix} \mathcal{L}_\mu + 2g|\Psi_0|^2 & g\Psi_0^2 \\ g\Psi_0^{*2} & \mathcal{L}_\mu + 2g|\Psi_0|^2 \end{pmatrix}, \qquad \sigma_3 = \begin{pmatrix} 1 & 0 \\ 0 & -1 \end{pmatrix}$$

is positive semi-definite. Then, as shown in Ref. [301], the operator $\mathcal{B}_{\rm GP}$ has only real eigenvalues, and the solutions of Eq. (4.29), together with the vector $(u_a, v_a)^{\rm T}$ of Eq. (4.32), form a complete set.

sought as eigenvector of $\mathcal{B}^2_{\rm GP}$ with eigenvalue zero, and chosen so as to share with the $(u_\nu, v_\nu)^{\rm T}$ and $(u_0, v_0)^{\rm T}$ adequate biorthonormality relations, as explained in Refs. [294, 296].

With this basis at hand, the field operators are expanded as

$$\begin{pmatrix} \delta\hat\Psi(\mathbf{r}) \\ \delta\hat\Psi^\dagger(\mathbf{r}) \end{pmatrix} = \frac{1}{\mathrm{i}\hbar}\hat Q \begin{pmatrix} \psi_0(\mathbf{r}) \\ -\psi_0^*(\mathbf{r}) \end{pmatrix} + \hat P \begin{pmatrix} \psi_a(\mathbf{r}) \\ \psi_a^*(\mathbf{r}) \end{pmatrix} + \sum_\nu \hat b_\nu \begin{pmatrix} u_\nu(\mathbf{r}) \\ v_\nu(\mathbf{r}) \end{pmatrix} + \hat b_\nu^\dagger \begin{pmatrix} v_\nu^*(\mathbf{r}) \\ u_\nu^*(\mathbf{r}) \end{pmatrix}, \tag{4.33}$$

where $\hat b_\nu$ and $\hat b_\nu^\dagger$ are defined in Eq. (4.23), and the coefficients $\hat Q$ and $\hat P$ are defined by

$$\hat P = \int \mathrm{d}\mathbf{r} \left[\psi_0^*(\mathbf{r})\delta\hat\Psi(\mathbf{r}) + \psi_0(\mathbf{r})\delta\hat\Psi^\dagger(\mathbf{r})\right] \tag{4.34}$$

$$\hat Q = \mathrm{i}\hbar \int \mathrm{d}\mathbf{r} \left[\psi_a^*(\mathbf{r})\delta\hat\Psi(\mathbf{r}) - \psi_a(\mathbf{r})\delta\hat\Psi^\dagger(\mathbf{r})\right]. \tag{4.35}$$

These operators $\hat P$ and $\hat Q$ are Hermitian and satisfy the commutation relation $[\hat Q, \hat P] = \mathrm{i}\hbar$. Finally, replacing the field operators by expressions (4.33) in Hamiltonian (4.17) leads to the expansion (4.21).

As explained above, the last term in Hamiltonian (4.21) describes non-interacting, bosonic quasi-particle excitations. Let us now briefly comment on the $\hat P^2$. Unlike the $\hat b_\nu$ and $\hat b_\nu^\dagger$ operators, $\hat P$ is Hermitian and commutes with Hamiltonian $\hat K_2$. Therefore, the $\hat P$ operator plays no role in the time dynamics of the fluctuations field $\delta\hat\Psi$, which is given by the Heisenberg equation of motion $\mathrm{i}\hbar\partial_t\delta\hat\Psi = [\delta\hat\Psi, \hat K_2]$. And neither does the $\hat Q$ operator which appears in the expansion of the field operators have an influence on their dynamics. According to Refs. [294, 296], $\hat Q$ and $\hat P$ should be interpreted as a collective phase coordinate and its conjugate momentum.[9] The $\hat P^2$ contribution to the Hamiltonian is attributed to the use of an approach which does not conserve the number of atoms [270, 294, 296, 301], and is shown to result in a phase diffusion of the condensate [294, 296]. We shall regard this part of the Hamiltonian as resulting from a spurious mode [301], and concentrate on the quasi-particle part.

4.1.2 Bogolyubov excitations in the density-phase picture

Let us now turn to the representation of the field operator in the density-phase picture: $\hat\Psi(\mathbf{r}) = \mathrm{e}^{\mathrm{i}\hat\theta(\mathbf{r})}\sqrt{\hat n(\mathbf{r})}$. Then, as shown in section 3.3.1, the grand-canonical Hamiltonian rewrites

$$\begin{aligned} \hat K = & \int \mathrm{d}\mathbf{r} \left\{ \frac{\hbar^2}{2m}\left[(\nabla\sqrt{\hat n})^2 + \sqrt{\hat n}(\nabla\hat\theta)^2\sqrt{\hat n} + \mathrm{i}\nabla\sqrt{\hat n}\nabla\hat\theta\sqrt{\hat n} - \mathrm{i}\sqrt{\hat n}\nabla\hat\theta\nabla\sqrt{\hat n}\right] + [V(\mathbf{r}) - \mu]\,\hat n \right\} \\ & + \frac{g}{2}\int \mathrm{d}\mathbf{r}\sqrt{\hat n}\,\mathrm{e}^{-\mathrm{i}\hat\theta}\hat n\,\mathrm{e}^{\mathrm{i}\hat\theta}\sqrt{\hat n}\,. \end{aligned} \tag{4.36}$$

For sufficiently strong mean-field interactions, the Bose gas close to the ground state has weak density fluctuations.[10] This allows for an expansion of the density operator around a classical field:

$$\hat n(\mathbf{r}) = n_0(\mathbf{r}) + \delta\hat n(\mathbf{r}) \qquad [\|\delta\hat n(\mathbf{r})\| \ll n_0(\mathbf{r})]. \tag{4.37}$$

[9] The $\hat P^2$ contribution represents a kinetic term. The difference with a harmonic oscillator, for instance, is that no potential term quadratic in $\hat Q$ appears in the Hamiltonian, so that the collective motion associated with $\hat Q$ and $\hat P$ is unbounded.

[10] The validy of this assumption is checked a posteriori in the theory. See e.g. Ref. [251].

While no assumption is made on the phase $\hat{\theta}$, it is shown in Ref. [264] that weak density fluctuations also imply weak fluctuations of the phase *gradient* $\nabla\hat{\theta}$. The grand-canonical Hamiltonian $\hat{K}$ is then expanded in powers of $\delta\hat{n}$ and $\nabla\hat{\theta}$. The two fields can be regarded as infinitesimal quantities of the same order [270,296]. Then, the expansion takes the form $\hat{K} = \hat{K}_0 + \hat{K}_1 + \cdots$ where the subscripts indicate the total order in $\delta\hat{n}$ and $\nabla\hat{\theta}$. As before, the hierarchy is truncated after the second order to obtain a Hamiltonian which is quadratic in the fluctuations.

Mean-field density profile

To zeroth order, we obtain the functional

$$K_0[n_0] = \int \mathrm{d}\mathbf{r}\sqrt{n_0(\mathbf{r})}\left\{-\frac{\hbar^2\nabla^2}{2m} + V(\mathbf{r}) + \frac{g}{2}n_0(\mathbf{r}) - \mu\right\}\sqrt{n_0(\mathbf{r})} \tag{4.38}$$

and the Gross-Pitaevskii equation

$$\left[-\frac{\hbar^2\nabla^2}{2m} + V(\mathbf{r}) + gn_0(\mathbf{r}) - \mu\right]\sqrt{n_0}(\mathbf{r}) = 0, \tag{4.39}$$

which determine the mean-field features studied in chapter 3. The ground-state solution $\sqrt{n_0(\mathbf{r})}$ has the same properties as the field $\psi_0(\mathbf{r}) = \Psi_0(\mathbf{r})/\sqrt{N_0}$ of the previous section, which can be chosen to be real-valued and positive in the ground state.

Density and phase fluctuations

As $n_0(\mathbf{r})$ is a solution of the GPE (4.39), the first order $\hat{K}_1$ vanishes, and we have again

$$\hat{K} \simeq K_0[n_0] + \hat{K}_2. \tag{4.40}$$

A modal expansion of the fields $\delta\hat{n}$ and $\hat{\theta}$, and of the Hamiltonian, is obtained from the analysis of $\hat{K}_2$. At this level, the density-phase picture gives rise to a few more technicalities than the approach with the field operators $\delta\hat{\Psi}$ and $\delta\hat{\Psi}^\dagger$, in particular because of commutation relations. As shown in Ref. [256], the expansion of the Hamiltonian is left unchanged,

$$\hat{K}_2 = \tilde{K}_2 + \alpha\hat{P}^2 + \sum_\nu \epsilon_\nu \hat{b}_\nu^\dagger \hat{b}_\nu. \tag{4.41}$$

The bosonic annihilation and creation operators $\hat{b}$ and $\hat{b}^\dagger$ are now obtained from the quantum fields as

$$\hat{b}_\nu = \int \mathrm{d}\mathbf{r}\left[\frac{f_\nu^{+*}(\mathbf{r})}{2\sqrt{n_0(\mathbf{r})}}\delta\hat{n}(\mathbf{r}) - \mathrm{i}\sqrt{n_0(\mathbf{r})}f_\nu^{-*}(\mathbf{r})\hat{\theta}(\mathbf{r})\right] \tag{4.42}$$

and its Hermitian conjugate. The functions f_ν^+ and f_ν^- are determined as the solutions of the set of equations

$$\left[-\frac{\hbar^2\nabla^2}{2m} + V(\mathbf{r}) - \mu + \ gn_0(\mathbf{r})\right] f_\nu^+(\mathbf{r}) \ = \ \epsilon_\nu f_\nu^-(\mathbf{r}) \tag{4.43}$$

$$\left[-\frac{\hbar^2\nabla^2}{2m} + V(\mathbf{r}) - \mu + 3gn_0(\mathbf{r})\right] f_\nu^-(\mathbf{r}) \ = \ \epsilon_\nu f_\nu^+(\mathbf{r}), \tag{4.44}$$

for $\epsilon_\nu > 0$. The identification $f_\nu^\pm(\mathbf{r}) = u_\nu(\mathbf{r}) \mp v_\nu(\mathbf{r})$ shows that this set of equations is equivalent to the BdGEs (4.24) and (4.25).[11] The functions f_ν^+ and f_ν^- are normalized so that

$$\int \mathrm{d}\mathbf{r} \left[f_\nu^{+*}(\mathbf{r}) f_{\nu'}^-(\mathbf{r}) + f_\nu^{-*}(\mathbf{r}) f_{\nu'}^+(\mathbf{r}) \right] = 2\delta_{\nu,\nu'}. \tag{4.45}$$

Finally, the modal expansions of the phase and density fluctuations are

$$\hat{\theta}(\mathbf{r}) = \frac{1}{2\mathrm{i}\sqrt{n_0(\mathbf{r})}} \sum_\nu \left[f_\nu^+(\mathbf{r}) \hat{b}_\nu - f_\nu^{+*}(\mathbf{r}) \hat{b}_\nu^\dagger \right] - \frac{1}{\hbar} \hat{Q} \tag{4.46}$$

$$\delta\hat{n}(\mathbf{r}) = \sqrt{n_0(\mathbf{r})} \sum_\nu \left[f_\nu^-(\mathbf{r}) \hat{b}_\nu + f_\nu^{-*}(\mathbf{r}) \hat{b}_\nu^\dagger \right] + 2\sqrt{n_0(\mathbf{r})} \psi_a(\mathbf{r}) \hat{P}, \tag{4.47}$$

where $\psi_a(\mathbf{r})$ is a real-valued function [256]. The $\hat{P}$ and $\hat{Q}$ operators can be left aside as a consequence of the lack of particle conservation in Hamiltonian (4.40). Thus, f^+ and f^-, which are associated with regular modes of the Bogolyubov Hamiltonian, are identified as wave-functions of the phase and density fluctuations, respectively. The coupling of Eqs. (4.43) and (4.44) shows that an elementary excitation of the weakly-interacting Bose gas carries both phase and density fluctuations, albeit in different proportions.

As pointed out by Popov [297] (see also Ref. [256]), the set of equations obtained in the phase-density representation turns out to be equivalent to those obtained from the usual Bogolyubov-de Gennes theory, where a shift is applied to the field operator, $\hat{\Psi} = \sqrt{n_0} + \delta\hat{\Psi}$, and $\hat{K}$ is expanded up to quadratic terms in the fluctuation $\delta\hat{\Psi}$ (see section 4.1.1). The latter approach assumes weak fluctuations of both the phase and the density around a unique classical field $\sqrt{n_0}$ which breaks the phase symmetry of the Hamiltonian. The phase-density picture, on the contrary, does not rely on this assumption, and proves suitable for the description of condensates as well as quasi-condensates. The derivation of the BdGEs in the density-phase picture therefore offers a useful extension of the standard Bogolyubov theory.

It is also worth emphasizing that the elementary excitations described by this set of equations are essentially the same as in approaches which conserve the number of particles. In such approaches, the excitation spectrum is exacly the same. Remarkably, however, the spurious modes are absent from Hamiltonian and field operators [296]. This justifies neglecting their role in non-conserving approaches. Finally, the regular modes of the conserving approach are the same as those of the non-conserving approach up to a projection orthogonally to the condensate wave function [296]. It is easily checked that this projection does not change any of the conclusions below.

4.1.3 Summary

The GPE

$$\left[-\frac{\hbar^2\nabla^2}{2m} + V(\mathbf{r}) + g n_0(\mathbf{r}) - \mu \right] \sqrt{n_0}(\mathbf{r}) = 0, \tag{4.48}$$

[11] Several sign conventions for the coherence factors u and v coexist in the literature [see the footnote above Eq. (4.23)]. For u and v, we follow here the notations of Refs. [296], and construct f^+ and f^- so as to associate them with phase and density fluctuations, respectively, as e.g. in Ref. [251]. As a mnemonic device, we observe that for low-energy excitations, f^+ is large, and f^- is small. On the other hand, if $(u, -v)$ is used instead of (u, v), then the superscripts in f^+ and f^- indicate that f^+ and f^- are the sum and the difference of the coherence factors u and v, respectively (it goes the other way round here).

and the BdGEs

$$\left[-\frac{\hbar^2\nabla^2}{2m}+V(\mathbf{r})-\mu+\ gn_0(\mathbf{r})\right]f_\nu^+(\mathbf{r}) = \epsilon_\nu f_\nu^-(\mathbf{r}) \tag{4.49}$$

$$\left[-\frac{\hbar^2\nabla^2}{2m}+V(\mathbf{r})-\mu+3gn_0(\mathbf{r})\right]f_\nu^-(\mathbf{r}) = \epsilon_\nu f_\nu^+(\mathbf{r}), \tag{4.50}$$

form a closed set which describes the ground-state and excitations of the Bose gas, as obtained from a quadratic expansion of Hamiltonian $\hat{K}$ in the quantum fluctuation fields. Equations (4.49) and (4.50) determine the energy spectrum and the wave functions of non-interacting, bosonic quasi-particles which form the elementary excitation of the Bose gas. Interactions between these quasi-particles only arise with higher-order terms in the expansion of $\hat{K}$, which we neglect here. Therefore, to study the properties of the Bose gas close to equilibrium at zero temperature, in the external potential $V(\mathbf{r})$, we are left with the sole modes defined by the GPE (4.48) and BdGEs (4.49) and (4.50).

Let us now examine the solutions of these equations in the absence of an external potential. These solutions provide a useful starting point for the case of weak potentials.

4.1.4 Homogeneous case

When no external potential is present ($V = 0$), and the system is either infinite or required to have periodic boundary conditions, the density profile is homogeneous ($n_0 = \mu/g$), and the BdGEs reduce to

$$-\frac{\hbar^2\nabla^2}{2m}f_\nu^+(\mathbf{r}) = \epsilon_\nu f_\nu^-(\mathbf{r}) \tag{4.51}$$

$$\left[-\frac{\hbar^2\nabla^2}{2m}+2\mu\right]f_\nu^-(\mathbf{r}) = \epsilon_\nu f_\nu^+(\mathbf{r}). \tag{4.52}$$

The solutions of these equations are plane-wave modes

$$\begin{pmatrix} f_{\mathbf{k}}^+(\mathbf{r}) \\ f_{\mathbf{k}}^-(\mathbf{r}) \end{pmatrix} = \begin{pmatrix} \sqrt{\rho_k} \\ 1/\sqrt{\rho_k} \end{pmatrix} \mathrm{e}^{\mathrm{i}\mathbf{k}.\mathbf{r}} \tag{4.53}$$

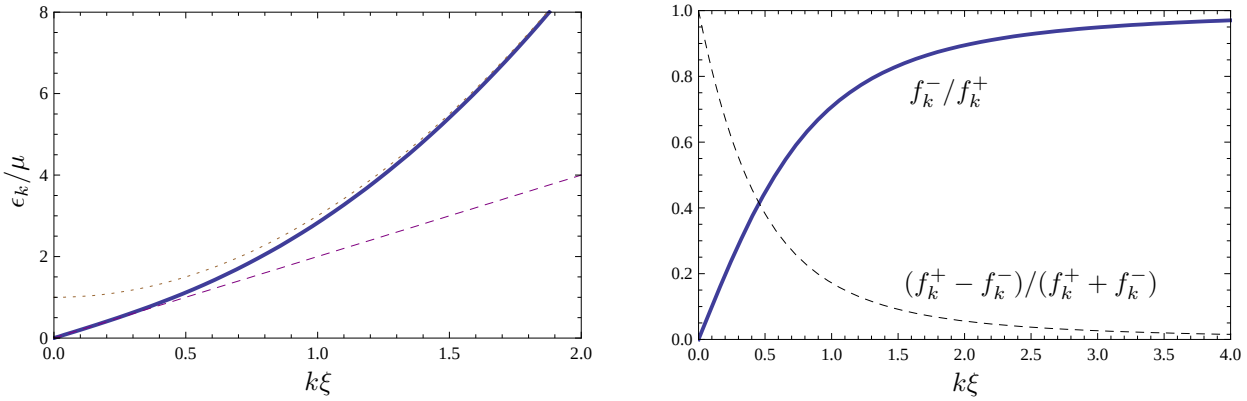
with wave vector $\mathbf{k}$ and energy

$$\epsilon_k = \sqrt{\frac{\hbar^2k^2}{2m}\left(2\mu+\frac{\hbar^2k^2}{2m}\right)} = 2\mu\sqrt{k^2\xi^2\left(1+k^2\xi^2\right)}. \tag{4.54}$$

In these expressions, we have used $\xi = \hbar/\sqrt{4m\mu}$ and defined

$$\rho_k = \frac{\mu}{\epsilon_k}+\sqrt{1+\left(\frac{\mu}{\epsilon_k}\right)}. \tag{4.55}$$

This coefficient also writes $\rho_k = \sqrt{1+1/(k\xi)^2}$, or $\rho_k = \epsilon_k/E_k$, where $E_k = \hbar^2k^2/2m$ is the energy of a bare particle with same wave vector $\mathbf{k}$. The coefficients ρ_k stands for the ratio of the functions f_k^+ and f_k^-.



(a) Homogeneous dispersion relation

(b) Quasi-particle coherence factors

Figure 4.1: (a) Dispersion relation of Bogolyubov quasi-particles in the absence of external potential (blue solid line). The dashed purple line and the dotted brown line correspond to the low- and high-energy limits given by Eqs. (4.56) and (4.57), respectively. (b) Coefficient of the Bogolyubov transformation as a function of the quasi-particle energy. The blue solid line indicates the ratio f_k^-/f_k^+ of relative density fluctuations to phase fluctuations carried by the quasi-particle. The black dashed line represents the relative weight $|v_k|/u_k = (f_k^+ - f_k^-)/(f_k^+ + f_k^-)$ of the particle and hole components in the BQP [see transformation (4.23)].

The quasi-particle dispersion relation (4.54) is plotted in Fig. 4.1(a). It crosses over from a linear dispersion relation at low energy,

$$\epsilon_k \sim \hbar c k \qquad [k\xi \to 0], \tag{4.56}$$

to a free-particle dispersion relation plus a mean-field offset at high energy,

$$\epsilon_k \sim g n_0 + \frac{\hbar^2 k^2}{2m} \qquad [k\xi \to \infty], \tag{4.57}$$

with $gn_0 = \mu$. The coefficient $c = \sqrt{gn_0/m}$ is well known to correpond to the macroscopic velocity of sound in the Bose gas [290].

Figure 4.1(b) shows the relative amplitude of the coherence factors of the Bogolyubov transformation. The ratio $f_k^-/f_k^+ = 1/\rho_k$ drops to zero for $k\xi \to 0$, indicating that the low-energy, long-wavelength excitations hardly carry density fluctuations, and are mostly phase-like excitations. The ratio $|v_k|/u_k = (f_k^+ - f_k^-)/(f_k^+ + f_k^-)$ shows that these long-wavelength quasi-particles consist in nearly equal parts of a bare particle and a bare hole [248]. The high-energy, short-wavelength quasi-particles, on the other hand, resemble bare particles.

4.2 Perturbation expansion for Bogolyubov quasi-particles in weak potentials

The BdGEs are difficult to solve for arbitrary potentials. The first reason for this is the presence of the density term n_0, which is determined by the non-linear GPE. What is more, the BdGEs (4.49) and (4.50) themselves form a set of two coupled, second-order differential

equations, which amounts to a differential problem of order four. In the following, we develop a perturbative approach, valid in the limit of a weak potential $V(\mathbf{r})$, which enables us to solve Eqs. (4.48), (4.49) and (4.50) rigorously, and to interpret the scattering and localization of BQPs in simple physical terms.

We now assume that V is a weak potential with vanishing spatial average ($\langle V\rangle = 0$) and standard deviation $|V_{\rm R}| = \sqrt{\langle V^2\rangle}$. The potential is said to be weak whenever $|V_{\rm R}| \ll \mu$.[12] We will focus on disorder in section 4.3. Note, however, that the perturbative approach introduced here is general, and V need not be random. In any case, we write the auto-correlation function of V as

$$\langle V(\mathbf{r})V(\mathbf{r}')\rangle = V_{\rm R}^2 c_2[(\mathbf{r}-\mathbf{r}')/\sigma_{\rm R}], \tag{4.58}$$

where $\sigma_{\rm R}$ stands either for a typical correlation length of V in the random case, or for a characteristic length scale in the periodic case.

4.2.1 Ground-state density background

Solving the BdGEs requires knowledge of the density background $n_0(\mathbf{r})$, which is determined by the GPE. In the case of a weak potential, the GPE can be solved perturbatively. We reproduce here the results of the analysis carried out in section 3.3.3.

In general, the density n_0 can be written

$$n_0(\mathbf{r}) = \frac{\mu + \Delta - \widetilde{V}(\mathbf{r})}{g}, \tag{4.59}$$

where $\widetilde{V}(\mathbf{r}) = g\langle n_0\rangle - g n_0(\mathbf{r})$ is the fluctuating part of the density modulations, and $\Delta = g\langle n_0\rangle - \mu$ is the deviation equation of state $\mu = g n_0$ obtained in the homogeneous case.

Both $\widetilde{V}$ and Δ vanish for $V = 0$, and remain small for a weak external potential V and strong-enough repulsive interactions. Expansions of $\widetilde{V}$ and Δ in the form

$$\widetilde{V}(\mathbf{r}) = \widetilde{V}^{(1)}(\mathbf{r}) + \widetilde{V}^{(2)}(\mathbf{r}) + \dots \tag{4.60}$$

$$\Delta = \Delta^{(1)} + \Delta^{(2)} + \dots, \tag{4.61}$$

where the superscripts indicate increasing powers of $V_{\rm R}/\mu$, are obtained from a perturbation expansion of the GPE. The first-order terms read

$$\Delta^{(1)} = 0 \tag{4.62}$$

and

$$\widetilde{V}^{(1)}(\mathbf{r}) = \int \mathrm{d}\mathbf{r}' G_\xi(\mathbf{r}-\mathbf{r}')V(\mathbf{r}'), \tag{4.63}$$

where the convolution kernel G_ξ has a simple Lorentzian shape in Fourier space, namely

$$\widetilde{V}^{(1)}(\mathbf{q}) = \frac{V(\mathbf{q})}{1 + (|\mathbf{q}|\xi)^2}. \tag{4.64}$$

[12] We have shown in chapter 3 that a less stringent criterion on the strength of the potential is sufficient to ensure weak modulations of the ground-state density profile, due to smoothing. See also Ref. [242].

Equation (4.63) defines a smoothed potential, the root-mean-square amplitude of which satisfies

$$\widetilde{V}_{\rm R}^{(1)} \equiv \sqrt{\langle \widetilde{V}^{(1)} \rangle} \leq V_{\rm R}. \tag{4.65}$$

We assume that this result holds for the exact $\widetilde{V}(\mathbf{r})$, i.e. $\widetilde{V}_{\rm R} \leq V_{\rm R}$.

The leading-order deviation from the homogeneous equation of state is obtained as

$$\Delta^{(2)} = \frac{V_{\rm R}^2}{2\mu} \left[I_1 - I_2 \right], \tag{4.66}$$

where

$$I_n \left(\frac{\xi}{\sigma_{\rm R}} \right) = \frac{\sigma_{\rm R}^d}{(2\pi)^{d/2}} \int {\rm d}\mathbf{q} \frac{\hat{c}_2(\mathbf{q}\sigma_{\rm R})}{[1 + (|\mathbf{q}|\xi)^2]^n}, \tag{4.67}$$

and $\hat{c}_2$ is the Fourier transform of the reduced autocorrelation function c_2. The functions I_1 and I_2 satisfy $0 \leq I_2 \leq I_1 \leq 1$, so that $0 \leq \Delta^{(2)} \leq V_{\rm R}^2/(2\mu)$.

4.2.2 Decoupling basis for the Bogolyubov-de Gennes equations

With the help of Eq. (4.59), and without approximation at this stage, the BdGEs (4.49) and (4.50) can be cast into

$$\left[-\frac{\hbar^2}{2m}\nabla^2 + V + \Delta - \widetilde{V} \right] f_\nu^+ = \epsilon_\nu f_\nu^- \tag{4.68}$$

$$\left[-\frac{\hbar^2}{2m}\nabla^2 + 2\mu + V + 3\Delta - 3\widetilde{V} \right] f_\nu^- = \epsilon_\nu f_\nu^+, \tag{4.69}$$

where Δ, $V(\mathbf{r})$ and $\widetilde{V}(\mathbf{r})$ are small compared to μ. As $n_0(\mathbf{r})$ is the ground-state solution of the GPE (4.48), thermodynamical and dynamical stability is ensured [253, 301], and we need only consider real-valued, strictly positive eigenvalues of the BdGEs. Now, given such an eigenvalue ϵ_ν, we are interested in the properties of the corresponding mode $\{f_\nu^+(\mathbf{r}), f_\nu^-(\mathbf{r})\}$.

The $\{f^+, f^-\}$ representation of the BQP components is not the most convenient, as f^+ and f^- are strongly coupled by the right-hand-side terms of Eqs. (4.68) and (4.69) even in the absence of an external potential. Following the approach we developed in Ref. [307], which is detailed in appendix G, we introduce the linear transformation

$$g_\nu^+(\mathbf{r}) = +\sqrt{\rho_\nu} f_\nu^+(\mathbf{r}) + \frac{1}{\sqrt{\rho_\nu}} f_\nu^-(\mathbf{r}) \tag{4.70}$$

$$g_\nu^-(\mathbf{r}) = -\frac{1}{\sqrt{\rho_\nu}} f_\nu^+(\mathbf{r}) + \sqrt{\rho_\nu} f_\nu^-(\mathbf{r}), \tag{4.71}$$

where ρ_ν is chosen so as to cancel the coupling between $g_\nu^+(\mathbf{r})$ and $g_\nu^-(\mathbf{r})$ in the homogeneous case ($V = 0$):

$$\rho_\nu = \frac{\mu}{\epsilon_\nu} + \sqrt{1 + \left(\frac{\mu}{\epsilon_\nu} \right)^2}. \tag{4.72}$$

Here ρ_ν is a shorthand notation for ρ_{ϵ_ν}. This expression defines a function of the eigenvalue ϵ_ν which does not depend on the details of the specific mode under consideration.[13] Then, in the basis of the $g^\pm_\nu(\mathbf{r})$ functions, the BdGEs take the form:[14]

$$\frac{\hbar^2 k_\nu^2}{2m} g_\nu^+ = -\frac{\hbar^2}{2m}\nabla^2 g_\nu^+ + \left[V - \frac{3+\rho_\nu^2}{1+\rho_\nu^2}(\widetilde{V}-\Delta)\right] g_\nu^+ - \frac{2\rho_\nu}{1+\rho_\nu^2}(\widetilde{V}-\Delta) g_\nu^- \tag{4.73}$$

$$-\frac{\hbar^2 \beta_\nu^2}{2m} g_\nu^- = -\frac{\hbar^2}{2m}\nabla^2 g_\nu^- + \left[V - \frac{1+3\rho_\nu^2}{1+\rho_\nu^2}(\widetilde{V}-\Delta)\right] g_\nu^- - \frac{2\rho_\nu}{1+\rho_\nu^2}(\widetilde{V}-\Delta) g_\nu^+, \tag{4.74}$$

where

$$\frac{\hbar^2 k_\nu^2}{2m} = \sqrt{\mu^2+\epsilon_\nu^2} - \mu \tag{4.75}$$

$$\frac{\hbar^2 \beta_\nu^2}{2m} = \sqrt{\mu^2+\epsilon_\nu^2} + \mu. \tag{4.76}$$

Both k and β are real-valued, positive functions of the energy ϵ, so that the associated g^+ and g^- functions are essentially of the oscillating and the evanescent type, respectively, owing to the signs of the left-hand-side terms in Eqs. (4.73) and (4.74).[15]

This qualitative property of the g^+ and g^- components is consistent with the limit of a vanishing external potential ($V = 0$, and thus $\widetilde{V} = 0$, $\Delta = 0$), where the equations for g^+ and g^- are decoupled:

$$-\frac{\hbar^2}{2m}\nabla^2 g_\nu^+ = \frac{\hbar^2 k_\nu^2}{2m} g_\nu^+ \tag{4.77}$$

$$-\frac{\hbar^2}{2m}\nabla^2 g_\nu^- = -\frac{\hbar^2 \beta_\nu^2}{2m} g_\nu^-. \tag{4.78}$$

This set of differential equations has obvious solutions of the form

$$(g^+(\mathbf{r}), g^-(\mathbf{r})) \propto \mathrm{e}^{\pm i\mathbf{k}.\mathbf{r}}(1,0) \qquad \text{and} \qquad (g^+(\mathbf{r}), g^-(\mathbf{r})) \propto \mathrm{e}^{\pm \boldsymbol{\beta}.\mathbf{r}}(0,1). \tag{4.79}$$

The first family of solutions corresponds to oscillating, plane-wave BQP modes with wave vector $\mathbf{k}$, such that $k_\nu = |\mathbf{k}| \equiv k$. The energy $\epsilon_\nu = \epsilon_k$ of these modes is given by Eq. (4.75), which coincides with the usual Bogolyubov dispersion relation (4.54). The second family in (4.79) corresponds to monotonous functions which grow or decay exponentially at rate β in space. These modes are forbidden if the system is infinite or required to have periodic boundary conditions. In other words, for $V = 0$, the g^- component of BQPs vanishes identically, while g^+ is non-zero.

In the presence of an external potential, the g^- component does not vanish identically, due to the coupling to g^+ in Eqs. (4.73) and (4.74). Note also that the BQPs are no longer characterized by a well-defined wave vector for $V \neq 0$. Therefore, Eqs. (4.75) and (4.76) should be understood as definitions of some auxiliary quantities k_ν and β_ν which depend on the BQP energy ϵ_ν. In general, Eq. (4.75) is not a dispersion relation.

[13] This definition is consistent with the coefficient ρ_k introduced in Eq. (4.55) for the homogeneous case.

[14] See Eqs. (G.16) and (G.17) in appendix G.

[15] We call essentially evanescent a function ψ which has negative kinetic term $-\hbar^2\nabla^2\psi/(2m\psi)$ in the spatial average.

4.2.3 Effective Schrödinger equation (first order)

While the g_ν^- function vanishes identically in the absence of an external potential, this is no longer true when V couples g_ν^- to g_ν^+ via Eqs. (4.73) and (4.74). For a weak external potential, however, all the terms introduced by g_ν^- in Eq. (4.73) are at least of second order in $V_{\rm R}$, so that we can neglect the third term on the r.h.s of Eq. (4.73).[16] Similarly, we neglect the terms of order two and higher in the expansion of the factor $\widetilde{V} - \Delta$ which appears between brackets. Then, we are left with the following closed equation for g_ν^+, valid to first order in $V_{\rm R}$:

$$-\frac{\hbar^2}{2m}\nabla^2 g_\nu^+(\mathbf{r}) + \mathcal{V}_{\epsilon_\nu}(\mathbf{r}) g_\nu^+(\mathbf{r}) \simeq \frac{\hbar^2 k_\nu^2}{2m} g_\nu^+(\mathbf{r}), \tag{4.80}$$

where

$$\mathcal{V}_{\epsilon_\nu}(\mathbf{r}) = V(\mathbf{r}) - \frac{3+\rho_\nu^2}{1+\rho_\nu^2}\widetilde{V}^{(1)}(\mathbf{r}). \tag{4.81}$$

Equation (4.80) is formally equivalent to a Schrödinger equation for a bare particle of energy $\hbar^2 k_\nu^2/2m$ in an effective potential $\mathcal{V}_{\epsilon_\nu}(\mathbf{r})$.[17] This potential differs from both the bare potential $V(\mathbf{r})$ and the smoothed potential $\widetilde{V}(\mathbf{r})$, and depends explicitly on the BQP energy ϵ_ν via the parameter ρ_ν. Note also that the potential $\mathcal{V}_{\epsilon_\nu}$ has a vanishing average.

To gain more insight on $\mathcal{V}_\epsilon(\mathbf{r})$, let us turn to Fourier space:

$$\mathcal{V}_\epsilon(\mathbf{q}) = V(\mathbf{q}) - \frac{3+\rho^2}{1+\rho^2}\widetilde{V}^{(1)}(\mathbf{q}). \tag{4.82}$$

By virtue of Eq. (4.64), we obtain

$$\mathcal{V}_\epsilon(\mathbf{q}) = V(\mathbf{q})\left[1 - \frac{3+\rho^2}{1+\rho^2}\frac{1}{1+(|\mathbf{q}|\xi)^2}\right]. \tag{4.83}$$

Since $\rho \geq 1$ according to Eq. (4.72), we easily find that $|\mathcal{V}_\epsilon(\mathbf{q})| \leq |V(\mathbf{q})|$ for any Fourier component $\mathbf{q}$ and any BQP energy ϵ. Hence, keeping in mind that $\mathcal{V}_\epsilon$ results from the competition of the bare potential V and the ground-state density background n_0 in the BdGEs, we term $\mathcal{V}_\epsilon$ a *screened* potential. The screening thus affects all Fourier components of the external potential. This result holds in any dimension. To illustrate these features of $\mathcal{V}_\epsilon$ in a 1D system, we have plotted in Fig. 4.2 the screened potential associated with a given realization of a speckle potential, in coordinate space and for two values of the BQP energy. Note that $\mathcal{V}_\epsilon(\mathbf{r})$ is significantly different from the *bare* potential $V(\mathbf{r})$ and the *smoothed* potential $\widetilde{V}(\mathbf{r})$.

Once Eq. (4.80) has been solved (possibly self-consistently) for g_ν^+, the function g_ν^- can be computed from g_ν^+. For $V_{\rm R} \ll \mu$, as shown in appendix G, the function g^- is everywhere much smaller than g^+, so that the second term in the r.h.s of Eq. (4.74) can be neglected, and we find

$$g_\nu^-(\mathbf{r}) \simeq \frac{2m}{\hbar^2\beta_\nu^2}\frac{2\rho_\nu}{1+\rho_\nu^2}\int \mathrm{d}\mathbf{r}' G_{1/\beta_\nu}(\mathbf{r}-\mathbf{r}')\widetilde{V}(\mathbf{r}')g_\nu^+(\mathbf{r}'), \tag{4.84}$$

where $G_{1/\beta}$ is the Green function associated with the differential operator $-(1/\beta)^2\nabla^2 + 1$. This function has a simple expression in Fourier space: $G_{1/\beta}(\mathbf{q}) = (2\pi)^{-d/2}/[1+(|\mathbf{q}|/\beta)^2]$.

[16] See appendix G and Eq. (4.84) in the present section.

[17] Note that the effective energy $\hbar^2 k_\nu^2/2m$ appearing in the Schrödinger-like equation (4.80) is different from the actual energy ϵ_ν of the considered BQP, as shown by Eq. (4.75).

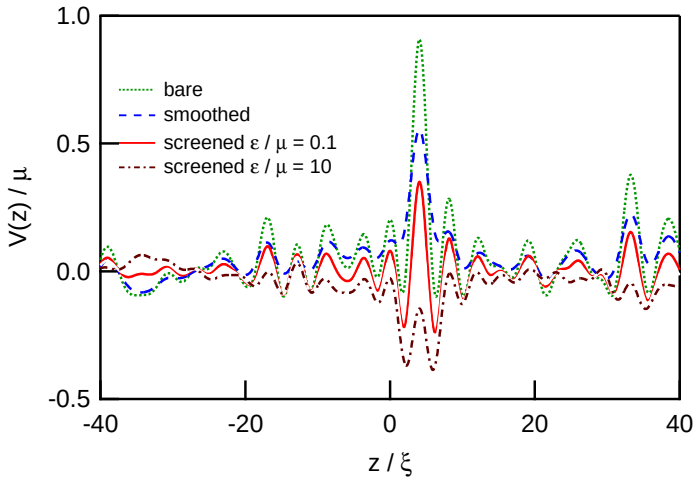


Figure 4.2: Plot of the screened potential $\mathcal{V}_\epsilon(z)$ for the same 1D speckle potential as in Fig. 3.3 ($\sigma_{\rm R} = \xi$, $V_{\rm R}/\mu = 0.1$), for $\epsilon/\mu = 0.1$ and $\epsilon/\mu = 10$. The bare potential $V(z)$ and the smoothed potential $\widetilde{V}(z)$ are shown for comparison.

For analytical purposes, the $g_\nu^\pm$ functions hence usefully replace the physically meaningful quantities $f_\nu^\pm$, which can readily be recovered by inverting transformation (4.70). In particular, as far as asymptotic localization properties in random potentials are concerned, Eq. (4.84) tells us that the typical amplitude of g_ν^- evolves parallel to the amplitude of g_ν^+ on intermediate to long length scales, if $\widetilde{V}$ is a potential with homogeneous statistical properties. In this respect, the benefit of the mapping of the exact BdGEs onto Eqs. (4.80) and (4.81) is that we can apply standard techniques for *bare* Schrödinger particles in weak random potentials, in any dimension, as long as these are consistent with the lowest-order approximation used to derive the effective equation (4.80). Similarly, the Schrödinger-like equation (4.80) can be used instead of the full BdGEs to capture the asymptotic properties of BQPs in isolated scattering events. Yet, the scattering and localization properties of BQPs differ substantially from those of usual bare particles, because of the peculiar features of the screened potential $\mathcal{V}_\epsilon(\mathbf{r})$.

4.2.4 Scattering by weak potentials

Before turning to random potentials, let us analyze the scattering of a BQP by a weak potential V of finite range. Since Eq. (4.80) has the form of a Schrödinger equation, we can apply standard results on the elastic scattering of Schrödinger particles.[18]

Consider a free particle of mass m and wave vector $\mathbf{k}$, described by a plane wave

$$\psi^{\rm in}(\mathbf{r}) = \mathrm{e}^{\mathrm{i}\mathbf{k}.\mathbf{r}} = \mathrm{e}^{\mathrm{i}kz}, \tag{4.85}$$

where $k = |\mathbf{k}|$ and the z-axis is oriented along $\mathbf{k}$ [see Fig.4.3(a)]. By definition this wave function solves the homogeneous wave equation $[\nabla^2 + k^2]\,\psi^{\rm in} = 0$. In the presence of a the potential V, the plane wave $\psi^{\rm in}$ is no longer a solution of the exact Schrödinger equation, and gives rise

[18] See e.g. §45 and §123 of Ref. [217].

to a scattered field $\psi^{\rm out}$. We assume that V has a finite range, or fall offs quickly outside a finite region of size a around the origin. In 3D, and at large distance r from the region where the amplitude of V is significant, the total wave-function $\psi = \psi^{\rm in} + \psi^{\rm out}$ is known to take the asymptotic form[19]

$$\psi \simeq {\rm e}^{{\rm i}kz} + f(k,\theta)\frac{{\rm e}^{{\rm i}kr}}{r}. \tag{4.86}$$

The function f is called the scattering amplitude. It depends on the scattering angle θ, that is, the angle between the z-axis and the direction of the scattered particle. Under the assumption that V is invariant by rotation around the z-axis, the scattering amplitude does not depend on the azimuthal angle ϕ around the z-axis. The differential cross-section ${\rm d}\sigma$ for scattering into a solid angle ${\rm d}\Omega$ around the direction (θ,ϕ) is given by ${\rm d}\sigma = |f(k,\theta)|^2{\rm d}\Omega$. In this direction, the scattered particle is locally a plane wave of wave vector $\mathbf{k}_{\rm f}$. Since the scattering is assumed to be elastic, we have $|\mathbf{k}_{\rm f}| = |\mathbf{k}|$ and $\mathbf{k}_{\rm f}.\mathbf{k} = k^2\cos(\theta)$.

For a weak potential, the scattering amplitude can be calculated in a perturbation expansion in powers of the scattering potential V. The leading-order result for the 3D case reads

$$f(\mathbf{k},\mathbf{k}_{\rm f}) = -\frac{m}{2\pi\hbar^2}\int {\rm d}\mathbf{r} V(\mathbf{r}){\rm e}^{-{\rm i}(\mathbf{k}_{\rm f}-\mathbf{k}).\mathbf{r}}. \tag{4.87}$$

This expression is simply proportional to the Fourier component $V(\mathbf{q})$, where $\hbar\mathbf{q} = \hbar(\mathbf{k}_{\rm f} - \mathbf{k})$ is the momentum transferred to the particle. The approximation made here is called the Born approximation in collision theory [308]. Its validity depends on the typical amplitude U of the potential V, the range a and the long-distance fall-off of V, the momentum $\hbar k$ of the particle, and the dimension of space. In 3D, the Born approximation usually holds if V falls off quickly enough, and any of the conditions $U \ll \hbar^2/ma^2$ or $U \ll (\hbar^2/ma^2)ka$ is satisfied [217].[20] We assume that this is the case here.

Since the first-order approximation leading to Eqs. (4.86) and (4.87) is consistent with the derivation of the effective Schrödinger equation (4.80), these results also apply upon replacement of V by $\mathcal{V}_\epsilon$ and ψ by g^+. To compare the scattering amplitudes of a BQP and a bare particle with same wave vector $\mathbf{k}$, we need only compare the Fourier components $V(\mathbf{q})$ and $\mathcal{V}_\epsilon(\mathbf{q})$, where

[19] The total field $\psi = \psi^{\rm in} + \psi^{\rm out}$ is an exact solution of the Schrödinger equation $\left[\nabla^2 + k^2\right]\psi = (2m/\hbar^2)V\psi$ if and only if $\left[\nabla^2 + k^2\right]\psi^{\rm out} = (2m/\hbar^2)V\psi$. This equation can be solved formally for $\psi^{\rm out}$ by considering the right-hand side as an inhomogeneous term, and using the Green function associated with the operator $-\nabla^2 + k^2$. Adding $\psi^{\rm int}$, this leads to the Lippmann-Schwinger equation

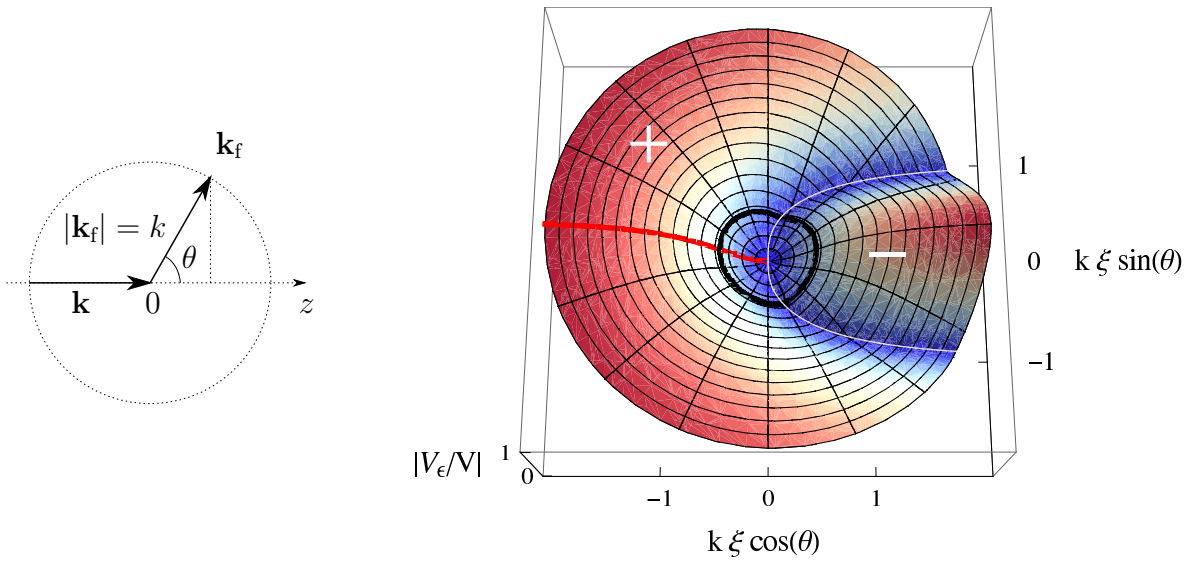
$$\psi(\mathbf{r}) = \psi^{\rm int}(\mathbf{r}) + \frac{2m}{\hbar^2}\int {\rm d}\mathbf{r}' G_k^{+,d{\rm D}}(\mathbf{r}'-\mathbf{r})V(\mathbf{r}')\psi(\mathbf{r}'),$$

with

$$G_k^{+,1{\rm D}}(\mathbf{r}) = \frac{{\rm e}^{{\rm i}k|\mathbf{r}|}}{2{\rm i}k}, \qquad G_k^{+,2{\rm D}}(\mathbf{r}) = \frac{H_0^{(1)}(k|\mathbf{r}|)}{4{\rm i}}, \qquad G_k^{+,3{\rm D}}(\mathbf{r}) = -\frac{{\rm e}^{{\rm i}k|\mathbf{r}|}}{4\pi|\mathbf{r}|},$$

where $H_0^{(1)}$ is a Hankel function of the first kind [306]. In the Born approximation, ψ is simply replaced by $\psi^{\rm int}$ under the integral. Then, the asymptotic expression for the 3D case and expression (4.87) are obtained from the far-field expansion $|\mathbf{r} - \mathbf{r}'| \simeq r - (\mathbf{r}'.\mathbf{r})/r$ in the Green function $G_k^{+,3{\rm D}}$.

[20] In 1D, the condition of validity is derived as $U \ll (\hbar^2/ma^2)ka$, and the perturbation theory breaks down at low k, where the amplitude of the scattered wave diverges as $1/k$. Note that the Born approximation defined here differs from the Born approximation of the 1D Lyapunov exponent introduced in chapter 2 in the sense that the latter approximation is of second order in the potential amplitude.



(a) Scattering process (b) Relative scattering amplitude of a Bogolyubov quasi-particle

Figure 4.3: (a) Schematic of the process of elastic scattering. (b) Relative scattering amplitude $|\mathcal{V}_\epsilon(\mathbf{k}_\mathrm{f}-\mathbf{k})/V(\mathbf{k}_\mathrm{f}-\mathbf{k})|$ of BQPs, as compared to bare particles in the same potential V, with the same initial and final wave vectors $\mathbf{k}$ and $\mathbf{k}_\mathrm{f}$. The ratio appears in polar coordinates $(k\xi,\theta)$, where $k = |\mathbf{k}| = |\mathbf{k}_\mathrm{f}|$, and θ is the BQP deflection angle ($\mathbf{k}_\mathrm{f}.\mathbf{k} = k^2\cos\theta$). The magnitude of this ratio ranges from 0 (blue, complete screening) to 1 (red, no screening). The thin white line indicates the zeros of the function. Note that the function changes sign on this line, and takes negative values in a sector of forward scattering. The radial coordinate can also be read in terms of the energy ϵ of the scattering BQP. The closed, thick black line, defined by $\epsilon/\mu = 1$ (i.e. $k\xi \simeq 0.46$), serves as guide for the eye. The red solid line corresponds to elastic backscattering ($\theta = \pi$) and represents the screening function $\mathcal{S}(k\xi)$ introduced in section 4.3.

$\mathbf{q} = \mathbf{k}_\mathrm{f} - \mathbf{k}$, and $\mathbf{k}_\mathrm{f}$ describes the final scattering state. Rewriting Eq. (4.83), we have

$$\frac{\mathcal{V}_\epsilon(\mathbf{q})}{V(\mathbf{q})} = 1 - \frac{3+\rho^2}{1+\rho^2}\frac{1}{1+(|\mathbf{q}|\xi)^2}. \tag{4.88}$$

The ratio of scattering amplitudes immediately follows as

$$\frac{\mathcal{V}_\epsilon(\mathbf{k}_\mathrm{f}-\mathbf{k})}{V(\mathbf{k}_\mathrm{f}-\mathbf{k})} = \frac{2(k\xi)^2}{1+2(k\xi)^2} \times \frac{2(k\xi)^2(1-\cos\theta)-\cos\theta}{2(k\xi)^2(1-\cos\theta)+1}, \tag{4.89}$$

where we have used the fact that $\rho^2 = 1+1/(k\xi)^2$ and $|\mathbf{k}_\mathrm{f}-\mathbf{k}|^2 = 2k^2(1-\cos\theta)$. This expression depends only on the norm k of the initial or final wave vectors, and on the scattering angle θ. The second term in the product on the r.h.s of Eq. (4.89) is the angular envelope function introduced in Ref. [309], where the angular dependence of the scattering of BQP was studied in a 2D geometry. Remarkably, this angular dependence simply derives here from the Fourier spectrum of the effective potential $\mathcal{V}_\epsilon$.

Expression (4.89) is plotted in Fig. 4.3(b). The vertical coordinate and the color code indicate the magnitude of $|\mathcal{V}_\epsilon(\mathbf{k}_\mathrm{f}-\mathbf{k})/V(\mathbf{k}_\mathrm{f}-\mathbf{k})|$, as a function of the polar coordinates $(k\xi,\theta)$. The distance from the origin of the graph represents the magnitude $k = |\mathbf{k}| = \mathbf{k}_\mathrm{f}$ of the wave vector of the BQP. The cartesian coordinates $k\xi\cos\theta$ and $k\xi\sin\theta$ represent the projections of

the final wave vector $\mathbf{k}_\mathrm{f}$ along the z-axis and an orthogonal direction. Figure 4.3(b) shows that the scattering of BQPs is suppressed at small wave vectors (low energy), in comparison with bare particles with the same wave vector. At large wave vectors (high energy), on the other hand, the ratio of BQP and bare-particle scattering amplitudes approaches one in absolute magnitude, except for a narrow angular region where its changes sign due to the interplay of the external potential and the density background of the Bose gas. The presence of this node in the angular scattering structure has been analyzed in Ref. [309]. We checked by expanding the k-dependent angular pattern in expression (4.89) on spherical harmonics that the scattering of BQPs is dominated by p-wave scattering for $k\xi \ll 1$ ($\epsilon \ll \mu$), and by s-wave scattering for $k\xi \gg 1$ ($\epsilon \gg \mu$), as discussed in Ref. [309].

In conclusion, the BQP scattering properties derived here agree with those reported in Ref. [309], and demonstrate the efficiency of the Schrödinger-like equation (4.80).

4.3 Anderson localization of Bogolyubov quasi-particles in one-dimension

We now assume that V is a weak 1D random potential, and we apply perturbation theory to calculate the Lyapunov exponent (inverse localization length) of the BQPs. Our analysis is based on the effective Schrödinger equation (4.80).

4.3.1 Phase formalism in the Born approximation

In 1D, the Lyapunov exponent γ_k of a bare particle of energy $E_k = \hbar^2 k^2/2m$ in a random potential $V(z)$ is simply related to the amplitude of backscattering from V. For a weak disorder, this exponent can be extracted from a perturbation expansion in the phase formalism discussed in chapter 2. In the lowest-order (Born) approximation, the Lyapunov exponent reads:[21]

$$\gamma_k \simeq \frac{\sqrt{2\pi}}{8k^2}\left(\frac{2m}{\hbar^2}\right)^2 C_2(2k), \tag{4.90}$$

where $C_2(q)$ is the Fourier transform of the two-point autocorrelation function $C_2(z)$ of the potential. In this formulation, $V(z)$ has a vanishing average, and k thus stands for the mean wave vector of the particle under consideration. The quantity k, rather than the related energy E_k, is the meaningful quantity in the interference effect which causes Anderson localization of the wave function in space. Applying this result to the Schrödinger-like equation (4.80), we derive the Lyapunov exponent Γ of a BQP of energy ϵ in the Born approximation:

$$\Gamma \simeq \frac{\sqrt{2\pi}}{8k^2}\left(\frac{2m}{\hbar^2}\right)^2 \mathcal{C}_\epsilon(2k), \tag{4.91}$$

where $\mathcal{C}_\epsilon(q)$ is the Fourier transform of the two-point correlator of $\mathcal{V}_\epsilon(z)$, and k is the mean wave vector, which depends on ϵ through Eq. (4.75) as we are now dealing with BQPs. From

[21] See Eq. (2.34) in section 2.2.2.

the Wiener-Khinchin theorem, we have $\mathcal{C}_\epsilon(q) \propto \langle|\mathcal{V}_\epsilon(q)|^2\rangle$, so that, according to Eq. (4.82), the relevant spectral component of $\mathcal{V}_\epsilon$ for the calculation of Γ is

$$\mathcal{V}_\epsilon(2k) = V(2k) - \frac{3+\rho^2}{1+\rho^2}\widetilde{V}^{(1)}(2k). \tag{4.92}$$

Then, inserting Eq. (4.64) into Eq. (4.92), and taking advantage of the equality $\rho^2 = 1+1/(k\xi)^2$, we obtain

$$\mathcal{V}_\epsilon(2k) = \mathcal{S}(k\xi)V(2k), \tag{4.93}$$

where

$$\mathcal{S}(k\xi) = \frac{2(k\xi)^2}{1+2(k\xi)^2}. \tag{4.94}$$

Finally, Eq. (4.91) can be rewritten as

$$\Gamma \simeq [\mathcal{S}(k\xi)]^2\gamma_k, \tag{4.95}$$

where[22]

$$\gamma_k \simeq \frac{\sqrt{2\pi}}{32}\left(\frac{V_{\rm R}}{\mu}\right)^2 \frac{\sigma_{\rm R}}{k^2\xi^4}\hat{c}_2(2k\sigma_{\rm R}). \tag{4.96}$$

Equation (4.95), together with Eqs. (4.94) and (4.96), completely determines the Lyapunov exponent of a BQP in a weak, correlated, 1D random potential.

Remarkably, Eq. (4.95) shows that the Lyapunov exponent Γ of a BQP can be simply related to the exponent of a bare Schrödinger particle with the same average wave vector k [307]. The function $\mathcal{S}(k\xi)$ which appears in the prefactor in Eq. (4.95) is plotted in Fig. 4.4. It is worth noting that $\mathcal{S}(k\xi)$ coincides with the value of expressions (4.88) and (4.89) for $\mathbf{k}_{\rm f} = -\mathbf{k}$ or, equivalently, $\theta = \pi$. Therefore, $S(k\xi)$ can be interpreted as the ratio of the backscattering amplitudes of a BQP and a bare particle with the same mean wave vector k, in the same potential. The influence of the $\mathcal{S}(k\xi)$ factor on localization properties will be discussed below.

4.3.2 Localization regimes

The combination of Eqs. (4.95) and (4.96) yields a unique expression for the Lyapunov exponent of BQPs:

$$\Gamma \simeq \frac{\sqrt{2\pi}}{8}\left(\frac{V_{\rm R}}{\mu}\right)^2 \frac{k^2\sigma_{\rm R}}{[1+2(k\xi)^2]^2}\hat{c}_2(2k\sigma_{\rm R}). \tag{4.97}$$

Expression (4.97) shows that apart from the quadratic dependence on the potential amplitude $V_{\rm R}$, which is characteristic of the Born approximation for the Lyapunov exponent, the dimensionless quantity $\Gamma\xi$ depends only on two parameters $k\xi$ and $\sigma_{\rm R}/\xi$. We recall however that this expression aggregates three distinct contributions [see Eqs. (4.95) and (4.96)]: i) a $1/k^2$ term which is representative of the kinetic energy of a bare particle, ii) the squared screening function $\mathcal{S}(k\xi)^2$, and iii) the spectral density of disorder $V_{\rm R}^2\sigma_{\rm R}\hat{c}_2(2k\sigma_{\rm R})$ at wave vector $2k$. Hereafter, we discuss the role of these various contributions.

[22] This expression derives from Eq. (4.90) with $\mu = \hbar^2/4m\xi^2$, and $\hat{c}_2$ is the Fourier transform of the reduced auto-correlation function defined in Eq. (4.58).

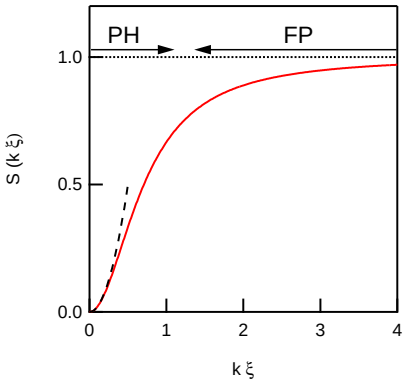


Figure 4.4: Screening function $\mathcal{S}(k\xi)$. The dashed lines show the asymptotic behaviors in the phonon [$\mathcal{S}(\epsilon) \simeq 2(k\xi)^2$ for $k\xi \ll 1$] and free-particle [$\mathcal{S}(\epsilon) \simeq 1$ for $k\xi \gg 1$] regimes.

Screening in the phonon regime

Let us first discuss the case of a white-noise potential [310], which is obtained by the limiting process $\sigma_{\rm R} \to 0$, $V_{\rm R} \to \infty$, $V_{\rm R}^2\sigma_{\rm R} = \text{const}$, in which the spectral density $\hat{c}_2$ uniformly approaches a flat distribution with an amplitude of the order of one. In this limit, the disorder spectrum plays no special role, and we are left with the competition of the $1/k^2$ and $\mathcal{S}(k\xi)^2$ terms.

Figure 4.4 shows that the magnitude of $S(k\xi)$ changes significantly depending on whether $k\xi$ is smaller or larger than one. For BQPs in a homogeneous Bose gas, this threshold corresponds to the crossover from pair excitations with a linear dispersion relation $\epsilon_k \simeq \hbar c k$ for $\epsilon_k \ll \mu$ and $k\xi \ll 1$ (phonon regime; PH) to nearly single-particle excitations with a quadratic dispersion relation $\epsilon_k \simeq E_k = (\hbar^2/2m)k^2$ for $\epsilon \gg \mu$ and $k\xi \gg 1$(free-particle regime; FP).[23] In the free-particle regime, we have $\mathcal{S} \simeq 1$ and $\Gamma \sim 1/k^2 \sim 1/\epsilon$. In other words, BQPs localize exactly like bare Schrödinger particles in this regime, as expected. In the phonon regime, on the contrary, the kinetic term is dominated by the $\mathcal{S}^2$ factor, which is approximately quartic in k (or ϵ). We then get the scaling $\Gamma \sim k^2 \sim \epsilon^2$, which is consistent with known results on the localization of acoustic phonons in 1D [65, 311].

Interestingly, Eq. (4.95) combines the two limiting models in a unified picture, and provide a physical interpretation for the decreasing localization of phonon modes with decreasing energy. The function $\mathcal{S}$ reflects the competition of the bare external potential V and the interaction of the BQPs with the quasi-BEC density background gn_0, which appears here as $\widetilde{V}$. In particular, the strong decay of $\mathcal{S}$ in the phonon regime can be interpreted as an increasing screening of the external potential by the static quasi-BEC background, which adapts to the long-wavelength modulations of the potential (see Sec. 3.3.3).

[23] See section 4.1.4.

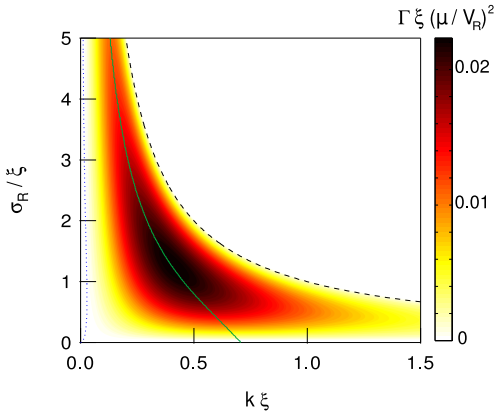


Figure 4.5: Contour plot of the Lyapunov exponent of BQPs in a speckle potential, as given by Eq. (4.100). Beyond $k\sigma_{\rm R} = 1$ (black dashed line), the Lyapunov exponent vanishes completely in the Born approximation, due to the finite support of the speckle power spectrum. The green solid line represents the wave vector of maximum localization for each ratio $\sigma_{\rm R}/\xi$. The blue dotted line encloses the region $\epsilon \lesssim \epsilon_\Delta$ (i.e. $k \lesssim k_\Delta$) discussed in section 4.4.2.

Correlated potentials

To analyze the role of the correlation length $\sigma_{\rm R}$ in Eq. (4.97), we consider a speckle potential with reduced auto-correlation function

$$c_2(u) = \sin(u)^2/u^2, \tag{4.98}$$

as in section 2.3. The Fourier spectrum of c_2, i.e. the reduced power spectrum of V, is

$$\hat{c}_2(k\sigma_{\rm R}) = \sqrt{\frac{\pi}{2}}\left(1 - \frac{k\sigma_{\rm R}}{2}\right)\Theta\left(1 - \frac{k\sigma_{\rm R}}{2}\right), \tag{4.99}$$

where Θ is the Heaviside step function, so that Eq. (4.97) reads

$$\Gamma \simeq \frac{\pi}{8}\left(\frac{V_{\rm R}}{\mu}\right)^2 \frac{k^2\sigma_{\rm R}(1-k\sigma_{\rm R})}{[1+2(k\xi)^2]^2}\Theta(1-k\sigma_{\rm R}). \tag{4.100}$$

This expression is plotted in Fig. 4.5. Correlation, that is, the finiteness of $\sigma_{\rm R}$, introduces several features we now comment on.

Effective mobility edge - Equation (4.100) shows that the Lyapunov exponent Γ_ϵ vanishes identically for $k\sigma_{\rm R} > 1$ (see also Figs. 4.5 and 4.6). This feature originates from the special correlation properties of speckle potentials, the power spectrum of which has a high-momentum cutoff [see Eq. (4.99)]. Because of this cutoff, the power spectrum contains no $2k$ component able to backscatter a wave travelling with wave vector $k > 1/\sigma_{\rm R}$ according to the process $+k \to -k$ in the Born approximation [34]. Higher-order terms in the expansion are expected to carry contributions to γ_k and Γ which do not all vanish identically for $k\sigma_{\rm R} > 1$, but their larger power dependence on the small parameter $V_{\rm R}/\mu$ makes them negligible for our purposes.

As a matter of fact, the third-order contribution to Γ, proportional to $V_{\rm R}^3$, can be shown to vanish abruptly for momenta above the same cutoff at $1/\sigma_{\rm R}$, so that corrections to Eq. (4.100) beyond that cutoff scale as $V_{\rm R}^4$ at least.[24] Hence, we recover for BQPs the physics of effective mobility edges discussed for pure Schrödinger particles in chapter 2. This behavior is specific to potentials with cutoffs in their Fourier-transformed correlation functions [34, 182, 219, 220, 222].

Localization maxima - In the white-noise limit, the BQPs localize best for $k\xi = 1/\sqrt{2}$ (i.e. $\epsilon = \sqrt{3}\mu$), that is, in the crossover region between the phonon and the free-particle regime [310]. This behavior results from the competition of bare kinetic energy and mean-field interactions via the screening effect, as discussed above. With correlations, however, the detailed statistical properties of the disorder enter the competition as well. In model (4.99), the wave vector of maximum localization $k_{\rm max}$ decreases with increasing correlation length $\sigma_{\rm R}$. More generally, it can be checked from Eq. (4.97) that for any correlated disorder with monotonously decreasing power spectrum akin to model (4.99), the wave vector of maximum localization is shifted to lower values than the corresponding white-noise value. The locus of $k_{\rm max}$ as a function of the correlation and the healing lengths is plotted in green in Fig. 4.5. For each $\sigma_{\rm R}/\xi$ ratio, we indeed find a unique maximum $k_{\rm max}$ with

$$k_{\rm max} \simeq \frac{1}{\sqrt{2}\,\xi}\left(1 - \frac{\sigma_{\rm R}/\xi}{2\sqrt{2}}\right), \qquad \sigma_{\rm R} \ll \xi, \tag{4.101}$$

$$k_{\rm max} \simeq \frac{2}{3\,\sigma_{\rm R}}, \qquad \sigma_{\rm R} \gg \xi. \tag{4.102}$$

These asymptotic expressions show that $k_{\rm max}$ is controlled by the longest length scale in the problem. Finally, we find an absolute maximum at fixed ξ for $\sigma_{\rm R} = \sqrt{3/2}\,\xi$ and $k\xi = 1/\sqrt{6}$, which yields a localization length

$$L_{\rm max}(\xi) = \Gamma^{-1}_{\rm max}(\xi) = \frac{512\sqrt{6}}{9\pi}\left(\frac{\mu}{V_{\rm R}}\right)^2 \xi. \tag{4.103}$$

Current experiments with ultracold atoms implement random potentials with correlation lengths of the order of $\sigma_{\rm R} \simeq 0.25\mu$m [29, 31, 172], which yields $L_{\rm max} \simeq 230\mu$m for $V_{\rm R} = 0.2\mu$. Since this value can be of the order of or even smaller than the system size, we conclude that localization of BQPs in ultracold (quasi-) BECs is relevant for present-day experiments. It remains to be determined whether the localization length of BQPs could be measured, for instance, in Bragg spectroscopy experiments [266, 312–315]. The localization of BQP modes in coordinate space implies a broadening of the dynamic structure factor $S(\omega, \mathbf{q})$ [249, 316]. Further studies would be required to assess other sources of broadening (as e.g. the finite size of the system, the finite life-time of the quasi-particles, the finite duration of the Bragg pulse,...).

4.3.3 Validity of the leading-order result

Before turning to some numerical tests, let us review the validity conditions of the leading-order result discussed above. The result (4.95) requires (i) the first-order smoothing solution which consists in replacing $\widetilde{V}$ by $\widetilde{V}^{(1)}$ in Eq. (4.59), (ii) the first-order decoupling of the g^+

[24] See section 4.4.3.

and g^- modes that leads to Eq. (4.80), and (iii) the Born approximation (4.90) to be valid. A *weak disorder* condition $\widetilde{V}_{\rm R} \ll \mu$ alone ensures (i) and (ii). Note that this condition of weak disorder imposes a less stringent criterion on the bare potential V (i.e. on the ratio $V_{\rm R}/\mu$), since smoothing reduces the amplitude of $\widetilde{V}$ with respect to V. As for requirement (iii), the regime of validity of the Lyapunov exponent derived for *bare Schrödinger particles* in a weak-disorder expansion is in itself a subtle issue, as the successive terms in the perturbation series all depend on the disorder amplitude and the kinetic energy of the particle. The resulting asymptotic series is well-behaved in the high-energy limit. A precise inspection of the low-energy limit (see e.g. Ref. [207]), where the terms of the series blow up, is necessary to exhibit a rigorous criterion of validity for a truncated perturbation expansion. For single particles, $\gamma_k \ll k$ is usually retained as a satisfactory criterion (see Ref. [86] and the end of section 2.2.3). In physical terms, this inequality means that the localization length should exceed the typical wavelength of the particle. This sets a $V_{\rm R}$-dependent lower bound on the single-particle energies for which the perturbative result is meaningful. Translating the above criterion to BQPs ($\Gamma \ll k$), we obtain

$$\frac{V_{\rm R}}{\mu}\sqrt{\frac{\sigma_{\rm R}}{\xi}}\sqrt{\hat{c}(2k\sigma_{\rm R})} \ll (k\xi)^{3/2} + \frac{1}{2(k\xi)^{1/2}}. \tag{4.104}$$

This validity condition resembles the corresponding one for Schrödinger particles, namely $(V_{\rm R}/\mu)\sqrt{\sigma_{\rm R}/\xi}\sqrt{\hat{c}(2k\sigma_{\rm R})} \ll (k\xi)^{3/2}$, which is derived from expression (4.96). As expected, the two coincide in the FP regime ($k \gg 1/\xi$). However, they differ significantly in the PH regime ($k \ll 1/\xi$). Indeed, for free particles, perturbation theory always breaks down at low energy (i.e. $k \to 0$). In contrast, for BQPs in the PH regime, the strong screening of the random potential leads to a completely different condition: $(V_{\rm R}/\mu)\sqrt{\sigma_{\rm R}/\xi}\sqrt{\hat{c}(2k\sigma_{\rm R})} \ll 1/(k\xi)^{1/2}$. The latter is always valid at low energy, under the assumption e.g. that $\hat{c}(2k\sigma_{\rm R})$ is bounded for $k \to 0$. We thus find that the validity condition (4.104) is easily satisfied on the whole spectrum by a potential that is weak enough, i.e. for $(V_{\rm R}/\mu)\sqrt{(\sigma_{\rm R}/\xi)} \ll 1$.

4.3.4 Numerical calculations

In order to test the accuracy of the perturbative approach introduced in this section, we performed numerical calculations of the Lyapunov exponent of BQPs in a 1D speckle potential, for various $\sigma_{\rm R}/\xi$ ratios (see Fig. 4.6). We briefly outline the numerical procedure below. The speckle potential is produced as explained in chapter 1. We focus here on the computation of the GPE ground state and Bogolyubov excitations, and the extraction of the Lyapunov exponent.

In a first step, we determined the ground-state solution n_0 of the GPE (4.48), using propagation in imaginary time with a Crank-Nicholson scheme [317,318]. As a precise determination of $n_0(z)$ is required for a correct calculation of the low-energy eigenmodes of the BdGEs (4.49) and (4.50), we compared the result of this procedure with a smoothing expansion including up to ten perturbation orders (see appendix E). The values of Δ computed with the two methods for $\sigma_{\rm R} = \sqrt{3/2}\,\xi$ agreed within a relative difference $\delta\Delta/\Delta$ of 0.3% for $V_{\rm R} = 0.05$ and 3% for $V_{\rm R} = 0.20$, while the r.m.s. difference of the computed density profiles typically amounted to a few $10^{-4}V_{\rm R}/g$ and $10^{-2}V_{\rm R}/g$ respectively. Periodic boundary conditions were used to avoid corrections to the equation of state solely due to kinetic terms at the boundaries of the system.

In a second step, the BdGEs (4.49) and (4.50) were solved for eigen-energies and eigenmodes. The density profile $n_0(z)$ obtained numerically was included in the exact BdGEs (4.49) and (4.50), and the associated differential operator was put in a discretized form in a one-dimensional box with zero Dirichlet boundary conditions (see comment below). Eigenvalues and eigenvectors of the resulting large, non-Hermitian band matrices were obtained for a limited set of target energies using the MATLAB software, and the underlying standard ARPACK routines. Diagonalization was preferred over open-end transfer-matrix calculations, or traditional methods for boundary-value problems, like shooting [319], as the propagation by a first-order differential operator $\xi\partial_z$ or a second-order operator $\xi^2\partial_z^2$, as described in appendix G, leads to an exponential divergence on the length scale of a few healing lengths due to the coupling into evanescent modes.

Despite the large system size of up to 2×10^6 discretization steps, the "diagonalization" routines proved efficient for band matrices with 4 or 6 diagonals (depending on the ordering of the BQP components), as used to represent the Bogolyubov differential operator with zero Dirichlet boundary conditions.[25] Periodic boundary conditions increase the number of diagonals to 8 or 10, respectively. In this case, the same routines required much more computational resources, and eigenstates could be computed only at the expense of losing several (typically two or three) orders of magnitude in the achievable system size. As large systems are needed for a precise numerical estimate of the Lyapunov exponent, zero Dirichlet boundary conditions were preferred. These boundary conditions are not strictly consistent with those imposed on the ground-state density. We checked that this choice had no noticeable effect on the eigenstates with quasi-particle energies down to $10^{-3}\mu$, in a periodic potential with similar amplitude and length scales as those of the speckle potential.

Finally, the Lyapunov exponent Γ of a BQP mode was obtained by computing estimators of

$$-\lim_{z\to\infty} \frac{\langle \ln[r(z)/r(z_0)]\rangle}{|z-z_0|}, \tag{4.105}$$

where $r = \sqrt{f^2 + (\partial_z f)^2/k^2}$ (see section 2.2.1), and the real-valued function f under scrutiny was chosen as f^+ for simplicity. We checked that, exchanging f^+ for the other eigenvector component f^-, or the derived functions $g^\pm$, the results agreed within 5% for all the parameters in this study, including the low-energy limit. In expression (4.105), the value z_0 is the position of the localization center, which varies from eigenstate to eigenstate. The disorder average was performed over 200 randomly generated speckle patterns, and the box size was chosen large enough (of the order of 10^5 correlations length) so as to approach the stationary distribution of the logarithm at infinity in the far wings of the computed eigenfunctions, for a wide range of $\sigma_{\rm R}/\xi$ and $k\xi$ parameters altogether.

The numerical data shown in Fig. 4.6 are in good agreement with the predictions of Eq. (4.100), plotted in solid lines. Even for $V_{\rm R}/\mu = 0.05$, as used in this figure, result (4.100) is in excellent qualitative and fair quantitative agreement with the numerical data on the whole spectral range studied here, which spans the phonon regime and the transition to the free-particle regime. As shown in the figure, the observable discrepancies can be attributed mostly to fluctuation terms which contribute to the exact Lyapunov exponent Γ beyond the second

[25] Working with 6 diagonals decreases the number of zeros on the "significant" diagonals of the matrix. This saves storage space. The efficiency of the diagonalization procedure, however, does not significantly depend on this choice.

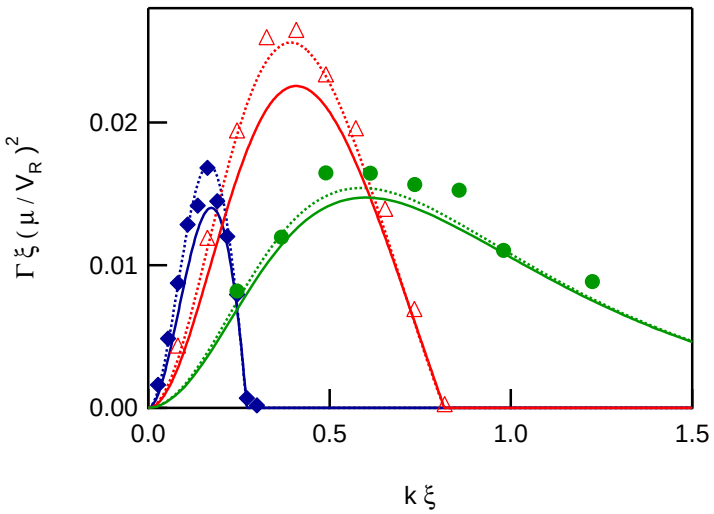


Figure 4.6: Numerical calculation of the Lyapunov exponent of BQPs in a speckle potential for $\sigma_R = 3.7\,\xi$ (blue diamonds), $\sigma_R = \sqrt{3/2}\,\xi$ (red open triangles), and $\sigma_R = 0.4\,\xi$ (green dots), and $V_R/\mu = 0.05$. The solid lines are given by Eq. (4.100), and the dashed lines to small corrections of the order of V_R^3 (see text).

order in V_R. The dashed lines in the figure are discussed in section 4.4.3. These contributions do not change overtly the qualitative behavior of the Lyapunov exponent Γ. In the numerical study, these contributions show up because of the intermediate values of V_R/μ which we have used.[26] The choice of V_R/μ was motived by experimental relevance and numerical tractability for an entire set of σ_R/ξ and $k\xi$ parameters. These fluctuation corrections to Γ are expected to be negligible for lower V_R/μ. At any rate, these numerical results validate our perturbative approach.

4.4 Beyond the Born approximation

4.4.1 Discussion

In section 4.2, simplified equations for the coherence factors of the BQPs were obtained by introducing auxiliary functions g^+ and g^-, and by developping a first-order perturbation theory in the potential amplitude V_R. Carried out at this order, the procedure allowed the oscillating $g^+(\mathbf{r})$ functions to be completely decoupled from the evanescent $g^-(\mathbf{r})$, and the exact density background $n_0(\mathbf{r})$ of the Bose gas to be replaced by a first-order approximation.

In section 4.3, this approach was applied to the problem of Anderson localization of BQPs in a 1D geometry. It was shown that for the BQPs of low energy ϵ, in the phonon regime, the disorder is strongly screened by the mean-field interactions, and that the Lyapunov exponent Γ of

[26] Note that the small deviations from Eq. (4.100) which appear in the data of Ref. [307] are smaller than those of the present work, for comparable parameters. The present results are actually more acurate, as only a lowest-order smoothing expansion was used to compute the density n_0 in Ref. [307].

BQPs drops to zero for $\epsilon \to 0$.[27] This result, derived in the framework of the Born approximation for the Lyapunov exponent, is in stark contrast with the case of bare Schrödinger particles. For those bare particles, the Born approximation and higher-order perturbation terms of the Lyapunov exponent diverge in the limit of vanishing energy. For BQPs, the $1/k^2$ divergence of the bare-particle exponent in the Born approximation is dominated by the quartic dependence of the screening factor $\mathcal{S}(k\xi)^2$ in the limit $k \to 0$. One might wonder whether such a screening persists at all individual orders of the perturbation expansion of the Lyapunov exponent Γ, or whether the screening in the leading-order result is only accidental, and hides divergences of individual higher orders. From the bare-particle case, we know that this can be the case although the exact result is finite (as opposed to infinite) for $k = 0$ [207], and one might wonder whether the low-energy properties of BQPs are, likewise, non-trivial.

This question also arises for the excitation spectrum. In a potential which is bounded below, the density of states of bare particles is known to take the non-perturbative form of a Lifshits tail at the bottom of the spectrum (see chapter 3). For BQPs, the effective potential $\mathcal{V}_\epsilon$ derived in the first-order perturbation theory has a vanishingly small effect on quasi-particles with energy ϵ approaching zero (in the leading-order scattering theory at least; see Fig. 4.3(b) in this respect), so that the bottom of the spectrum is unlikely to be dominated by those rare events in the potential which give rise to a Lifshits tail.[28]

The consideration of the spectrum and the strength of localization of elementary excitations is of prime importance for the characterization of the disordered Bose gas. Deviations both from the $\Gamma \propto \epsilon^2$ dependence of the Lyapunov exponent and from a constant density of states at low energy have been reported in Refs. [244, 289] for the regime of strong disorder, close to the transition of the weakly-interacting Bose gas from superfluid to insulator. In the following section, we shall simply examine some features which arise one step beyond the leading-order perturbation theory.

4.4.2 Decoupling beyond the first-order approximation

Equation (4.80) is obtained from the BdGE (4.73) by keeping only the potential terms which are of first order in $V_{\rm R}$. For the description of the scattering and localization of BQPs beyond the Born approximation on the basis of such a Schrödinger-like equation, higher-order terms in Eq. (4.73) need to be considered as well, so as to keep track consistently of all terms of the same order.

Schrödinger-like equation

We revisit here the approximation of Eq. (4.73) by Eq. (4.80) to include second-order terms. It turns out (see appendix G) that a new Schrödinger-like equation for g^+, which contains all

[27] See Eq. (4.97). We assume again that $\hat{c}_2(2k\sigma_{\rm R})$ is bounded when $k \to 0$. Note also that this result is consistent with a hand-waving continuity argument, based on the observation that the extended ground-state density profile which solves the GPE is also a solution of the BdGEs for zero energy.

[28] Taking the limit $\epsilon \to 0$ in Eq.(4.81), we are left with $V(\mathbf{r}) - \widetilde{V}^{(1)}(\mathbf{r})$, a potential with suppressed *long*-wavelength components. The rare, wide potential wells hosting the lowest Lifshits states should therefore also be suppressed.

the next order terms, can be derived for BQPs of low energy, such that $k \ll \min(1/\sigma_{\rm R}, 1/\xi)$.[29] This equation takes the form

$$\frac{\hbar^2 k^2}{2m} g^+ \simeq -\frac{\hbar^2}{2m}\nabla^2 g^+ + \left[\mathcal{V}_\epsilon(\mathbf{r}) + \mathcal{V}_n(\mathbf{r}) + \mathcal{V}_-(\mathbf{r})\right] g^+, \tag{4.106}$$

where $\mathcal{V}_\epsilon$ is the screened potential (4.81), and $\mathcal{V}_n$ and $\mathcal{V}_-$ are potentials proportional to $V_{\rm R}^2$:

$$\mathcal{V}_n(\mathbf{r}) = -\frac{3+\rho^2}{1+\rho^2}\left[\widetilde{V}^{(2)}(\mathbf{r}) + \Delta^{(2)}\right] \tag{4.107}$$

$$\mathcal{V}_-(\mathbf{r}) = -\frac{8m\rho^2}{\hbar^2\beta^2\left(1+\rho^2\right)^2}\int \mathrm{d}\mathbf{r}' G_{1/\beta}(\mathbf{r}-\mathbf{r}')\widetilde{V}^{(1)}(\mathbf{r})\widetilde{V}^{(1)}(\mathbf{r}'). \tag{4.108}$$

The potential term $\mathcal{V}_n$ follows from a second-order expansion of the ground-state density profile, and $\mathcal{V}_-$ originates from the coupling between g^+ and g^-.

Kinetic term (phase formalism)

In constrast to $\mathcal{V}_\epsilon$, the potentials $\mathcal{V}_n$ and $\mathcal{V}_-$ do not have a vanishing average. Equation (4.107), for instance, displays an offset proportional to $\Delta^{(2)}$. We define $\mathcal{V}_n' = \mathcal{V}_n - \langle\mathcal{V}_n\rangle$ and $\mathcal{V}_-' = \mathcal{V}_- - \langle\mathcal{V}_-\rangle$ as the fluctuations of $\mathcal{V}_n$ and $\mathcal{V}_-$ around their mean. Then, Eq. (4.106) rewrites

$$\frac{\hbar^2 k'^2}{2m} g^+ \simeq -\frac{\hbar^2}{2m}\nabla^2 g^+ + \left[\mathcal{V}_\epsilon(\mathbf{r}) + \mathcal{V}_n'(\mathbf{r}) + \mathcal{V}_-'(\mathbf{r})\right] g^+, \tag{4.109}$$

where $\hbar^2 k'^2/2m$ is build to absorb the averages $\langle\mathcal{V}_n\rangle$ and $\langle\mathcal{V}_-\rangle$. Its expression is worked out as

$$\frac{\hbar^2 k'^2}{2m} = \frac{\hbar^2 k^2}{2m} - \frac{3+\rho^2}{1+\rho^2}\Delta^{(2)} + \frac{\epsilon^2}{2\mu}D^{(2)}(\epsilon), \tag{4.110}$$

where k still follows the definition (4.75), and $D^{(2)}(\epsilon)$ is the offset term

$$D^{(2)}(\epsilon) = \frac{16m\mu\rho^2}{\hbar^2\beta^2\epsilon^2\left(1+\rho^2\right)^2}\int \mathrm{d}\mathbf{r} G_{1/\beta}(\mathbf{r})\langle\widetilde{V}^{(1)}(\mathbf{0})\widetilde{V}^{(1)}(\mathbf{r})\rangle. \tag{4.111}$$

The function $D^{(2)}(\epsilon)$ is proportional to $(V_{\rm R}/\mu)^2$. It depends on the model of potential and the ratio $\sigma_{\rm R}/\xi$, and tends to a finite value when $\epsilon \to 0$. The $\Delta^{(2)}$ term has been documented in section 4.2.1.

Since $\langle\mathcal{V}_\epsilon\rangle = \langle\mathcal{V}_n'\rangle = \langle\mathcal{V}_-'\rangle = 0$, expression (4.110) is identified as the average kinetic term $\langle -\hbar^2\nabla^2 g^+/2mg^+\rangle$ in the second-order Schrödinger-like equation for g^+, and k' appears as the corresponding average "wave vector". The quantities $\hbar^2 k'^2/2m$ and k' differ slightly from their counterparts $\hbar^2 k^2/2m$ and k, which hold in the homogeneous case and in the first-order approach. In particular, $\hbar^2 k'^2/2m$ also depends on the amplitude of the bare potential V. The values of k'^2 and k^2 as a function of energy are shown in Fig. 4.7 for a weak random potential. The difference between the two functions is visible only on a small energy interval at the bottom of the BQP spectrum, displayed in the inset.

[29] This equation might actually cover the whole BQP spectrum with good accuracy. See in this respect the end of section 4.4.3 below.

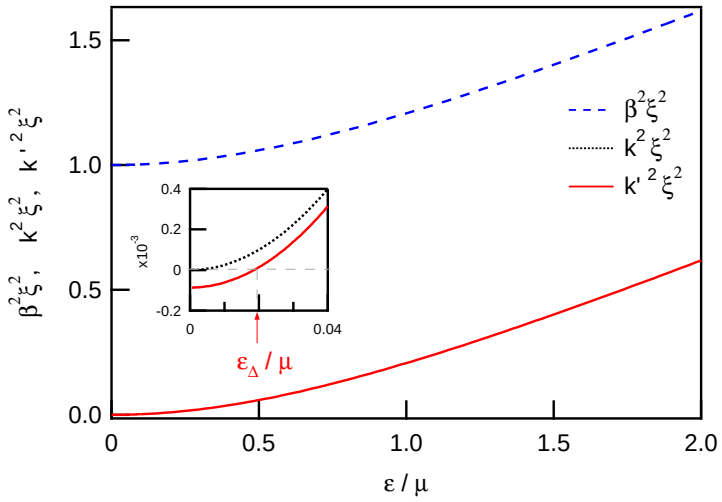


Figure 4.7: Values of k'^2 (solid red line) and k^2 (black dotted line) as a function of the BQP energy ϵ, for a speckle potential with $V_{\rm R} = 0.05\mu$ and $\sigma_{\rm R}/\xi = \sqrt{3/2}$ (and hence $\Delta \simeq 1.7{\times}10^{-4}\mu$). The value of β^2 (blue dashed line) is shown for comparison. The inset shows the low-energy region around $\epsilon_\Delta \simeq 0.02\mu$.

Remark Note that the kinetic term $\langle -\hbar^2\nabla^2\psi/2m\psi\rangle$ used in the phase formalism differs from the actual kinetic energy $-(\hbar^2/2m)\int \psi^*\nabla^2\psi$. In particular, it can be shown that only *some* of the terms in Eq. (4.110) correspond to a renormalization of the kinetic energy. The phase formalism nevertheless isolates $\langle -\hbar^2\nabla^2\psi/2m\psi\rangle$ as the relevant quantity which determines the oscillatory behavior and the localization of a wave function ψ.

In the low-energy limit, the last term in Eq. (4.110) becomes negligible even compared to $\Delta^{(2)}$, and we obtain the low-energy and small-$V_{\rm R}$ expansion [see Eq. (G.34) in appendix G]

$$\frac{\hbar^2 k'^2}{2m} \simeq -\Delta^{(2)} + \frac{\epsilon^2}{2\mu}, \tag{4.112}$$

where, according to Eqs. (4.66) and (4.67),

$$\Delta^{(2)} = \frac{V_{\rm R}^2\sigma_{\rm R}^d}{2(2\pi)^{d/2}\mu}\int {\rm d}\mathbf{q}\frac{(|\mathbf{q}|\xi)^2\hat{c}_2(\mathbf{q}\sigma_{\rm R})}{[1+(|\mathbf{q}|\xi)^2]^2}. \tag{4.113}$$

In this expression (4.112), $\Delta^{(2)}$ can be replaced by Δ for simplicity. We introduce the energy

$$\epsilon_\Delta = \sqrt{2\mu\Delta} \tag{4.114}$$

which, for $V_{\rm R} < \mu$, compares with other energy scales as shown in Fig. 4.8. For $\epsilon \gg \epsilon_\Delta$, the quantity $\hbar^2k'^2/2m$ need not be distinguished from $\hbar^2k^2/2m$ (see Fig. 4.7). For $\epsilon \lesssim \epsilon_\Delta$, on the other hand, $\hbar^2k'^2/2m$ becomes negative. This implies that, for BQPs in this limit of the spectrum, the regions of space where $g^+(\mathbf{r})$ decays or grows exponentially, possibly alternatively, should exceed in volume those regions where $g^+(\mathbf{r})$ accumulates phase. From the consideration of cases without disorder, e.g. bare Schrödinger particles in a periodic potential, we know that

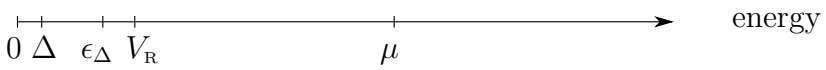


Figure 4.8: Ordering of the energy scales appearing in this chapter, for a weak potential of root-mean-square amplitude $V_{\rm R} \ll \mu$, where μ is the chemical potential of the Bose gas. The deviation Δ from the homogeneous equation of state is introduced in section 4.2.1, and the energy ϵ_Δ is defined in Eq. (4.114). The BQP energies ϵ span the whole positive axis.

this does *not* generally imply the presence of a gap in the spectrum, or localization.[30] In particular, it should be emphasized that Eq. (4.112) is *not* a dispersion relation. On the other hand, Schrödinger particles are usually strongly localized when their average kinetic energy is small or negative. It is therefore useful to examine the origin and the possible implications of the energy scale ϵ_Δ.

Here, the potential is indeed random, but we can argue that $\hbar^2 k'^2/2m < 0$ should not be taken as an indication of a localization of the BQPs, and should instead be related to the form of the GPE ground state, which is extended. We recall that $\hbar^2 k'^2/2m$ stands for the average value of $-\hbar^2\nabla^2 g^+/(2mg^+)$ in Eq. (4.106), which is a second-order approximation of the BdGE (4.73) in powers of $V_{\rm R}$. Taking the limit $\epsilon \to 0$ in Eq. (4.73), we find[31]

$$\left[-\frac{\hbar^2\nabla^2}{2m} + V + gn_0 - \mu\right] g_0^+ = 0. \tag{4.115}$$

In this limit, the function g^+ coincides with the GPE solution $\sqrt{n_0}$. Now, using the second-order approximation $gn_0 - \mu \simeq \Delta^{(2)} - \widetilde{V}^{(1)} - \widetilde{V}^{(2)}$ and taking the spatial average of Eq. (4.115) with $\langle V\rangle = \langle\widetilde{V}^{(1)}\rangle = \langle\widetilde{V}^{(2)}\rangle = 0$, we obtain

$$\left\langle \frac{-\hbar^2\nabla^2\sqrt{n_0}}{2m\sqrt{n_0}} \right\rangle = \left\langle \frac{-\hbar^2\nabla^2 g_0^+}{2mg_0^+} \right\rangle \simeq -\Delta^{(2)}. \tag{4.116}$$

Hence, a negative kinetic term does not necessarily imply a large Lyapunov exponent. This statement is true for ground-state $\sqrt{n_0} = g_0^+$ (which solves the non-linear GPE and has a vanishing Lyapunov exponent), and might be extended to regular BQP modes with small energy $\epsilon > 0$, in a hand-waving continuity argument.

4.4.3 Lyapunov exponent in one dimension

We apply the 1D phase formalism of chapter 2 to the Schrödinger-like equation (4.106) for g^+, and retain the terms up to order $V_{\rm R}^3$ in the expression of the Lyapunov exponent. Using Eqs. (2.34) and (2.79), we obtain

$$\Gamma \simeq \Gamma^{(2)}_{\mathcal{V}_\epsilon,\mathcal{V}_\epsilon} + \Gamma^{(3)}_{\mathcal{V}_\epsilon,\mathcal{V}_n} + \Gamma^{(3)}_{\mathcal{V}_\epsilon,\mathcal{V}_-} + \Gamma^{(3)}_{\mathcal{V}_\epsilon,\mathcal{V}_\epsilon,\mathcal{V}_\epsilon} \tag{4.117}$$

[30] Particles near the bottom of the first Bloch band, with energy below the mean value of the periodic potential, have a negative "kinetic term". They are nevertheless described by extended Bloch waves. Their *pseudo-momentum* should be distinguished from $\hbar k'$.

[31] For $\epsilon \to 0$, we have $k \to 0$ and $\rho \to \infty$. We use $\widetilde{V} - \Delta = \mu - gn_0$, which follows from the definition (4.59).

where

$$\Gamma^{(2)}_{\mathcal{V}_\epsilon,\mathcal{V}_\epsilon} = \frac{1}{4}\left(\frac{2m}{\hbar^2 k}\right)^2 \int_{-\infty}^{0} \mathrm{d}z_1 \langle \mathcal{V}_\epsilon(0)\mathcal{V}_\epsilon(z_1)\rangle \cos(2kz_1) \tag{4.118}$$

$$\Gamma^{(3)}_{\mathcal{V}_\epsilon,\mathcal{V}_n} = \frac{1}{4}\left(\frac{2m}{\hbar^2 k}\right)^2 \int_{-\infty}^{0} \mathrm{d}z_1 \big[\langle \mathcal{V}_\epsilon(0)\mathcal{V}_n(z_1)\rangle + \langle \mathcal{V}_n(0)\mathcal{V}_\epsilon(z_1)\rangle\big] \cos(2kz_1) \tag{4.119}$$

$$\Gamma^{(3)}_{\mathcal{V}_\epsilon,\mathcal{V}_-} = \frac{1}{4}\left(\frac{2m}{\hbar^2 k}\right)^2 \int_{-\infty}^{0} \mathrm{d}z_1 \big[\langle \mathcal{V}_\epsilon(0)\mathcal{V}_-(z_1)\rangle + \langle \mathcal{V}_-(0)\mathcal{V}_\epsilon(z_1)\rangle\big] \cos(2kz_1) \tag{4.120}$$

$$\Gamma^{(3)}_{\mathcal{V}_\epsilon,\mathcal{V}_\epsilon,\mathcal{V}_\epsilon} = -\frac{1}{4}\left(\frac{2m}{\hbar^2 k}\right)^3 \int_{-\infty}^{0} \mathrm{d}z_1 \int_{-\infty}^{z_1} \mathrm{d}z_2 \langle \mathcal{V}_\epsilon(0)\mathcal{V}_\epsilon(z_1)\mathcal{V}_\epsilon(z_2)\rangle \sin(2kz_2). \tag{4.121}$$

The exponents (4.118) and (4.121) follow from a simple application of the formulas found for Schrödinger particles to the potential $\mathcal{V}_\epsilon$, which is first order in V_R. The term $\Gamma^{(2)}_{\mathcal{V}_\epsilon,\mathcal{V}_\epsilon}$ is equal to the Lyapunov exponent (4.91) found in the Born approximation for BQPs. The contributions (4.119) and (4.121) also correspond to the Born approximation of the phase formalism for Schrödinger particles. Here they involve the two-point cross-correlators between $\mathcal{V}_\epsilon$, $\mathcal{V}_n$ and $\mathcal{V}_-$ which arise in the expansion of the two-point autocorrelation function of the complete potential of Eq. (4.106).

For the derivation of the Lyapunov exponent (4.117), we started from Eq. (4.106). In this equation, the potential does not have zero average, and k is not the average wave vector. In principle, the standard phase formalism should be applied to Eq. (4.109) instead, and k, $\mathcal{V}_n$ and $\mathcal{V}_-$ should be replaced by k', $\mathcal{V}'_n$ and $\mathcal{V}'_-$ in expressions (4.118) to (4.121). Here we take advantage of the fact that, when using k, $\mathcal{V}_n$ and $\mathcal{V}_-$, the error made on the Lyapunov exponent should be proportional to V_R^4, i.e. beyond the scope of the present calculation. Indeed, if V_A and V_B are two potentials with zero mean, and δ_A and δ_B are offsets, then we have $\langle (V_A+\delta_A)(V_B+\delta_B)\rangle = \langle V_A V_B\rangle + \delta_A\delta_B$, and the error made on a the two-point correlator scales as $\delta_A\delta_B$. In the case of $\mathcal{V}_n$ and $\mathcal{V}_-$, the offsets are proportional to V_R^2, and we may argue that errors made in any of the expressions (4.118) to (4.121) is of fourth order at least.[32]

Remarkably, all the contributions to the Lyapunov exponent (4.117) can be expressed as functions of the correlation functions of the bare potential V, by going to Fourier space. The resulting expressions are cumbersome, but share generic features. While the second-order term $\Gamma^{(2)}_{\mathcal{V}_\epsilon,\mathcal{V}_\epsilon}$ satisfies

$$\Gamma^{(2)}_{\mathcal{V}_\epsilon,\mathcal{V}_\epsilon} \propto \left(\frac{V_\mathrm{R}}{\mu}\right)^2 \frac{\sigma_\mathrm{R}}{k^2\xi^4} \left[\mathcal{S}(k\xi)\right]^2 \hat{c}_2(2k\sigma_\mathrm{R}), \tag{4.122}$$

where $\mathcal{S}(k\xi)$ is the screening factor defined in Eq. (4.94) and shown in Fig. 4.4, and $\hat{c}_2$ is the Fourier transform of the reduced two-point correlator of the *bare* potential, the third-order terms all follow

$$\Gamma^{(3)} \propto \left(\frac{V_\mathrm{R}}{\mu}\right)^3 \frac{\sigma_\mathrm{R}^{\alpha+1}}{k^{\alpha+2}\xi^{2\alpha+4}} \mathcal{S}(k\xi) \int \mathrm{d}q\, F(q) \hat{c}_3(q, 2k\sigma_\mathrm{R}) \tag{4.123}$$

where $\alpha \in \{0,1\}$, $F(q)$ is some function or distribution parametrized by the energy ϵ, and $\hat{c}_3$ is the Fourier transform of the reduced three-point correlation function. For simplicity, we have

[32] The argument may need to be made rigorous by a careful inspection of the perturbation expansion. Here we assume that the argument is valid.

assumed that the bare potential V is isotropic. This form resembles the bare-particle result

$$\gamma_{\rm iso}^{(3)} = -\frac{1}{32}\left(\frac{V_{\rm R}}{\mu}\right)^3 \frac{\sigma_{\rm R}^2}{k^3\xi^6}\int {\rm d}q \frac{\hat{c}_3(q,2k\sigma_{\rm R})}{q} \tag{4.124}$$

derived from Eq. (2.99) with $\hat{c}_3(q_1,q_2) = \hat{c}_3(-q_1,-q_2)$. In particular, from expression (4.123) we deduce that all third-order contributions vanish identically if the bispectrum $\hat{c}_3$ of the bare potential has a finite support, as in the bare-particle case.

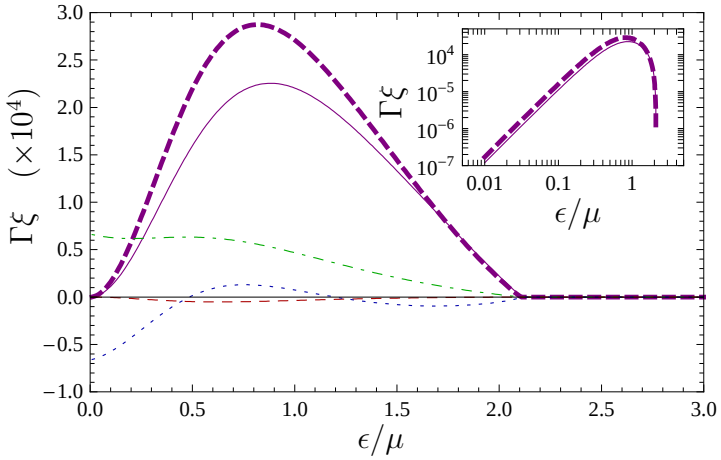
Figure 4.9 displays the result of a numerical evaluation of formula (4.117) for a speckle potential with field-field correlator $c_a(u) = \sin(u)/u$ (see section 2.3.2), and various correlation lengths $\sigma_{\rm R}$.[33] The third-order Lyapunov exponent indeed drops to zero at a critical energy corresponding to $k\sigma_{\rm R} = 1$. Qualitatively, this Lyapunov exponent behaves like the Born approximation shown in thin solid line. In particular, as shown in the inset, the Lyapunov exponent still has a dependence $\Gamma \sim \epsilon^2$ for $\epsilon \to 0$. The contribution stemming from the coupling of g^+ and g^-, shown in red dashed line, appears to be much smaller than all the other third-order contributions, and supports the idea that the decoupling of g^+ and g^- is indeed a legitimate approach. It also suggests that the effective potential (4.106), which has been derived on the basis of a low-energy approximation of the coupling between g^+ and g^- (see appendix G), might be accurate to second order in $V_{\rm R}$ over the whole BQP spectrum. Interestingly, and in spite of the screening factor $\mathcal{S}(k\xi)$ appearing in expression (4.123), the contributions $\Gamma^{(3)}_{\mathcal{V}_\epsilon,\mathcal{V}_n}$ and $\Gamma^{(3)}_{\mathcal{V}_\epsilon,\mathcal{V}_\epsilon,\mathcal{V}_\epsilon}$ do not drop to zero in the limit $\epsilon \to 0$. The functions $F(q)$ in (4.123) would therefore require further analysis. Remarkably, however, the contributions $\Gamma^{(3)}_{\mathcal{V}_\epsilon,\mathcal{V}_n}$ and $\Gamma^{(3)}_{\mathcal{V}_\epsilon,\mathcal{V}_\epsilon,\mathcal{V}_\epsilon}$ appear to cancel out exactly in the limit $\epsilon \to 0$, although they seem to have quite distinct origins in the perturbation theory. As this cancellation is most probably not accidental, it would be interesting to search for a representation which does not separate the two.

Finally, we refer to the numerical data of Fig. 4.6, where result (4.117) appears in dashed lines. The data points show a fair qualitative and quantitative agreement with the estimated correction beyond the Born approximation for BQPs (for the largest $\sigma_{\rm R}/\xi$ ratios at least). The discrepancy observed for the smallest $\sigma_{\rm R}/\xi$ ratio was shown to persist after averaging over a larger number of realizations of the random potential, and is probably due to even-higher orders in the Lyapunov exponent.

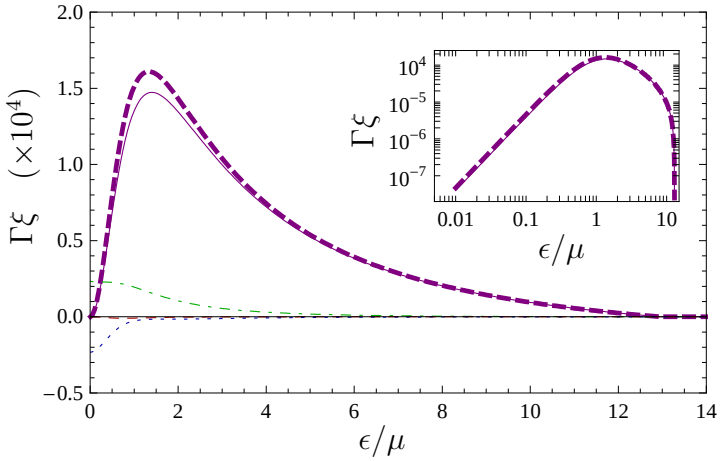
As the low-energy limit of the spectrum is of great physical relevance, but also seems technically more demanding, it would be interesting to explore it numerically. This limit of the spectrum, however, is also the most challenging to explore numerically, as large systems sizes and averaging over larger statistical samples are probably required. The ground-state density also needs to be computed with good accuracy. In spite of an encouraging similarity in the density profile obtained by standard propagation in imaginary time and a higher-order smoothing algorithm (see the figures of section 4.3.4), the two numerical methods produced contrasting BQP behavior at the very bottom of the spectrum.[34] The profile obtained from propagation in imaginary time with a Crank-Nicholson scheme produced a gapless spectrum (down to the level spacing associated with the finite size of the box used for the computations),

[33] We checked that the case $\sigma_{\rm R}/\xi \simeq 0.4$ of Fig. 4.9(b) essentially displays the features found closer to the white-noise limit (for even smaller $\sigma_{\rm R}/\xi$ ratios).

[34] Precisely, such a behavior was observed for $\epsilon \lesssim 10^{-2}\mu$ for the parameters of Fig. 4.6, i.e. in a puzzling vicinity of the energy scale ϵ_Δ discussed around Eq. (4.114). For the three sets of data displayed in Fig. 4.6, ϵ_Δ is of the order of $2\times 10^{-2}\mu$, which corresponds to $k_\Delta\xi \simeq 10^{-2}$.



(a) Speckle potential with $\sigma_{\rm R}/\xi \simeq 1.2$



(b) Speckle potential with $\sigma_{\rm R}/\xi \simeq 0.4$

Figure 4.9: Lyapunov exponent of BQPs one order beyond the Born approximation, in speckle potentials with $V_{\rm R}/\mu = 0.1$. The thick dashed line corresponds to result (4.117), which is the sum of the Born approximation [purple solid line, Eqs. (4.118) and (4.96)] and third-order contributions originating from: i) the screened potential $\mathcal{V}_\epsilon$ and the second-order expansion of the quasi-BEC density profile [green dash-dotted line, Eq. (4.119)], ii) the third-order Lyapunov exponent for $\mathcal{V}_\epsilon$ [blue dotted line, Eq. (4.121)], iii) $\mathcal{V}_\epsilon$ and the coupling between g^+ and g^- [red dashed line, Eq. (4.120)]. Inset: log-log plot of the Lyapunov exponents in the Born approximation, and one step beyond. At low energy, both scale as $\Gamma \sim \epsilon^2$.

but the modes of lowest energy displayed a re-increasing Lyapunov exponent and rather erratic wave functions, suggesting numerical artifacts. With the smoothing algorithm, on the other hand, the computed Lyapunov exponent monotonously dropped at low energy, but the BQP spectrum displayed a (very small) energy gap. This suggests that a precise control of the ground-state density (and boundary conditions) is required for the precise study of the low-energy excitations. It is also worth emphasizing that the low-energy physics of the disordered quasi-BEC cannot simply be brought to higher energies by increasing the strength of disorder with random potentials which are unbounded, like speckle potentials, since fragmentation is then very quickly reached.

4.5 Conclusion

In this chapter, we described the scattering and 1D localization of elementary excitations in an inhomogeneous weakly-interacting Bose-condensed gas. In such a Bose gas, the elementary excitations are, to a very good approximation, quasi-particles described by the Bogolyubov-de Gennes theory. In this framework, the quasi-particles have no mutual interaction, but experience the external potential V imposed on the system, as well as the mean-field interaction potential created by the density background of the condensed atoms. We addressed the case where the chemical potential μ of the Bose gas (and hence also the strength of the mean-field interaction term) is much larger than the amplitude $V_{\rm R}$ of the external potential. As shown in chapter 3, this condition ensures that the Bose gas lies deep in the superfluid regime.

We developed a perturbation theory around the exact time-independent Bogolyubov-de Gennes equations governing the quasi-particle modes. In this perturbation expansion, the only small parameter is $V_{\rm R}/\mu$. The approach presented in this chapter differs in this respect from a number of standard approximations: (i) the approximation of the Bogolyubov-de Gennes equations by *classical* hydrodynamical equations, which confine the theory to excitations of typical wavelength $\lambda \gg \xi$ (i.e. energy $\epsilon \ll \mu$), where ξ is the healing length of the condensate [253,310], (ii) the Thomas-Fermi approximation of the ground-state density profile, which is valid only under the assumption $\xi \ll \sigma_{\rm R}$, where $\sigma_{\rm R}$ is the typical (minimal) length scale on which the external potential varies [310], (iii) when V is random, a white-noise approximation which requires at least $\sigma_{\rm R} \ll \lambda$ [233,310]. The approach developed here holds for any ordering of the length scales ξ, $\sigma_{\rm R}$ and λ.

For a weak potential ($V_{\rm R} \ll \mu$), the Bogolyubov-de Gennes equations map approximately onto a Schrödinger equation, with an effective potential $\mathcal{V}_\epsilon$ which depends on the bare potential V, the condensate density background, and the quasi-particle energy. An inspection of the Fourier components of $\mathcal{V}_\epsilon$ reveals that the scattering of Bogolyubov quasi-particles is suppressed in the low-energy phonon regime ($\epsilon \lesssim \mu$), due to the efficient screening of the long-wavelength modulations of the external potential V by the condensate density background. In particular, screening affects the backscattering amplitude of Bogolyubov quasi-particles in the phonon regime. These results hold in any dimension.

Localization of Bogolyubov quasi-particles in a random potential was studied in a 1D geometry. The Lyapunov exponent of the quasi-particle excitations was obtained by applying the phase formalism of chapter 2 to the effective potential $\mathcal{V}_\epsilon$. The phase formalism captures the spatial decay of the quasi-particle modes in a simple fashion, and allows for the consideration of correlated random potentials. In particular, the applicability of this technique is not

restricted to (i) Gaussian disorder, (ii) (uncorrelated) white-noise potentials or (iii) models of non-overlapping impurities, which are tractable analytically with transfer matrix methods [310].

Our results show a suppression of the localization of Bogolyubov quasi-particles for $\epsilon/\mu \to 0$, which is consistent with known results on the localization of phonons [65] and studies in the white-noise limit [310]. The potential $\mathcal{V}_\epsilon$ provides a physical interpretation of this result in terms of screening, and a unified description of the phonon ($\epsilon \ll \mu$) and free-particle ($\epsilon \gg \mu$) regimes. In the free-particle regime, the Lyapunov exponent asymptotically approaches the exponent of a bare Schrödinger particle. In uncorrelated potentials, the Lyapunov exponent of Bogolyubov quasi-particles thus falls off as $1/\epsilon$ in the high energy limit, and admits a maximum around $\epsilon \simeq \mu$ [310], at the crossover between the phonon and free-particle regimes.

In correlated potentials, the strength of localization is also determined by the detailed Fourier spectrum of the correlation functions. In particular, the energy for which the strongest localization is observed depends on the competition of the healing length ξ and the correlation length σ_{R}. When the power spectrum of the random potential has a finite support, effective mobility edges arise as in the bare-particle case discussed in chapter 2.

At second order in V_{R}/μ, the effective Schrödinger equation displays the first correction to the relation between the energy of the quasi-particle and its average wave vector. The Lyapunov exponent Γ calculated one step beyond the Born approximation is qualitatively similar to leading-order result. In particular, Γ scales as ϵ^2 in the limit $\epsilon \to 0$, for the correlated speckle potential studied here. This result is probably generic at this level of the perturbation theory.

Screening is expected to be present also for stronger disorder. It remains to be determined how screening and strong disorder compete to shape the spectrum and the spatial properties of the elementary excitations of the Bose gas at low energy.

Conclusion

In this thesis we have studied localization effects induced by the presence of quenched (static) disorder in non-interacting and weakly-interacting one-dimensional Bose gases.

In chapter 2, we have concentrated on the one-dimensional Anderson localization of non-interacting particles in correlated potentials. Our study has been motivated by the realization that the localization properties of ultracold atoms in speckle potentials are strongly affected by the presence of a high-momentum cutoff in the power spectrum of such random potentials, beyond which the Lyapunov exponent vanishes in the Born approximation [29,34]. While general results establish that all single-particle states are exponentially localized in 1D, the question as to how localization occurs beyond such a cutoff was open. We have calculated the Lyapunov exponent in a weak-disorder expansion, two orders beyond the usual Born approximation. Our results are general, and apply to potentials which may be e.g. correlated, non-Gaussian, or asymmetric about the mean. We have shown that exponential localization occurs beyond the momentum cutoff in speckle potentials, due to higher-order scattering processes, and shown that the Lyapunov exponent undergoes a sharp drop across the cutoff for weak disorder, in agreement with the existence of an effective mobility edge in 1D.

The remaining part of the thesis has been devoted to localization effects in interacting one-dimensional Bose gases. In chapter 3, we have examined the ground state of a weakly-interacting, disordered Bose gas, and established a diagram of the zero-temperature quantum states as a function of the chemical potential and the disorder strength. We have identified three regimes: a regime of delocalized disordered (quasi-) BEC for weak disorder and strong mean-field interactions, a Lifshits-glass regime at very weak interactions or strong disorder, and an intermediate regime of fragmented BEC. In the regime of fragmented BEC, the Bose gas is a compressible insulator, identified with the Bose glass expected at weak interactions. No phase transition, but a crossover is expected between the regimes of Lifshits glass and fragmented BEC. In the Lifshits glass regime, the Bose gas populates a small number of strongly localized single-particle states. The crossover to the regime of fragmented BEC proceeds as an increasing number of single-particle states are populated and start developing overlaps. We have discussed the location of the crossover boundary on the basis of scaling arguments. Conversely, the crossover from BEC to fragmented BEC occurs as the amplitude of the density modulations imposed on the Bose gas by the random potential becomes large. We have derived the shape of the corresponding boundary from a precise analysis of the ground-state density modulations, and emphasized the role of the correlation length of the disorder in driving the Bose gas either into the smoothing regime or into the Thomas-Fermi regime. Finally, we have derived mean-field equations of state in the limiting BEC and Lifshits-glass regimes, which we have found to be in agreement with numerical calculations.

In chapter 4, finally, we have considered the elementary excitations of a disordered, weakly-interacting Bose gas deep in the (quasi-) BEC regime. In dilute Bose gases, these elementary excitations are accurately described by non-interacting Bogolyubov quasi-particles (BQPs).

For weak external potentials, we have mapped the exact Bogolyubov-de Gennes equations governing the quasi-particle modes on a Schrödinger-like equation. The effective potential of this equation accounts for the combined effect of the external potential and the mean-field density background on the quasi-particles, and shows that the low-energy excitations are screened from the external potential by the density background. Specializing to the one-dimensional geometry, we have shown that BQPs undergo Anderson localization, and we have derived the corresponding Lyapunov exponent in the Born approximation. While BQPs localize as bare Schrödinger particles at high energy, their localization is suppressed by screening in the phonon regime at low energy. In uncorrelated potentials, the strongest localization occurs for an excitation energy of the order of the chemical potential. In general, the energy of strongest localization is determined by the competition of the healing length of the quasi-condensate and the correlation length of the disorder. In the low-energy limit, which is important to characterize the disordered Bose gas, a quadratic dependence of the Lyapunov exponent on the BQP energy has been found, and shown to persist one order beyond the Born approximation.

Outlook

Anderson localization and the phenomena associated with the interplay of disorder and interactions in quantum systems form an important field of research in condensed-matter physics. Since 2005, experiments with ultracold atomic gases have multiplied to address the physics of disordered systems [15], and the high degree of control of these systems offers original prospects [16]. Systematic experimental investigations into the interplay of disorder and interactions are just starting, focusing in particular on the weakly-interacting regime of one-dimensional Bose gases [33]. A special emphasis has been set in this thesis on analytical approaches which take statistical correlations of the disorder into account. Correlations are present in any realistic random potential, and may change the qualitative behavior of disordered systems. Two such effects have been presented in this thesis. The first one is the possibility of an effective mobility edge in 1D, revealed in the studies of Refs. [29, 34] and analyzed in detail in chapter 2. The second one is the different power-law dependence of the boundary between the regimes of BEC and fragmented BEC, which reflects the importance of the smoothing of the disorder in the interacting Bose gas. As the statistical properties of disordered optical potentials are well controlled in experiments with ultracold atoms, the effects of both interactions and statistical correlations should be observable in ongoing and future experiments.

From the theoretical point of view, we identify several possible extensions of our work and directions of future research. First, in connection with the Anderson localization of single particles in 1D, a possible extension would be the analysis of fluctuations around the Lyapunov exponent in correlated potentials. Such fluctuations are an important aspect of localization [81]. For uncorrelated potentials, the full probability distribution of the fluctuations is known from the solution of Fokker-Planck equations [75,86]. These equations cannot be solved for arbitrary correlations. The phase formalism, on the other hand, may be used to calculate not only the average exponential decay, but also all the higher moments. Such calculations would be relevant to analyze deviations from the Gaussian fluctuations (1.13) and possible deviations from one-parameter scaling in correlated potentials. A few first steps have been made in this direction, and preliminary results, to be checked, indicate a departure from Gaussian fluctuations in non-Gaussian disorder.

Second, in connection with the characterization of the disordered weakly-interacting Bose gas, an important task would be to develop beyond-mean-field approaches to describe many-body correlations. Possibles avenues to analyze the crossover between Lifshits glass and fragmented BEC, the fragmented BEC itself, and the insulator-superfluid transition would be multi-orbital mean-field calculations, modeling of the Bose gas with Josephson junctions, and Bogolyubov theory. The two latter approaches have been recently used in Refs. [244, 289] to describe some aspects of the transition from superfluid to Bose glass.

Finally, the study of the Anderson localization of Bogolyubov quasi-particles in disordered BECs could be pursued both theoretically and experimentally. Theoretically, it would be interesting to describe the localization of BQPs in higher dimensions, using diagrammatic approaches to quantum transport [320]. An original feature in such developments would be the anisotropic scattering of BQPs (see Ref. [309] and section 4.2.4). In principle, the screening of low-energy excitations from the disorder by the ground-state background could lead to a striking result, namely the possible existence of two mobility edges in 3D. In such a scenario, a first delocalization transition would occur at high-energy, as for bare particles, and a second one would occur towards the low energies, as the effect of disorder is suppressed in the limit of vanishing BQP energy. Conversely, we can speculate about a regime of parameters where no BQP state would be localized at all. Experimentally, the Anderson localization of BQPs should be observable with Bragg-spectroscopy techniques, which allow the excitation of a (quasi-) condensate at given wave vector and energy [315].

APPENDIX A

Correlation functions of speckle potentials

We derive in this appendix the correlation functions of speckle potentials. Such potentials have been presented in section 1.3.3. In brief, they derive from a light intensity pattern $I(\mathbf{r})$:

$$V(\mathbf{r}) = V_{\mathrm{R}} \left(\frac{I(\mathbf{r})}{\langle I \rangle} - 1 \right) \qquad \text{with} \qquad I(\mathbf{r}) \propto |\mathcal{E}(\mathbf{r})|^2, \tag{A.1}$$

where $|V_{\mathrm{R}}| = \sqrt{\langle V^2 \rangle}$ is the root-mean-square amplitude of the potential, the sign of V_{R} might be positive or negative [see Eq. (1.44)], and $\mathcal{E}$ is the electric field amplitude, which is taken as a scalar. The field $\mathcal{E}$ is a complex Gaussian random field, which is assumed to have homogeneous statistical properties. Its two-point correlation function $C_{\mathcal{E}}(\mathbf{r}) = \langle \mathcal{E}(\mathbf{r}_0)\mathcal{E}(\mathbf{r}_0 + \mathbf{r}) \rangle$ has a cutoff at some critical value k_c for Fourier components in the transverse plane [see Eqs. (1.51) and (1.52)].[1] We use this cutoff to define the correlation length σ_{R} of speckle potentials:

$$\sigma_{\mathrm{R}} \equiv \frac{1}{k_c}. \tag{A.2}$$

Speckle correlation functions

The correlation functions of V are defined as

$$C_n(\mathbf{r}_1, \ldots, \mathbf{r}_{n-1}) = \langle V(\mathbf{r} + \mathbf{r}_1) \cdots V(\mathbf{r} + \mathbf{r}_{n-1}) \rangle, \tag{A.3}$$

and we introduce reduced correlation functions c_n to scale out the disorder amplitude and the correlation length:

$$C_n(\mathbf{r}_1, \mathbf{r}_2, \cdots, \mathbf{r}_{n-1}) = V_{\mathrm{R}}^n c_n(\mathbf{u}_1, \mathbf{u}_2, \cdots, \mathbf{u}_{n-1}), \tag{A.4}$$

where $\mathbf{u}_i = \mathbf{r}_i/\sigma_{\mathrm{R}}$. Accordingly, we may write the speckle potential as

$$V(\mathbf{r}) = V_{\mathrm{R}} \times \left(|a\left(\mathbf{r}/\sigma_{\mathrm{R}}\right)|^2 - \langle |a\left(\mathbf{r}/\sigma_{\mathrm{R}}\right)|^2 \rangle \right), \tag{A.5}$$

where the function $a(\mathbf{u})$ is proportional to the electric field amplitude $\mathcal{E}(\mathbf{r})$, and is therefore a (circular) complex Gaussian random field [181]. As a consequence of the Gaussian moment theorem, the n-point correlation functions of $|a|^2$ factorize into products of two-point correlators:

$$\langle a_0^* \cdots a_{n-1}^* a_0 \cdots a_{n-1} \rangle = \sum_{\Pi \in S_n} \langle a_0^* a_{\Pi(0)} \rangle \cdots \langle a_{n-1}^* \cdots a_{\Pi(n-1)} \rangle, \tag{A.6}$$

[1] For simplicity, we do not discuss the "longitudinal" correlation function of the speckle field. In turns out that this longitudinal component also has a sharp cutoff in the Fourier spectrum [321].

where a_p is a shorthand for $a(\mathbf{u}_p)$, and Π runs trough the $n!$ permutations of $[\![0, n-1]\!]$. The properties of expression (A.6) are entirely determined by the field-field correlator

$$c_a(\mathbf{u}_1) = \langle a^*(\mathbf{u}_0) a(\mathbf{u}_0 + \mathbf{u}_1) \rangle. \tag{A.7}$$

Properties of the reduced field correlator

Owing to the expansion $\langle |a|^4 \rangle = 2\langle |a|^2 \rangle^2$, the normalization $V_{\mathrm{R}} = \sqrt{\langle V^2 \rangle}$ imposes

$$c_a(\mathbf{0}) = \langle |a|^2 \rangle = 1. \tag{A.8}$$

Homogeneity of the statistical properties of the speckle field implies

$$c_a(-\mathbf{u}) = c_a^*(\mathbf{u}), \tag{A.9}$$

which ensures that the Fourier transform $\hat{c}_a$ is real. As noted above, a key property of the electric field-field correlator $C_{\mathcal{E}}$ in a speckle pattern is that it bears no Fourier components beyond the high-momentum cutoff k_c in the "transverse plane" (the plane perpendicular to the optical axis in Fig. 1.10). Denoting by $c_a^\perp(\mathbf{u})$ the restriction of $c_a(\mathbf{u})$ to vectors in that plane, we find that $c_a^\perp(\mathbf{u})$ has a compact support, bounded above by one:

$$\hat{c}_a^\perp(\mathbf{q}) = 0 \quad \text{for } |\mathbf{q}| > 1 = k_c \sigma_{\mathrm{R}}. \tag{A.10}$$

In this thesis, we only consider geometries which are confined to the transverse plane. Then, the correlator c_a coincides with $c_a^\perp$, and has the same cutoff.

Reduced correlation functions of the speckle potential

In Eq. (A.6) we almost recognize the n-point correlation function of the potential. Because the average of $\langle |a|^2 \rangle$ has been substracted from the definition of the potential, we obtain instead

$$c_n(\mathbf{u}_1, \ldots, \mathbf{u}_{n-1}) = \sum_{\Pi \in S'_n} c_a(\mathbf{u}_{\Pi(0)} - \mathbf{u}_0) c_a(\mathbf{u}_{\Pi(1)} - \mathbf{u}_1) \cdots c_a(\mathbf{u}_{\Pi(n-1)} - \mathbf{u}_{n-1}), \tag{A.11}$$

where $\mathbf{u}_0 = \mathbf{0}$ and S'_n is the ensemble of the permutations of $[\![0, n-1]\!]$ which leave no element unchanged. Since $c_a(\mathbf{0}) = 1$, the number of those permutations is

$$c_n(\mathbf{0}, \ldots, \mathbf{0}) = \frac{\langle (I - \langle I \rangle)^n \rangle}{\langle I \rangle^n} = \langle I \rangle^{-n} \sum_{p=0}^{n} \frac{n!}{p!(n-p)!} (-1)^p \langle I \rangle^p \langle I^{n-p} \rangle = \sum_{p=0}^{n} (-1)^p \frac{n!}{p!}, \tag{A.12}$$

where we have used the fact that $\langle I^m \rangle = m! \langle I \rangle^m$ [181]. With this, the first few correlators read

$$\begin{aligned}
c_2(\mathbf{u}) &= |c_a(\mathbf{u})|^2 && \text{(A.13)} \\
c_3(\mathbf{u}, \mathbf{v}) &= c_a(\mathbf{u}) c_a(\mathbf{v} - \mathbf{u}) c_a(-\mathbf{v}) + \text{c.c.} && \text{(A.14)} \\
c_4(\mathbf{u}, \mathbf{v}, \mathbf{w}) &= c_4^A(\mathbf{u}, \mathbf{v}, \mathbf{w}) + c_4^B(\mathbf{u}, \mathbf{v}, \mathbf{w}) + c_4^C(\mathbf{u}, \mathbf{v}, \mathbf{w}) \\
&\quad + [c_4^D(\mathbf{u}, \mathbf{v}, \mathbf{w}) + \text{c.c.}] + [c_4^E(\mathbf{u}, \mathbf{v}, \mathbf{w}) + \text{c.c.}] + [c_4^F(\mathbf{u}, \mathbf{v}, \mathbf{w}) + \text{c.c.}], && \text{(A.15)}
\end{aligned}$$

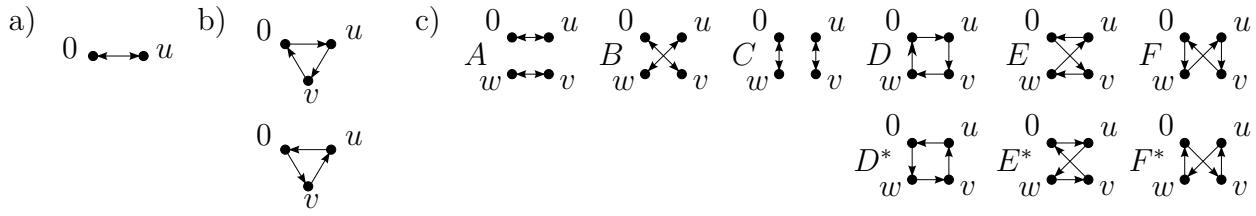


Figure A.1: Graphical representation of the components of the correlators c_n [a) $n = 2$, b) $n = 3$, c) $n = 4$] for speckle potentials V such that $\langle V \rangle = 0$. The correlators are obtained by drawing all possible ways to connect the n points in closed, oriented, possibly disconnected paths, without leaving isolated points.

where

$$c_4^A(\mathbf{u},\mathbf{v},\mathbf{w}) = |c_a(\mathbf{u})|^2 |c_a(\mathbf{w}-\mathbf{v})|^2 \tag{A.16}$$
$$c_4^B(\mathbf{u},\mathbf{v},\mathbf{w}) = |c_a(\mathbf{v})|^2 |c_a(\mathbf{u}-\mathbf{w})|^2 \tag{A.17}$$
$$c_4^C(\mathbf{u},\mathbf{v},\mathbf{w}) = |c_a(\mathbf{w})|^2 |c_a(\mathbf{v}-\mathbf{u})|^2 \tag{A.18}$$

and

$$c_4^D(\mathbf{u},\mathbf{v},\mathbf{w}) = c_a(\mathbf{u}) c_a(\mathbf{v}-\mathbf{u}) c_a(\mathbf{w}-\mathbf{v}) c_a(-\mathbf{w}) \tag{A.19}$$
$$c_4^E(\mathbf{u},\mathbf{v},\mathbf{w}) = c_a(\mathbf{v}) c_a(\mathbf{w}-\mathbf{v}) c_a(\mathbf{u}-\mathbf{w}) c_a(-\mathbf{u}) \tag{A.20}$$
$$c_4^F(\mathbf{u},\mathbf{v},\mathbf{w}) = c_a(\mathbf{w}) c_a(\mathbf{u}-\mathbf{w}) c_a(\mathbf{v}-\mathbf{u}) c_a(-\mathbf{v}). \tag{A.21}$$

The terms (A.16) to (A.18) may be called the Gaussian part of the four-point correlation function, as they factorize into two-point correlators, and the terms (A.19) to (A.21), with their complex conjugates, would form the non-Gaussian part. All these term can be constructed in a pictorial approach shown in Fig. A.1, where the correlators are obtained from all the possible ways to connect n points in closed, oriented, but possibly disconnected paths. The prescription $\langle V \rangle = 0$ amounts to excluding all graphs with isolated points. In expressions (A.14) and (A.15), the complex conjugates corresponds to paths with reversed direction [compare e.g. Eq. (A.14) and Fig. A.1(b)]. It is therefore clear that the correlation functions of the speckle potential are all symmetric with respect to a simultaneous change of sign of all the coordinates, whatever the form of the field correlator c_a is. This symmetry is essentially due to the Gaussian nature of the underlying electric field, the group structure of S_n, and the fact that for every permutation (path) Π left in S'_n, its inverse (the reversed path) Π^{-1} is also in S'_n.

APPENDIX B

Fourth-order Lyapunov exponent in a speckle potential

In this appendix we calculate the fourth perturbation order of the Lyapunov exponent of a single particle in a 1D speckle potential. The particle is described by the 1D Schrödinger equation

$$\left[-\frac{\hbar^2\nabla^2}{2m} + V(z)\right]\psi(z) = E\psi(z), \tag{B.1}$$

where V is a speckle potential (see section 1.3.3). The wave function ψ is assumed to be real and to correspond to an eigenstate of the Schrödinger operator. Then, the Lyapunov exponent is defined as

$$\gamma = -\lim_{|z-z_0|} \frac{\langle \ln[r(z)/r(z_0)]\rangle}{|z-z_0|}, \tag{B.2}$$

where $r = \sqrt{\psi^2 + (\partial_z\psi)^2/k^2}$, and k is related to the energy through $E = \hbar^2k^2/2m$.

For weak disorder, the Lyapunov exponent can be calculated in a perturbation expansion

$$\gamma = \gamma^{(2)} + \gamma^{(3)} + \gamma^{(4)} + \cdots, \tag{B.3}$$

where the superscripts indicate increasing powers of the potential amplitude V_{R}. Generic expressions for $\gamma^{(n)}$ $(n = 2, 3, 4)$ have been expounded in chapter 2. The general form is

$$\gamma^{(n)} = \left(\frac{\epsilon_{\mathrm{R}}}{k\sigma_{\mathrm{R}}}\right)^n f_n(k\sigma_{\mathrm{R}}), \tag{B.4}$$

where $\epsilon_{\mathrm{R}} = 2m\sigma_{\mathrm{R}}^2 V_{\mathrm{R}}/\hbar^2$, the parameter σ_{R} is the correlation length of the disorder, and f_n is a function which depends on the reduced n-point correlation function c_n of the potential [see Eqs. (2.95) to (2.100)].

In speckle potentials, the correlation functions are all determined by a field-field correlator c_a which has a cutoff in Fourier space (see appendix A):

$$\hat{c}_a(q) = 0 \quad \text{for } |q| > \kappa_c = 1. \tag{B.5}$$

The functions f_2 and f_3 for speckle potentials have been derived in section 2.3.1. Here we present the results of a calculation of the function f_4 for arbitrary c_a, as well as the specific speckle potential studied in section 2.3.2.

Correlation functions

The reduced four-point correlation function of a 1D speckle potential reads (see appendix A)

$$\begin{aligned} c_4(u,v,w) &= c_4^A(u,v,w) + c_4^B(u,v,w) + c_4^C(u,v,w) \\ &\quad + [c_4^D(u,v,w) + \text{c.c.}] + [c_4^E(u,v,w) + \text{c.c.}] + [c_4^F(u,v,w) + \text{c.c.}], \end{aligned} \tag{B.6}$$

where c_4^A, c_4^B and c_4^C are the factorized ("Gaussian") components

$$c_4^A(u,v,w) = |c_a(u)|^2 |c_a(w-v)|^2 \tag{B.7}$$
$$c_4^B(u,v,w) = |c_a(v)|^2 |c_a(u-w)|^2 \tag{B.8}$$
$$c_4^C(u,v,w) = |c_a(w)|^2 |c_a(v-u)|^2, \tag{B.9}$$

and c_4^D, c_4^E and c_4^F are the unfactorized parts

$$c_4^D(u,v,w) = c_a(u)c_a(v-u)c_a(w-v)c_a(-w) \tag{B.10}$$
$$c_4^E(u,v,w) = c_a(v)c_a(w-v)c_a(u-w)c_a(-u) \tag{B.11}$$
$$c_4^F(u,v,w) = c_a(w)c_a(u-w)c_a(v-u)c_a(-v). \tag{B.12}$$

The f_4 function

Here we calculate the function f_4 starting from formula (2.92):

$$\begin{aligned} f_4(\kappa) &= -\frac{1}{8} \lim_{\eta_i \to 0^+} \int_{-\infty}^{0} \mathrm{d}u \int_{-\infty}^{u} \mathrm{d}v \int_{-\infty}^{v} \mathrm{d}w \; c_4(u,v,w)\, \mathrm{e}^{\eta_1 u + \eta_2 v + \eta_3 w} \times \\ &\qquad \{\cos[2\kappa(-u+v+w)] + 2\cos[2\kappa w]\}. \end{aligned} \tag{B.13}$$

Integral (B.13) is split into terms of the form

$$I_\kappa^L = \lim_{\eta_i \to 0^+} \int_{-\infty}^{0} \mathrm{d}u \int_{-\infty}^{u} \mathrm{d}v \int_{-\infty}^{v} \mathrm{d}w \, c_4^L(u,v,w)\, \mathrm{e}^{\eta_1 u + \eta_2 v + \eta_3 w}\, \mathrm{e}^{\mathrm{i}2\kappa w} \tag{B.14}$$
$$J_\kappa^L = \lim_{\eta_i \to 0^+} \int_{-\infty}^{0} \mathrm{d}u \int_{-\infty}^{u} \mathrm{d}v \int_{-\infty}^{v} \mathrm{d}w \, c_4^L(u,v,w)\, \mathrm{e}^{\eta_1 u + \eta_2 v + \eta_3 w}\, \mathrm{e}^{\mathrm{i}2\kappa(-u+v+w)}, \tag{B.15}$$

where $L = A, B, C, D, E, F$. Then, we obtain $f_4(\kappa)$ as the sum

$$\begin{aligned} f_4(\kappa) = -\frac{1}{16}\mathrm{Re}\,[\quad & 2I_\kappa^A + 2I_{-\kappa}^A + \; J_\kappa^A + \; J_{-\kappa}^A + \\ & 2I_\kappa^B + 2I_{-\kappa}^B + \; J_\kappa^B + \; J_{-\kappa}^B + \\ & 2I_\kappa^C + 2I_{-\kappa}^C + \; J_\kappa^C + \; J_{-\kappa}^C + \\ & 4I_\kappa^D + 4I_{-\kappa}^D + 2J_\kappa^D + 2J_{-\kappa}^D + \\ & 4I_\kappa^E + 4I_{-\kappa}^E + 2J_\kappa^E + 2J_{-\kappa}^E + \\ & 4I_\kappa^F + 4I_{-\kappa}^F + 2J_\kappa^F + 2J_{-\kappa}^F \quad]. \end{aligned} \tag{B.16}$$

As calculating all the terms in (B.16) is a lengthy task, we do not reproduce all the details here. Let us simply outline the principle of the calculation by an example.

Example

Consider the integral I_κ^A for the part of the correlation function which reads[1]

$$c_4^A(u,v,w) = c_a(u)c_a(-u)c_a(w-v)c_a(v-w). \tag{B.17}$$

Going to Fourier space, we have

$$\begin{aligned} I_\kappa^A &= \lim_{\eta_i\to 0^+} \frac{1}{(2\pi)^2} \iiiint \mathrm{d}q_1\,\mathrm{d}q_2\,\mathrm{d}q_3\,\mathrm{d}q_4\,\hat{c}_a(q_1)\hat{c}_a(q_2)\hat{c}_a(q_3)\hat{c}_a(q_4)\times \\ &\quad \int_{-\infty}^{0}\mathrm{d}u\int_{-\infty}^{u}\mathrm{d}v\int_{-\infty}^{v}\mathrm{d}w\,\mathrm{e}^{\mathrm{i}u(q_1-q_2-\mathrm{i}\eta_1)}\mathrm{e}^{\mathrm{i}v(-q_3+q_4-\mathrm{i}\eta_2)}\mathrm{e}^{\mathrm{i}w(q_3-q_4+2\kappa-\mathrm{i}\eta_3)}. \end{aligned} \tag{B.18}$$

The triple integral in coordinate space evaluates to

$$\begin{aligned} &\int_{-\infty}^{0}\mathrm{d}u\int_{-\infty}^{u}\mathrm{d}v\int_{-\infty}^{v}\mathrm{d}w\,\mathrm{e}^{\mathrm{i}u(q_1-q_2-\mathrm{i}\eta_1)}\mathrm{e}^{\mathrm{i}v(-q_3+q_4-\mathrm{i}\eta_2)}\mathrm{e}^{\mathrm{i}w(q_3-q_4+2\kappa-\mathrm{i}\eta_3)} = \\ &\qquad \frac{\mathrm{i}}{(q_1-q_2+2\kappa-\mathrm{i}\eta_1-\mathrm{i}\eta_2-\mathrm{i}\eta_3)(2\kappa-\mathrm{i}\eta_2-\mathrm{i}\eta_3)(q_3-q_4+2\kappa-\mathrm{i}\eta_3)}. \end{aligned} \tag{B.19}$$

Taking the limit $\eta_i \to 0^+$ and using the identity

$$\lim_{\eta\to 0^+}\frac{1}{q-\mathrm{i}\eta} = \mathcal{P}\left(\frac{1}{q}\right) + \mathrm{i}\pi\delta(q), \tag{B.20}$$

where $\mathcal{P}(1/q)$ denotes the Cauchy principal value, we obtain

$$\begin{aligned} I_\kappa^A &= \frac{\mathrm{i}}{(2\pi)^2}\iiiint \mathrm{d}q_1\,\mathrm{d}q_2\,\mathrm{d}q_3\,\mathrm{d}q_4\,\hat{c}_a(q_1)\hat{c}_a(q_2)\hat{c}_a(q_3)\hat{c}_a(q_4)\times \\ &\quad \left[\frac{1}{q_1-q_2+2\kappa}+\mathrm{i}\pi\delta(q_1-q_2+2\kappa)\right]\times\frac{1}{2\kappa}\times\left[\frac{\mathrm{i}}{q_3-q_4+2\kappa}+\mathrm{i}\pi\delta(q_3-q_4+2\kappa)\right], \end{aligned} \tag{B.21}$$

where we have dropped the $\mathcal{P}$ symbol for simplicity. Taking the real part, we find

$$\mathrm{Re}[I_\kappa^A] = 2R_1^\kappa, \tag{B.22}$$

where R_1^κ is defined as

$$R_\kappa^1 = -\frac{1}{8\pi\kappa}\int \mathrm{d}q\,\overbrace{\hat{c}_a(q)\hat{c}_a(q+2\kappa)}\times\iint \mathrm{d}q\,\mathrm{d}q'\frac{\hat{c}_a(q)\hat{c}_a(q')}{q-q'+2\kappa}\qquad (c_4^A,\kappa_c). \tag{B.23}$$

The brace in this expression indicates a product of field correlators c_a which vanishes when κ exceeds a certain threshold. This threshold is equal κ_c in R_κ^1, so that R_κ^1 vanishes for $\kappa > \kappa_c$.

[1] This is simple rewriting of Eq. (B.7), owing to the property $c_a(-u) = c_a(u)^*$.

Other terms

The other terms in Eq. (B.16) are calculated along the lines of $\mathrm{Re}[I^A_\kappa]$. We find that they are determined by a number of "elementary" building blocks R^i_κ:

$$\begin{aligned}
\mathrm{Re}[I^A_\kappa] &= 2R^1_\kappa && \text{(B.24)}\\
\mathrm{Re}[J^A_\kappa] &= R^1_\kappa && \text{(B.25)}\\
\mathrm{Re}[I^B_\kappa] &= 2R^2_\kappa + R^3_\kappa && \text{(B.26)}\\
\mathrm{Re}[J^B_\kappa] &= R^4_\kappa && \text{(B.27)}\\
\mathrm{Re}[I^C_\kappa] &= R^5_\kappa && \text{(B.28)}\\
\mathrm{Re}[J^C_\kappa] &= R^6_\kappa && \text{(B.29)}\\
\mathrm{Re}[I^D_\kappa] &= 3R^7_\kappa + R^8_\kappa && \text{(B.30)}\\
\mathrm{Re}[J^D_\kappa] &= 2R^9_\kappa + R^{10}_\kappa + R^{11}_\kappa && \text{(B.31)}\\
\mathrm{Re}[I^E_\kappa] &= R^{12}_\kappa + R^{12}_{-\kappa} + R^{13}_\kappa + R^{14}_\kappa && \text{(B.32)}\\
\mathrm{Re}[J^E_\kappa] &= R^{15}_\kappa + R^{15}_{-\kappa} - R^{10}_\kappa + R^{11}_\kappa && \text{(B.33)}\\
\mathrm{Re}[I^F_\kappa] &= 2R^{16}_\kappa + R^{17}_\kappa + R^8_{-\kappa} && \text{(B.34)}\\
\mathrm{Re}[J^F_\kappa] &= 2R^{12}_\kappa + R^{18}_\kappa + R^{14}_\kappa && \text{(B.35)}
\end{aligned}$$

Note that some R^i_κ terms appear several times in Eqs. (B.24) to (B.35).

On the table of the following pages we have listed the expressions of the R^i_κ terms for an arbitrary field-field correlator $\hat{c}_a$ and for

$$\hat{c}_a(q) = \sqrt{\pi/2}\,\Theta(1-|q|), \qquad \text{(B.36)}$$

where Θ is the Heaviside step function. The terms R^i_κ all have a cutoff, indicated in the right column. Braces in the left column indicate which correlators introduce the largest cutoff. The expressions for $\mathrm{Re}[I^L_{-\kappa}]$ are obtained from those listed for $\mathrm{Re}[I^L_{+\kappa}]$ by substituting κ for $-\kappa$ in the R^i_κ terms. For field-field correlators c_a which are even in Fourier space, such as (B.36), the substitution leaves the integrals R^i_κ unchanged. In the explicit expressions for the simple speckle potential (B.36) listed in the table, κ should be read as $|\kappa|$.

Ultimately, with the elements listed in the table, the function f_4 for a speckle potential reads

$$\begin{aligned}
f_4(\kappa) = -\frac{1}{16}\Big\{ \quad & 5R^1_\kappa + 4R^2_\kappa + 2R^3_\kappa + R^4_\kappa + \\
& 2R^5_\kappa + R^6_\kappa + 12R^7_\kappa + 8R^8_\kappa + \\
& 4R^9_\kappa + 4R^{11}_\kappa + 12R^{12}_\kappa + 4R^{13}_\kappa + \\
& 6R^{14}_\kappa + 4R^{15}_\kappa + 8R^{16}_\kappa + 4R^{17}_\kappa + \\
& 5R^1_{-\kappa} + \cdots \\
& \qquad\qquad \cdots + 4R^{17}_{-\kappa} \quad \Big\} \qquad \text{(B.37)}
\end{aligned}$$

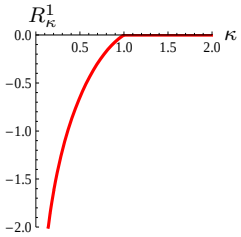
It turns out that the R^{10} and R^{18} terms do not appear in the final sum for f_4.

Remark **-** The results obtained for the "Gaussian" component of the speckle potentials (integrals $R^\kappa_i, i = 1..6$ below) are expressed both as functions of the field-field correlated c_a and as functions of the two-point correlator c_2. In the latter form, they apply not only to speckle potentials, but also to other models of disorder.

$$R^1_\kappa = +\frac{1}{4\kappa}\overbrace{\hat{c}_2(2\kappa)}\int \mathrm{d}q\frac{\hat{c}_2(q+2\kappa)}{q}$$
$$= -\frac{1}{8\pi\kappa}\iiint \mathrm{d}q_1\mathrm{d}q_2\mathrm{d}q_3\frac{\overbrace{\hat{c}_a(q_1)\hat{c}_a(q_1+2\kappa)}\,\hat{c}_a(q_2)\hat{c}_a(q_3)}{q_2-q_3+2\kappa}$$

Cutoff: $\kappa_c \equiv 1$
Appears in: I^A, J^A
$R^1_{-\kappa} = R^1_\kappa$

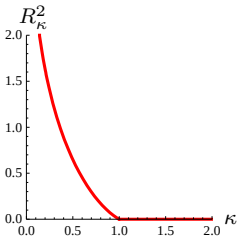
$$R^1_\kappa = \Theta(1-\kappa)\frac{\pi}{8}\frac{1-\kappa}{\kappa}\{(1-\kappa)\ln(1-\kappa)+2\kappa\ln(\kappa)-(1+\kappa)\ln(1+\kappa)\}$$



$$R^2_\kappa = -\frac{1}{2}\overbrace{\hat{c}_2(2\kappa)}\int \mathrm{d}q\frac{\hat{c}_2(q)}{q(q+2\kappa)}$$
$$= -\frac{1}{4\pi}\iiint \mathrm{d}q_1\mathrm{d}q_2\mathrm{d}q_3\frac{\overbrace{\hat{c}_a(q_1)\hat{c}_a(q_1+2\kappa)}\,\hat{c}_a(q_2)\hat{c}_a(q_3)}{(q_3-q_2)(q_3-q_2+2\kappa)}$$

Cutoff: $\kappa_c \equiv 1$
Appears in: I^B
$R^2_{-\kappa} = R^2_\kappa$

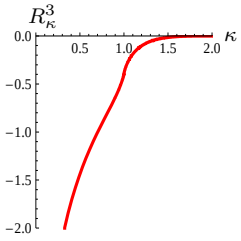
$$R^2_\kappa = \Theta(1-\kappa)\frac{\pi}{8}\frac{1-\kappa}{\kappa}\{-(1-\kappa)\ln(1-\kappa)-2\kappa\ln(\kappa)+(1+\kappa)\ln(1+\kappa)\}$$

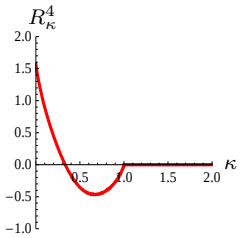
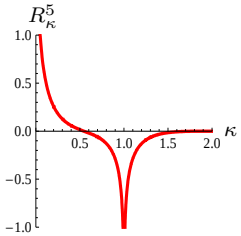
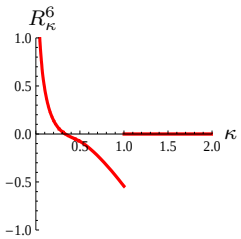


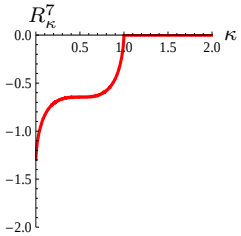
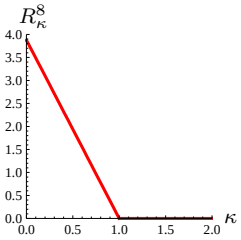
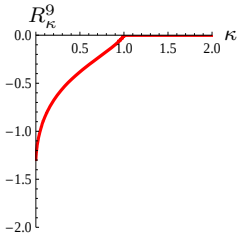
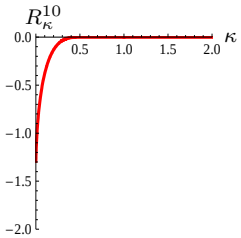
$$R^3_\kappa = +\frac{1}{2}\int \mathrm{d}q\frac{\overbrace{\hat{c}_2(q)\hat{c}_2(q+2\kappa)}}{q(q+2\kappa)}$$
$$= -\frac{1}{4\pi}\iiint \mathrm{d}q_1\mathrm{d}q_2\mathrm{d}q_3\frac{\overbrace{\hat{c}_a(q_1)\hat{c}_a(q_2)\hat{c}_a(q_3)\hat{c}_a(-q_1+q_2+q_3-2\kappa)}}{(q_2-q_1)(q_1-q_2+2\kappa)}$$

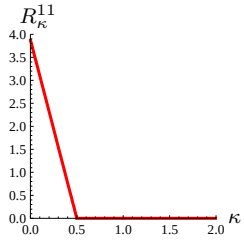
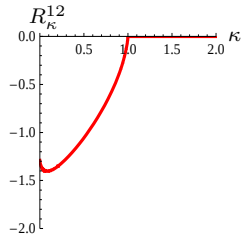
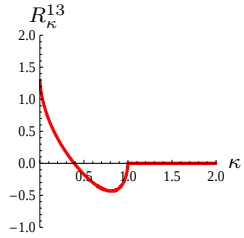
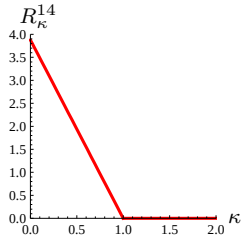
Cutoff: $2\kappa_c \equiv 2$
Appears in: I^B
$R^3_{-\kappa} = R^3_\kappa$

$$R^3_\kappa = \Theta(1-\kappa)\frac{\pi}{8}\left\{2-3\kappa+2\frac{1-\kappa}{\kappa}\ln(1-\kappa)+4\ln(\kappa)\right\}$$
$$+\Theta(\kappa-1)\Theta(2-\kappa)\frac{\pi}{8}\left\{-2+\kappa+2\frac{1-\kappa}{\kappa}\ln(\kappa-1)\right\}$$



$R_\kappa^4 = \int \frac{\mathrm{d}q}{q} \overbrace{\partial\hat{c}_2(q-2\kappa)[\hat{c}_2(q+2\kappa)}^{} - \overbrace{\hat{c}_2(2\kappa)}^{}]$	Cutoff: $\kappa_c \equiv 1$ Appears in: J^B $R_{-\kappa}^4 = R_\kappa^4$
$R_\kappa^4 = \Theta(1/2-\kappa)\frac{\pi}{4}\{2-6\kappa-(1+\kappa)\ln(1-\kappa)+2\kappa\ln(\kappa)+(1-\kappa)\ln(1+\kappa)\}$ $+\Theta(\kappa-1/2)\Theta(1-\kappa)\frac{\pi}{4}\{-2+2\kappa+(1-\kappa)\ln(1-\kappa)-2(1-\kappa)\ln(\kappa)$ $+(1-\kappa)\ln(1+\kappa)\}$	
$R_\kappa^5 = -\frac{1}{2}\int \frac{\mathrm{d}q}{q}\left\{\overbrace{\partial\hat{c}_2(q)[\hat{c}_2(q+2\kappa)}^{} - \hat{c}_2(2\kappa)]\right.$ $\left. + \overbrace{\hat{c}_2(q)[\partial\hat{c}_2(q+2\kappa)}^{} - \partial\hat{c}_2(2\kappa)]\right\}$	Cutoff: $2\kappa_c \equiv 2$ Appears in: I^C $R_{-\kappa}^5 = R_\kappa^5$
$R_\kappa^5 = \Theta(1-\kappa)\frac{\pi}{8}\{-4+6\kappa+(2-\kappa)\ln(1-\kappa)-2(1+\kappa)\ln(\kappa)\}$ $+\Theta(\kappa-1)\Theta(2-\kappa)\frac{\pi}{8}\{4-2\kappa+\kappa\ln(\kappa-1)\}$	
$R_\kappa^6 = -\frac{1}{2}\int \frac{\mathrm{d}q}{q}\left\{\overbrace{\partial\hat{c}_2(q-2\kappa)[\hat{c}_2(q+2\kappa)}^{} - \overbrace{\hat{c}_2(2\kappa)}^{}]\right.$ $\left. + \overbrace{\hat{c}_2(q-2\kappa)[\partial\hat{c}_2(q+2\kappa)}^{} - \overbrace{\partial\hat{c}_2(2\kappa)}^{}]\right\}$	Cutoff: $\kappa_c \equiv 1$ Appears in: J^C $R_{-\kappa}^6 = R_\kappa^6$
$R_\kappa^6 = \Theta(1/2-\kappa)\frac{\pi}{4}\{-2+6\kappa+2\ln(1-\kappa)-\ln(\kappa)-\ln(1+\kappa)\}$ $+\Theta(\kappa-1/2)\Theta(1-\kappa)\frac{\pi}{4}\{2-2\kappa+\ln(\kappa)-\ln(1+\kappa)\}$	

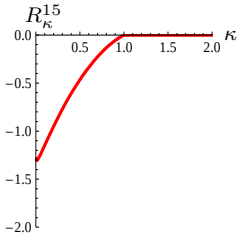
$R_\kappa^7 = -\frac{1}{4\pi}\iiint \mathrm{d}q_1\mathrm{d}q_2\mathrm{d}q_3 \frac{\overbrace{\hat{c}_a(q_1)\hat{c}_a(q_1+2\kappa)}\,\hat{c}_a(q_2)\hat{c}_a(q_3)}{(q_2-q_1)(q_3-q_1)}$	Cutoff: $\kappa_c \equiv 1$ Appears in: I^D
$R_\kappa^7 = \Theta(1-\kappa)\frac{\pi}{8}\{-2\mathrm{Li}_2(1)+2(1-\kappa)\ln(1-\kappa)\ln(\kappa)-(1-\kappa)\ln^2(1-\kappa)+\kappa\ln^2(\kappa)$ $+2\mathrm{Li}_2(\kappa)\}$	
$R_\kappa^8 = \frac{\pi}{4}\int \mathrm{d}q_1\,\overbrace{\hat{c}_a(q_1)^3\hat{c}_a(q_1+2\kappa)}$	Cutoff: $\kappa_c \equiv 1$ Appears in: I^D, I^F
$R_\kappa^8 = \Theta(1-\kappa)\frac{\pi^3}{8}(1-\kappa)$	
$R_\kappa^9 = -\frac{1}{4\pi}\iiint \mathrm{d}q_1\mathrm{d}q_2\mathrm{d}q_3 \frac{\overbrace{\hat{c}_a(q_1)\hat{c}_a(q_1+2\kappa)}\,\hat{c}_a(q_2)\hat{c}_a(q_3)}{(q_2-q_1+2\kappa)(q_3-q_1)}$	Cutoff: $\kappa_c \equiv 1$ Appears in: J^D
$R_\kappa^9 = \Theta(1-\kappa)\frac{\pi}{16}\{3\kappa\mathrm{Li}_2(1)-4\ln(2)\kappa\ln(1-\kappa)+4\ln(2)\kappa\ln(\kappa)$ $+2(1+\kappa)\ln(1-\kappa)\ln(1+\kappa)-2(1+\kappa)\ln(1-\kappa)\ln(\kappa)+\kappa\ln^2(\kappa)$ $-2\kappa\mathrm{Li}_2(2-\frac{1}{k})+2\kappa\mathrm{Li}_2(-\kappa)+2(1-\kappa)\mathrm{Li}_2(\frac{-\kappa}{1-\kappa})-2(1+\kappa)\mathrm{Li}_2(\frac{1-\kappa}{1+\kappa})$ $-2(1-\kappa)\mathrm{Li}_2(\frac{1-2\kappa}{1-\kappa})\Big\}$	
$R_\kappa^{10} = -\frac{1}{4\pi}\iiint \mathrm{d}q_1\mathrm{d}q_2\mathrm{d}q_3 \frac{\overbrace{\hat{c}_a(q_1-2\kappa)\hat{c}_a(q_1+2\kappa)}\,\hat{c}_a(q_2)\hat{c}_a(q_3)}{(q_2-q_1)(q_3-q_1)}$	Cutoff: $\frac{\kappa_c}{2} \equiv \frac{1}{2}$ Appears in: J^D, J^E $R_{-\kappa}^{10} = R_\kappa^{10}$ Canceled in f_4
$R_\kappa^{10} = \Theta(1/2-\kappa)\frac{\pi}{4}\{\mathrm{Li}_2(1)+(1-\kappa)\ln^2(1-\kappa)-2(1-\kappa)\ln(1-\kappa)\ln(\kappa)-\kappa\ln^2(\kappa)$ $-2\mathrm{Li}_2(\kappa)\}$	

$R_\kappa^{11} = \frac{\pi}{4}\int \mathrm{d}q_1 \hat{c}_a(q_1)^2 \overbrace{\hat{c}_a(q_1-2\kappa)\hat{c}_a(q_1+2\kappa)}$	Cutoff: $\frac{\kappa_c}{2} \equiv \frac{1}{2}$ Appears in: J^D, J^E $R_{-\kappa}^{11} = R_\kappa^{11}$
$R_\kappa^{11} = \Theta(1/2-\kappa)\frac{\pi^3}{4}(\frac{1}{2}-\kappa)$	
$R_\kappa^{12} = -\frac{1}{4\pi}\iiint \mathrm{d}q_1\mathrm{d}q_2\mathrm{d}q_3 \frac{\overbrace{\hat{c}_a(q_1)\hat{c}_a(q_1+2\kappa)}\hat{c}_a(q_2)\hat{c}_a(q_3)}{(q_1-q_3+2\kappa)(q_2-q_3+2\kappa)}$	Cutoff: $\kappa_c \equiv 1$ Appears in: I^E, J^F
$R_\kappa^{12} = \Theta(1-\kappa)\frac{\pi}{16}\{-4(1-\kappa)\mathrm{Li}_2(1) - (1-\kappa)\ln^2(1-\kappa) - \kappa\ln^2(\kappa)$ $+2(1+\kappa)\ln(\kappa)\ln(1+\kappa) + 2(1+\kappa)\mathrm{Li}_2(-\kappa) + 2\kappa\mathrm{Li}_2(\kappa)\}$	
$R_\kappa^{13} = -\frac{1}{4\pi}\iiint \mathrm{d}q_1\mathrm{d}q_2\mathrm{d}q_3 \frac{\overbrace{\hat{c}_a(q_1)\hat{c}_a(q_1+2\kappa)}\hat{c}_a(q_2)\hat{c}_a(q_3)}{(q_2-q_1)(q_1-q_3+2\kappa)}$	Cutoff: $\kappa_c \equiv 1$ Appears in: I^E $R_{-\kappa}^{13} = R_\kappa^{13}$
$R_\kappa^{13} = \Theta(1-\kappa)\frac{\pi}{16}\{4(1-\kappa)\mathrm{Li}_2(1) - 2(1-\kappa)\ln^2(1-\kappa) - 2\kappa\ln^2(\kappa)$ $+4(1+\kappa)\ln(\kappa)\ln(1+\kappa) + 4\kappa\mathrm{Li}_2(\kappa) + 4(1+\kappa)\mathrm{Li}_2(-\kappa)\}$	
$R_\kappa^{14} = \frac{\pi}{4}\int \mathrm{d}q_1 \overbrace{\hat{c}_a(q_1)^2\hat{c}_a(q_1+2\kappa)^2}$	Cutoff: $\kappa_c \equiv 1$ Appears in: I^E, J^F $R_{-\kappa}^{14} = R_\kappa^{14}$
$R_\kappa^{14} = \Theta(1-\kappa)\frac{\pi^3}{8}(1-\kappa)$	

$$R_\kappa^{15} = -\frac{1}{4\pi}\iiint \mathrm{d}q_1\mathrm{d}q_2\mathrm{d}q_3 \frac{\overbrace{\hat{c}_a(q_1)\hat{c}_a(q_1+2\kappa)}\,\hat{c}_a(q_2)\hat{c}_a(q_3)}{(q_1-q_3+4\kappa)(q_2-q_3+2\kappa)}$$

Cutoff: $\kappa_c \equiv 1$
Appears in: J^E

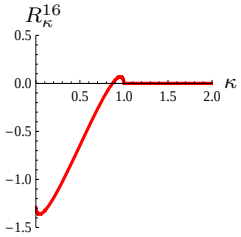
$$\begin{aligned}R_\kappa^{15} &= \Theta(1-\kappa)\frac{\pi}{16}\{(-2+3\kappa)\mathrm{Li}_2(1) - 2\ln(2)(1-\kappa)\ln(1-\kappa) - 4\ln(2)\kappa\ln(\kappa)\\ &+2\ln(2)(1+\kappa)\ln(1+\kappa) - 2\kappa\ln^2(\kappa) + 4(1+\kappa)\ln(\kappa)\ln(1+\kappa)\\ &-2(1+\kappa)\ln^2(1+\kappa) - 2\kappa\mathrm{Li}_2(2-\frac{1}{\kappa}) + 2\mathrm{Li}_2(-\kappa) + 2\mathrm{Li}_2(\kappa) + 2(1-\kappa)\mathrm{Li}_2(\frac{-2\kappa}{1-\kappa})\\ &-2(1-\kappa)\mathrm{Li}_2(\frac{1-2\kappa}{1-\kappa})\Big\}\end{aligned}$$



$$R_\kappa^{16} = -\frac{1}{4\pi}\iiint \mathrm{d}q_1\mathrm{d}q_2\mathrm{d}q_3 \frac{\overbrace{\hat{c}_a(q_1)\hat{c}_a(q_1+2\kappa)}\,\hat{c}_a(q_2)\hat{c}_a(q_3)}{(q_1-q_2+2\kappa)(q_3-q_2)}$$

Cutoff: $\kappa_c \equiv 1$
Appears in: I^F

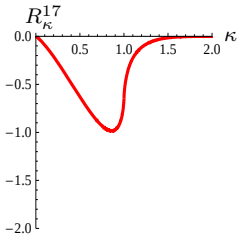
$$\begin{aligned}R_\kappa^{16} &= \Theta(1-\kappa)\frac{\pi}{16}\{(-4+6\kappa)\mathrm{Li}_2(1) + (1-\kappa)\ln^2(1-\kappa) - 2(1-\kappa)\ln(1-\kappa)\ln(\kappa)\\ &-\kappa\ln^2(\kappa) - 2\mathrm{Li}_2(\kappa)\}\end{aligned}$$



$$R_\kappa^{17} = -\frac{1}{4\pi}\iiint \mathrm{d}q_1\mathrm{d}q_2\mathrm{d}q_3 \frac{\overbrace{\hat{c}_a(q_1)\hat{c}_a(q_2)\hat{c}_a(q_3)\hat{c}_a(q_1-q_2+q_3+2\kappa)}}{(q_1-q_2+2\kappa)(q_2-q_3)}$$

Cutoff: $2\kappa_c \equiv 2$
Appears in: I^F

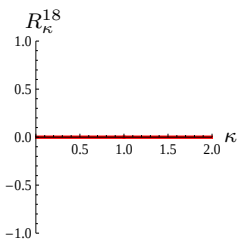
$$\begin{aligned}R_\kappa^{17} &= \Theta(1-\kappa)\frac{\pi}{16}\{-2\kappa\mathrm{Li}_2(1) - 2(1-\kappa)\ln^2(1-\kappa) + 4(1-\kappa)\ln(1-\kappa)\ln(\kappa)\\ &+4(1+\kappa)\ln(\kappa)\ln(1+\kappa) + 4(1+\kappa)\mathrm{Li}_2(-\kappa) + 4\mathrm{Li}_2(\kappa)\}\\ &+\Theta(\kappa-1)\Theta(2-\kappa)\frac{\pi}{16}\{-2\kappa\mathrm{Li}_2(1) + 2(\kappa-1)\ln^2(\kappa-1) - 4\kappa\ln(\kappa)\ln(\kappa-1)\\ &-4\kappa\mathrm{Li}_2(1-\kappa)\}\end{aligned}$$



$$R_\kappa^{18} = -\frac{1}{4\pi}\iiint \mathrm{d}q_1\mathrm{d}q_2\mathrm{d}q_3 \frac{\overbrace{\hat{c}_a(q_1)\hat{c}_a(q_2)\hat{c}_a(q_3)\hat{c}_a(q_1-q_2+q_3+4k)}}{(q_1-q_2+2\kappa)(q_2-q_3-2\kappa)}$$

Cutoff: $\kappa_c \equiv 1$
Appears in: J^F
$R_{-\kappa}^{18} = -R_\kappa^{18}$
Canceled in f_4

$$R_\kappa^{18} = 0$$



APPENDIX C

The dilogarithm function Li_2

The dilogarithm function [227], plotted in Fig. C.1 below, is defined by

$$\mathrm{Li}_2(x) = \sum_{k=1}^{\infty} \frac{x^k}{k^2} = \int_x^0 \frac{\ln(1-t)}{t} \mathrm{d}t \tag{C.1}$$

on the real-valued domain $x \in]-\infty, 1]$. It is a specialization of the polylogarithm function $\mathrm{Li}_s(x) = \sum_{k=1}^{\infty} x^k/k^s$ for $s = 2$, and arises in chapter 2 from the integration of the natural logarithm, as can be seen in the definition above.

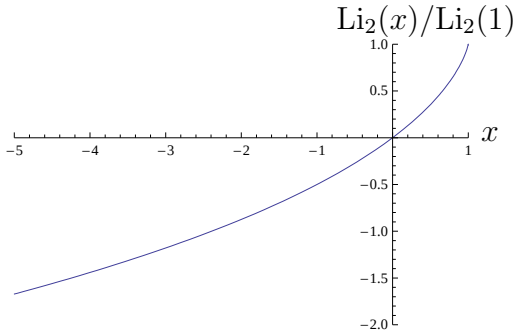


Figure C.1: Dilogarithm function on the domain $]-\infty, 1]$, normalized by $\mathrm{Li}_2(1) = \pi^2/6$.

The dilogarithm satisfies a number of functional identities. We quote here the most useful ones in the context of chapter 2 and appendix B:

$$\mathrm{Li}_2(x) + \mathrm{Li}_2(1-x) = \frac{\pi^2}{6} - \ln(x)\ln(1-x) \tag{C.2}$$

$$\mathrm{Li}_2(1-x) + \mathrm{Li}_2(1-1/x) = -\frac{1}{2}\ln^2(x). \tag{C.3}$$

These identities can be used to rewrite some of the contributions to the function f_4 of Eq. (2.129) and the expressions listed in appendix B in a different fashion. Let us also give a few limiting values which are relevant for the analysis:

$$\mathrm{Li}_2(1) = \zeta(2) = \frac{\pi^2}{6} \tag{C.4}$$

$$\mathrm{Li}_2(1/2) = \frac{\pi^2}{12} - \frac{1}{2}\ln^2(2) \tag{C.5}$$

$$\mathrm{Li}_2(0) = 0 \tag{C.6}$$

$$\mathrm{Li}_2(x) \sim -\frac{1}{2}\ln^2(-x) \qquad [x \to -\infty]. \tag{C.7}$$

Here ζ is Riemann's zeta function.

APPENDIX D

Gross-Pitaevskii equation in standard geometries

At the level of the mean field, the ground-state density profile $n_0(\mathbf{r})$ of weakly-interacting bosons with chemical potential μ is determined by the Gross-Pitaevskii equation (GPE)

$$\left[-\frac{\hbar^2\nabla^2}{2m} + V_{\rm ext}(\mathbf{r}) + g n_0(\mathbf{r}) - \mu\right]\sqrt{n_0(\mathbf{r})} = 0, \tag{D.1}$$

where g is the coupling constant of the bosons (assumed to be positive) and $V_{\rm ext}$ is the external potential (see section 3.3.2).

We review here well-known results on the ground-state solution of the GPE in a few geometries which are relevant to the study of chapter 3. We focus on the ground-state wave function $\sqrt{n_0}$ and on the equation of state, which relates the chemical potential μ to the number of bosons, $N = \int n_0$, or their average density $\langle n_0\rangle$ in the system.

The simple cases presented below also provide an elementary illustration of the competition of the energy and length scales which shape the ground-state density profile. The same type of competition is analyzed in the case of random potentials in chapters 3 and 4.

Free space

In free space, the potential and kinetic energy terms vanish in the GPE, so that the density profile is homogeneous:

$$n_0(\mathbf{r}) = \frac{\mu}{g}. \tag{D.2}$$

The system has an infinite number of particles, but a finite density determined by the chemical potential $\mu > 0$. The equation of state then reads

$$\mu = g\langle n_0\rangle, \tag{D.3}$$

where $\langle n_0\rangle$ is the average number of bosons per unit volume. These results obviously hold for a constant potential V_0 and a chemical potential $\mu = g\langle n_0\rangle + V_0 > V_0$.

1D box potential

Consider a one-dimensional box $[-L, L]$ with N bosons, i.e. an average density $\langle n_0\rangle = N/2L$. The potential $V_{\rm ext}(z)$ is assumed to vanish identically inside the box. If periodic boundary conditions are imposed, the problem is translation invariant, the density profile is homogeneous

and the equation of state reads $\mu = gN/2L$. If, on the other hand, the density profile is required to vanish on the box boundaries, i.e. if we consider

$$V_{\text{ext}}(z) = \begin{cases} 0 & \text{if } |z| < L \\ +\infty & \text{otherwise} \end{cases}, \tag{D.4}$$

then kinetic terms arise because of the inhomogeneity of the density profile, and the full non-linear GPE needs to be solved.

Density profile

Simple solutions of the GPE exist for piece-wise constant potentials [277, 279]. For the 1D box potential (D.4), we find

$$\sqrt{n_0(z)} = \sqrt{\frac{N}{2L}} \sqrt{\frac{\eta\,\mathcal{K}(\eta)}{\mathcal{K}(\eta) - \mathcal{E}(\eta)}}\, \text{sn}\left[\left(\frac{z}{L} + 1\right) \mathcal{K}(\eta); \eta\right], \tag{D.5}$$

where $\text{sn}(u;\eta)$ is a Jacobi elliptic function [280]. The parameter η is determined as the unique solution on the interval $[0, 1]$ of the equation $2\left[\mathcal{K}(\eta) - \mathcal{E}(\eta)\right] = E_g/E_L$, where $E_g = gN/2L$ is the average mean-field interaction energy, $E_L = \hbar^2/2mL^2$ is a kinetic energy associated with the boundaries (and, roughly, with the single-particle ground-state energy in the same potential). The functions $\mathcal{K}$ and $\mathcal{E}$ are called complete elliptic integrals of the first and second kind, respectively [280].

The Thomas-Fermi approximation

Expression (D.5) is plotted in Fig. D.1 for various ratios of E_g and E_L. The density profile "buldges" with increasing E_g/E_L. For dominating mean-field interaction energy ($E_g/E_L \gg 1$), the density is almost homogeneous over the entire system. At the boundaries, it drops to zero on the length scale of a few ξ, where ξ is the healing length, defined from the chemical potential μ as $\xi = \hbar/\sqrt{4m\mu}$.

The qualitative shape of this density profile is a very well known result. We may take it as a trivial illustration of the fact that, *when the mean-field interaction energy dominates the kinetic energy associated with the spatial scale of the variations of the potential, the density profile almost perfectly adapts to the local value of the potential.* In other words, quantum kinetic terms play a marginal role in this limit. In the present case, the potential is flat inside the box, so the density profile approaches a flat distribution. This result generalizes to inhomogeneous potentials, and forms the basis of the well-known Thomas-Fermi approximation for weakly interacting gases.

In this thesis, we examine certain regimes where the length scale of the variations of the potential *does* play a role, invalidating the Thomas-Fermi approximation (see chapters 3 and 4).

Equation of state

In the absence of interactions, the chemical potential μ is simply equal to the single-particle ground-state energy $\pi^2 E_L/4$. Approaching the Thomas-Fermi limit ($E_g/E_L \gg 1$), we have

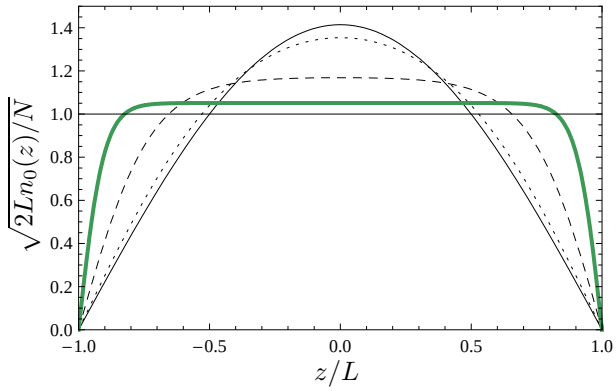


Figure D.1: Ground-state solution of the Gross-Pitaevskii equation in a 1D potential box of size $2L$ with zero Dirichlet boundary conditions. The profiles $\sqrt{n_0(z)}$ depend on the competition of the mean-field interaction energy $E_g = gN/2L$ and the kinetic energy $E_L = \hbar^2/2mL^2$ associated with the boundaries. The curves follow from the analytical solution (D.5), with values of η such that $E_g/E_L = 0, 1, 10, 100, \infty$ (in solid, dotted, dashed, thick, and flat solid line respectively).

$\mu \sim E_g$, that is, $\mu \sim g\langle n_0 \rangle$, as expected from the homogeneous limit.[1] Since we have $\mu \sim E_g$ in this limit, the criterion $E_g/E_L \gg 1$ can also be written $\xi \ll L$.

Harmonic trap

Let now $V_{\rm ext}$ be a d-dimensional harmonic trap with isotropic frequency ω,

$$V_{\rm ext}(\rho) = \frac{1}{2} m\omega^2 \rho^2, \tag{D.6}$$

where ρ is the distance from the trap centre.

Non-interacting case

In the absence of interactions, the bosons populate the ground-state of the harmonic oscillator, with density

$$n_0(\rho) = \frac{N}{(\sqrt{\pi} a_{\rm ho})^d} \mathrm{e}^{-\rho^2/a_{\rm ho}^2}, \tag{D.7}$$

where $a_{\rm ho}$ is the harmonic oscillator length [32]

$$a_{\rm ho} = \sqrt{\hbar/m\omega}. \tag{D.8}$$

The corresponding chemical potential is

$$\mu = \frac{d}{2} \hbar\omega. \tag{D.9}$$

[1] The exact result is found as

$$\mu = \frac{(1+\eta)\mathcal{K}(\eta)}{2[\mathcal{K}(\eta) - \mathcal{E}(\eta)]} E_g,$$

which for $E_g/E_L \gg 1$ expands as $\mu \simeq E_g(1 + \sqrt{2E_L/E_g})$.

Thomas-Fermi limit

The interacting case has no simple analytic solution. As in the 1D box potential, however, the Thomas-Fermi limit, where the mean-field interactions or the chemical potential by far exceed the ground-state single-particle kinetic energy, is easy to discuss. The Thomas-Fermi limit is obtained here for

$$\mu \gg \hbar\omega \tag{D.10}$$

or, equivalently,

$$\xi \ll a_{\rm ho}, \tag{D.11}$$

with $\xi = \hbar/\sqrt{4m\mu}$.

Density profile - An inspection of the GPE shows that the kinetic energy associated with the oscillator ground-state has a relative contribution of order $(\xi/a_{\rm ho})^2 \ll 1$ to the chemical potential. In the Thomas-Fermi regime, the kinetic term in the GPE is usually simply discarded, so that the density profile reads

$$n_0(\mathbf{r}) \simeq \begin{cases} \frac{\mu - V_{\rm ext}(\mathbf{r})}{g} & \text{if } V_{\rm ext}(\mathbf{r}) < \mu \\ 0 & \text{otherwise} \end{cases} . \tag{D.12}$$

For the harmonic trap (D.6), this approximation gives the cloud the shape of an inverted parabola:

$$n_0(\rho) \simeq \begin{cases} \frac{\mu}{g}\left(1 - \rho^2/R^2\right) & \text{if } \rho < R = \sqrt{\frac{2\mu}{m\omega^2}} \\ 0 & \text{otherwise} \end{cases} . \tag{D.13}$$

The Thomas-Fermi approximation breaks down only in a small region at the edges of the cloud, where the kinetic energy plays an important role and the density smoothly drops to zero [32].

Equation of state - Integration of the density profile (D.13) yields the equation of state[2]

$$gN \simeq \frac{(2\pi)^{d/2}\mu^{1+d/2}}{\Gamma\left(\frac{d}{2}+2\right)(m\omega^2)^{d/2}} \tag{D.14}$$

or, equivalently,

$$\mu \simeq \left[(2\pi)^{-d/2}\Gamma\left(\frac{d}{2}+2\right)(m\omega^2)^{d/2} gN\right]^{2/(2+d)} , \tag{D.15}$$

with $m\omega^2 = \hbar\omega a_{\rm ho}^{-2}$.

Intermediate regime

In the intermediate regime, the density profile changes continuously from the oscillator ground-state Gaussian into the Thomas-Fermi inverted parabola, and the equation of state crosses

[2] Γ is the gamma function [280], with the relevant values $\Gamma(5/2) = 3\sqrt{\pi}/4$, $\Gamma(2) = 2$, and $\Gamma(7/2) = 15\sqrt{\pi}/8$.

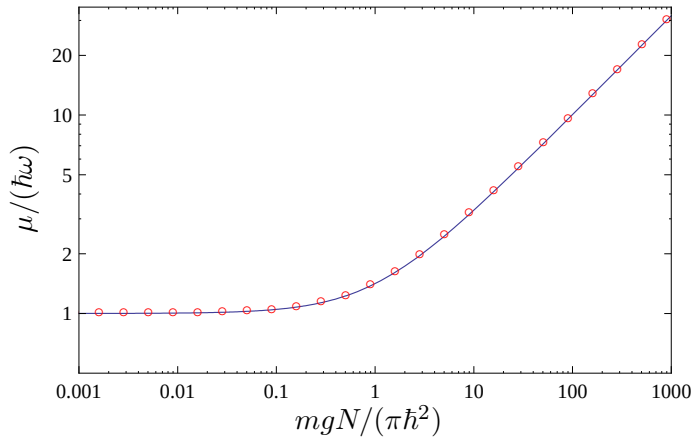


Figure D.2: Equation of state in a 2D harmonic trap (ω is the trapping frequency, g the 2D coupling constant, and N the number of atoms in the 2D geometry). The solid line is given by Eq. (D.16), and the red circles represent data obtained by solving the 2D GPE numerically.

over from the oscillator ground-state energy (D.9) to expression (D.15) for increasing mean-field interactions. In the particular case $d = 2$, an efficient interpolation between the two limiting regimes is provided by

$$\mu = \sqrt{(\hbar\omega)^2 + \frac{m\omega^2}{\pi} gN}. \tag{D.16}$$

To our knowledge, it is difficult to provide a rigorous justification of this formula [322]. However, numerical calculations seem to be in perfect agreement with this expression. We solved the 2D GPE for the ground state, using standard schemes of propagation in imaginary time [317,318]. The numerical results, shown in Fig. D.2, agree with formula (D.16) within 1% over the whole range of parameters.

APPENDIX E

Perturbative solution of the Gross-Pitaevskii equation for a weak potential

We determine here the ground-state solution of the Gross-Pitaevskii equation (GPE)

$$\left[-\frac{\hbar^2\nabla^2}{2m} + V(\mathbf{r}) + gn_0(\mathbf{r}) - \mu\right]\sqrt{n_0}(\mathbf{r}) = 0 \tag{E.1}$$

for a potential V with typical amplitude $V_{\rm R}$ such that

$$V_{\rm R} \ll \mu \qquad \text{or} \qquad V_{\rm R} \ll g\langle n_0\rangle, \tag{E.2}$$

where $\langle n_0\rangle$ is average number of bosons per unit volume. Averages are here understood in the spatial sense. If V is a random potential, we assume that its statistical properties are independent of absolute position in the system, and statistical averages then coincide with spatial averages.

Any of the assumptions in (E.2) allows to seek an exact solution in the form

$$n_0(\mathbf{r}) = n_0^{(0)} + \delta n_0(\mathbf{r}) \tag{E.3}$$

where $n_0^{(0)}$ is the homogeneous solution found in the absence of potential (see below), and $\delta n_0(\mathbf{r})$ is a small perturbation which satisfies $|\delta n_0(\mathbf{r})| \ll n_0^{(0)}$. The perturbation is found as an expansion

$$\delta n_0(\mathbf{r}) = n_0^{(1)}(\mathbf{r}) + n_0^{(2)}(\mathbf{r}) + \cdots, \tag{E.4}$$

where the superscripts indicate increasing powers of $V_{\rm R}$.

Solution (E.3) can always be written

$$n_0(\mathbf{r}) = \frac{\mu - \widetilde{V}(\mathbf{r}) + \Delta}{g}, \tag{E.5}$$

where

$$\widetilde{V}(\mathbf{r}) = g\langle n_0\rangle - gn_0(\mathbf{r}) \tag{E.6}$$

is a field with vanishing average, and the offset term

$$\Delta = g\langle n_0\rangle - \mu \tag{E.7}$$

measures the deviation from the equation of state obtained in the unperturbed case ($\mu = g\langle n_0\rangle$). The quantities $\widetilde{V}$ and Δ have their own expansion in powers of $V_{\rm R}$, which are identified term by term from the $\mathbf{r}$-dependent and constant parts in the expansion of $n_0(\mathbf{r})$.

In general, Δ does not vanish, and the perturbation expansion takes a slightly different form depending on whether the chemical potential μ or the average density $\langle n_0 \rangle$ is kept constant in the process. In the latter case, for instance, the chemical potential is also expanded. We therefore present both derivations below.

Expansion at fixed chemical potential

In this section, the GPE is solved for a given chemical potential. Accordingly, the invariant length scale in the problem is the healing length

$$\xi = \frac{\hbar}{\sqrt{4m\mu}}, \tag{E.8}$$

the GPE rewrites

$$\left[-2\xi^2\nabla^2 - 1 + \frac{V(\mathbf{r})}{\mu} + \frac{g n_0(\mathbf{r})}{\mu}\right]\sqrt{n_0(\mathbf{r})} = 0, \tag{E.9}$$

the unperturbed solution (obtained for $V = 0$) is

$$n_0^{(0)} = \frac{\mu}{g}, \tag{E.10}$$

and the small parameter of the expansion is

$$\beta = \frac{V_{\mathrm{R}}}{\mu}. \tag{E.11}$$

Form (E.9) suggests an expansion of the square root of the density as

$$\sqrt{n_0(\mathbf{r})} = \sqrt{\frac{\mu}{g}}\ \left[\phi^{(0)}(\mathbf{r}) + \phi^{(1)}(\mathbf{r}) + \phi^{(2)}(\mathbf{r}) + \ldots\right], \tag{E.12}$$

where $\phi^{(0)}(\mathbf{r}) = 1$ is the solution in the absence of external potential, and the functions $\phi^{(n)}(\mathbf{r})$ are real-valued. We thus have

$$n_0(\mathbf{r}) = \frac{\mu}{g}\ \sum_{i,j}\phi^{(i)}(\mathbf{r})\phi^{(j)}(\mathbf{r}), \tag{E.13}$$

and the quantities of interest at any order in the expansion series are readily obtained by collecting the terms at the corresponding order:

$$n_0^{(n)}(\mathbf{r}) \;=\; \frac{\mu}{g}\sum_{\substack{0\le i,j\le n\\ i+j=n}}\phi^{(i)}(\mathbf{r})\phi^{(j)}(\mathbf{r}) \qquad \text{for } n \ge 0, \tag{E.14}$$

whence

$$\Delta^{(0)} \;=\; 0 \tag{E.15}$$

$$\Delta^{(n)} \;=\; \mu \sum_{\substack{0\le i,j\le n\\ i+j=n}}\langle\phi^{(i)}\phi^{(j)}\rangle \qquad \text{for } n \ge 1, \tag{E.16}$$

and

$$\widetilde{V}^{(0)}(\mathbf{r}) = 0 \tag{E.17}$$

$$\widetilde{V}^{(n)}(\mathbf{r}) = \Delta^{(n)} - \mu \sum_{\substack{0\le i,j\le n \\ i+j=n}} \phi^{(i)}(\mathbf{r})\phi^{(j)}(\mathbf{r}) \qquad \text{for } n \ge 1. \tag{E.18}$$

The functions $\phi^{(n)}(\mathbf{r})$ are determined by inserting the perturbation series (E.12) into the GPE (E.9) and by collecting the terms of order n. The explicit calculation of $\phi^{(n)}$ becomes increasingly tedious for larger n values, as the number of terms involved grows like n^2. Yet, the above perturbation hierarchy produces a simple recursion formula which can be used in analytical or numerical calculations. Following the procedure outlined above, for all $n \ge 1$, we obtain

$$\phi^{(n)} = -\frac{1}{2} G_\xi * \left[\frac{V}{\mu}\phi^{(n-1)} + \sum_{\substack{i+j+k=n \\ 0\le i,j,k\le n-1}} \phi^{(i)}\phi^{(j)}\phi^{(k)} \right] \tag{E.19}$$

In this expression, $G_\xi(\mathbf{r})$ is the Green function associated with the operator $-\xi^2\nabla^2 + 1$, and the star denotes the convolution product

$$(f * g)(\mathbf{r}) = \int \mathrm{d}\mathbf{r}'\ f(\mathbf{r}-\mathbf{r}')g(\mathbf{r}'). \tag{E.20}$$

The convolution kernel G_ξ is best written in Fourier space, where it takes a simple Lorentzian form:

$$G_\xi(\mathbf{q}) = \frac{(2\pi)^{-d/2}}{1 + (|\mathbf{q}|\xi)^2}. \tag{E.21}$$

The Fourier transform is defined here as

$$f(\mathbf{q}) = (2\pi)^{-d/2} \int \mathrm{d}\mathbf{r} f(\mathbf{r}) \mathrm{e}^{-\mathrm{i}\mathbf{q}.\mathbf{r}}. \tag{E.22}$$

Applying the recursive procedure up to second order, we find

$$\phi^{(0)} = 1 \tag{E.23}$$

$$\phi^{(1)} = -\frac{1}{2\mu} G_\xi * V \tag{E.24}$$

$$\phi^{(2)} = \frac{1}{8\mu^2} G_\xi * \left[2V(G_\xi * V) - 3(G_\xi * V)^2 \right]. \tag{E.25}$$

Then, using Eqs. (E.16) and (E.18), we find

$$\Delta^{(1)} = 0 \tag{E.26}$$

$$\widetilde{V}^{(1)} = G_\xi * V \tag{E.27}$$

and

$$\Delta^{(2)} = \frac{1}{4\mu} \left\langle G_\xi * \left[2V(G_\xi * V) - 3(G_\xi * V)^2 \right] + (G_\xi * V)^2 \right\rangle \tag{E.28}$$

$$\widetilde{V}^{(2)} = \Delta^{(2)} - \frac{1}{4\mu} \left\{ G_\xi * \left[2V(G_\xi * V) - 3(G_\xi * V)^2 \right] + (G_\xi * V)^2 \right\}. \tag{E.29}$$

Note, in particular, that the leading-order fluctuation field $\widetilde{V}^{(1)}$ has a very simple form:

$$\widetilde{V}^{(1)}(\mathbf{r}) = \int \mathrm{d}\mathbf{r}'\, G_\xi(\mathbf{r}-\mathbf{r}')V(\mathbf{r}') \tag{E.30}$$

$$\widetilde{V}^{(1)}(\mathbf{q}) = \frac{V(\mathbf{q})}{1+(|\mathbf{q}|\xi)^2}. \tag{E.31}$$

The leading-order deviation from the homogeneous equation of state, on the other hand, is readily rewritten as

$$\Delta^{(2)} = \frac{1}{2\mu}\left\langle V(G_\xi * V) - (G_\xi * V)^2 \right\rangle. \tag{E.32}$$

Introducing the autocorrelation function[1]

$$C_2(\mathbf{r}) = \langle V(\mathbf{r}')V(\mathbf{r}'+\mathbf{r})\rangle, \tag{E.33}$$

and its reduced version c_2 defined by

$$C_2(\mathbf{r}) = V_{\mathrm{R}}^2 c_2(\mathbf{r}/\sigma_{\mathrm{R}}), \tag{E.34}$$

where σ_{R} is chosen as a characteristic scale of variation of the potential V, we finally obtain

$$\Delta^{(2)} = \frac{V_{\mathrm{R}}^2\sigma_{\mathrm{R}}^d}{2(2\pi)^{d/2}\mu}\int \mathrm{d}\mathbf{q}\, \frac{(|\mathbf{q}|\xi)^2}{\left[1+(|\mathbf{q}|\xi)^2\right]^2}\hat{c}_2(\mathbf{q}\sigma_{\mathrm{R}}). \tag{E.35}$$

Expansion at fixed average density

The GPE (E.1) is now solved for a given average density $\langle n_0\rangle$. As the perturbation orders differ from those obtained at fixed chemical potential, the quantities are here labeled with a bar (e.g. $\bar{\beta}$ instead of β) to avoid any ambiguity as to which quantities change or remain unchanged. The invariant length scale in the problem is now

$$\bar{\xi} = \frac{\hbar}{\sqrt{4mg\langle n_0\rangle}}, \tag{E.36}$$

the GPE rewrites

$$\left[-2\bar{\xi}^2\nabla^2 - \frac{\bar{\mu}}{g\langle n_0\rangle} + \frac{V(\mathbf{r})}{g\langle n_0\rangle} + \frac{\bar{n_0}(\mathbf{r})}{\langle n_0\rangle}\right]\sqrt{\bar{n_0}(\mathbf{r})} = 0, \tag{E.37}$$

the unperturbed solution is

$$\bar{n}_0^{(0)} = \langle n_0\rangle \tag{E.38}$$

$$\bar{\mu}^{(0)} = g\langle n_0\rangle, \tag{E.39}$$

and the small parameter of the expansion is

$$\bar{\beta} = \frac{V_{\mathrm{R}}}{g\langle n_0\rangle}. \tag{E.40}$$

[1]Note that, since averages are here understood in the spatial sense, the autocorrelation function C_2 takes only one argument, whether V is random or not.

The square root of the density and the chemical potential are expanded as

$$\sqrt{\bar{n_0}(\mathbf{r})} = \sqrt{\langle n_0\rangle}\left[\bar{\phi}^{(0)}(\mathbf{r}) + \bar{\phi}^{(1)}(\mathbf{r}) + \bar{\phi}^{(2)}(\mathbf{r}) + \ldots\right] \tag{E.41}$$

$$\bar{\mu} = g\langle n_0\rangle\left[\bar{m}^{(0)} + \bar{m}^{(1)} + \bar{m}^{(2)} + \ldots\right] \tag{E.42}$$

with

$$\bar{\phi}^{(0)}(\mathbf{r}) = 1 \tag{E.43}$$

$$\bar{m}^{(0)} = 1. \tag{E.44}$$

The density follows as

$$\bar{n_0}(\mathbf{r}) = \langle n_0\rangle \sum_{i,j} \bar{\phi}^{(i)}(\mathbf{r})\bar{\phi}^{(j)}(\mathbf{r}) \tag{E.45}$$

$$\bar{n}_0^{(n)}(\mathbf{r}) = \langle n_0\rangle \sum_{\substack{0\le i,j\le n\\ i+j=n}} \bar{\phi}^{(i)}(\mathbf{r})\bar{\phi}^{(j)}(\mathbf{r}) \qquad \text{for } n \ge 0. \tag{E.46}$$

As the average density is kept constant, the offset introduced by the potential between the chemical potential and the average mean-field energy is now carried by $\bar{\mu}$, and the higher-order terms of $\bar{n_0}(\mathbf{r})$ have only fluctuations. Therefore, defining

$$\bar{\tilde{V}}(\mathbf{r}) = g\langle n_0\rangle - g\bar{n}_0(\mathbf{r}) \tag{E.47}$$

$$\bar{\Delta} = g\langle n_0\rangle - \bar{\mu}, \tag{E.48}$$

so that

$$\bar{n}_0(\mathbf{r}) = \frac{\bar{\mu} - \bar{\tilde{V}}(\mathbf{r}) + \bar{\Delta}}{g}, \tag{E.49}$$

we obtain

$$\bar{\Delta}^{(0)} = 0 \tag{E.50}$$

$$\bar{\Delta}^{(n)} = -\bar{\mu}^{(n)} = -g\langle n_0\rangle\bar{m}^{(n)} \qquad \text{for } n \ge 1 \tag{E.51}$$

and

$$\bar{\tilde{V}}^{(0)}(\mathbf{r}) = 0 \tag{E.52}$$

$$\bar{\tilde{V}}^{(n)}(\mathbf{r}) = -g\bar{n}_0^{(n)} = -g\langle n_0\rangle \sum_{\substack{0\le i,j\le n\\ i+j=n}} \bar{\phi}^{(i)}(\mathbf{r})\bar{\phi}^{(j)}(\mathbf{r}) \qquad \text{for } n \ge 1. \tag{E.53}$$

A perturbation hierarchy is obtained by inserting expressions (E.41) and (E.42) into the Gross-Pitaevskii equation (E.37), and collecting the terms of order n. Because of the modified chemical potential, the perturbation hierarchy now takes the following form for $n \ge 1$:

$$\bar{\phi}^{(n)} = -\frac{1}{2}G_{\bar{\xi}} * \left[\frac{V}{g\langle n_0\rangle}\bar{\phi}^{(n-1)} + \sum_{\substack{i+j+k=n\\ 0\le i,j,k\le n-1}} \bar{\phi}^{(i)}\bar{\phi}^{(j)}\bar{\phi}^{(k)} - \sum_{n'=1}^{n-1} \bar{m}^{(n')}\bar{\phi}^{(n-n')}\right] + \frac{\bar{m}^{(n)}}{2}. \tag{E.54}$$

The additional unknown $\bar{m}^{(n)}$ is determined from the requirement that

$$\begin{aligned}\bar{n}_0^{(n)} &= 2\bar{\phi}^{(n)} + \sum_{n'=1}^{n-1} \bar{\phi}^{(n')}\bar{\phi}^{(n-n')} \\ &= -G_{\bar{\xi}} * [\cdots] + \bar{m}^{(n)} + \sum_{n'=1}^{n-1} \bar{\phi}^{(n')}\bar{\phi}^{(n-n')} \end{aligned} \tag{E.55}$$

should vanish in the mean, so that for all $n \geq 1$

$$\bar{m}^{(n)} = \left\langle G_{\bar{\xi}} * \left[\frac{V}{g\langle n_0\rangle}\bar{\phi}^{(n-1)} + \sum_{\substack{i+j+k=n \\ 0\leq i,j,k\leq n-1}} \bar{\phi}^{(i)}\bar{\phi}^{(j)}\bar{\phi}^{(k)} - \sum_{n'=1}^{n-1} \bar{m}^{(n')}\bar{\phi}^{(n-n')} \right] - \sum_{n'=1}^{n-1} \bar{\phi}^{(n')}\bar{\phi}^{(n-n')} \right\rangle . \tag{E.56}$$

Equations (E.43), (E.44), (E.54) and (E.56) completely determine all terms of the perturbation series at fixed average density.

Up to second order, we find

$$\bar{m}^{(0)} = 1 \tag{E.57}$$

$$\bar{\phi}^{(0)} = 1 \tag{E.58}$$

$$\bar{m}^{(1)} = 0 \tag{E.59}$$

$$\bar{\phi}^{(1)} = -\frac{1}{2g\langle n_0\rangle} G_{\bar{\xi}} * V \tag{E.60}$$

$$\bar{m}^{(2)} = -\frac{1}{4(g\langle n_0\rangle)^2} \langle G_{\bar{\xi}} * \left[2V(G_{\bar{\xi}} * V) - 3(G_{\bar{\xi}} * V)^2\right] + (G_{\bar{\xi}} * V)^2\rangle \tag{E.61}$$

$$\bar{\phi}^{(2)} = \frac{1}{8(g\langle n_0\rangle)^2} G_{\bar{\xi}} * \left[2V(G_{\bar{\xi}} * V) - 3(G_{\bar{\xi}} * V)^2\right] + \frac{\bar{m}^{(2)}}{2}. \tag{E.62}$$

Then, using Eqs. (E.51) and (E.53) we obtain

$$\bar{\Delta}^{(1)} = 0 \tag{E.63}$$

$$\tilde{\bar{V}}^{(1)} = G_{\bar{\xi}} * V \tag{E.64}$$

and

$$\bar{\Delta}^{(2)} = \frac{1}{4g\langle n_0\rangle} \left\langle G_{\bar{\xi}} * \left[2V(G_{\bar{\xi}} * V) - 3(G_{\bar{\xi}} * V)^2\right] + (G_{\bar{\xi}} * V)^2 \right\rangle \tag{E.65}$$

$$\tilde{\bar{V}}^{(2)} = \bar{\Delta}^{(2)} - \frac{1}{4g\langle n_0\rangle} \left\{ G_{\bar{\xi}} * \left[2V(G_{\bar{\xi}} * V) - 3(G_{\bar{\xi}} * V)^2\right] + (G_{\bar{\xi}} * V)^2 \right\}, \tag{E.66}$$

that is, the same expressions as in the first section of this appendix upon replacement of μ and ξ by the invariant quantities $g\langle n_0\rangle$ and $\bar{\xi}$.

Let us finish with a few comments.

First, as μ and $g\langle n_0\rangle$ (or ξ^2 and $\bar{\xi}^2$, respectively) are different in the presence of an external potential (differences arise from the second order in $V_{\rm R}$), the formal equivalence of the results

obtained for Δ and $\bar{\Delta}$ on the one hand, and ξ and $\bar{\xi}$ on the other hand, is not expected to hold with higher-order terms.

Second, both approaches produce the same qualitative results [compare Eqs. (E.27), (E.64), (E.28), and (E.65)]. The quantitative differences arising with higher-order terms are expected to be relevant for moderate potential strengths, and negligible for sufficiently weak potentials.

Finally, the perturbation expansion and the recursive schemes presented above can be used in numerical calculations to solve the GPE equation for the ground-state. This approach offers an efficient alternative to propagation in imaginary time for small and moderate potential strengths. In principle, it is possible to use any of the two above schemes (either at fixed chemical potential, or at fixed average density) in such a numerical calculation. If an average density $g\langle n_0\rangle$ is imposed in the physical problem and the algorithm for fixed chemical potential is used, it is possible to start with $g\langle n_0\rangle$ as input for μ, then compute Δ, then use $g\langle n_0\rangle - \Delta$ as a new input estimate for μ, and so on, till convergence is reached. It is however more convenient to use directly the suitable among the two perturbation schemes presented above.

APPENDIX F

Lifshits tail in a speckle potential

We examine here the low-energy spectrum of the 1D Schrödinger problem

$$\left[\frac{\hbar^2}{2m}\frac{\mathrm{d}^2}{\mathrm{d}z^2} + V(z)\right]\chi_\nu(z) = E_\nu\chi_\nu(z) \tag{F.1}$$

in the case where $V(z)$ is a speckle potential.

Lifshits tails

In disordered systems, the single-particle density of states $\mathcal{D}(E)$ is strongly affected at low energies. At the level of the cumulative density of states

$$\mathcal{N}(E) = \int_{-\infty}^{E} \mathrm{d}E'\mathcal{D}(E'), \tag{F.2}$$

this leads to the formation of so-called Lifshits tails in the spectrum [282, 283]. The eigenstates which belong to the Lifshits tail are created by the ocurrence of rare fluctuations in the potential (see section 3.4.1). In particular, if the random potential is bounded below by some minimum value

$$V_{\min} = \min(V), \tag{F.3}$$

the asymptotic behavior of the cumulative density of state $\mathcal{N}(E)$ when E approaches $V_{\min}$ from above is described by a stretched exponential which drops to zero at $E = V_{\min}$. In the seminal analysis by I.M. Lifshits [282, 283], the stretched exponential takes the form

$$\mathcal{N}(E) \sim C'\mathrm{e}^{-C''/\sqrt{E-V_{\min}}} \qquad [E \to V_{\min}^+]. \tag{F.4}$$

In general, the precise form of the Lifshits tail depends on the statistical properties of the random potential [197, 281]. The asymptotic form (F.4) was confirmed for various forms of impurity potentials [204, 323, 324], including potentials of randomly placed impurities with correlated single-impurity potential [324]. In the latter case, the single-impurity potential $f(z)$ which determines the autocorrelation function is required to decay faster than $1/|z|^3$ at infinity for result (F.4) to hold. On the other hand, if $f(z)$ decays as $1/|z|^\alpha$ with $1 < \alpha < 3$, then the stretched exponential takes a slightly different form [197, 281, 325]:

$$\mathcal{N}(E) \sim C'\mathrm{e}^{-C''(E-V_{\min})^{-\frac{1}{\alpha-1}}} \qquad [E \to V_{\min}^+]. \tag{F.5}$$

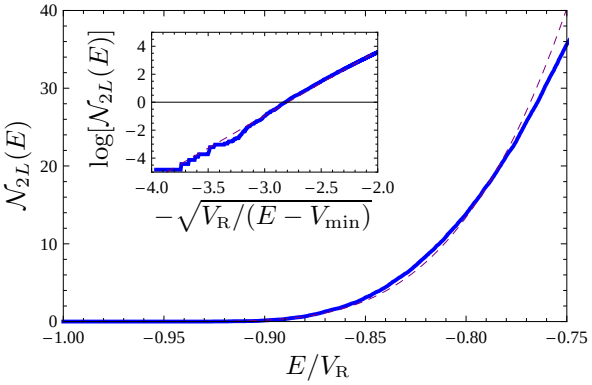


Figure F.1: Cumulative density of states in a speckle potential and fit of the low-energy tail by the law (F.4). The autocorrelation function of the potential is $C_2(z) = V_{\rm R}^2 \mathrm{sinc}(z/\sigma_{\rm R})^2$, with $2m\sigma_{\rm R}^2 V_{\rm R}/\hbar^2 = 1$. The minimum of the potential is $V_{\rm min} = -V_{\rm R}$. The quantity $\mathcal{N}_{2L}(E)$ is the average number of states up to energy E in a system of size $2L$. In the limit of large L, it becomes representative of $2L\mathcal{N}(E)$. Here the numerical data (blue solid line) was obtained by direct diagonalization in a box of size $2L = 5\times 10^3 \sigma_{\rm R}$, and averaged over 250 potential samples. The data is arranged for a linear fit (see inset). The result of this fit (dashed purple line) is reproduced in Fig. 3.6.

The different power dependence in the stretched exponential is characterized by the limit[1]

$$\lim_{E\to V_{\rm min}^+} \frac{\ln\left[-\ln[\mathcal{N}(E)]\right]}{\ln[E-V_{\rm min}]} \tag{F.6}$$

which, for a tail of the form (F.5), is equal to $-1/(\alpha-1)$ and, for Lifshits tail of the form (F.4), is equal to $-1/2$.

Speckle potentials

Figure F.1 shows the result of a numerical study of the low-energy spectrum in a speckle potential with autocorrelation function $C_2(z) = V_{\rm R}^2 \mathrm{sinc}(z/\sigma_{\rm R})^2$ and $V_{\rm R}/E_\sigma = 1$, where $E_\sigma = \hbar^2/2m\sigma_{\rm R}^2$. The dashed line is a fit with law (F.4), which turns out to provide a good approximation of the cumulative density of states in the low-energy tail of the spectrum.

A more thorough analysis was carried out with larger system sizes, and for various ratios of the amplitude $V_{\rm R}$ and the "correlation energy" E_σ. The result displayed in Fig. F.2 suggest possible deviations from law (F.4), as no clear convergence of the exponent (F.6) towards a unique value, e.g. 1/2, was observed.[2] The inset of Fig. F.2, on the other hand, suggests

[1] For clarity, we leave aside normalizations by the dimensions of C' and C''. The limit computed in Eq. (F.6) is called *Lifshits exponent* in Ref. [281]. This exponent is zero for a periodic potential [281]. Note also that it provides only a weak form of the asymptotic expressions in (3.131) and (F.5), as it hides possible weak dependencies (e.g. sub-power-law dependencies of C'' and power-law dependencies of C') on $E - V_{\rm min}$.

[2] The reduced autocorrelation function $c_2(u) = \sin(u)^2/u^2$ used in our studies with speckle potential might be said to fall between a $1/|u|^2$ and a $1/|u|^3$ decay of correlations. As a consequence, a law of the type (F.5) could be observed. And yet, the low-energy tail in speckle potentials may differ significantly from those results for

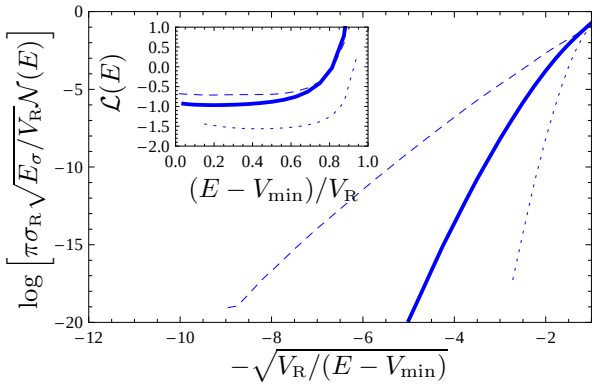


Figure F.2: Asymptotic behavior of the cumulative density of states $\mathcal{N}(E)$ in the Lifshits tail of a speckle potential with autocorrelation function $C_2(z) = V_{\mathrm{R}}^2 \mathrm{sinc}(z/\sigma_{\mathrm{R}})^2$ and minimum $V_{\min} = -V_{\mathrm{R}}$. The cumulative density of state was computed numerically for $V_{\mathrm{R}}/E_\sigma = 0.1, 1, 10$ (in dotted, solid and dashed lines, respectively), where $E_\sigma = \hbar^2/2m\sigma_{\mathrm{R}}^2$. The data was obtained from transfer matrix calculations by counting the nodes of the wave functions at a given energy. System sizes of the order of $10^8\sigma_{\mathrm{R}}$ were used, and averaging was performed over 10 realizations of the speckle potential. Inset: attempt to observe the convergence of $\mathcal{L}(E) = \ln[-\ln[\pi\sigma_{\mathrm{R}}\sqrt{E_\sigma/V_{\mathrm{R}}}\mathcal{N}(E)]]/\ln[(E-V_{\min})/V_{\mathrm{R}}]$ to a limit of the type (F.6).

that a convergence might be reached for much larger system sizes (not necessarily to a value independent of V_{R}/E_σ, though). Remarkably, the behavior which is closest to a convergence to an exponent of the order of $1/2$ is observed for the largest ratio of V_{R}/E_σ (i.e. $V_{\mathrm{R}}/E_\sigma = 10$). In the regime $V_{\mathrm{R}}/E_\sigma \gg 1$, the random potential has wide modulations of large amplitude, akin to infinitely deep potential wells with large, variables widths. The original argument of Lifshits might apply in this limiting regime and lead to an exponent $1/2$.

A precise determination of the full asymptotic form of the CDoS for generic speckle potentials would require further analytical or numerical studies which lie beyond the scope of the present work. At any rate, the stretched exponential (F.4) provides a good description of the Lifshits tail in the speckle potentials studied in this thesis. It should also be noted that the description of the Lifshits glass presented in chapter 3 does not depend qualitatively on the precise form of the Lifshits tail.

correlated impurity potentials. The Lifshits tails are created by rare configurations where the potential assumes values close to the minimum $V_{\min}$ on one or several correlation lengths. In this sense, these configurations involve a large number of "points". Except for a few simple cases, their probability is likely not to be captured entirely by the two-point correlation function, and to depend on higher-order correlation functions or, ultimately, on the entire probability density of the potential.

APPENDIX G

Decoupling basis for the Bogolyubov-de Gennes equations

In chapter 4 we develop a perturbation theory to solve the Bogolyubov-de Gennes equations (BdGEs)

$$\left[-\frac{\hbar^2}{2m}\nabla^2 + V(\mathbf{r}) + \Delta - \widetilde{V}(\mathbf{r})\right] f_\nu^+(\mathbf{r}) = \epsilon_\nu f_\nu^-(\mathbf{r}) \tag{G.1}$$

$$\left[-\frac{\hbar^2}{2m}\nabla^2 + 2\mu + V(\mathbf{r}) + 3\Delta - 3\widetilde{V}(\mathbf{r})\right] f_\nu^-(\mathbf{r}) = \epsilon_\nu f_\nu^+(\mathbf{r}), \tag{G.2}$$

where V is a weak potential, and Δ and $\widetilde{V}$, which derive from the fluctuations and the average value of the mean-field interaction term gn_0, are also small quantities. The differential problem of Eqs. (G.1) and (G.2) is parametrized by the energy ϵ_ν, and we wish to solve this set of equations for $f_\nu^+(\mathbf{r})$ and $f_\nu^-(\mathbf{r})$. Even in the absence of external potential ($V = 0$, and hence $\widetilde{V} = 0$, $\Delta = 0$), the two above equations are strongly coupled by the terms on the right-hand side. We show in this appendix that this technical difficulty is circumvented by the introduction of auxiliary functions g^+ and g^-, in the basis of which the BdGEs are decoupled to zeroth order in the amplitude of the potential, and which prove convenient for a perturbative solution of the BdGEs.

Matrix formulation

To gain insight into the structure of the BdGEs, we cast them into the algebraic form

$$\xi^2\nabla^2 F(\mathbf{r}) = \mathcal{F}_\epsilon(\mathbf{r})F(\mathbf{r}), \tag{G.3}$$

where

$$F(\mathbf{r}) = \begin{pmatrix} f^+(\mathbf{r}) \\ f^-(\mathbf{r}) \end{pmatrix}, \tag{G.4}$$

and $\mathcal{F}_\epsilon(\mathbf{r})$ is a real-valued, symmetric matrix which expands as $\mathcal{F}_\epsilon(\mathbf{r}) = \mathcal{F}_\epsilon^{(0)} + \delta\mathcal{F}(\mathbf{r})$, with

$$\mathcal{F}_\epsilon^{(0)} = \begin{pmatrix} 0 & -\epsilon/2\mu \\ -\epsilon/2\mu & 1 \end{pmatrix} \tag{G.5}$$

$$\delta\mathcal{F}(\mathbf{r}) = \frac{1}{2\mu}\begin{pmatrix} V(\mathbf{r}) + \Delta - \widetilde{V}(\mathbf{r}) & 0 \\ 0 & V(\mathbf{r}) + 3\Delta - 3\widetilde{V}(\mathbf{r}) \end{pmatrix}. \tag{G.6}$$

The two differential equations on f^+ and f^- associated with Eq. (G.3) are strongly coupled via the off-diagonal terms in $\mathcal{F}_\epsilon^{(0)}$. Since $\delta\mathcal{F}$ is small (at most of first order in $V_{\rm R}$), it is worth working in the basis which diagonalizes $\mathcal{F}_\epsilon^{(0)}$. Indeed, although the change of basis may introduce (coupling) off-diagonal terms in $\delta\mathcal{F}$, these terms will remain small. We will show that this approach is suitable for the set-up of a perturbation theory.

Solutions in the homogeneous case

In the absence of an external potential ($V = 0$), the matrix $\delta\mathcal{F}(\mathbf{r})$ vanishes identically. Then, the matrix $\mathcal{F}_\epsilon(\mathbf{r}) = \mathcal{F}_\epsilon^{(0)}$ has two eigenvalues,

$$\frac{1-\sqrt{1+(\epsilon/\mu)^2}}{2} \equiv -k^2\xi^2 \tag{G.7}$$

$$\frac{1+\sqrt{1+(\epsilon/\mu)^2}}{2} \equiv +\beta^2\xi^2, \tag{G.8}$$

respectively associated to the eigenvectors

$$F_k \propto \begin{pmatrix} \sqrt{\rho_\epsilon} \\ 1/\sqrt{\rho_\epsilon} \end{pmatrix} \quad \text{and} \quad F_\beta \propto \begin{pmatrix} -1/\sqrt{\rho_\epsilon} \\ \sqrt{\rho_\epsilon} \end{pmatrix}, \tag{G.9}$$

where

$$\rho_\epsilon = \frac{\mu}{\epsilon} + \sqrt{1+\left(\frac{\mu}{\epsilon}\right)^2}. \tag{G.10}$$

How do these solutions compare with the well-known results reported in section 4.1.4 ?

For simplicity, let us restrict our discussion to the 1D case[1]. Since Eq. (G.3) is of second order, each eigenspace corresponds to two possible solutions of the BdGEs. First, the solutions corresponding to $+\beta^2\xi^2$ have the form $e^{\pm\beta z}F_\beta$, and either grow or decrease exponentially. Here, the system is infinite, or required to have periodic boundary conditions. Since no solution of Eq. (G.3) in the subspace spanned by these eigenvectors can satisfy the boundary conditions on both boundaries of the system, these modes are forbidden in the case of vanishing V. Second, the solutions corresponding to $-k^2\xi^2$ are $e^{\pm ikz}F_k$, which are *oscillating* (plane-wave) modes. These modes are allowed for $V = 0$. They correspond to the well-known physical solutions of the BdGEs (4.49) and (4.50), reported in section 4.1.4.

Inhomogeneous case

The above procedure allowed us to decouple the BdGEs in homogenous space. Let us now introduce the external potential $V(\mathbf{r})$. Working in the eigenbasis of $\mathcal{F}_\epsilon^{(0)}$, equation (G.3) reads

$$\xi^2\nabla^2 G(\mathbf{r}) = \mathcal{G}_\epsilon(\mathbf{r})G(\mathbf{r}). \tag{G.11}$$

where

$$G(\mathbf{r}) = P_\epsilon^{-1}F(\mathbf{r}), \tag{G.12}$$

[1]The conclusions are naturally extended to higher dimensions.

and P_ϵ^{-1} is the inverse of the transformation matrix from the F-basis to the G-basis, i.e. [2]

$$P_\epsilon^{-1} = \begin{pmatrix} \sqrt{\rho_\epsilon} & 1/\sqrt{\rho_\epsilon} \\ -1/\sqrt{\rho_\epsilon} & \sqrt{\rho_\epsilon} \end{pmatrix}. \tag{G.13}$$

The matrix $\mathcal{G}_\epsilon(\mathbf{r})$ represents the Bogolyubov-de Gennes equations in the G-basis, and expands as $\mathcal{G}_\epsilon(\mathbf{r}) = \mathcal{G}_\epsilon^{(0)} + \delta\mathcal{G}_\epsilon(\mathbf{r})$, where

$$\mathcal{G}_\epsilon^{(0)} = \begin{pmatrix} -k^2\xi^2 & 0 \\ 0 & \beta^2\xi^2 \end{pmatrix} \tag{G.14}$$

and $\delta\mathcal{G}_\epsilon(\mathbf{r}) = P_\epsilon^{-1}\delta\mathcal{F}(\mathbf{r})P_\epsilon$, that is,

$$\delta\mathcal{G}_\epsilon = \frac{1}{2\mu}\begin{pmatrix} V - \frac{3+\rho_\epsilon^2}{1+\rho_\epsilon^2}(\widetilde{V}-\Delta) & -\frac{2\rho_\epsilon}{1+\rho_\epsilon^2}(\widetilde{V}-\Delta) \\ -\frac{2\rho_\epsilon}{1+\rho_\epsilon^2}(\widetilde{V}-\Delta) & V - \frac{1+3\rho_\epsilon^2}{1+\rho_\epsilon^2}(\widetilde{V}-\Delta) \end{pmatrix}. \tag{G.15}$$

In Eq. (G.14), k and β are functions of ϵ defined exactly as in Eqs. (G.7) and (G.8). The benefit of the transformation from the F-basis to the G-basis is that a weak external potential only weakly couples the two equations associated to Eq. (G.11), via $\delta\mathcal{G}_\epsilon$. Since now the coupling terms are at most of first order in V (as $\widetilde{V}_{\rm R} \leq V_{\rm R}$ and $2\rho_\epsilon/(1+\rho_\epsilon^2) \leq 1$), we can promote the G-basis as a suitable representation, which takes into account the full structure of the BdGEs, and which allows for a perturbative approach in the case of weak disorder.

Approximate mapping onto Schrödinger-like equations

For the sake of clarity, let us first write explicitly the two equations associated to Eq. (G.11), which are now weakly coupled, and still parametrized by the BQP energy ϵ :

$$-\frac{\hbar^2}{2m}\nabla^2 g^+ + \left[V - \frac{3+\rho^2}{1+\rho^2}(\widetilde{V}-\Delta)\right] g^+ - \frac{2\rho}{1+\rho^2}(\widetilde{V}-\Delta)g^- = +\frac{\hbar^2 k^2}{2m} g^+ \tag{G.16}$$

$$-\frac{\hbar^2}{2m}\nabla^2 g^- + \left[V - \frac{1+3\rho^2}{1+\rho^2}(\widetilde{V}-\Delta)\right] g^- - \frac{2\rho}{1+\rho^2}(\widetilde{V}-\Delta)g^+ = -\frac{\hbar^2 \beta^2}{2m} g^-. \tag{G.17}$$

Here g^+ and g^- are the components of the quasi-particle in the G-basis, $G(\mathbf{r}) = (g^+(\mathbf{r}), g^-(\mathbf{r}))^{\rm T}$. They are obtained from f^+ and f^- via transformation (G.12):

$$g^\pm(\mathbf{r}) = \pm\rho^{\pm 1/2} f^+(\mathbf{r}) + \rho^{\mp 1/2} f^-(\mathbf{r}). \tag{G.18}$$

We have dropped the subscript in ρ_ϵ for conciseness. The coefficients on the right-hand side of Eqs. (G.16) and (G.17) are defined as in Eqs. (G.7) and (G.8), and read

$$\frac{\hbar^2 k^2}{2m} = \sqrt{\mu^2 + \epsilon^2} - \mu \tag{G.19}$$

$$\frac{\hbar^2 \beta^2}{2m} = \sqrt{\mu^2 + \epsilon^2} + \mu. \tag{G.20}$$

Equations (G.16) and (G.17) are equivalent to the BdGEs, without any approximation. We now develop the perturbation theory in the G-basis.

[2] For simplicity, we leave easide a normalization which would make P_ϵ unitary. This choice does not affect Eqs. (4.73), (4.74) and following.

First-order terms

Since Eqs. (G.16) and (G.17) are weakly coupled, we can resort to the following self-consistent approach. We assume that g^- is smaller than g^+ by at least one order in $V_{\rm R}/\mu$ for small $V_{\rm R}$, and we neglect the second term on the left-hand side of Eq. (G.17). Then, solving the latter equation for g^-, we obtain[3]

$$g^-(\mathbf{r}) \simeq \frac{2m}{\hbar^2\beta^2}\frac{2\rho}{1+\rho^2}\int \mathrm{d}\mathbf{r}' G_{1/\beta}(\mathbf{r}-\mathbf{r}')\widetilde{V}^{(1)}(\mathbf{r}')g^+(\mathbf{r}'), \tag{G.21}$$

where $G_{1/\beta}(\mathbf{q}) = (2\pi)^{-d/2}/[1+(|\mathbf{q}|/\beta)^2]$ is the Green function associated with the differential operator $-(1/\beta)^2\nabla^2+1$, written in Fourier space. The positive smoothing function $G_{1/\beta}$ satisfies $\int \mathrm{d}\mathbf{r}' G_{1/\beta}(\mathbf{r}') = 1$, and decays on the length scale $1/\beta$, which is smaller than the healing length ξ and than $1/k$, i.e. the typical length scale over which g^+ varies. Thus, owing to the fact that $2m/(\hbar^2\beta^2) < 1/\mu$ and $2\rho/(1+\rho^2) < 1$, we can safely write

$$|g^-(\mathbf{r})| \;<\; \frac{1}{\mu}\int \mathrm{d}\mathbf{r}' G_{1/\beta}(\mathbf{r}-\mathbf{r}') \times |\widetilde{V}^{(1)}(\mathbf{r}')| \times |g^+(\mathbf{r}')|.$$

Then, in terms of orders of magnitude,

$$\begin{aligned} |g^-| \;&\lesssim\; \frac{\widetilde{V}_{\rm R}^{(1)}}{\mu}|g^+|\int \mathrm{d}\mathbf{r}' G_{1/\beta}(\mathbf{r}-\mathbf{r}') \\ &\lesssim\; \frac{\widetilde{V}_{\rm R}^{(1)}}{\mu}|g^+| \ll |g^+|, \end{aligned} \tag{G.22}$$

which is consistent with our initial assumption, i.e. g^- is small compared to g^+. Figure G.1 displays numerical results which corroborate expression (G.21). As for the data of Fig. G.2, they confirm that g^- is a term of order $\widetilde{V}_{\rm R}^{(1)}/\mu$ at most as compared to g^+, over the entire BQP spectrum.

From the upper bound (G.22), we infer that the third term on the left-hand side of Eq. (G.16) is of the order of $\widetilde{V}_{\rm R}^{(1)}(\widetilde{V}_{\rm R}^{(1)}/\mu)|g^+|$ at most, while the second term contains terms scaling as $V_{\rm R}|g^+|$. Hence, we neglect the former contribution, and obtain a closed equation for g^+ that is valid up to first order in $\widetilde{V}_{\rm R}^{(1)}/\mu$:

$$-\frac{\hbar^2}{2m}\nabla^2 g^+ + \mathcal{V}_\epsilon(\mathbf{r})g^+ \simeq \frac{\hbar^2k^2}{2m}g^+, \tag{G.23}$$

where

$$\mathcal{V}_\epsilon(\mathbf{r}) = V(\mathbf{r}) - \frac{3+\rho^2}{1+\rho^2}\widetilde{V}^{(1)}(\mathbf{r}). \tag{G.24}$$

These are the expressions reproduced in Eqs. (4.80) and (4.81), which form the basis of our approach to study the spatial properties of BQP modes.

[3]Note that Δ is at least of second order in $V_{\rm R}$ (see section 4.2.1 or appendix E).

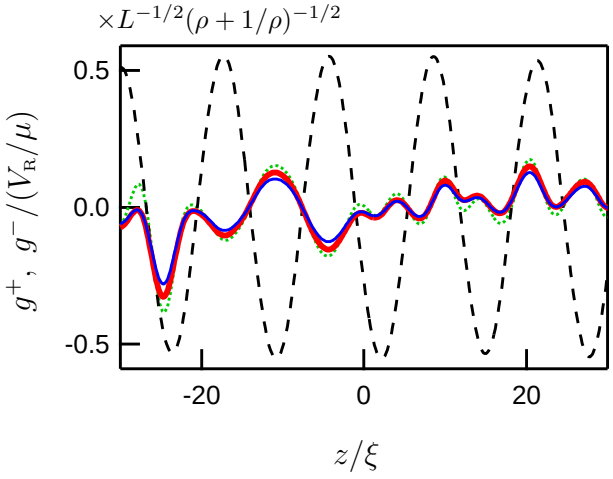


Figure G.1: Components of a BQP mode in the G-basis. This eigenmode was computed for a speckle potential with $V_R = 0.05\mu$ and $\sigma_R/\xi = \sqrt{3/2}$, and has energy $\epsilon \simeq 1.1\mu$. The g^+ and g^- components obtained numerically are given by the black dashed line and the blue solid line, respectively. The thick red line represents the convolution formula (G.21), and the green dotted line the somewhat cruder approximation (G.26) to g^-. Note that all the representations of g^- have been rescaled by μ/V_R for better comparison with g^+. With the parameters above, the smoothed potential $\widetilde{V}^{(1)}$ has root-mean-square amplitude $\widetilde{V}^{(1)}_R \simeq 0.6\, V_R$.

Second-order terms - offset and fluctuations

We now consider explicitly the terms in Eq. (G.16) that are of second order in V_R.[4] Their discussion takes a technical twist, but allows for the determination of a precise range of validity of the simple effective equation (4.80).

The second term on the left-hand side of Eq. (G.16) contains both a fluctuation term $\widetilde{V}^{(2)}$ and an offset $\Delta^{(2)}$ which are proportional to V_R^2.[5] Likewise, the crossed term $\widetilde{V}g^-$ introduces elements of order $(V_R^2/\mu)|g^+|$ into Eq. (G.16). Since g^- itself is of order $(V_R/\mu)|g^+|$, we need only consider the contribution of $\widetilde{V}^{(1)}g^-$ in $\widetilde{V}g^-$. This contribution reads

$$\frac{2\rho}{1+\rho^2}\widetilde{V}^{(1)}(\mathbf{r})g^-(\mathbf{r}) \simeq \frac{2m}{\hbar^2\beta^2}\frac{4\rho^2}{[1+\rho^2]^2}\widetilde{V}^{(1)}(\mathbf{r})\int \mathrm{d}\mathbf{r}' G_{1/\beta}(\mathbf{r}-\mathbf{r}')\widetilde{V}^{(1)}(\mathbf{r}')g^+(\mathbf{r}'), \tag{G.25}$$

where we have used approximation (G.21), which is valid to the required order. As the g^+ function appears in the integrand of Eq. (G.25), the latter expression cannot be used as such to reduce Eq. (G.16) to a closed Schrödinger-like equation for g^+. In the low-energy limit, however, the contribution of g^- may be simplified. For $k \ll \min(1/\sigma_R, 1/\xi)$, we expect g^+ to vary much more slowly than the other quantities in the integrand of Eq. (G.21), and we can use the approximation

$$g^-(\mathbf{r}) \simeq \frac{2m}{\hbar^2\beta^2}\frac{2\rho}{1+\rho^2}g^+(\mathbf{r})\int \mathrm{d}\mathbf{r}' G_{1/\beta}(\mathbf{r}-\mathbf{r}')\widetilde{V}(\mathbf{r}'). \tag{G.26}$$

[4] We now drop the distinction between smoothed and bare amplitudes (e.g. between $\widetilde{V}^{(1)}_R$ and V_R) in the discussion of orders of magnitude.

[5] Expressions for $\widetilde{V}^{(2)}$ and $\Delta^{(2)}$ are given in section 4.2.1 and in Eqs. (E.28) and (E.29) of appendix E.

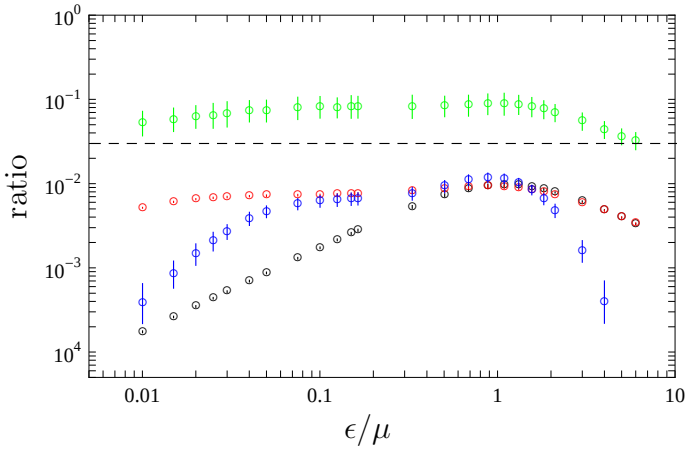


Figure G.2: Relative amplitude of g^+ and g^- as a function of the BQP energy ϵ, for speckle potentials with $V_{\rm R} = 0.05\mu$ and $\sigma_{\rm R}/\xi = \sqrt{3/2}$. The amplitudes are measured with help of the envelope functions $r_\pm = \sqrt{g^{\pm 2} + (\partial_z g^\pm/k)^2}$. The circles show: the maximum value of $r_-(z)/r_+(z)$ in systems as large as $10^5\sigma_{\rm R}$[green], the fraction of space where $r_-(z) > (\widetilde{V}_{\rm R}^{(1)}/\mu)\, r_+(z)$ [blue], the ratio $\left[\int r_-^2 / \int r_+^2\right]^{1/2}$ [red] and the ratio $\left[\int |g^-|^2 / \int |g^+|^2\right]^{1/2}$ [black] as a function of the BQP energy. The data was averaged over 200 realizations, and the small vertical bars denote plus or minus two standard deviations. The black dashed line corresponds to the value of $\widetilde{V}_{\rm R}^{(1)}/\mu$.

In this regime, g^+ can also be taken out of the integral in formula (G.25). Hence, we get a new closed equation for g^+, which now comprises all the terms up to order $V_{\rm R}^2$ and is legitimate in the low-energy limit:

$$\begin{aligned}\frac{\hbar^2 k^2}{2m} g^+ \;\simeq\; & -\frac{\hbar^2}{2m}\nabla^2 g^+ + \left[\mathcal{V}_\epsilon(\mathbf{r}) - \frac{3+\rho^2}{1+\rho^2}\left(\widetilde{V}^{(2)}(\mathbf{r}) - \Delta^{(2)}\right)\right] g^+ \\ & -\frac{2m}{\hbar^2\beta^2}\frac{4\rho^2}{(1+\rho^2)^2}\left[\widetilde{V}^{(1)}(\mathbf{r})\int \mathrm{d}\mathbf{r}' G_{1/\beta}(\mathbf{r}-\mathbf{r}')\widetilde{V}^{(1)}(\mathbf{r}')\right] g^+. \end{aligned} \tag{G.27}$$

We identify the two last terms on the right-hand side with a potential acting on g^+. Its expression is rather cumbersome. We shall nevertheless try and go one step beyond the first-order perturbation theory of Eqs. (G.23) and (G.24), in order to discuss possible limitations. In particular, the discussion which follows is based on the observation that the potential on the right-hand side of Eq. (G.27) contains fluctuations around the mean, and an offset, which is obtained by taking the spatial average of that potential.

From the analysis in chapter 2, we recall that the Lyapunov exponent of a Schrödinger particle in a random potential directly depends on the n-point autocorrelation functions C_n of the potential: $C_2 \propto V_{\rm R}^2, C_3 \propto V_{\rm R}^3, \ldots$ These correlation functions tend to zero at large separations, because the potential is taken with zero average.[6] Here, the random potential acting on g^+ is the sum of several contributions. The Lyapunov exponent derived from Eq. (G.27) therefore depends on the autocorrelators as well as the cross-correlators of these various contributions.

[6] We refer to the discussion around Eq. (1.23).

In particular, the second-order fluctuations on the right-hand side of Eq. (G.27) contribute to the Lyapunov exponent Γ by terms of order V_{R}^3 (when these fluctuations are crossed with $\mathcal{V}_\epsilon$, which is of order V_{R}, to build a two-point cross-correlator of order V_{R}^3) and higher. We do not detail here these higher-order contributions to the Lyapunov exponent, and concentrate instead on the offset terms, which have to be isolated from the fluctuations for the calculations of the Lyapunov exponent to hold.

When offset terms are introduced into the potential of a Schrödinger equation, they renormalize the parameter $\hbar^2k^2/2m$, and modify, for instance, the Fourier component $\mathbf{k}$ at which the correlation functions entering the Lyapunov exponent are evaluated. An inspection of Eq. (G.27) shows that the right-hand side indeed contains an offset, proportional to V_{R}^2. We can define a corrected kinetic term which cancels this offset:

$$\frac{\hbar^2k'^2}{2m} = \frac{\hbar^2k^2}{2m} - \frac{3+\rho^2}{1+\rho^2}\Delta^{(2)} + \frac{\epsilon^2}{2\mu}D^{(2)}(\epsilon). \tag{G.28}$$

Here k is still defined by Eq. (G.19), and

$$D^{(2)}(\epsilon) = \frac{16m\mu\rho^2}{\hbar^2\beta^2\epsilon^2\left(1+\rho^2\right)^2}\int \mathrm{d}\mathbf{r}\, G_{1/\beta}(\mathbf{r})\langle\widetilde{V}^{(1)}(\mathbf{0})\widetilde{V}^{(1)}(\mathbf{r})\rangle \tag{G.29}$$

is introduced to absorb the average value of the term proportional to g^+ on the second line of Eq. (G.27) at the leading order. Since the last two terms in Eq. (G.28) are proportional to V_{R}^2, significant changes in the relation linking the BQP energy and the average kinetic term will indeed be restricted to a range of low energies, which has yet to be defined.

Expression (G.29) is easily evaluated in terms of the reduced auto-correlation function of the bare potential V:

$$D^{(2)}(\epsilon) = \frac{V_{\mathrm{R}}^2(2\pi)^{-d/2}\sigma_{\mathrm{R}}^d}{\mu^2\beta^2\xi^2\left(2\beta^2\xi^2-1\right)^2}\int \mathrm{d}\mathbf{q}\frac{\hat{c}(\mathbf{q}\sigma_{\mathrm{R}})}{\left(1+\frac{\mathbf{q}^2}{\beta^2}\right)\left(1+\mathbf{q}^2\xi^2\right)^2} \tag{G.30}$$

and expanded as

$$D^{(2)}(\epsilon) = \left(\frac{V_{\mathrm{R}}}{\mu}\right)^2\left[I_3 - \left(I_3+\frac{I_4}{4}\right)\left(\frac{\epsilon}{\mu}\right)^2 + \underset{\frac{\epsilon}{\mu}\to 0}{\mathrm{O}}\left(\frac{\epsilon^4}{\mu^4}\right)\right] \tag{G.31}$$

where I_n is defined by

$$I_n\left(\frac{\xi}{\sigma_{\mathrm{R}}}\right) = \frac{\sigma_{\mathrm{R}}^d}{(2\pi)^{d/2}}\int \mathrm{d}\mathbf{q}\frac{\hat{c}_2(\mathbf{q}\sigma_{\mathrm{R}})}{[1+(|\mathbf{q}|\xi)^2]^n}, \tag{G.32}$$

as in section 3.3.3, and $\hat{c}_2$ is the Fourier transform of the reduced autocorrelation function of the bare potential V. Note that with this definition the leading deviation $\Delta^{(2)}$ is cast into [see Eq. (3.76)]

$$\Delta^{(2)} = \frac{V_{\mathrm{R}}^2}{2\mu}\left[I_1 - I_2\right]. \tag{G.33}$$

Finally, using Eqs.(G.31) and (G.33), we obtain a low-energy expansion of Eq. (G.28) as

$$\frac{\hbar^2k'^2}{2m} \simeq -\Delta^{(2)} + \frac{\epsilon^2}{2\mu}\left[1+\left(\frac{V_{\mathrm{R}}}{\mu}\right)^2\left(I_3+\frac{I_2-I_1}{2}\right)\right]. \tag{G.34}$$

This expression is actually already the product of the low-energy approximation (G.26), which may put into question the meaning and accuracy of the terms proportional to ϵ^2 in expression (G.34). The $\Delta^{(2)}$ term, on the other hand, is a safe term, as can be seen by taking the limit $\epsilon \to 0$ (and hence, $\rho \to \infty$) in Eq. (G.16) or (G.21).

Let us emphasize that the terms in Eq. (G.28) do not necessarily (all) correspond to a renormalization of the average kinetic energy. However, they do correspond to a renormalization of the average wave vector which should be relevant in scattering processes and localization.

Bibliography

[1] P. W. Anderson, "Absence of Diffusion in Certain Random Lattices", *Phys. Rev.* **109**, 1492 (1958).

[2] A. Lagendijk, B. van Tiggelen, and D. S. Wiersma, "Fifty years of Anderson localization", *Physics Today* **62**, 24 (2009).

[3] S. John, "Localization of Light", *Physics Today* **44**, 32 (1991).

[4] R. L. Weaver, "Anderson localization of ultrasound", *Wave Motion* **12**, 129 (1990).

[5] A. Aspect and M. Inguscio, "Anderson localization of ultracold atoms", *Physics Today* **62**, 30 (2009).

[6] J. A. Hertz, L. Fleishman, and P. W. Anderson, "Marginal Fluctuations in a Bose Glass", *Phys. Rev. Lett.* **43**, 942 (1979).

[7] M. Ma, B. I. Halperin, and P. A. Lee, "Strongly disordered superfluids: Quantum fluctuations and critical behavior", *Phys. Rev. B* **34**, 3136 (1986).

[8] T. Giamarchi and H. J. Schulz, "Localization and Interaction in One-Dimensional Quantum Fluids", *EPL (Europhys. Lett.)* **3**, 1287 (1987).

[9] D. Belitz and T. R. Kirkpatrick, "The Anderson-Mott transition", *Rev. Mod. Phys.* **66**, 261 (1994).

[10] J. D. Reppy, "Superfluid Helium in Porous Media", *J. Low Temp. Phys.* **87**, 205 (1992).

[11] I. S. Beloborodov, A. V. Lopatin, V. M. Vinokur, and K. B. Efetov, "Granular electronic systems", *Rev. Mod. Phys.* **79**, 469 (2007).

[12] M. H. Anderson, J. R. Ensher, M. R. Matthews, C. E. Wieman, and E. A. Cornell, "Observation of Bose-Einstein Condensation in a Dilute Atomic Vapor", *Science* **269**, 198 (1995).

[13] C. C. Bradley, C. A. Sackett, J. J. Tollett, and R. G. Hulet, "Evidence of Bose-Einstein Condensation in an Atomic Gas with Attractive Interactions", *Phys. Rev. Lett.* **75**, 1687 (1995).

[14] K. B. Davis, M. O. Mewes, M. R. Andrews, N. J. van Druten, D. S. Durfee, D. M. Kurn, and W. Ketterle, "Bose-Einstein Condensation in a Gas of Sodium Atoms", *Phys. Rev. Lett.* **75**, 3969 (1995).

[15] L. Fallani, C. Fort, and M. Inguscio, "Bose-Einstein Condensates in Disordered Potentials", *Adv. At. Mol. Opt. Phys.* **56**, 119 (2008).

[16] L. Sanchez-Palencia and M. Lewenstein, "Disordered quantum gases under control", *Nat. Phys.* **6**, 87 (2010).

[17] W. Ketterle, D. Durfee, and D. Stamper-Kurn, in *Bose-Einstein condensation in atomic gases, Proceedings of the International School of Physics ¨Enrico Fermi¨, Course CXL*, edited by M. Inguscio, S. Stringari, and C. Wieman (IOS Press, Amsterdam, 1999), e-print: arXiv:cond-mat/9904034.

[18] I. Bloch, J. Dalibard, and W. Zwerger, "Many-body physics with ultracold gases", *Rev. Mod. Phys.* **80**, 885 (2008).

[19] M. Lewenstein, A. Sanpera, V. Ahufinger, B. Damski, A. Sen, and U. Sen, "Ultracold atomic gases in optical lattices: mimicking condensed matter physics and beyond", *Adv. Phys.* **56**, 243 (2007).

[20] M. Greiner, O. Mandel, T. Esslinger, T. W. Hänsch, and I. Bloch, "Quantum phase transition from a superfluid to a Mott insulator in a gas of ultracold atoms", *Nature* **415**, 39 (2002).

[21] Z. Hadzibabic, P. Kruger, M. Cheneau, B. Battelier, and J. Dalibard, "Berezinskii-Kosterlitz-Thouless crossover in a trapped atomic gas", *Nature* **441**, 1118 (2006).

[22] P. Horak, J.-Y. Courtois, and G. Grynberg, "Atom cooling and trapping by disorder", *Phys. Rev. A* **58**, 3953 (1998).

[23] G. Grynberg, P. Horak, and C. Mennerat-Robilliard, "Spatial diffusion of atoms cooled in a speckle field", *EPL (Europhys. Lett.)* **49**, 424 (2000).

[24] B. Damski, J. Zakrzewski, L. Santos, P. Zoller, and M. Lewenstein, "Atomic Bose and Anderson Glasses in Optical Lattices", *Phys. Rev. Lett.* **91**, 080403 (2003).

[25] J. E. Lye, L. Fallani, M. Modugno, D. Wiersma, C. Fort, and M. Inguscio, "Bose-Einstein Condensate in a Random Potential", *Phys. Rev. Lett.* **95**, 070401 (2005).

[26] D. Clément, A. F. Varón, M. Hugbart, J. A. Retter, P. Bouyer, L. Sanchez-Palencia, D. M. Gangardt, G. V. Shlyapnikov, and A. Aspect, "Suppression of Transport of an Interacting Elongated Bose-Einstein Condensate in a Random Potential", *Phys. Rev. Lett.* **95**, 170409 (2005).

[27] C. Fort, L. Fallani, V. Guarrera, J. E. Lye, M. Modugno, D. S. Wiersma, and M. Inguscio, "Effect of Optical Disorder and Single Defects on the Expansion of a Bose-Einstein Condensate in a One-Dimensional Waveguide", *Phys. Rev. Lett.* **95**, 170410 (2005).

[28] T. Schulte, S. Drenkelforth, J. Kruse, W. Ertmer, J. Arlt, K. Sacha, J. Zakrzewski, and M. Lewenstein, "Routes Towards Anderson-Like Localization of Bose-Einstein Condensates in Disordered Optical Lattices", *Phys. Rev. Lett.* **95**, 170411 (2005).

[29] J. Billy, V. Josse, Z. Zuo, A. Bernard, B. Hambrecht, P. Lugan, D. Clément, L. Sanchez-Palencia, P. Bouyer, and A. Aspect, "Direct observation of Anderson localization of matter waves in a controlled disorder", *Nature* **453**, 891 (2008).

[30] G. Roati, C. D'Errico, L. Fallani, M. Fattori, C. Fort, M. Zaccanti, G. Modugno, M. Modugno, and M. Inguscio, "Anderson localization of a non-interacting Bose-Einstein condensate", *Nature* **453**, 895 (2008).

[31] D. Clément, A. F. Varón, J. A. Retter, L. Sanchez-Palencia, A. Aspect, and P. Bouyer, "Experimental study of the transport of coherent interacting matter-waves in a 1D random potential induced by laser speckle", *New J. Phys.* **8**, 165 (2006).

[32] F. Dalfovo, S. Giorgini, L. P. Pitaevskii, and S. Stringari, "Theory of Bose-Einstein condensation in trapped gases", *Rev. Mod. Phys.* **71**, 463 (1999).

[33] B. Deissler, M. Zaccanti, G. Roati, C. D'Errico, M. Fattori, M. Modugno, G. Modugno, and M. Inguscio, "Delocalization of a disordered bosonic system by repulsive interactions", e-print arXiv:0910.5062v1.

[34] L. Sanchez-Palencia, D. Clément, P. Lugan, P. Bouyer, G. V. Shlyapnikov, and A. Aspect, "Anderson Localization of Expanding Bose-Einstein Condensates in Random Potentials", *Phys. Rev. Lett.* **98**, 210401 (2007).

[35] E. Akkermans and G. Montambaux, *Mesoscopic Physics of Electrons and Photons* (Cambridge University Press, Cambridge, 2007).

[36] Y. Imry, *Introduction to mesoscopic physics, second edition* (Oxford University Press, Oxford, 2002).

[37] P. A. Lee and T. V. Ramakrishnan, "Disordered electronic systems", *Rev. Mod. Phys.* **57**, 287 (1985).

[38] N. Ashcroft and D. Mermin, *Solid State Physics* (Saunders College, Philadelphia, 1976).

[39] L. Van den dries, C. Van Haesendonck, Y. Bruynseraede, and G. Deutscher, "Two-Dimensional Localization in Thin Copper Films", *Phys. Rev. Lett.* **46**, 565 (1981).

[40] D. Vollhardt and P. Wölfle, "Diagrammatic, self-consistent treatment of the Anderson localization problem in $d \leq 2$ dimensions", *Phys. Rev. B* **22**, 4666 (1980).

[41] D. Vollhardt and P. Wölfle, in *Electronic phase transitions*, edited by W. Hanke and Y. V. Kopaev (Elsevier Science, Amsterdam, 1992), Chap. 1, pp. 1–78.

[42] S. E. Skipetrov and B. A. van Tiggelen, "Dynamics of Anderson Localization in Open 3D Media", *Phys. Rev. Lett.* **96**, 043902 (2006).

[43] B. Kramer and A. MacKinnon, "Localization: theory and experiment", *Reports on Progress in Physics* **56**, 1469 (1993).

[44] I. Aleiner, B. Altshuler, and M. Gershenson, "Interaction effects and phase relaxation in disordered systems", *Waves in Random Media* **9**, 201 (1999).

[45] R. Kuhn, *Coherent Transport of Matter Waves in Disordered Optical Potentials*, Ph.D. thesis, University of Bayreuth, Germany, and University of Nice Sophia-Antipolis, France, 2007.

[46] F. Evers and A. D. Mirlin, "Anderson transitions", *Rev. Mod. Phys.* **80**, 1355 (2008).

[47] L. Pezzé, B. Hambrecht, and L. Sanchez-Palencia, "Dipole oscillations of a Fermi gas in a disordered trap: Damping and localization", *EPL (Europhys. Lett.)* **88**, 30009 (2009).

[48] N. F. Mott, "Electrons in disordered structures", *Adv. Phys.* **16**, 49 (1967).

[49] M. H. Cohen, H. Fritzsche, and S. R. Ovshinsky, "Simple Band Model for Amorphous Semiconducting Alloys", *Phys. Rev. Lett.* **22**, 1065 (1969).

[50] N. Mott, "Electrons in glass", *Rev. Mod. Phys.* **50**, 203 (1978).

[51] N. Mott, "The mobility edge since 1967", *J. Phys. C: Solid State Phys.* **20**, 3075 (1987).

[52] M. Schreiber and H. Grussbach, "Multifractal wave functions at the Anderson transition", *Phys. Rev. Lett.* **67**, 607 (1991).

[53] E. Abrahams, P. W. Anderson, D. C. Licciardello, and T. V. Ramakrishnan, "Scaling Theory of Localization: Absence of Quantum Diffusion in Two Dimensions", *Phys. Rev. Lett.* **42**, 673 (1979).

[54] M. C. W. van Rossum and T. M. Nieuwenhuizen, "Multiple scattering of classical waves: microscopy, mesoscopy, and diffusion", *Rev. Mod. Phys.* **71**, 313 (1999).

[55] J. T. Edwards and D. J. Thouless, *J. Phys. C: Solid State Phys.* **5**, 807 (1972).

[56] D. C. Licciardello and D. J. Thouless, "Constancy of Minimum Metallic Conductivity in Two Dimensions", *Phys. Rev. Lett.* **35**, 1475 (1975).

[57] D. C. Licciardello and D. J. Thouless, "Conductivity and mobility edges for two-dimensional disordered systems", *J. Phys. C: Solid State Phys.* **8**, 4157 (1975).

[58] D. Vollhardt and P. Wölfle, "Scaling Equations from a Self-Consistent Theory of Anderson Localization", *Phys. Rev. Lett.* **48**, 699 (1982).

[59] J. L. Pichard and G. Sarma, "Finite size scaling approach to Anderson localisation", *J. Phys. C: Solid State Phys.* **14**, L127 (1981).

[60] D. J. Thouless, "A relation between the density of states and range of localization for one dimensional random systems", *J. Phys. C: Solid State Phys.* **5**, 77 (1972).

[61] D. C. Herbert and R. Jones, "Localized states in disordered systems", *J. Phys. C: Solid State Phys.* **4**, 1145 (1971).

[62] J. L. Pichard and G. Andre, "Many-Channel Transmission: Large Volume Limit of the Distribution of Localization Lengths and One-Parameter Scaling", *EPL (Europhys. Lett.)* **2**, 477 (1986).

[63] R. Landauer, "Spatial variation of currents and fields due to localized scatterers in metallic conduction", *IBM J. Res. Dev.* **1**, 223 (1957).

[64] R. Landauer, "Electrical resistance of disordered one-dimensional lattices", *Philos. Mag.* **21**, 863 (1970).

[65] K. Ishii, "Localization of Eigenstates and Transport Phenomena in the One-Dimensional Disordered System", *Prog. Theor. Phys. Suppl.* **53**, 77 (1973).

[66] P. W. Anderson, D. J. Thouless, E. Abrahams, and D. S. Fisher, "New method for a scaling theory of localization", *Phys. Rev. B* **22**, 3519 (1980).

[67] O. N. Dorokhov, "Transmission coefficient and the localization length of an electron in N bound disordered chains", *JETP Lett.* **36**, 318 (1982).

[68] O. N. Dorokhov, "Electron localization in a multichannel conductor", *Sov. Phys. JETP* **58**, 606 (1983).

[69] P. A. Mello, "Central-limit theorems on groups", *J. Math. Phys.* **27**, 2876 (1986).

[70] Y. Imry, "Active Transmission Channels and Universal Conductance Fluctuations", *EPL (Europhys. Lett.)* **1**, 249 (1986).

[71] B. Derrida, K. Mecheri, and J. Pichard, "Lyapounov exponents of products of random matrices : weak disorder expansion. - Application to localisation", *J. Physique* **48**, 733 (1987).

[72] O. N. Dorokhov, "Solvable model of multichannel localization", *Phys. Rev. B* **37**, 10526 (1988).

[73] P. A. Mello, P. Pereyra, and N. Kumar, "Macroscopic approach to multichannel disordered conductors", *Ann. Phys.* **181**, 290 (1988).

[74] P. A. Mello, "Macroscopic approach to universal conductance fluctuations in disordered metals", *Phys. Rev. Lett.* **60**, 1089 (1988).

[75] C. W. J. Beenakker, "Random-matrix theory of quantum transport", *Rev. Mod. Phys.* **69**, 731 (1997).

[76] K. A. Muttalib, P. Wölfle, and V. A. Gopar, "Conductance distribution in quasi-one-dimensional disordered quantum wires", *Ann. Phys.* **308**, 156 (2003).

[77] V. I. Oseledec, "A multiplicative ergodic theorem. Lyapunov characteristic numbers for dynamical systems", *Trans. Mosc. Math. Soc.* **19**, 197 (1968).

[78] H. Furstenberg, "Non-commuting random products", *Trans. Am. Math. Soc.* **108**, 377 (1963).

[79] J. P. Eckmann and D. Ruelle, "Ergodic theory of chaos and strange attractors", *Rev. Mod. Phys.* **57**, 617 (1985).

[80] P. Bougerol and J. Lacroix, *Products of random matrices with applications to Schrödinger operators* (Birkhäuser, Basel, 1985).

[81] B. van Tiggelen, in *Diffuse Waves in Complex Media*, edited by J. P. Fouque (Kluwer, Dordrecht, 1999), pp. 1–63, ISBN: 978-0-7923-5680-6.

[82] F. m. c. Delyon, Y.-E. Lévy, and B. Souillard, "Approach à la Borland to Multidimensional Localization", *Phys. Rev. Lett.* **55**, 618 (1985).

[83] C.A. Müller and D. Delande, lecture notes from Les Houches Physics School in Singapore, June 2009, in preparation.

[84] S. A. van Langen, P. W. Brouwer, and C. W. J. Beenakker, "Nonperturbative calculation of the probability distribution of plane-wave transmission through a disordered waveguide", *Phys. Rev. E* **53**, R1344 (1996).

[85] J.-L. Pichard and M. Sanquer, "Quantum conductance fluctuations and maximum entropy ensembles for the transfer matrix", *Physica A* **167**, 66 (1990).

[86] I. M. Lifshits, S. A. Gredeskul, and L. A. Pastur, *Introduction to the theory of disordered systems* (Wiley, New York, 1988).

[87] J. Sak and B. Kramer, "Transmission of particles through a random one-dimensional potential", *Phys. Rev. B* **24**, 1761 (1981).

[88] H. Hu, A. Strybulevych, J. H. Page, S. E. Skipetrov, and B. A. van Tiggelen, "Localization of ultrasound in a three-dimensional elastic network", *Nat. Phys.* **4**, 1745 (2008).

[89] S. Faez, A. Strybulevych, J. H. Page, A. Lagendijk, and B. A. van Tiggelen, "Observation of Multifractality in Anderson Localization of Ultrasound", *Phys. Rev. Lett.* **103**, 155703 (2009).

[90] R. Dalichaouch, J. P. Armstrong, S. Schultz, P. M. Platzman, and S. L. McCall, "Microwave localization by two-dimensional random scattering", *Nature* **354**, 53 (1991).

[91] A. A. Chabanov, M. Stoytchev, and A. Z. Genack, "Statistical signatures of photon localization", *Nature* **404**, 850 (2000).

[92] D. S. Wiersma, P. Bartolini, A. Lagendijk, and R. Righini, "Localization of light in a disordered medium", *Nature* **390**, 671 (1997).

[93] M. Störzer, P. Gross, C. M. Aegerter, and G. Maret, "Observation of the Critical Regime Near Anderson Localization of Light", *Phys. Rev. Lett.* **96**, 063904 (2006).

[94] T. Schwartz, G. Bartal, S. Fishman, and M. Segev, "Transport and Anderson localization in disordered two-dimensional photonic lattices", *Nature* **446**, 52 (2007).

[95] Y. Lahini, A. Avidan, F. Pozzi, M. Sorel, R. Morandotti, D. N. Christodoulides, and Y. Silberberg, "Anderson Localization and Nonlinearity in One-Dimensional Disordered Photonic Lattices", *Phys. Rev. Lett.* **100**, 013906 (2008).

[96] F. L. Moore, J. C. Robinson, C. Bharucha, P. E. Williams, and M. G. Raizen, "Observation of Dynamical Localization in Atomic Momentum Transfer: A New Testing Ground for Quantum Chaos", *Phys. Rev. Lett.* **73**, 2974 (1994).

[97] F. L. Moore, J. C. Robinson, C. F. Bharucha, B. Sundaram, and M. G. Raizen, "Atom Optics Realization of the Quantum δ-Kicked Rotor", *Phys. Rev. Lett.* **75**, 4598 (1995).

[98] J. Chabé, G. Lemarié, B. Grémaud, D. Delande, P. Szriftgiser, and J. C. Garreau, "Experimental Observation of the Anderson Metal-Insulator Transition with Atomic Matter Waves", *Phys. Rev. Lett.* **101**, 255702 (2008).

[99] G. Labeyrie, F. de Tomasi, J.-C. Bernard, C. A. Müller, C. Miniatura, and R. Kaiser, "Coherent Backscattering of Light by Cold Atoms", *Phys. Rev. Lett.* **83**, 5266 (1999).

[100] D. R. Grempel, R. E. Prange, and S. Fishman, "Quantum dynamics of a nonintegrable system", *Phys. Rev. A* **29**, 1639 (1984).

[101] G. Casati, I. Guarneri, and D. L. Shepelyansky, "Anderson Transition in a One-Dimensional System with Three Incommensurate Frequencies", *Phys. Rev. Lett.* **62**, 345 (1989).

[102] S. E. Skipetrov, A. Minguzzi, B. A. van Tiggelen, and B. Shapiro, "Anderson Localization of a Bose-Einstein Condensate in a 3D Random Potential", *Phys. Rev. Lett.* **100**, 165301 (2008).

[103] T. Giamarchi, in *Quantum phenomena in mesoscopic systems (Proceedings of the International School of Physics "Enrico Fermi", Vol. CLI)*, edited by B. Altshuler, V. Tognetti, and A. Tagliacozzo (IOS Press, Amsterdam, 2003), Chap. 14, pp. 303–337.

[104] E. Abrahams, S. V. Kravchenko, and M. P. Sarachik, "Metallic behavior and related phenomena in two dimensions", *Rev. Mod. Phys.* **73**, 251 (2001).

[105] B. L. Altshuler and A. G. Aronov, "Zero bias anomaly in tunnel resistance and electron-electron interaction", *Solid State Commun.* **30**, 115 (1979).

[106] B. L. Altshuler, A. G. Aronov, and P. A. Lee, "Interaction Effects in Disordered Fermi Systems in Two Dimensions", *Phys. Rev. Lett.* **44**, 1288 (1980).

[107] D. Basko, I. Aleiner, and B. Altshuler, "Metal-insulator transition in a weakly interacting many-electron system with localized single-particle states", *Ann. Phys.* **321**, 1126 (2006).

[108] A. M. Finkel'stein, "Weak localization and coulomb interaction in disordered systems", *Z. Phys. B: Cond. Matt.* **56**, 189 (1984).

[109] S. V. Kravchenko, G. V. Kravchenko, J. E. Furneaux, V. M. Pudalov, and M. D'Iorio, "Possible metal-insulator transition at $B = 0$ in two dimensions", *Phys. Rev. B* **50**, 8039 (1994).

[110] C. J. Pethick and H. Smith, *Bose-Einstein Condensation in Dilute Gases* (Cambridge University Press, Cambridge, 2001).

[111] A. J. Leggett, "Bose-Einstein condensation in the alkali gases: Some fundamental concepts", *Rev. Mod. Phys.* **73**, 307 (2001).

[112] Y. Shapira and G. Deutscher, "Semiconductor-superconductor transition in granular Al-Ge", *Phys. Rev. B* **27**, 4463 (1983).

[113] A. T. Fiory and A. F. Hebard, "Electron Mobility, Conductivity, and Superconductivity near the Metal-Insulator Transition", *Phys. Rev. Lett.* **52**, 2057 (1984).

[114] J. Reppy, " ^{4}He as a dilute bose gas", *Physica B+C* **126**, 335 (1984).

[115] B. C. Crooker, B. Hebral, E. N. Smith, Y. Takano, and J. D. Reppy, "Superfluidity in a Dilute Bose Gas", *Phys. Rev. Lett.* **51**, 666 (1983).

[116] J. Bardeen, L. N. Cooper, and J. R. Schrieffer, "Theory of Superconductivity", *Phys. Rev.* **108**, 1175 (1957).

[117] W. Buckel and R. Hilsch, "Einfluß der Kondensation bei tiefen Temperaturen auf den elektrischen Widerstand und die Supraleitung für verschiedene Metalle", *Z. Phys. A: Hadrons and Nuclei* **138**, (1954).

[118] A. A. Abrikosov and L. P. Gorkov, *Sov. Phys. JETP* **8**, 1090 (1958).

[119] A. A. Abrikosov and L. P. Gorkov, *Sov. Phys. JETP* **9**, 220 (1959).

[120] P. W. Anderson, *J. Phys. Chem. Solids* **11**, 26 (1959).

[121] T. Giamarchi and H. J. Schulz, "Anderson localization and interactions in one-dimensional metals", *Phys. Rev. B* **37**, 325 (1988).

[122] T. P. Devereaux and D. Belitz, "Magnetic pair breaking in disordered superconducting films", *Phys. Rev. B* **53**, 359 (1996).

[123] A. Frydman, O. Naaman, and R. C. Dynes, "Universal transport in two-dimensional granular superconductors", *Phys. Rev. B* **66**, 052509 (2002).

[124] M. Bretz, "Heat Capacity of Multilayer He^4 on Graphite", *Phys. Rev. Lett.* **31**, 1447 (1973).

[125] G. K. S. Wong, P. A. Crowell, H. A. Cho, and J. D. Reppy, "Superfluid critical behavior in the presence of a dilute correlated impurity", *Phys. Rev. B* **48**, 3858 (1993).

[126] P. A. Crowell, F. W. Van Keuls, and J. D. Reppy, "Superfluid-Insulator Transition in ^{4}He Films Adsorbed in Vycor Glass", *Phys. Rev. Lett.* **75**, 1106 (1995).

[127] P. A. Crowell, F. W. Van Keuls, and J. D. Reppy, "Onset of superfluidity in ^{4}He films adsorbed on disordered substrates", *Phys. Rev. B* **55**, 12620 (1997).

[128] M. P. A. Fisher, P. B. Weichman, G. Grinstein, and D. S. Fisher, "Boson localization and the superfluid-insulator transition", *Phys. Rev. B* **40**, 546 (1989).

[129] D. K. K. Lee and J. M. F. Gunn, "Bosons in a random potential: condensation and screening in a dense limit", *J. Phys.: Condens. Matter* **2**, 7753 (1990).

[130] R. T. Scalettar, G. G. Batrouni, and G. T. Zimanyi, "Localization in interacting, disordered, Bose systems", *Phys. Rev. Lett.* **66**, 3144 (1991).

[131] W. Krauth, N. Trivedi, and D. Ceperley, "Superfluid-insulator transition in disordered boson systems", *Phys. Rev. Lett.* **67**, 2307 (1991).

[132] K. Huang and H.-F. Meng, "Hard-sphere Bose gas in random external potentials", *Phys. Rev. Lett.* **69**, 644 (1992).

[133] K. G. Singh and D. S. Rokhsar, "Disordered bosons: Condensate and excitations", *Phys. Rev. B* **49**, 9013 (1994).

[134] V. Ahufinger, L. Sanchez-Palencia, A. Kantian, A. Sanpera, and M. Lewenstein, "Disordered ultracold atomic gases in optical lattices: A case study of Fermi-Bose mixtures", *Phys. Rev. A* **72**, 063616 (2005).

[135] M. P. A. Fisher, G. Grinstein, and S. M. Girvin, "Presence of quantum diffusion in two dimensions: Universal resistance at the superconductor-insulator transition", *Phys. Rev. Lett.* **64**, 587 (1990).

[136] N. F. Mott, "The Basis of the Electron Theory of Metals, with Special Reference to the Transition Metals", *Proc. Phys Soc. A* **62**, 416 (1949).

[137] A. Georges, G. Kotliar, W. Krauth, and M. J. Rozenberg, "Dynamical mean-field theory of strongly correlated fermion systems and the limit of infinite dimensions", *Rev. Mod. Phys.* **68**, 13 (1996).

[138] M. Imada, A. Fujimori, and Y. Tokura, "Metal-insulator transitions", *Rev. Mod. Phys.* **70**, 1039 (1998).

[139] F. D. M. Haldane, "Effective Harmonic-Fluid Approach to Low-Energy Properties of One-Dimensional Quantum Fluids", *Phys. Rev. Lett.* **47**, 1840 (1981).

[140] G. G. Batrouni, R. T. Scalettar, and G. T. Zimanyi, "Quantum critical phenomena in one-dimensional Bose systems", *Phys. Rev. Lett.* **65**, 1765 (1990).

[141] T. Giamarchi, "Resistivity of a one-dimensional interacting quantum fluid", *Phys. Rev. B* **46**, 342 (1992).

[142] D. Jaksch, C. Bruder, J. I. Cirac, C. W. Gardiner, and P. Zoller, "Cold Bosonic Atoms in Optical Lattices", *Phys. Rev. Lett.* **81**, 3108 (1998).

[143] D. Jaksch and P. Zoller, "The cold atom Hubbard toolbox", *Ann. Phys.* **315**, 52 (2005).

[144] R. Jördens, N. Strohmaier, K. Günter, H. Moritz, and T. Esslinger, "A Mott insulator of fermionic atoms in an optical lattice", *Nature* **455**, 204 (2008).

[145] U. Schneider, L. Hackermüller, S. Will, T. Best, I. Bloch, T. A. Costi, R. W. Helmes, D. Rasch, and A. Rosch, "Metallic and Insulating Phases of Repulsively Interacting Fermions in a 3D Optical Lattice", *Science* **322**, 1520 (2008).

[146] W. Zwerger, "Mott-Hubbard transition of cold atoms in optical lattices", *J. Opt. B: Quantum Semiclass. Opt.* **5**, S9 (2003).

[147] T. Giamarchi, *Quantum Physics in One Dimension* (Oxford University Press, New York, 2004).

[148] S. Rapsch, U. Schollwock, and W. Zwerger, "Density matrix renormalization group for disordered bosons in one dimension", *EPL (Europhys. Lett.)* **46**, 559 (1999).

[149] N. V. Prokof'ev and B. V. Svistunov, "Comment on ¨One-Dimensional Disordered Bosonic Hubbard Model: A Density-Matrix Renormalization Group Study¨", *Phys. Rev. Lett.* **80**, 4355 (1998).

[150] K. G. Singh and D. S. Rokhsar, "Real-space renormalization study of disordered interacting bosons", *Phys. Rev. B* **46**, 3002 (1992).

[151] L. Zhang and M. Ma, "Real-space renormalization-group study of hard-core dirty bosons", *Phys. Rev. B* **45**, 4855 (1992).

[152] L. Pitaevskii and S. Stringari, *Bose-Einstein Condensation* (Oxford Science Publication, 2003).

[153] L. Landau and E. Lifshitz, *Course of Theoretical Physics; Statistical Physics, Part 1* (Butterworth-Heinemann, Oxford, 1980).

[154] O. Penrose, "On the quantum mechanics of helium II", *Philos. Mag.* **42**, 1373 (1951).

[155] O. Penrose and L. Onsager, "Bose-Einstein Condensation and Liquid Helium", *Phys. Rev.* **104**, 576 (1956).

[156] C. N. Yang, "Concept of Off-Diagonal Long-Range Order and the Quantum Phases of Liquid He and of Superconductors", *Rev. Mod. Phys.* **34**, 694 (1962).

[157] C. J. Pethick and L. P. Pitaevskii, "Criterion for Bose-Einstein condensation for particles in traps", *Phys. Rev. A* **62**, 033609 (2000).

[158] R. A. Aziz, A. R. Janzen, and M. R. Moldover, "Ab Initio Calculations for Helium: A Standard for Transport Property Measurements", *Phys. Rev. Lett.* **74**, 1586 (1995).

[159] N. Bogolyubov, "Theory of superfluidity", *J. Phys. USSR* **11**, 23 (1947).

[160] M. Schellekens, R. Hoppeler, A. Perrin, J. V. Gomes, D. Boiron, A. Aspect, and C. I. Westbrook, "Hanbury Brown Twiss Effect for Ultracold Quantum Gases", *Science* **310**, 648 (2005).

[161] P. McCullagh, *Tensor Methods in Statistics* (Chapman & Hall, London, 1987).

[162] B. I. Halperin, "Green's Functions for a Particle in a One-Dimensional Random Potential", *Phys. Rev.* **139**, A104 (1965).

[163] H. L. Frisch and S. P. Lloyd, "Electron Levels in a One-Dimensional Random Lattice", *Phys. Rev.* **120**, 1175 (1960).

[164] B. I. Halperin and M. Lax, "Impurity-Band Tails in the High-Density Limit. I. Minimum Counting Methods", *Phys. Rev.* **148**, 722 (1966).

[165] B. I. Halperin and M. Lax, "Impurity-Band Tails in the High-Density Limit. II. Higher Order Corrections", *Phys. Rev.* **153**, 802 (1967).

[166] A. Iomin, "Lyapunov exponents in one-dimensional disordered systems with long-range memory", *Phys. Rev. E* **79**, 062102 (2009).

[167] J. Zittartz and J. S. Langer, "Theory of Bound States in a Random Potential", *Phys. Rev.* **148**, 741 (1966).

[168] T. Kinoshita, T. Wenger, and D. S. Weiss, "Observation of a One-Dimensional Tonks-Girardeau Gas", *Science* **305**, 1125 (2004).

[169] B. Paredes, A. Widera, V. Murg, O. Mandel, S. Fölling, I. Cirac, G. V. Shlyapnikov, T. W. Hänsch, and I. Bloch, "Tonks-Girardeau gas of ultracold atoms in an optical lattice", *Nature* **429**, 277 (2004).

[170] Y. P. Chen, J. Hitchcock, D. Dries, M. Junker, C. Welford, and R. G. Hulet, "Phase coherence and superfluid-insulator transition in a disordered Bose-Einstein condensate", *Phys. Rev. A* **77**, 033632 (2008).

[171] D. Clément, P. Bouyer, A. Aspect, and L. Sanchez-Palencia, "Density modulations in an elongated Bose-Einstein condensate released from a disordered potential", *Phys. Rev. A* **77**, 033631 (2008).

[172] M. White, M. Pasienski, D. McKay, S. Q. Zhou, D. Ceperley, and B. DeMarco, "Strongly Interacting Bosons in a Disordered Optical Lattice", *Phys. Rev. Lett.* **102**, 055301 (2009).

[173] L. Fallani, J. E. Lye, V. Guarrera, C. Fort, and M. Inguscio, "Ultracold Atoms in a Disordered Crystal of Light: Towards a Bose Glass", *Phys. Rev. Lett.* **98**, 130404 (2007).

[174] A. E. Leanhardt, Y. Shin, A. P. Chikkatur, D. Kielpinski, W. Ketterle, and D. E. Pritchard, "Bose-Einstein Condensates near a Microfabricated Surface", *Phys. Rev. Lett.* **90**, 100404 (2003).

[175] J. Estève, C. Aussibal, T. Schumm, C. Figl, D. Mailly, I. Bouchoule, C. I. Westbrook, and A. Aspect, "Role of wire imperfections in micromagnetic traps for atoms", *Phys. Rev. A* **70**, 043629 (2004).

[176] U. Gavish and Y. Castin, "Matter-Wave Localization in Disordered Cold Atom Lattices", *Phys. Rev. Lett.* **95**, 020401 (2005).

[177] B. Paredes, F. Verstraete, and J. I. Cirac, "Exploiting Quantum Parallelism to Simulate Quantum Random Many-Body Systems", *Phys. Rev. Lett.* **95**, 140501 (2005).

[178] P. Massignan and Y. Castin, "Three-dimensional strong localization of matter waves by scattering from atoms in a lattice with a confinement-induced resonance", *Phys. Rev. A* **74**, 013616 (2006).

[179] P. W. Courteille, B. Deh, J. Fortágh, A. Günther, S. Kraft, C. Marzok, S. Slama, and C. Zimmermann, "Highly versatile atomic micro traps generated by multifrequency magnetic field modulation", *J. Phys. B: At. Mol. Opt. Phys.* **39**, 1055 (2006).

[180] J. W. Goodman, *Laser speckle and related phenomena* (Springer, Berlin, 1975).

[181] J. W. Goodman, *Speckle Phenomena in Optics : Theory and Applications* (Roberts and Company Publishers, Englewood, Colorado, 2007).

[182] F. M. Izrailev and A. A. Krokhin, "Localization and the Mobility Edge in One-Dimensional Potentials with Correlated Disorder", *Phys. Rev. Lett.* **82**, 4062 (1999).

[183] L. Sanchez-Palencia, D. Clément, P. Lugan, P. Bouyer, and A. Aspect, "Disorder-induced trapping versus Anderson localization in Bose-Einstein condensates expanding in disordered potentials", *New J. Phys.* **10**, 045019 (2008).

[184] S. Aubry and G. André, "Analyticity breaking and Anderson localization in noncommensurate lattices", *Ann. Israel Phys. Soc.* **3**, 133 (1980).

[185] A. A. Abrikosov and I. A. Ryzhkin, "Conductivity of quasi-one-dimensional metal systems", *Adv. Phys.* **27**, 147 (1978).

[186] P. Erdös and R. C. Herndon, "Theories of electrons in one-dimensional disordered systems", *Adv. Phys.* **31**, 65 (1982).

[187] A. A. Gogolin, "Electron localization and hopping conductivity in one-dimensional disordered systems", *Phys. Rep.* **86**, 1 (1982).

[188] N. F. Mott and W. D. Twose, "The theory of impurity conduction", *Adv. Phys.* **10**, 107 (1961).

[189] R. E. Borland, "The Nature of the Electronic States in Disordered One-Dimensional Systems", *Proc. Roy. Soc. A* **274**, 529 (1963).

[190] M. E. Gertsenshtein and V. B. Vasil'ev, "Waveguides with Random Inhomogeneities and Brownian Motion In the Lobachevsky Plane", *Theor. Probab. Appl.* **4**, 391 (1959).

[191] V. L. Berezinskii, "Kinetics of a quantum particle in a one-dimensional random potential", *Sov. Phys. JETP* **38**, 620 (1974).

[192] K. B. Efetov, "Supersymmetry and theory of disordered metals", *Adv. Phys.* **32**, 53 (1983).

[193] I. Y. Goldsheid, S. A. Molchanov, and L. A. Pastur, "A pure point spectrum of the one dimensional Schrödinger operator", *Funct. Anal. Appl.* **11**, 1 (1977).

[194] S. A. Molchanov, "The structure of eigenfunctions of one-dimensional unordered structures", *Math. USSR Izv.* **12**, 69 (1978).

[195] R. Carmona, "Exponential localization in one dimensional disordered systems", *Duke Math. J.* **49**, 191 (1982).

[196] A. Figotin, F. Germinet, A. Klein, and P. Müller, "Persistence of Anderson localization in Schrödinger operators with decaying random potentials", *Ark. Mat.* **45**, 15 (2007).

[197] H. Leschke, P. Müller, and S. Warzel, "A survey of rigorous results on random Schrödinger operators for amorphous solids", *Markov Processes and Related Fields* **9**, 729 (2003).

[198] H. Leschke, P. Müller, and S. Warzel, in *Interacting Stochastic Systems*, edited by J.-D. Deuschel and A. Greven (Springer, Berlin, 2005), pp. 119–151.

[199] Y. Lahini, R. Pugatch, F. Pozzi, M. Sorel, R. Morandotti, N. Davidson, and Y. Silberberg, "Observation of a Localization Transition in Quasiperiodic Photonic Lattices", *Phys. Rev. Lett.* **103**, 013901 (2009).

[200] D. H. Dunlap, H.-L. Wu, and P. W. Phillips, "Absence of localization in a random-dimer model", *Phys. Rev. Lett.* **65**, 88 (1990).

[201] S. D. Bièvre and F. Germinet, "Dynamical localization for the random dimer model", *J. Stat. Phys.* **98**, 1135 (2000).

[202] S. Jitomirskaya, H. Schulz-Baldes, and G. Stolz, "Delocalization in Random Polymer Models", *Commun. Math. Phys.* **233**, 27 (2003).

[203] D. Clément, *Propriétés statiques et dynamiques d'un condensat de Bose-Einstein dans un potentiel aléatoire*, Ph.D. thesis, Université Pierre et Marie Curie, Paris, France, 2007, in French, available online under http://tel.archives-ouvertes.fr/tel-00262463/en/.

[204] J. M. Luttinger and H. K. Sy, "Low-Lying Energy Spectrum of a One-Dimensional Disordered System", *Phys. Rev. A* **7**, 701 (1973).

[205] J. M. Luttinger, "Asymptotic density of electronic energy levels for a simple model of a disordered system", *Phys. Rev. B* **13**, 4555 (1976).

[206] T. Nieuwehhuizen, "Exact electronic spectra and inverse localization lengths in one-dimensional random systems", *Physica* **120A**, 468 (1983).

[207] B. Derrida and E. Gardner, "Lyapounov exponent of the one dimensional Anderson model : weak disorder expansions", *J. Physique* **45**, 1283 (1984).

[208] F. M. Izrailev, S. Ruffo, and L. Tessieri, "Classical representation of the one-dimensional Anderson model", *J. Phys. A: Math. Gen.* **31**, 5263 (1998).

[209] H. Prüfer, "Neue Herleitung der Sturm-Liouvilleschen Reihenentwicklung stetiger Funktionen", *Math. Ann.* **95**, 499 (1926).

[210] *Sturm-Liouville Theory*, edited by W. O. Amrein, A. M. Hinz, and D. P. Pearson (Birkhäuser, Basel, 2005).

[211] S. Kotani and B. Simon, "Localization in general one-dimensional random systems", *Commun. Math. Phys.* **112**, 103 (1987).

[212] F. V. Atkinson, *Discrete and Continuous Boundary Problems* (Academic Press, New York, 1964).

[213] D. Adamova, J. Horejsi, and I. Ulehla, "The Atkinson-Prüfer transformation and the eigenvalue problem for coupled systems of Schrödinger equations", *J. Phys. A: Math. Gen.* **17**, 2621 (1984).

[214] L. Greenberg, Technical report TR91-24, University of Maryland (unpublished).

[215] M. Marletta, "Numerical solution of eigenvalue problems for Hamiltonian systems", *Adv. Comput. Math.* **2**, 155 (1994).

[216] C. R. Maple and M. Marletta, "Solving Hamiltonian systems arising from ODE eigenproblems", *Numerical Algorithms* **22**, 263 (1999).

[217] L. Landau and E. Lifshitz, *Course of Theoretical Physics; Quantum Mechanics, Third Edition* (Butterworth-Heinemann, Oxford, 1977).

[218] E. Gardner, C. Itzykson, and B. Derrida, "The Laplacian on a random one-dimensional lattice", *J. Phys. A: Math. Gen.* **17**, 1093 (1984).

[219] L. Tessieri, "Delocalization phenomena in one-dimensional models with long-range correlated disorder: a perturbative approach", *J. Phys. A: Math. Gen.* **35**, 9585 (2002).

[220] E. Gurevich and O. Kenneth, "Lyapunov exponent for the laser speckle potential: A weak disorder expansion", *Phys. Rev. A* **79**, 063617 (2009).

[221] R. C. Kuhn, C. Miniatura, D. Delande, O. Sigwarth, and C. A. Müller, "Localization of Matter Waves in Two-Dimensional Disordered Optical Potentials", *Phys. Rev. Lett.* **95**, 250403 (2005).

[222] P. Lugan, A. Aspect, L. Sanchez-Palencia, D. Delande, B. Gremaud, C. A. Müller, and C. Miniatura, "One-dimensional Anderson localization in certain correlated random potentials", *Phys. Rev. A* **80**, 023605 (2009).

[223] D. Hansel and J. F. Luciani, "On diffusion equations for dynamical systems driven by noise", *J. Stat. Phys.* **54**, 971 (1989).

[224] D. Delande, private communication.

[225] F. M. Izrailev and N. M. Makarov, "Anomalous transport in low-dimensional systems with correlated disorder", *J. Phys. A: Math. Gen.* **38**, 10613 (2005).

[226] F. M. Izrailev and N. M. Makarov, "Selective transparency of single-mode waveguides with surface scattering", *Opt. Lett.* **26**, 1604 (2001).

[227] L. Lewin, *Polylogarithms and associated functions* (North-Holland, Amsterdam, 1981).

[228] A. A. Gogolin, V. I. Melnikov, and E. I. Rashba, "Conductivity in a disordered one-dimensional system induced by electron-phonon interaction", *Sov. Phys. JETP* **69**, 327 (1976).

[229] A. A. Gogolin, "Electron density distribution for localized states in one-dimensional disordered system", *Sov. Phys. JETP* **71**, 1912 (1976).

[230] G. E. Astrakharchik, J. Boronat, J. Casulleras, and S. Giorgini, "Superfluidity versus Bose-Einstein condensation in a Bose gas with disorder", *Phys. Rev. A* **66**, 023603 (2002).

[231] V. Yukalov and R. Graham, "Bose-Einstein-condensed systems in random potentials", *Phys. Rev. A* **75**, 023619 (2007).

[232] V. I. Yukalov, E. P. Yukalova, K. V. Krutitsky, and R. Graham, "Bose-Einstein-condensed gases in arbitrarily strong random potentials", *Phys. Rev. A* **76**, 053623 (2007).

[233] S. Giorgini, L. Pitaevskii, and S. Stringari, "Effects of disorder in a dilute Bose gas", *Phys. Rev. B* **49**, 12938 (1994).

[234] A. V. Lopatin and V. M. Vinokur, "Thermodynamics of the Superfluid Dilute Bose Gas with Disorder", *Phys. Rev. Lett.* **88**, 235503 (2002).

[235] G. M. Falco, A. Pelster, and R. Graham, "Thermodynamics of a Bose-Einstein condensate with weak disorder", *Phys. Rev. A* **75**, 063619 (2007).

[236] M. Modugno, "Collective dynamics and expansion of a Bose-Einstein condensate in a random potential", *Phys. Rev. A* **73**, 013606 (2006).

[237] M. Albert, T. Paul, N. Pavloff, and P. Leboeuf, "Dipole Oscillations of a Bose-Einstein Condensate in the Presence of Defects and Disorder", *Phys. Rev. Lett.* **100**, 250405 (2008).

[238] N. Bilas and N. Pavloff, "Propagation of a Dark Soliton in a Disordered Bose-Einstein Condensate", *Phys. Rev. Lett.* **95**, 130403 (2005).

[239] T. Paul, P. Leboeuf, N. Pavloff, K. Richter, and P. Schlagheck, "Nonlinear transport of Bose-Einstein condensates through waveguides with disorder", *Phys. Rev. A* **72**, 063621 (2005).

[240] T. Paul, P. Schlagheck, P. Leboeuf, and N. Pavloff, "Superfluidity versus Anderson Localization in a Dilute Bose Gas", *Phys. Rev. Lett.* **98**, 210602 (2007).

[241] T. Paul, M. Albert, P. Schlagheck, P. Leboeuf, and N. Pavloff, "Anderson localization of a weakly interacting one-dimensional Bose gas", *Phys. Rev. A* **80**, 033615 (2009).

[242] L. Sanchez-Palencia, "Smoothing effect and delocalization of interacting Bose-Einstein condensates in random potentials", *Phys. Rev. A* **74**, 053625 (2006).

[243] P. Lugan, D. Clement, P. Bouyer, A. Aspect, M. Lewenstein, and L. Sanchez-Palencia, "Ultracold Bose Gases in 1D Disorder: From Lifshits Glass to Bose-Einstein Condensate", *Phys. Rev. Lett.* **98**, 170403 (2007).

[244] L. Fontanesi, M. Wouters, and V. Savona, "Superfluid to Bose-Glass Transition in a 1D Weakly Interacting Bose Gas", *Phys. Rev. Lett.* **103**, 030403 (2009).

[245] T. Nattermann and V. L. Pokrovsky, "Bose-Einstein Condensates in Strongly Disordered Traps", *Phys. Rev. Lett.* **100**, 060402 (2008).

[246] G. M. Falco, T. Nattermann, and V. L. Pokrovsky, "Weakly interacting Bose gas in a random environment", *Phys. Rev. B* **80**, 104515 (2009).

[247] G. M. Falco, T. Nattermann, and V. L. Pokrovsky, "Localized states and interaction-induced delocalization in Bose gases with quenched disorder", *EPL (Europhys. Lett.)* **85**, 30002 (2009).

[248] D. Pines and P. Nozières, *The Theory of Quantum Liquids, Vol. II* (Perseus Books, Cambridge, Massachusetts, 1999).

[249] A. Fetter and J. Walecka, *Quantum Theory of Many-Particle Systems* (Dover Publications, Mineola, New York, 2003).

[250] M. Olshanii, "Atomic Scattering in the Presence of an External Confinement and a Gas of Impenetrable Bosons", *Phys. Rev. Lett.* **81**, 938 (1998).

[251] D. S. Petrov, G. V. Shlyapnikov, and J. T. M. Walraven, "Regimes of Quantum Degeneracy in Trapped 1D Gases", *Phys. Rev. Lett.* **85**, 3745 (2000).

[252] D. S. Petrov, M. Holzmann, and G. V. Shlyapnikov, "Bose-Einstein Condensation in Quasi-2D Trapped Gases", *Phys. Rev. Lett.* **84**, 2551 (2000).

[253] Y. Castin, in *Coherent atomic matter waves, Lecture Notes of Les Houches Summer School*, edited by R. Kaiser, C. Westbrook, and F. David (EDP Sciences and Springer-Verlag, 2000), "Bose-Einstein condensates in atomic gases: simple theoretical results", e-print: arXiv:cond-mat/0105058.

[254] E. H. Lieb and W. Liniger, "Exact Analysis of an Interacting Bose Gas. I. The General Solution and the Ground State", *Phys. Rev.* **130**, 1605 (1963).

[255] I. Bouchoule, N. J. Van Druten, and C. I. Westbrook, "Atom chips and one-dimensional Bose gases", to be published; e-print: arXiv:0901.3303.

[256] C. Mora and Y. Castin, "Extension of Bogoliubov theory to quasicondensates", *Phys. Rev. A* **67**, 053615 (2003).

[257] K. Mølmer, "Optical coherence: A convenient fiction", *Phys. Rev. A* **55**, 3195 (1997).

[258] N. M. Hugenholtz and D. Pines, "Ground-State Energy and Excitation Spectrum of a System of Interacting Bosons", *Phys. Rev.* **116**, 489 (1959).

[259] P. C. Hohenberg and P. C. Martin, "Microscopic theory of superfluid helium", *Ann. Phys.* **34**, 291 (1965).

[260] P. C. Hohenberg and P. C. Martin, "Microscopic theory of superfluid helium", *Ann. Phys.* **281**, 636 (2000).

[261] N. D. Mermin and H. Wagner, "Absence of Ferromagnetism or Antiferromagnetism in One- or Two-Dimensional Isotropic Heisenberg Models", *Phys. Rev. Lett.* **17**, 1133 (1966).

[262] P. C. Hohenberg, "Existence of Long-Range Order in One and Two Dimensions", *Phys. Rev.* **158**, 383 (1967).

[263] J. W. Kane and L. P. Kadanoff, "Long-Range Order in Superfluid Helium", *Phys. Rev.* **155**, 80 (1967).

[264] D. S. Petrov, *Bose-Einstein Condensation in Low-Dimensional Trapped Gases*, Ph.D. thesis, University of Amsterdam, 2003.

[265] T.-L. Ho and M. Ma, "Quasi 1 and 2d Dilute Bose Gas in Magnetic Traps: Existence of Off-Diagonal Order and Anomalous Quantum Fluctuations", *J. Low Temp. Phys.* **115**, 61 (1999).

[266] S. Richard, F. Gerbier, J. H. Thywissen, M. Hugbart, P. Bouyer, and A. Aspect, "Momentum Spectroscopy of 1D Phase Fluctuations in Bose-Einstein Condensates", *Phys. Rev. Lett.* **91**, 010405 (2003).

[267] M. Hugbart, J. Retter, F. Gerbier, A. Varón, S. Richard, J. Thywissen, D. Clément, P. Bouyer, and A. Aspect, "Coherence length of an elongated condensate", *Eur. Phys. J. D* **35**, 155 (2005).

[268] D. Hellweg, L. Cacciapuoti, M. Kottke, T. Schulte, K. Sengstock, W. Ertmer, and J. J. Arlt, "Measurement of the Spatial Correlation Function of Phase Fluctuating Bose-Einstein Condensates", *Phys. Rev. Lett.* **91**, 010406 (2003).

[269] S. I. Shevchenko, "On the theory of a Bose gas in a nonuniform field", *Sov. J. Low Temp. Phys.* **18**, 223 (1992).

[270] Y. Castin, in *Quantum Gases in low dimensions*, edited by L. Pricoupenko, H. Perrin, and M. Olshanii (EDP Sciences, Les Ulis, France, 2004), Vol. 116, pp. 89–132.

[271] H. Fröhlich, "A contradiction between quantum hydrodynamics and the existence of particles", *Physica* **34**, 47 (1967).

[272] D. T. Pegg and S. M. Barnett, "Phase properties of the quantized single-mode electromagnetic field", *Phys. Rev. A* **39**, 1665 (1989).

[273] E. H. Lieb, R. Seiringer, and J. Yngvason, "Bosons in a trap: A rigorous derivation of the Gross-Pitaevskii energy functional", *Phys. Rev. A* **61**, 043602 (2000).

[274] E. P. Gross, "Structure of a quantized vortex in boson systems", *Nuovo Cimento* **20**, 454 (1961).

[275] L. P. Pitaevskii, "Vortex Lines in an Imperfect Bose Gas", *Sov. Phys. JETP* **13**, 451 (1961).

[276] R. D´Agosta and C. Presilla, "States without a linear counterpart in Bose-Einstein condensates", *Phys. Rev. A* **65**, 043609 (2002).

[277] K. W. Mahmud, J. N. Kutz, and W. P. Reinhardt, "Bose-Einstein condensates in a one-dimensional double square well: Analytical solutions of the nonlinear Schrödinger equation", *Phys. Rev. A* **66**, 063607 (2002).

[278] N. Bilas and N. Pavloff, "Dark soliton past a finite-size obstacle", *Phys. Rev. A* **72**, 033618 (2005).

[279] R. Khomeriki, J. Leon, S. Ruffo, and S. Wimberger, "Nonlinear dynamics in double square-well potentials", *Theor. Math. Phys.* **152**, 1122 (2007).

[280] M. Abramowitz and I. A. Stegun, *Handbook of Mathematical Functions* (Dover, New York, 1972).

[281] W. Kirsch and B. Metzger, in *Spectral Theory and Mathematical Physics: A Festschrift in Honor of Barry Simons 60th Birthday* (AMS, 2007), pp. 649–698, preprint arXiv:math-ph/0608066.

[282] I. M. Lifshitz, "Structure of the energy spectrum of impurity bands in disordered solid solutions", *Sov. Phys. JETP* **17**, 1159 (1963).

[283] I. M. Lifshitz, "The energy spectrum of disordered systems", *Adv. Phys.* **13**, 483 (1964).

[284] A. Smerzi, S. Fantoni, S. Giovanazzi, and S. R. Shenoy, "Quantum Coherent Atomic Tunneling between Two Trapped Bose-Einstein Condensates", *Phys. Rev. Lett.* **79**, 4950 (1997).

[285] G. J. Milburn, J. Corney, E. M. Wright, and D. F. Walls, "Quantum dynamics of an atomic Bose-Einstein condensate in a double-well potential", *Phys. Rev. A* **55**, 4318 (1997).

[286] I. Zapata, F. Sols, and A. J. Leggett, "Josephson effect between trapped Bose-Einstein condensates", *Phys. Rev. A* **57**, R28 (1998).

[287] J. Javanainen and M. Y. Ivanov, "Splitting a trap containing a Bose-Einstein condensate: Atom number fluctuations", *Phys. Rev. A* **60**, 2351 (1999).

[288] F. S. Cataliotti, S. Burger, C. Fort, P. Maddaloni, F. Minardi, A. Trombettoni, A. Smerzi, and M. Inguscio, "Josephson Junction Arrays with Bose-Einstein Condensates", *Science* **293**, 843 (2001).

[289] V. Gurarie, G. Refael, and J. T. Chalker, "Excitations of One-Dimensional Bose-Einstein Condensates in a Random Potential", *Phys. Rev. Lett.* **101**, 170407 (2008).

[290] J. Gavoret and P. Nozières, "Structure of the perturbation expansion for the bose liquid at zero temperature", *Ann. Phys.* **28**, 349 (1964).

[291] E. Lifshitz and L. Pitaevksii, *Landau and Lifshitz: Course of Theoretical Physics; Statistical Physics, Part 2* (Butterworth-Heinemann, Oxford, 1980).

[292] S. Ianeselli, C. Menotti, and A. Smerzi, "Beyond the Landau criterion for superfluidity", *J. Phys. B: At. Mol. Opt. Phys.* **39**, S135 (2006).

[293] A. Griffin, "Conserving and gapless approximations for an inhomogeneous Bose gas at finite temperatures", *Phys. Rev. B* **53**, 9341 (1996).

[294] M. Lewenstein and L. You, "Quantum Phase Diffusion of a Bose-Einstein Condensate", *Phys. Rev. Lett.* **77**, 3489 (1996).

[295] C. W. Gardiner, "Particle-number-conserving Bogoliubov method which demonstrates the validity of the time-dependent Gross-Pitaevskii equation for a highly condensed Bose gas", *Phys. Rev. A* **56**, 1414 (1997).

[296] Y. Castin and R. Dum, "Low-temperature Bose-Einstein condensates in time-dependent traps: Beyond the $U(1)$ symmetry-breaking approach", *Phys. Rev. A* **57**, 3008 (1998).

[297] V. Popov, *Functional Integrals in Quantum Field Theory and Statistical Physics* (Reidel, Dordrecht, 1983).

[298] D. V. Fil and S. I. Shevchenko, "Collective excitations of a two-dimensional interacting Bose gas in external fields", *Phys. Rev. A* **64**, 013607 (2001).

[299] C. Mora and Y. Castin, "Ground State Energy of the Two-Dimensional Weakly Interacting Bose Gas: First Correction Beyond Bogoliubov Theory", *Phys. Rev. Lett.* **102**, 180404 (2009).

[300] P.-G. de Gennes, *Superconductivity of Metals and Alloys* (Benjamin, New York, 1966).

[301] J.-P. Blaizot and G. Ripka, *Quantum Theory of Finite Systems* (MIT Press, Cambridge, Massachusetts, 1986).

[302] V. Gurarie and J. T. Chalker, "Bosonic excitations in random media", *Phys. Rev. B* **68**, 134207 (2003).

[303] D. V. Skryabin, "Instabilities of vortices in a binary mixture of trapped Bose-Einstein condensates: Role of collective excitations with positive and negative energies", *Phys. Rev. A* **63**, 013602 (2000).

[304] K. Berg-Sørensen and K. Mølmer, "Bose-Einstein condensates in spatially periodic potentials", *Phys. Rev. A* **58**, 1480 (1998).

[305] N. N. Bogoliubov, "New method in the theory of superconductivity. I", *Sov. Phys. JETP* **7**, 41 (1958).

[306] P. M. Morse and H. Feshbach, *Methods of Theoretical Physics, Part I* (McGraw-Hill, New York, 1953).

[307] P. Lugan, D. Clement, P. Bouyer, A. Aspect, and L. Sanchez-Palencia, "Anderson Localization of Bogolyubov Quasiparticles in Interacting Bose-Einstein Condensates", *Phys. Rev. Lett.* **99**, 180402 (2007).

[308] M. Born, "Quantum mechanics in impact processes", *Z. Physik* **38**, 803 (1926).

[309] C. Gaul and C. A. Müller, "Anisotropic scattering of Bogoliubov excitations", *EPL (Europhys. Lett.)* **83**, 10006 (2008).

[310] N. Bilas and N. Pavloff, "Anderson localization of elementary excitations in a one-dimensional Bose-Einstein condensate", *Eur. Phys. J. D* **40**, 387 (2006).

[311] M. Y. Azbel, "Eigenstates and properties of random systems in one dimension at zero temperature", *Phys. Rev. B* **28**, 4106 (1983).

[312] J. Stenger, S. Inouye, A. P. Chikkatur, D. M. Stamper-Kurn, D. E. Pritchard, and W. Ketterle, "Bragg Spectroscopy of a Bose-Einstein Condensate", *Phys. Rev. Lett.* **82**, 4569 (1999).

[313] D. M. Stamper-Kurn, A. P. Chikkatur, A. Görlitz, S. Inouye, S. Gupta, D. E. Pritchard, and W. Ketterle, "Excitation of Phonons in a Bose-Einstein Condensate by Light Scattering", *Phys. Rev. Lett.* **83**, 2876 (1999).

[314] J. Steinhauer, R. Ozeri, N. Katz, and N. Davidson, "Excitation Spectrum of a Bose-Einstein Condensate", *Phys. Rev. Lett.* **88**, 120407 (2002).

[315] R. Ozeri, N. Katz, J. Steinhauer, and N. Davidson, "Colloquium: Bulk Bogoliubov excitations in a Bose-Einstein condensate", *Rev. Mod. Phys.* **77**, 187 (2005).

[316] F. Zambelli, L. Pitaevskii, D. M. Stamper-Kurn, and S. Stringari, "Dynamic structure factor and momentum distribution of a trapped Bose gas", *Phys. Rev. A* **61**, 063608 (2000).

[317] N. Parker, *Numerical Studies of Vortices and Dark Solitons in Atomic Bose-Einstein Condensates*, Ph.D. thesis, University of Durham, U.K., 2004.

[318] J. E. Williams, *The Preparation of Topological Modes in a Strongly-Coupled Two-Component Bose-Einstein Condensate*, Ph.D. thesis, University of Colorado, U.S.A., 1999.

[319] W. Press, S. Teukolsky, W. Vetterling, and B. Flannery, *Numerical Recipes 3rd Edition* (Cambridge University Press, Cambridge, 2007).

[320] R. C. Kuhn, O. Sigwarth, C. Miniatura, D. Delande, and C. A. Müller, "Coherent matter wave transport in speckle potentials", *New J. Phys.* **9**, 161 (2007).

[321] F. Jendrzejewski, private communication.

[322] F. Gerbier, "Quasi-1D Bose-Einstein condensates in the dimensional crossover regime", *EPL (Europhys. Lett.)* **66**, 771 (2004).

[323] T. P. Eggarter, "Some Exact Results on Electron Energy Levels in Certain One-Dimensional Random Potentials", *Phys. Rev. B* **5**, 3863 (1972).

[324] M. D. Donsker and S. R. S. Varadhan, "Asymptotics for the wiener sausage", *Commun. Pure Appl. Math.* **28**, 525 (1975).

[325] L. A. Pastur, "Behavior of some Wiener integrals as $t \to \infty$ and the density of states of Schrödinger equations with random potential", *Theor. Math. Phys.* **32**, 615 (1977).

Résumé

Ce mémoire présente une étude théorique des propriétés de localisation de gaz de Bose avec interactions faibles, en présence de désordre uni-dimensionnel. Nous abordons trois aspects de ces systèmes désordonnés. En premier lieu, nous étudions le cas d'un gaz sans interactions. Des résultats généraux stipulent que tous les états à une particule sont localisés en une dimension. Nous montrons que pour certaines classes de désordre corrélé, la dépendance de la longueur de localisation des atomes vis-à-vis de leur énergie est marquée par d'abruptes transitions à faible désordre. Ceci permet l'interprétation de résultats expérimentaux récents, au-delà des analyses précédentes. Dans un deuxième temps, nous étudions l'état fondamental d'un gaz avec interactions répulsives, et établissons un diagramme des états quantiques du système en fonction de l'amplitude du désordre et des interactions. Nous analysons les modulations de densité imposées au gaz par le désordre afin de décrire le passage du régime de condensat de Bose-Einstein délocalisé à celui de condensat fragmenté. Pour le régime des très faibles interactions, nous développons une description microscopique du système sur la base des états propres de basse énergie du hamiltonien à une particule. Ces résultats contribuent à la caractérisation de la phase de verre de Bose encore peu explorée aux faibles interactions. Enfin, nous étudions la localisation des excitations élémentaires du gaz de Bose dans le régime de (quasi-) condensat. Nous montrons que la localisation réduite des excitations de plus faible énergie est imputable à un écrantage efficace par le (quasi-) condensat des variations de grande longueur d'onde du potentiel extérieur.

Abstract

In this thesis, we theoretically investigate the localization properties of weakly-interacting Bose gases in the presence of one-dimensional disorder. We focus on three aspects of those disordered systems. First, we study the case of a non-interacting gas. According to general results, all single-particle states are localized in one dimension. We show that for certain classes of correlated disorder, the dependence of the localization length of the atoms on their energy undergoes sharp crossovers for weak disorder. These findings allow for the interpretation of recent experiments beyond previous analyses. Then, we examine the ground state of an interacting gas, and establish a diagram of the quantum states as a function of the strength of disorder and interactions. We analyze the density modulations imposed on the gas by the disorder, in order to describe the crossover from the regime of delocalized Bose-Einstein condensate to the regime of fragmented condensate. For the regime of very weak interactions, we develop a microscopic description of the system on the basis of the eigenstates of the single-particle Hamiltonian. These results contribute to characterizing the Bose-glass phase at weak interactions, which has yet to be explored thoroughly. Finally, we study the localization of the elementary excitations of the Bose gas in the (quasi-) condensate regime. We show that the suppressed localization of the excitations of lowest energy is due to an efficient screening by the (quasi-) condensate of the long-wavelength variations of the external potential.